Roles of nicotinic acetylcholine receptors in development, viability, and insecticide response, in *Drosophila melanogaster*

Danielle Christesen

ORCID: 0000-0002-5996-7123

Submitted in total fulfilment of the requirements of the degree of

Doctor of Philosophy

June 2021

School of Biosciences
Faculty of Science
The University of Melbourne

Abstract

The majority of excitatory neurotransmission in the insect brain occurs via nicotinic acetylcholine receptors (nAChRs), however knowledge of which nAChR subunits may be required in specific neurons is virtually absent. The ubiquity of nAChRs in the insect brain also makes them ideal molecular targets for many neuroactive insecticides. Mutations in specific nAChR subunits can confer high levels of resistance, but the fitness costs that may be associated with resistance alleles or with low-dose insecticide exposure are not fully understood. This thesis examines two *Drosophila* nAChR subunits with the most severe loss of function phenotypes, with a focus on their endogenous functions and their roles in insecticide response.

Chapter Two investigates the role of the Dα5 subunit in larval development. Preliminary observations had indicated that loss of Dα5 causes larval mortality and is associated with precocious wandering and moulting phenotypes. Here, these phenotypes are quantified and found to be associated with loss of ecdysis triggering hormone. Cell types requiring Dα5 were also narrowed-down to potentially include the prothoracic gland cells, or the neurons innervating the prothoracic gland. In insecticide exposure assays, loss of Dα5 was shown to not confer altered response to spinosad, suggesting that Dα5 may not be contributing to the primary spinosad target.

In *Chapter Three*, loss of the Dβ1 subunit is shown to result in pleiotropic consequences, including severely shortened longevity, reduced male courtship, limited locomotion, and unsuccessful wing expansion. Since wing expansion is controlled by a well-characterised hormone (bursicon) in a small and well-defined subset of neurons (the CCAP neurons), this phenotype was examined further. Removal of *Dβ1* specifically from CCAP neurons using somatic CRISPR was sufficient to disrupt wing expansion and loss of Dβ1 was shown to cause loss of the hormone bursicon. Together, these experiments identify CCAP neurons as a specific subset requiring Dβ1 for normal function.

Chapter Four extends findings from the previous chapter, by testing whether alternative *Dβ1* alleles, and a non-*Drosophila β1* subunit orthologue, can rescue the Dβ1 loss of function phenotypes. *Dβ1* cDNA rescue constructs containing the amino acid replacements R81T (found in resistant populations of aphids), and R81Q (naturally occurring in insensitive arachnids), were both found to rescue all elements of the Dβ1 phenotype, but only R81Q was found to confer high levels of imidacloprid resistance. The aphid subunit Mpβ1 was also able to rescue loss of Dβ1, and fully restored sensitivity to imidacloprid, revealing substantial functional conservation between the β1 subunits in these two species. This work provides a platform for studying resistance-conferring amino acid replacements in pest nAChR subunits within the *Drosophila* model.

Understanding the endogenous roles of nAChR subunits will be essential for characterising the function of every pathway in the insect brain. By characterising the roles of Dα5 and Dβ1, this thesis provides great insight into the fitness costs insects may endure when evolving insecticide resistance. It also reveals the developmental and behavioural pathways that may be affected when pest and non-pest species are chronically exposed to the low doses of insecticides that contaminate the environment.

Declaration

This is to certify that:

i. the thesis comprises only my original work towards the PhD except where indicated in the Preface;

ii. due acknowledgement has been made in the text to all other material used;

iii. the thesis is fewer than 100,000 words in length, exclusive of tables, maps, bibliographies, and appendices.

Signed:

Danielle Christesen

30 June 2021

Preface

I would like to acknowledge the following people for contributing directly to this work:

Chapter Two

- Dr Trent Perry, Ying Ting Yang, Joseph Nguyen – assisted with many attempts at Dα5 CRISPR
- Dr Hector Sandoval – created Dα5 deGradFP lines and assisted with confocal imaging
- Dr Julia Wang, Dr Felipe Martelli – performed confocal imaging for *Dα5$^{TG4\text{-}3'}$*

Chapter Three*

- Ying Ting Yang – created *Dβ1* CRISPR lines
- Ying Ting Yang - assisted with collection of embryos and larvae for multiple experiments
- Wei Chen – created *Dβ1-TG4* and performed confocal imaging for *Dβ1-TG4*

*This chapter is a manuscript that was accepted for publication in the journal *Genetics* in June 2021.

Chapter Four

- Dr Trent Perry – designed R81T mutagenesis primers, R81Q gBlocks, and *Mpβ1* cloning primers
- Dr Trent Perry – collected aphid samples
- Ying Ting Yang – assisted with longevity scoring
- Ying Ting Yang – assisted with collection of embryos and larvae for multiple experiments

Scholarships and funding

The following awards funded me during the course of my PhD candidature:

- Australian Postgraduate Award - to undertake a doctoral degree (2015 - 2018)

- Dame Margaret Blackwood Soroptimist Scholarship - to aid research and to aid travel to visit labs to discuss and develop research (2015, 2016)

- Bio21 Institute Student Travel Award - to aid travel to conferences and/or to visit labs and discuss and develop research (2019)

Acknowledgements

This thesis has been a huge undertaking, and I could not have done it without the advice, support, and encouragement of the many wonderful people around me.

Above all, my biggest thanks must go to my supervisors, Dr Trent Perry and Prof Philip Batterham. I was incredibly lucky to have two brilliant mentors who are equally as passionate about their science as they are about the welfare of their students. Trent, you were always full of ideas and suggestions, and eager to troubleshoot all my problems. You dedicated so much energy to my project and I know that all the future students that join the Perry Lab will be in the best hands. Phil, you have influenced so many scientists and it was a privilege to learn directly from you. The way you think about and communicate your science is so inspiring and you will always be someone I look up to. Thank you, Phil and Trent, for welcoming me into the Batterham/Perry lab family and for being the best supervisors a student could hope for.

Another massive thank you goes to Tinna Yang. Tinna, you taught me a huge proportion of the lab skills I know, and I continue to learn from you every day. You are the heart of the lab and I know there are dozens of students out there who are better scientists because of you. Thank you for your patience in the lab and, of course, for your friendship.

I am thankful to all past and present members of the Batterham/Perry lab, however a few people deserve special mentions. Dr Jason Somers and Chris Lumb, thank you for your guidance and patience when I was a new and clueless MSc student. Joseph Nguyen, Wei Chen, Dr Felipe Martelli, Natalia Hernandes, Dr Razi Ghazali, and Alex Giang, thank you all for your help with my project, and for making the Batterham/Perry lab such a fun and memorable place to work.

I would also like to express my gratitude to my committee members, A/Prof Meryl Davis, Dr Michael Murray, and Prof Alex Andrianopoulos. You always challenged me to think about my work in new ways, and no matter how nervous I was for every meeting, I always left

feeling like you were proud of me. I was lucky to have such a supportive team of academics guiding me.

One of the greatest experiences in my PhD was the opportunity to visit Prof Hugo Bellen's lab in Houston and I am incredibly grateful to Hugo, Dr Hector Sandoval, and Catherine Tasnier for overseeing my stay there. The pace and intensity of their research is mind-blowing and it was a privilege to be exposed to that environment so early in my career. My sincere thanks also go to Abhi and Dulce, who so warmly welcomed me into their home and adopted me into their family for my five-month stay.

Another highlight of my PhD was teaching and marking in a range of university subjects. An enormous thank you to Stephen Hardy, Dr Alexandre Fournier-Level, A/Prof Dawn Gleeson, and Dr Hayley Bugeja for entrusting me with the responsibility of teaching in your subjects - I had a ball and will miss working with all of you. I am also incredibly grateful to A/ Prof Paul Umina for the opportunity to work on the mite project and gain experience as a research assistant.

Last, but certainly not the least, I would like to thank my family - mum, dad and Bee. You have been incredibly supportive and have always tolerated my selfish work habits (not just during my PhD, but throughout school and uni). Thank you for always showing interest in my work, and doing such a good job explaining to people what I do. I love you!

My PhD would not have been possible nor as fulfilling without all the wonderful people acknowledged here (plus many others). I am endlessly grateful to all of you and value all the friendships I made along the way.

Table of Contents

Abstract iii

Declaration v

Preface vii

Scholarships and funding ix

Acknowledgements xi

Table of Contents xiii

List of Figures xvii

List of Tables xix

Chapter One: Introduction 1

1.1 Understanding the insect brain 3

1.2 Nicotinic acetylcholine receptors 4

1.2.1 nAChRs: subunit domains and topology 5

1.2.2 nAChRs: pentamer assembly 7

1.2.3 nAChRs: cholinergic signalling 11

1.2.4 Insect nAChR gene families 15

1.2.5 The *Drosophila* nAChR gene family 18

1.2.6 nAChRs as targets of insecticides 22

1.2.7 Endogenous roles of *Drosophila* nAChRs 24

1.3 Insect development 26

1.3.1 The *Drosophila* life cycle 26

1.3.2 Endocrine control of developmental transitions 28

1.4 Aims of this thesis 33

Chapter Two: Investigating the role of the Dα5 subunit in larval development 35

2.1 Introduction 37

2.1.1 Early descriptions of loss of Dα5 function 39

2.1.2 Cues for moulting and wandering 40

2.1.3 Chapter aims 41

2.2 Methods 42

2.2.1 Fly strains and maintenance 42

2.2.1.1 CRISPR strains 42

2.2.1.2 RNAi crosses 45

2.2.1.3 Overexpression crosses 45

2.2.1.4 deGradFP crosses 47

2.2.1.5 Complementation crosses 48

2.2.1.6 Genetic rescue crosses 48
2.2.1.7 BAC clone strains 48
2.2.1.8 "Mapping" lethality to the MiMIC insertion 49
2.2.2 Developmental mortality assays 51
2.2.3 Measuring body weight 51
2.2.4 Wandering assays 51
2.2.5 Larval movement assays 51
2.2.6 Feeding assays 52
2.2.7 Longevity assays 52
2.2.8 Fertility assays 53
2.2.9 Climbing assays 53
2.2.10 qRT-PCR 53
2.2.11 Semi-quantitative PCR 54
2.2.12 Confocal microscopy 57
2.2.13 Protein alignments 58
2.2.14 Western blotting 58

2.3 Results 60
2.3.1 Attempts to generate *Dα5* genomic deletions 60
2.3.2 MiMIC insertions in *Dα5* disrupt larval development 64
2.3.2.1 $D\alpha5^{Mi\text{-}5'}$ 64
2.3.2.2 $D\alpha5^{TG4\text{-}5'}$ and $D\alpha5^{TG4\text{-}3'}$ 67
2.3.3 Larvae have abnormal wandering, movement and feeding behaviours 68
2.3.3.1 Wandering 68
2.3.3.2 Movement 68
2.3.3.3 Feeding 70
2.3.4 Loss of Dα5 disrupts a hormone pathway 72
2.3.4.1 Comparison with existing literature 72
2.3.4.2 Hormone qRT-PCR 74
2.3.5 Dα5 may be required in the PG or PG neurons 75
2.3.5.1 Tissue-specific RNAi knockdown 75
2.3.5.2 TG4 expression patterns 79
2.3.6 Loss of Dα5 in adults 81
2.3.6.1 Post-larval deGradFP knockdown 81
2.3.6.2 Longevity, fertility, and climbing performance in heterozygous adults 84
2.3.7 Attempts to verify loss of Dα5 as the cause of mortality 86
2.3.7.1 Complementation crosses 86
2.3.7.2 Genetic rescue 89
2.3.7.3 BAC clone rescue 90
2.3.7.4 "Mapping" lethality to the MiMIC insertion 90
2.3.8 Analysis of Dα5's abnormal N-terminus 92
2.3.8.1 Bioinformatic analyses 92
2.3.8.2 Western blotting 97
2.3.9 The role of Dα5 in insecticide response 98

2.4 Discussion 99
2.4.1 A deeper look at the lethal phenotype 99
2.4.2 An underlying cause for the lethal phenotype 100
2.4.3 Linking loss of Dα5 and loss of ETH 101
2.4.4 Hypotheses on which cells need Dα5 102
2.4.4.1 Dα5 may be required in the PG cells 103
2.4.4.2 Dα5 may be required in the PGNs 104
2.4.4.3 Dα5 may be required in the PG driver neurons 105

2.4.4.4 Next steps for narrowing down cells of interest 105
2.4.5 Adult heterozygotes are healthy, or are they? 106
2.4.6 Is Dα5's essential role conserved among insects? 107
2.4.7 How important is the abnormal N-terminus? 108
2.4.8 The $D\alpha5^{Mi\text{-}5'}$ response to spinosad 108
2.4.9 Addressing issues with Dα5 strains 109
2.4.9.1 Complementation between Dα5 strains 110
2.4.9.2 Failed genetic rescue 110
2.4.9.3 A poorly visible GFP tag and ineffectual deGradFP 111
2.4.9.4 Dα5's aversion to CRISPR 112
2.4.10 Final comments 115

Chapter Three: Loss of the Dβ1 nicotinic acetylcholine receptor subunit disrupts bursicon-driver wing expansion and dimishes adult viability in *Drosophila melanogaster* **..... 117**

3.1 Abstract 119

3.2 Introduction 119

3.3 Methods 122
3.3.1 Fly strains and maintenance 122
3.3.2 Generating *Dβ1* genomic deletions using CRISPR-Cas9 122
3.3.3 Generating *Dβ1*-TG4 using CRIMIC 123
3.3.4 Generating cDNA rescue constructs 123
3.3.5 Developmental mortality assays 124
3.3.6 Wing morphology scoring 124
3.3.7 Longevity and fertility assays 124
3.3.8 Mating assays 125
3.3.9 Adult climbing assays 125
3.3.10 Larval movement assays 126
3.3.11 qRT-PCR 126
3.3.12 Data availability 127
3.4.2 Loss of *Dβ1* decreases fitness and disrupts wing expansion 129
3.4.3 Loss of *Dβ1* affects locomotor performance 132
3.4.4 Males lacking *Dβ1* spend less time courting and fail to initiate copulation 134
3.4.5 Pinpointing a neuronal subset that requires *Dβ1* 136

3.5 Discussion 140

Chapter Four: Establishing a rescue system for examining the conservation of β1 subunits and resistance-conferring mutations **..... 145**

4.1 Introduction 147
4.1.1 The R81T replacement 147
4.1.2 Using *Drosophila* to express alternative β1 subunits 148
4.1.3 Chapter aims 150

4.2 Methods 151
4.2.1 Fly strains and maintenance 151

4.2.1.1 Generating UAS-Dβ1^{R81T} 151
4.2.1.2 Generating Dβ1^{R81Q} 154
4.2.1.3 Generating Mpβ1 154
4.2.2 Developmental mortality assays 155
4.2.3 Wing morphology analysis 155
4.2.4 Longevity assays 155
4.2.5 Fertility assays 156
4.2.6 Climbing assays 156
4.2.7 Wiggle Index assays 156

4.3 Results 158
4.3.1 The *Dβ1^{R81T}, Dβ1^{R81Q} and Mpβ1* subunits restore native *Dβ1* function 158
4.3.2 Responses to imidacloprid exposure 161

4.4 Discussion 164
4.4.1 Dβ1^{R81T} 164
4.4.2 Dβ1^{R81Q} 166
4.4.3 *Mpβ1* 167
4.4.4 Future directions 168

Chapter Five: Discussion **..... 170**

5.1 Neuronal control of development 171

5.2 Implications of nAChR compensation 172

5.3 The trade-off between insecticide resistance and associated fitness costs 173

5.4 Concluding remarks 175

References 177

Appendix 1 CRISPR methods used in attempts to generate a *Dα5* genomic deletion **..... 196**

Appendix 2 Supplementary material for Christesen *et al.* 2021 (*Chapter Three*) **..... 202**

Appendix 3 gBlocks used to generate *Dβ1^{R81Q}* cDNA **..... 217**

List of Figures

Chapter One

Figure 1.1 nAChR subunit topology and pentamer assembly 6
Figure 1.2 Homomeric and heteromeric nAChRs 9
Figure 1.3 The position of nAChRs is dynamic 10
Figure 1.4 Channel gating 11
Figure 1.5 Cholinergic neurotransmission 12
Figure 1.6 Pre-synaptic and non-neuronal nAChRs 14
Figure 1.7 Tree of insect nAChR subunits 17
Figure 1.8 Expression of nAChR subunit genes in single-cell RNA-seq datasets 21
Figure 1.9 The *Drosophila* life cycle 27
Figure 1.10 Endocrine control of moulting 31
Figure 1.11 Pulses of 20E drive developmental transitions 32

Chapter Two

Figure 2.1 *Drosophila* nAChR subunit gene structure 38
Figure 2.2 The α7-like superclade 38
Figure 2.3 Known binding partners for Dα5 39
Figure 2.4 Key positions and insertion cassettes for fly strains used in *Chapter Two* 43
Figure 2.5 Timing of deGradFP experiments 47
Figure 2.6 BAC clones 49
Figure 2.7 "Mapping" lethality on $D\alpha5^{Mi\text{-}5'}$ chromosome 2 50
Figure 2.8 CRISPR target sites and plasmids 61
Figure 2.9 Evidence of CRISPR editing lost over subsequent generations 63
Figure 2.10 Evidence of CRISPR editing lost in subsequent DNA extractions 64
Figure 2.11 $D\alpha5^{Mi\text{-}5'}$ exhibits mid-moult mortality 65
Figure 2.12 $D\alpha5^{Mi\text{-}5'}$ has low larval body weight 66
Figure 2.13 Relative expression of nAChR subunits in $D\alpha5^{Mi\text{-}5'}$ larvae 66
Figure 2.14 $D\alpha5^{TG4\text{-}5'}$ and $D\alpha5^{TG4\text{-}3'}$ exhibit mid-moult mortality 67
Figure 2.15 $D\alpha5^{Mi\text{-}5'}$ and $D\alpha5^{TG4\text{-}3'}$ exhibit precocious wandering behaviour 69
Figure 2.16 $D\alpha5^{Mi\text{-}5'}$ larvae have reduced basal movement 70
Figure 2.17 $D\alpha5^{Mi\text{-}5'}$ larvae stop feeding during the second instar stage 71
Figure 2.18 Timing of observations for $D\alpha5^{Mi\text{-}5'}$ 72
Figure 2.19 Knockdown of *ETH* causes precocious wandering behaviour 74
Figure 2.20 Hormone levels in $D\alpha5^{Mi\text{-}5'}$ larvae 75
Figure 2.21 Pan-neuronal RNAi knockdown of *Dα5* causes eye phenotype 76
Figure 2.22 Relative expression of nAChR subunits in *da-GAL4* RNAi larvae 78
Figure 2.23 Semi-quantitative PCR analysis of *Dα5* in *da-GAL4* RNAi larvae 79
Figure 2.24 $D\alpha5^{TG4\text{-}5'}$ and $D\alpha5^{TG4\text{-}3'}$ are expressed in the CNS and PGNs 80
Figure 2.25 PG driver expression in the CNS 81
Figure 2.26 *Dα5-GFP* expression in the CNS 83
Figure 2.27 Fitness of heterozygous $D\alpha5^{Mi\text{-}5'}/D\alpha5^{w1118}$ adults 85
Figure 2.28 Complementation between different *Dα5* strains 87

Figure 2.29 *Dα5* cDNA is detectable in transheterozygotes 88
Figure 2.30 Ubiquitous expression of *UAS-Dα5cDNA* does not rescue $D\alpha5^{Mi\text{-}5'}$ 89
Figure 2.31 Lethality is associated with the MiMIC cassette 91
Figure 2.32 Abnormal N-terminus is restricted to the *Drosophila* genus and select dipterans 93
Figure 2.33 Western blotting indicates the abnormal N-terminus may be cleaved 97
Figure 2.34 Wiggle Index analysis following exposure to spinosad 98

Chapter Three

Figure 3.1 Genomic deletion of the *Dβ1* nAChR subunit gene 128
Figure 3.2 *Dβ1* deletion reduces adult fitness 130
Figure 3.3 *Dβ1* deletion affects larval crawling and adult climbing performance 133
Figure 3.4 Males lacking *Dβ1* fail to mate 135
Figure 3.5 *Dβ1* is required in CCAP neurons for bursicon-driven wing expansion 139

Chapter Four

Figure 4.1 Rescue crosses 153
Figure 4.2 *β1* alleles rescue mortality 159
Figure 4.3 *β1* alleles rescue adult longevity 159
Figure 4.4 *β1* alleles rescue fertility 160
Figure 4.5 *β1* alleles rescue wing morphology 160
Figure 4.6 The level of rescue of larval and adult locomotor performance varies between different *β1* alleles 161
Figure 4.7 Responses of different *β1* alleles to imidacloprid exposure 163

List of Tables

Chapter One

Table 1.1 Complete insect nAChR gene families 16
Table 1.2 *Drosophila* nAChR subunit genes 19
Table 1.3 *Drosophila* nAChR subtypes 20
Table 1.4 nAChR subunits involved in insecticide response 23
Table 1.5 Endogenous roles of nAChR subunits 25

Chapter Two

Table 2.1 Fly strains used throughout *Chapter Two* 44
Table 2.2 Fly strains used for RNAi 46
Table 2.3 Primers used in complementation experiments 48
Table 2.4 Primers flanking the $D\alpha5^{Mi\text{-}5'}$ insertion site 49
Table 2.5 qRT-PCR primers 55
Table 2.6 MIQE 56
Table 2.7 Semi-quantitative PCR primers 56
Table 2.8 Semi-quantitative PCR conditions 57
Table 2.9 Confocal microscopy antibodies 59
Table 2.10 Western blotting antibodies 59
Table 2.11 Attempted CRISPR strategies 62
Table 2.12 Comparison of $D\alpha5^{Mi\text{-}5'}$ with previously-reported phenotypes 73
Table 2.13 Most frequent stage of mortality for tissue-specific RNAi knockdown 76
Table 2.14 Sequence conservation amongst insect α5 and α7 subunits 95

Chapter Four

Table 4.1 Alignment of loop D amino acid residues from β1 (and equivalent) subunits 149
Table 4.2 Fly strains used in *Chapter Four* 152
Table 4.3 Primers used in *Chapter Four* 152
Table 4.4 Loop D amino acid residues based on sequencing of UAS-$D\beta1$ plasmids 153

Chapter One

Introduction

1.1 Understanding the insect brain

Insects are the most abundant animals on Earth (Bar-On *et al.* 2018). They contribute to our ecosystems in vital ways, providing services such as pollination and decomposition (Losey and Vaughan 2006). A minority of insect species are pests, acting as vectors of disease (Wilson *et al.* 2020) and causing immense damage to agricultural crops and livestock (Sharma *et al.* 2017). More recently, humans have bestowed yet another role upon insects - that of scientific research tool.

Studying insects can teach us profound lessons about biology in general, and no other species has been more impactful in this regard than the vinegar fly *Drosophila melanogaster* (Jennings 2011). Multiple Nobel Prizes have been awarded for discoveries that used this model species, from the role of chromosomes in inheritance in 1933, to the molecular mechanisms controlling circadian rhythm in 2017 (nobelprize.org). Thanks to the universality of the genetic code, and surprisingly high levels of conservation with many human disease-causing genes, *Drosophila* is also being used to diagnose the genetic causes of common and rare human diseases (Bellen *et al.* 2019).

Within the vast field of *Drosophila* research, the 21st century has seen a surge in attention towards the brain. Flies have the capacity to perform many complex behaviours, yet their brains are composed of a fairly manageable 100,000 neurons (far less daunting than the ~86 billion neurons in the human brain) (Scheffer *et al.* 2020). Thus, combined with the impressive range of genetic tools available in this species, the *Drosophila* brain is an ideal candidate for producing the first complete, functional wiring diagram of a centralised animal brain. While remarkable progress has been made in producing physical maps (connectomes) (Zheng *et al.* 2018, Li *et al.* 2020, Scheffer *et al.* 2020) and characterising the functions of many neurons, determining how every neuron interacts with others in different circuits to control behaviour is a huge ongoing challenge that will take many small steps to achieve.

One of the key pieces in this puzzle will be the nicotinic acetylcholine receptors (nAChRs). A large proportion of the *Drosophila* brain is described as cholinergic (Croset *et al.* 2018),

meaning the neurons communicate across synapses by releasing the neurotransmitter acetylcholine (ACh), which then binds to nAChRs in post-synaptic membranes. Numerous *Drosophila* behaviours and cognitive tasks are already known to rely on this nAChR-dependent signalling, from learning and memory, to mating and sleep (Shi *et al.* 2014, Wu *et al.* 2014, Barnstedt *et al.* 2016, Somers *et al.* 2017). Further, many neuroactive insecticides that we use to control insect pests also target these nAChRs (Sparks *et al.* 2020). Unravelling nAChR biology is therefore imperative for completing the functional map of the *Drosophila* brain, and for understanding how different insect species will be affected by insecticides present in the environment. This thesis examines nAChRs through both of these lenses.

1.2 Nicotinic acetylcholine receptors

nAChRs are widespread in the nervous systems of taxa across the animal kingdom (Bossy *et al.* 1988). From animals with a relatively simple brain, like worms, to the astoundingly complex nervous systems of humans, nAChRs always contribute to the machinery that facilitates neurotransmission. However, insect central nervous systems (CNS) stand out in the extent to which they are dominated by nAChR-dependent signalling (Lee and O'Dowd 1999, Breer and Sattelle 1987).

Insect brains are the second most concentrated source of nAChRs known to exist in nature, second only to the electric organ of the *Torpedo* electric ray where nAChRs were first discovered (Claudio and Rafferty 1977). In contrast, vertebrate nAChRs are primarily found in neuromuscular junctions and peripheral neurons and play a less dominant role in CNS function (Millar 2003). Nonetheless, this does not mean that vertebrate nAChRs are dispensable to vertebrate nervous systems. Mutations or other disruptions to human nAChRs have been implicated in the pathophysiology of a range of human conditions, including addiction disorders and neurodegenerative diseases (Albuquerque *et al.* 2009, Picciotto and Kenny 2013). Vertebrates are also sensitive to xenobiotic agonists and antagonists of nAChRs, including various drugs and toxins (Changeux *et al.* 1970, Arneric *et al.* 2007, Lebbe *et al.* 2014).

Thanks to relatively high levels of functional and structural conservation, we can study nAChRs in both vertebrate and invertebrate systems and gain transferable insight into nAChR biology. Indeed, most of our structural and pharmacological knowledge of nAChRs originates from work performed in vertebrate systems. The following sections cover this vertebrate-based work before returning to focus on what we already know about insect, and in particular *Drosophila,* nAChRs.

1.2.1 nAChRs: subunit domains and topology

Like all ligand-gated cation channels in the Cys-loop family, nAChRs are pentameric and are embedded in the cell membrane (Corringer *et al.* 2000, Karlin 2002). Considering the tertiary structure of individual nAChR subunits, all possess the same topology with five key domains: an N-terminal ligand binding domain (LBD), and four hydrophobic transmembrane domains (TM1-TM4) (**Figure 1.1**). These domains are arranged such that the large LBD is extracellular, where it can be accessed by ligands, with the TM domains then passing through the membrane four times so that the short C-terminus also sits on the extracellular side of the cell membrane. Each TM domain is joined by intracellular and extracellular loops, with the intracellular loop flanked by TM3 and TM4 being particularly variable in size and sequence between different subunits. A signal peptide (SP) is also present on each subunit, upstream of the LBD. Each of these regions plays a role in the function of the mature receptor, although certain domains are better characterised than others.

Understandably, the LBD receives a disproportionate amount of attention, both in terms of its interaction with its native ligand ACh and interactions with xenobiotics. It consists of six loops which contain key conserved residues. At the secondary level, these loops are arranged in the order D-A-E-B-F-C, but in the mature subunit they are arranged as A-B-C on what is known as the principal interface, and D-E-F on the complementary interface (**Figure 1.1**) (Corringer *et al.* 2000, Karlin 2002). ACh binds between the principal and complementary interfaces of two adjacent subunits, in a hydrophobic pocket formed by the

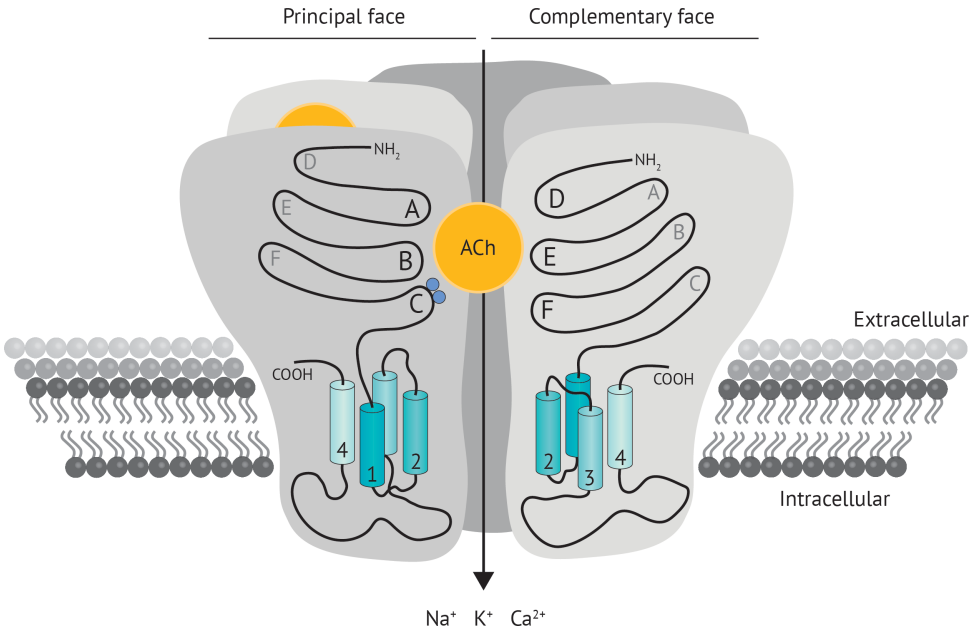


Figure 1.1 nAChR subunit topology and pentamer assembly

nAChRs consist of five individual subunits arranged symmetrically around a central ion channel. Each individual subunit has a large N-terminal ligand binding domain followed by four transmembrane domains, the second of which lines the central channel. Within the ligand binding domain, loops A, B and C form the principal face, while loops D, E and F form the complementary face. It is at the interface of two adjacent subunits that the ligand ACh binds, causing the channel to open and allowing cations to enter the cell. A di-cysteine motif at the apex of loop C (blue) is required for ACh binding and is found only in α subunits. (After Jones and Sattelle 2010).

six loops (Grutter and Changeux 2001). At the apex of loop C is a YXCC motif required for ACh binding (Kao *et al.* 1984; Karlin and Akabas 1995), however this motif only occurs in a subset of nAChR subunits called α subunits, and is absent in non-α subunits. This distinction between α and non-α subunits has implications at the quaternary level and will be addressed in a later section (*1.2.2*).

Whereas the LBD governs channel activation, the TM domains form the channel itself, through which, once opened, cations can traverse the cell membrane (Corringer *et al.* 2000, Karlin 2002). Of the four TM domains, TM2 is considered the most pertinent to receptor function as it is the domain that lines the channel. Meanwhile, TM1, TM3 and TM4 are thought to provide stability in the membrane (Tierney and Unwin 2000). Amino acid residues located near the ends of TM2 influence ion selectivity, and can govern whether a channel is more permeable to Na^+, K^+ or Ca^{2+} (Corringer *et al*. 2000, Karlin 2002). Thus, while TM domains tend to be conserved, variation in TM2 can provide a source of pharmacological variation among different subunits.

The most diverse region of an nAChR subunit is the large intracellular domain spanning TM3-TM4 (Stokes *et al.* 2015). While its function is less obvious than the LBD and the TM domains, there are some clues as to its role in the mature receptor, including the presence of conserved phosphorylation sites. These may influence the assembly of different subunits into pentamers, the trafficking of receptors to the cell membrane, or the spatial clustering of receptors at the cell surface (*section 1.2.2*) (Ren *et al.* 2005, Stokes *et al.* 2015).

Together, the LBD, TM domains and intracellular loop define nAChR subunits, but sequence variation in these regions provides pharmacological diversity between various subunits. Understanding these differences helps explain why certain subunits may be able to fulfil unique roles - it all depends on the nature of cholinergic signalling required at a given synapse. But in addition to this sequence-level diversity, what makes nAChRs such a diverse family of receptors is the many combinations of individual subunits that can potentially assemble together to form mature nAChR pentamers.

1.2.2 nAChRs: pentamer assembly

To form a mature nAChR, five subunits are arranged symmetrically to form a central ion channel (**Figure 1.1**) (Corringer *et al.* 2000, Karlin 2002). Whilst we have already seen that there is variation at the secondary level between different subunits, it is here at the quaternary level that the vast pharmacological repertoire of nAChRs is fully realised. If one

considers the size of nAChR gene families (for instance, the *D. melanogaster* genome has 10 subunits), then theoretically there are over 250 possible homomeric or heteromeric subtypes that could exist in a single fly brain. That number would be orders of magnitude higher if the exact arrangement of subunits within each subtype was also taken into account. But not all of these may necessarily exist or be functional. For instance, some pentameric combinations may consist of subunits that do not share an overlapping expression pattern. Another limiting factor is the YXCC motif required for ACh binding which is found only in α subunits. This means an α subunit must be present to form the principal interface and eliminates pentamers lacking α subunits from the potential pool of functional ACh-binding subtypes (**Figure 1.2**).

Correct assembly of these subtypes and their delivery to the cell membrane is a tightly controlled process, involving multiple steps and an assortment of machinery (**Figure 1.3**) (Millar and Harkness 2002, St John 2009). Subunits are first synthesised in the endoplasmic reticulum, then assembled into pentamers and exported to the Golgi body before being trafficked to their functional position in the cell membrane. Many accessory proteins are involved in this process, including some that are nAChR-specific such as RIC3 (Castillo *et al.* 2005). Once at the cell membrane, the position of nAChRs is not static. They can be internalised and then recycled back to the membrane, and eventually will be degraded via the ubiquitin-protease system. This movement of nAChRs occurs naturally, but can also be triggered by xenobiotic compounds (Harkness and Millar 2002, Martelli 2020, Nguyen *et al.* 2021). Thus, the presence of nAChRs at a given synapse is not just dependent upon the expression levels of constituent subunits, but also upon this dynamic movement of nAChRs at the post-translational level.

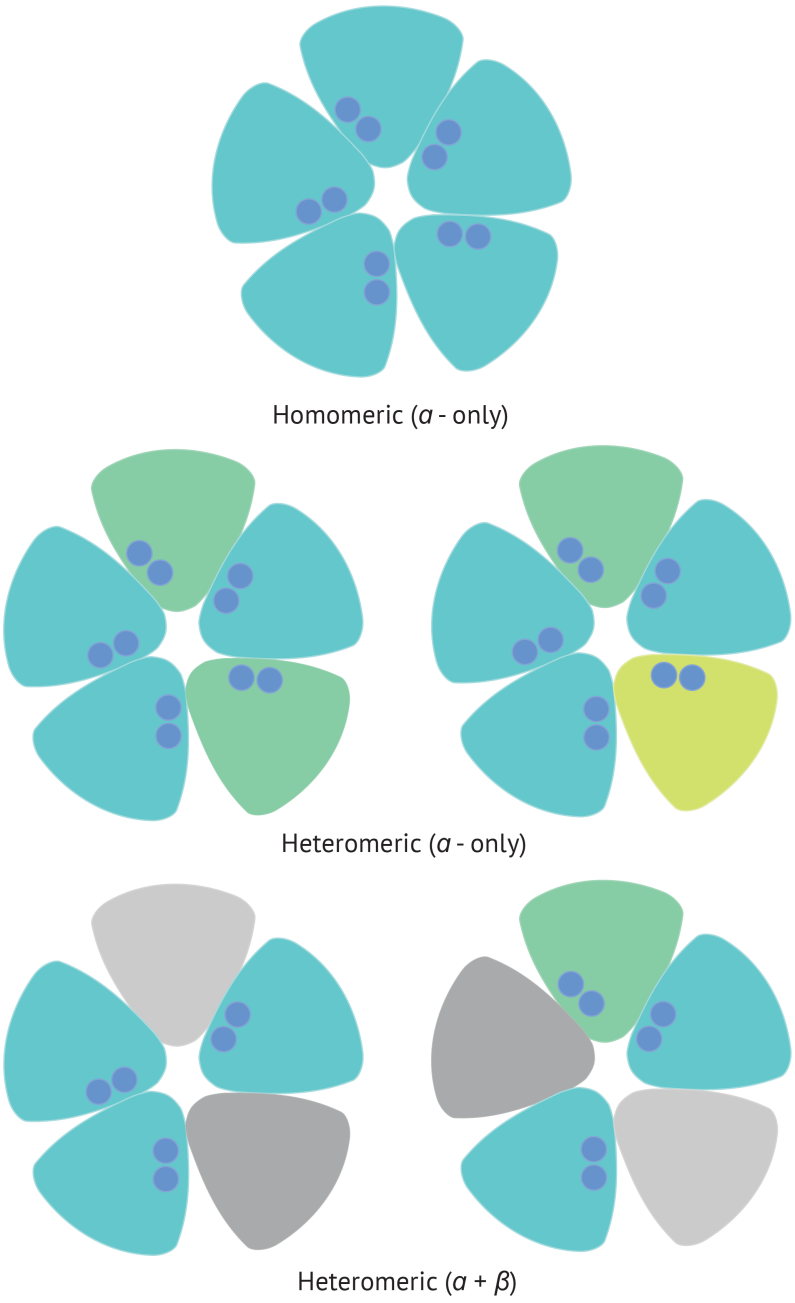


Figure 1.2 Homomeric and heteromeric nAChRs

nAChRs may be composed of the five identical subunits (homomeric) or five non-identical subunits (heteromeric). A di-cysteine motif (blue) required for ACh binding is present only in α subunits, making it unlikely that functional pentamers consisting only of non-α subunits would exist. The number of α subunits limits the number of ACh molecules that can be simultaneously bound to an individual pentamer.

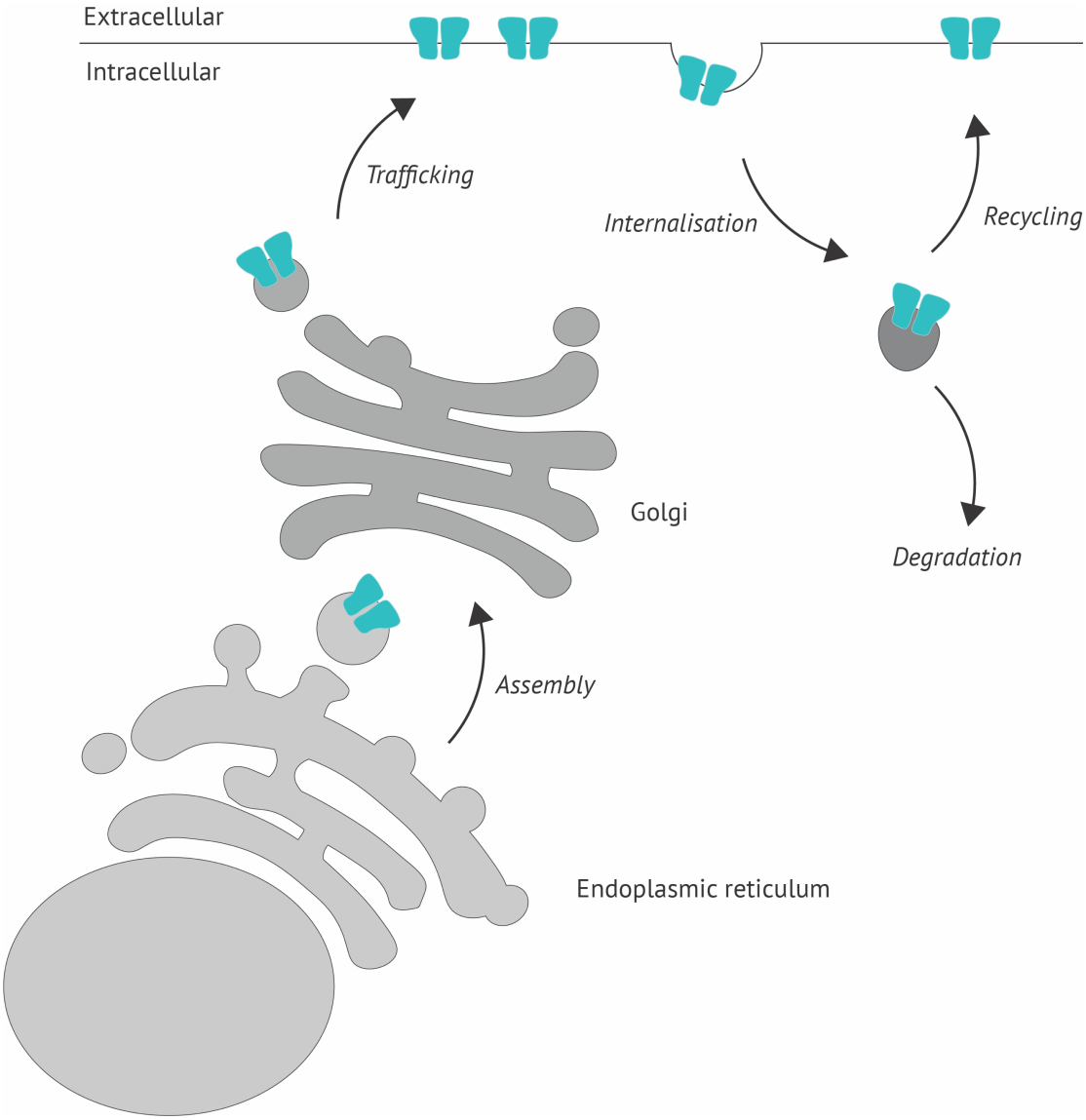


Figure 1.3 The position of nAChRs is dynamic

Once nAChRs have been synthesized and assembled in the endoplasmic reticulum, they are then trafficked, via secretory mechanisms in the Golgi, to their position in the cell membrane. It is here in the cell membrane that they function as ligand-gated cation channels. From the cell membrane, they can then be internalised via endocytosis, then recycled back to the membrane, or degraded by the ubiquitin-proteasome system.

1.2.3 nAChRs: cholinergic signalling

The mature nAChR, once assembled and positioned in the cell membrane, responds to ligand binding by undergoing conformational changes (Althoff *et al.* 2015, Nemecz *et al.* 2016). This channel gating involves three conformational states: closed, open, and desensitised (**Figure 1.4**). In the absence of ACh, the channel remains in a closed conformation, with hydrophobic residues blocking the passage of cations. Upon ACh binding there is hinging of the subunits, with the LBDs moving inwards and TM2s tilting outwards to open the central pore. This open state is unstable, leading to the final desensitised state where residues at the bottom of TM2 block the channel.

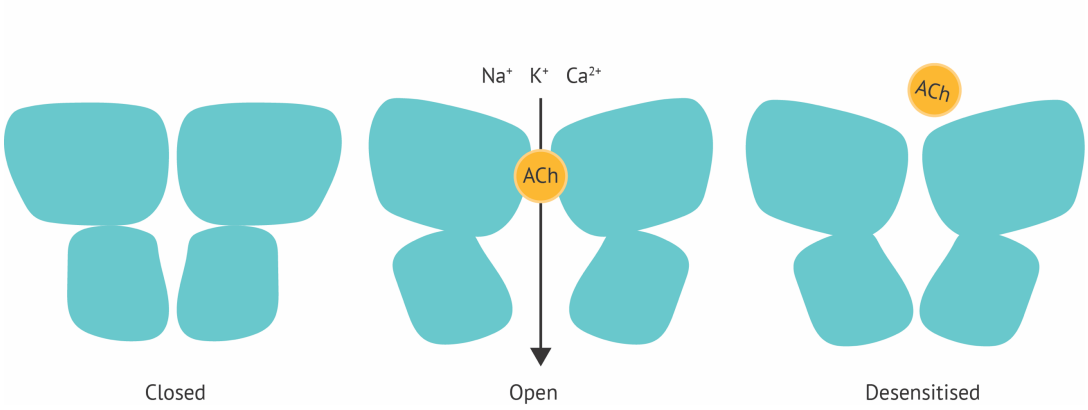


Figure 1.4 Channel gating

The nAChR ion channel can exist in one of three conformational states. When at rest, the channel is closed. Upon binding of ACh the subunits hinge between the LBD and TM domains to open the channel, allowing cations to flow into the cell. This open state is unstable. Immediately after the channel is opened, there is a brief period of desensitisation where residues in the TM domains block the passage of cations. (After Nemecz *et al.* 2016).

nAChRs often fulfil their role as ligand-gated cation channels in the post-synaptic membranes of neurons (English and Jones 2012) (**Figure 1.5**). At these cholinergic synapses, ACh is first packaged into vesicles in the pre-synaptic neuron by the vesicular ACh

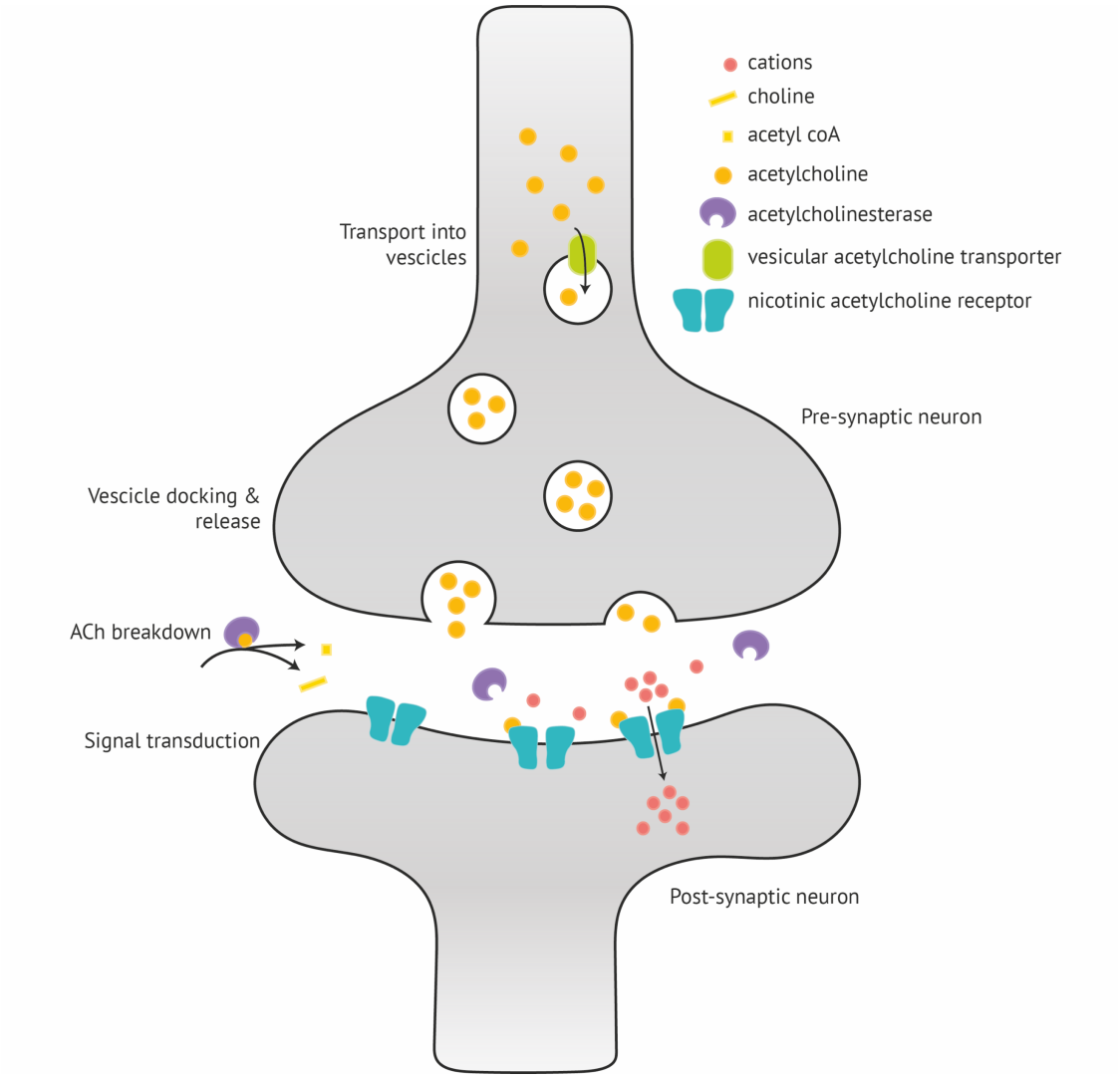


Figure 1.5 Cholinergic neurotransmission

In the pre-synaptic neuron, the vesicular acetylcholine transporter packs acetylcholine into vesicles. These vesicles dock at the pre-synaptic membrane to release acetylcholine into the synaptic cleft. Acetylcholine then binds to nAChRs in the post-synaptic membrane. This binding causes a conformational change to open the ion channel, allowing cations to rush into the post-synaptic neuron. Acetylcholine is then broken down in the synapse by acetylcholinesterase.

transporter. These vesicles then dock at the pre-synaptic membrane and release ACh across the synaptic cleft where it can briefly and reversibly bind to nAChRs in the post-synaptic membrane. This binding initiates the channel gating mechanism described above, resulting in the flow of cations into the post-synaptic neuron. The unbound ACh is then rapidly broken down by the enzyme acetylcholinesterase into inactive metabolites. The influx of cations into the post-synaptic cell can, if a threshold is passed, depolarise that cell and trigger an action potential, thus resulting in successful transduction of the neural signal.

Interestingly, the role of nAChRs in neurotransmission is not limited to the post-synaptic membrane - they can also be found in pre-synaptic axon terminals (Wonnacott 1997, Dani and Bertrand 2007, McKay *et al.* 2008) (**Figure 1.6**). As described above, neurotransmitters such as ACh must be packaged and released from vesicles in the pre-synaptic neuron. This release occurs in response to an influx of Ca^{2+} ions into the pre-synaptic neurons, and nAChRs often fulfil this role as pre-synaptic Ca^{2+} channels. A wide range of neurotransmitters, not just ACh, are known to be regulated in this way in vertebrates (McKay *et al.* 2008), however this pre-synaptic role is yet to be examined in insects.

The versatility of nAChRs extends even further to non-excitable cells outside the nervous system (Beckmann and Lips 2013) (**Figure 1.6**). In non-neuronal cells, nAChRs can function as Ca^{2+} channels, activating downstream Ca^{2+}-mediated intracellular pathways. In vertebrates, we know that some nAChR subtypes are more likely to form these non-neuronal receptors due to their expression pattern and high permeability to Ca^{2+}. For instance, the vertebrate $\alpha 7$ subunit is thought to function as a Ca^{2+} channel in a variety of non-neuronal cell types in vertebrates (Quik *et al.* 2015). Once again, this non-neuronal role of nAChRs is yet to be reported in insects.

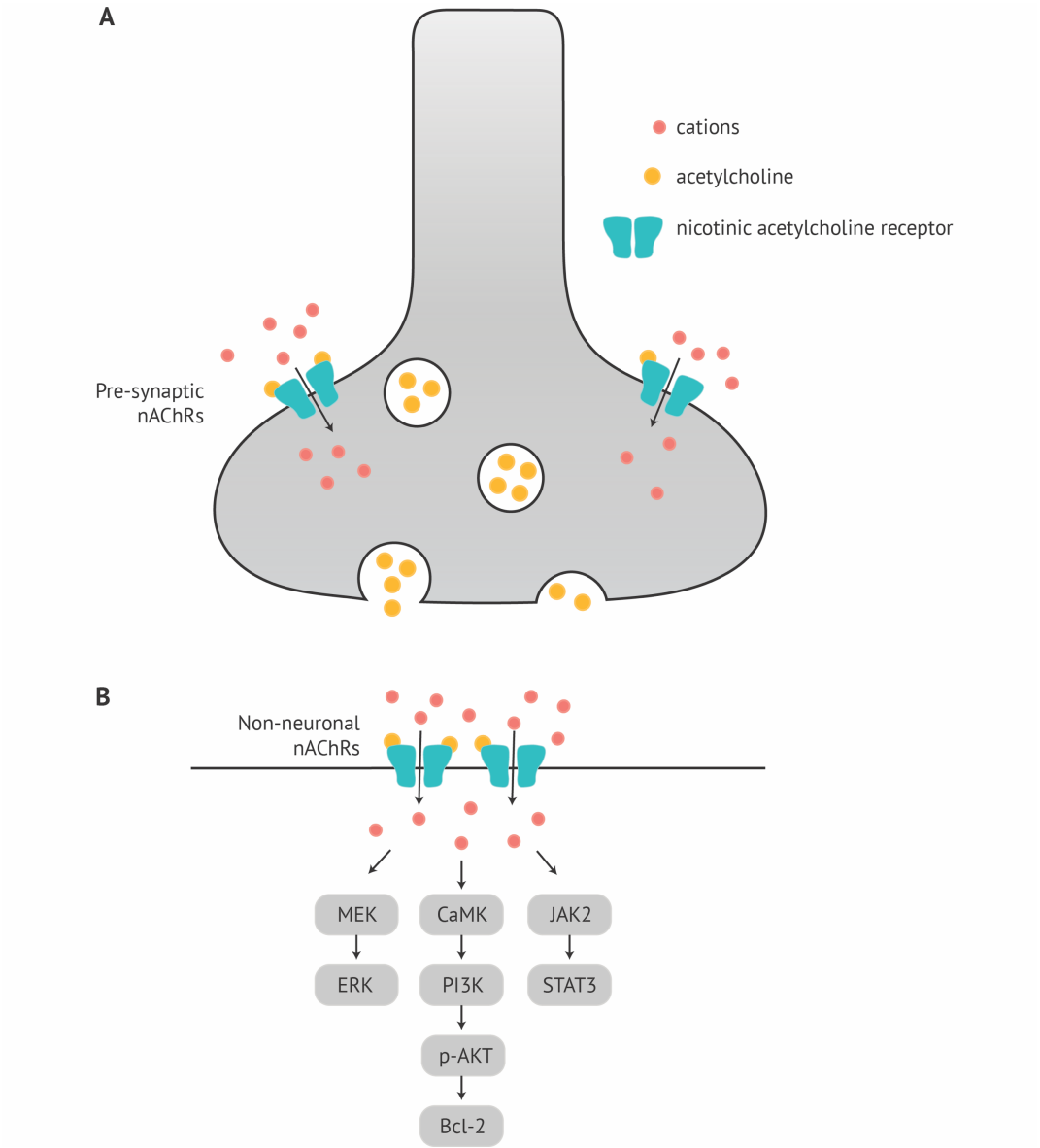


Figure 1.6 Pre-synaptic and non-neuronal nAChRs

(**A**) nAChRs can be found in pre-synaptic membranes where they act as Ca^{2+} channels to regulate neurotransmitter release. (**B**) Non-excitable cells outside the nervous system can also use nAChRs as Ca^{2+} channels. Here, nAChRs can activate a range of downstream Ca^{2+}-dependent signalling pathways. (After Quik *et al.* 2015).

1.2.4 Insect nAChR gene families

Compared to other members of the animal kingdom, insect nAChR gene families are quite compact (Jones and Sattelle 2010). In most insect genomes assembled to date, nAChR gene families are comprised of 10-12 subunits, far fewer than the 17 in vertebrates or 29 in worms (**Table 1.1**). Insects appear to possess a core set of nine conserved subunits (**Figure 1.7**). These include α subunits (α1-α8) and a β subunit (β1), although depending on the time of discovery, nomenclature can deviate, which can lead to confusion when comparing species. Among this core set, β1 is the most highly conserved subunit among insects. The α5/α6/α7 subunits are also a noteworthy group - these share the highest level of similarity with a vertebrate subunit (vertebrate α7), known for its ability to form functional homomeric pentamers and for its role in forming Ca^{2+} channels in pre-synaptic and non-neuronal membranes (Quik *et al.* 2015). Divergent subunits, those that do not belong in this core set, are also common amongst insect species. These subunits possess extremely low sequence similarity with other known subunits and their biological importance is unclear.

Despite the comparatively small size of insect nAChR gene families, there is still astounding capacity for diversity in the mature receptors. Aside from the multitude of possible pentameric combinations, and stoichiometric variations within that, there are other processes that can further expand the pharmacological repertoire. Alternative exons are a common feature of insect nAChR genes, allowing alternative splicing to occur under certain conditions (Sattelle *et al.* 2005). RNA A-I editing is another means of altering the final amino acid sequence of nAChR subunits. This form of nuclear RNA editing involves conversion of adenosine nucleosides to inosine, which is interpreted by the translation machinery as a guanosine, and this often occurs in key functional regions like the LBD and TM domains.

Table 1.1 Complete insect nAChR gene families

Species **Common name**	**Order**	**α Subunits**	**β Subunits**	**Total Subunits**	**Reference**
D. melanogaster Vinegar fly	Diptera	7	3	10	Sattelle *et al.* 2005
Anopheles gambiae African malaria mosquito	Diptera	9	1	10	Jones *et al.* 2005
Apis mellifera European honeybee	Hymenoptera	9	2	11	Jones *et al.* 2006
Tribolium castaneum Red flour beetle	Coleoptera	11	1	12	Jones and Sattelle 2007
Bombyx mori Silkworm	Lepidoptera	9	3	12	Shao *et al.* 2007
Acyrthosiphon pisum Pea aphid	Hemiptera	9	2	11	Dale *et al.* 2010
Nasonia vitripennis Parasitoid wasp	Hymenoptera	12	4	16	Jones *et al.* 2010
Helicoverpa armigera Cotton bollworm	Lepidoptera	9	3	12	Pearce *et al.* 2017
Locusta migratoria Migratory locust	Lepidoptera	9	2	11	Wang *et al.* 2015

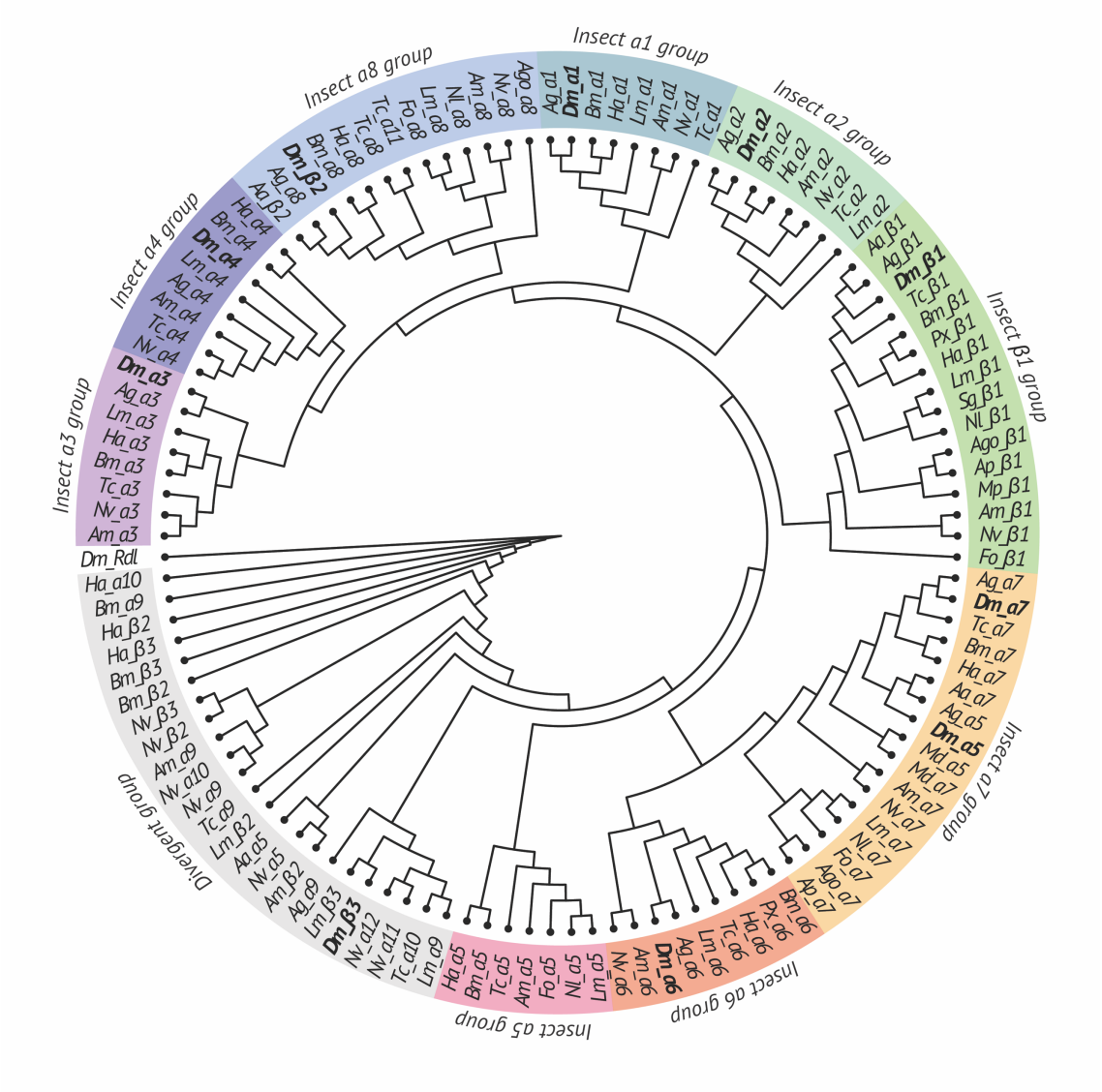


Figure 1.7 Tree of insect nAChR subunits

Phylogenetic tree of select insect nAChR subunits. Groups are named according to their insect nAChR classification. *D. melanogaster* subunits are featured in bold text. Amino acid sequences were aligned using Geneious Prime 2019.1.3 and the tree was generated in FigTree 1.4.4. Species: Aa, *Aedes aegypti*; Ag, *Anopheles gambiae;* Ago, *Aphis gossypii*; Am, *Apis mellifera*; Ap, *Acyrthosiphon pisum*; Bm, *Bombyx mori*; Dm, *D. melanogaster*; Fo, *Frankiniella occidentalis*; Ha, *Helicoverpa armigera*, Lm, *Locusta migratoria*; Md, *Musca domestica*; Nl, *Nilaparvata lugens*; Nv, *Nasonia vitripennis*; Px, *Plutella xylostella*; Sg, *Schistocerca gregaria*; Tc, *Tribolium castaneum*.

1.2.5 The *Drosophila* nAChR gene family

The discovery of the ten nAChR subunit genes in *D. melanogaster* spans 14 years and reflects the technology that was popular or available at the time (**Table 1.2**); from the pre-genome discovery of *Dβ1* via a hybridisation screen with *Torpedo* probes in 1986 (Hermans-Borgmeyer et al. 1986), to the post-genome discovery of *Dα5, Dα6* and *Dα7* via simple BLAST search in 2002 (Grauso *et al.* 2002). The 10 subunit genes are found on all major chromosomes, with one notable cluster on 3R containing *Dα1*, *Dα2* and *Dα2*. Direct linkage between these three is thought to facilitate coordinated expression and similar arrangements have been identified in vertebrates (Chamaon *et al.* 2002, Boulter *et al.* 1990). Structurally, there are a few unique subunits, but it is unknown whether these unusual features confer unique functional properties. The *Dα5* gene includes an abnormally large N-terminus upstream of the regular N-terminal SP and LBD (Grauso *et al.* 2002), and the *Dβ2* gene (a member of the insect *α8* group) has lost its α motif in *Drosophila* to become a β subunit (Jones and Sattelle 2010). Most unique of all is the *Dβ3* gene; formally classified as a divergent subunit, the Dβ3 subunit shares only up to 20% amino acid identity with other subunits (Lansdell and Millar 2002).

Until recently, there had been a technical roadblock in identifying combinations of *Drosophila* subunits that form functional subtypes. Heterologous expression studies had required coexpression of *Drosophila* subunits with vertebrate subunits to generate functional receptors (Lansdell and Millar 2000a, Schultz *et al.* 2000). Now, expression of *Drosophila*-only receptors has been achieved, thanks to the addition of the co-factors TMX3 and UNC-50 (Ihara *et al.* 2020), along with the previously identified co-factor RIC3 (Watson *et al.* 2010). Approximately 17 subtype combinations are now supported by empirical evidence (**Table 1.3**), and so far it appears the vertebrate α7-like subunits (Dα5, Dα6 and Dα7) may behave as an independent unit, only assembling into homomeric pentamers or heteromeric pentamers with each other (Lansdell *et al.* 2012). The work of Ihara *et al.* (2020) will accelerate the discovery and characterisation of more potential subtype combinations in the coming years, however determining the native subtypes that exist

Table 1.2 *Drosophila* nAChR subunit genes

Subunit	Alternative nomenclature	Insect nAChR group	Genomic location	Identification technique	Year published	Reference
Dα1	*ALS* (α-like subunit)	*Dα1*	3R	Hybridisation screen	1988	Bossy *et al.* 1988
Dα2	*SAD* (second α-like subunit *Drosophila*)	*Dα2*	3R	Hybridisation screen	1990	Jonas *et al*. 1990, Sawruk *et al.* 1990a
Dα3		*Dα3*	X	Hybridisation screen	1998	Schultz *et al.* 1998
Dα4	*redeye*	*Dα4*	3L	PCR	2000	Lansdell and Millar 2000a
Dα5		*Dα7*	2L	BLAST analysis	2002	Grauso *et al.* 2002
Dα6	*rsn* (resistance to spinosyns)	*Dα6*	2L	BLAST analysis	2002	Grauso *et al.* 2002
Dα7	*gfA* (giant fibre)	*Da7*	X	BLAST analysis	2002	Grauso *et al.* 2002
Dβ1	*ARD* (acetylcholine receptor *Drosophila*)	*Dβ1*	3L	Hybridisation screen	1986	Hermans-Borgmeyer *et al*. 1986
Dβ2	SBD (second β-like subunit *Drosophila*)	*α8*	3R	Hybridisation screen	1990	Sawruk *et al.* 1990b
Dβ3		Divergent	2L	EST clone sequencing	2002	Lansdell and Millar 2002

and working out the exact stoichiometries of different subunits in those subtypes remains another challenge. The existence of any of these subtype combinations will depend upon the co-expression of their subunits *in vivo*.

The expression patterns of *Drosophila* subunits have been examined over the years using a range of resources; from early *in situ* work (Ali 2012) and microarrays (Robinson *et al.* 2013), to RNA-seq (Contrino *et al.* 2012, Perry *et al.* 2021) and protein tagging (Nagarkar-Jaiswal *et al.* 2016), and more recently single-cell sequencing (Croset *et al.* 2018, Allen *et al.* 2020,

Table 1.3 *Drosophila* nAChR subtypes

Subtype	Technique used	Reference
Dα1 + Dβ1	Toxin binding assays Functional expression in *Xenopus* oocytes	Schloss *et al.* 1991 Ihara *et al.* 2020
Dα1 + Dα2	Co-IP and functional expression in *Xenopus* oocytes (with vertebrate β2)	Schulz *et al.* 2000
Dα3 + Dβ1	Co-IP and affinity chromatography	Chamaon *et al.* 2000
Dα1 + Dα2 + Dβ2	Co-IP and affinity chromatography	Chamaon *et al.* 2002
Dβ1 + Dβ2	Co-IP	Chamaon *et al.* 2002
Dβ3 + Dα2/Dα3/Dα4/Dβ2	Co-IP	Lansdell *et al.* 2002
Dα5 homomeric	Functional expression in *Xenopus* oocytes	Lansdell *et al.* 2012
Dα7 homomeric	Functional expression in *Xenopus* oocytes	Lansdell *et al*. 2012
Dα5 + Dα6	Functional expression in *Xenopus* oocytes Radioligand binding	Watson *et al.* 2010, Lansdell *et al.* 2012
Dα5 + Dα7	Functional expression in *Xenopus* oocytes	Lansdell *et al.* 2012
Dα5 + Dα6 + Dα7	Functional expression in *Xenopus* oocytes	Lansdell *et al.* 2012
Dα1 + Dα2 + Dβ1	Functional expression in *Xenopus* oocytes	Ihara *et al.* 2020
Dα1 + Dβ1 + Dβ2	Functional expression in *Xenopus* oocytes	Ihara *et al.* 2020
Dα1 + Dα2 + Dβ1 + Dβ2	Functional expression in *Xenopus* oocytes	Ihara *et al.* 2020

Ravenscroft *et al.* 2020) and T2A-GAL4 technologies (Diao *et al.* 2015, Chen 2021). Overall, most expression datasets are in agreement that the subunits are predominantly expressed in the CNS. Only the divergent subunit *Dβ3* is known to have an unusual expression pattern, with enriched expression in the heart and no expression in the CNS (Contrino *et al.* 2012, Croset *et al.* 2018, Allen *et al.* 2020). Temporal expression data indicates the subunits are most highly transcribed in the embryo and pupa: stages when the CNS is being built or remodelled and therefore undergoing the most significant changes (Contrino *et al.* 2012). Of the nine CNS subunits, single-cell RNA-seq reveals that *Dβ1* is the most highly and broadly expressed in various regions of the adult brain, followed by *Dα5* and *Dα6* (Croset *et al.* 2018, Allen *et al.* 2020) (**Figure 1.8**). Meanwhile, *Dα6, Dα1* and *Dα5* are the most broadly expressed in the larval brain (Ravenscroft *et al.* 2020). An exciting aspect of this new wave of single-cell data is that it tells us which subunits are co-expressed in any given neuron, giving insight into which subunits may be able to form functional subtypes, and in which endogenous signalling pathways they may function.

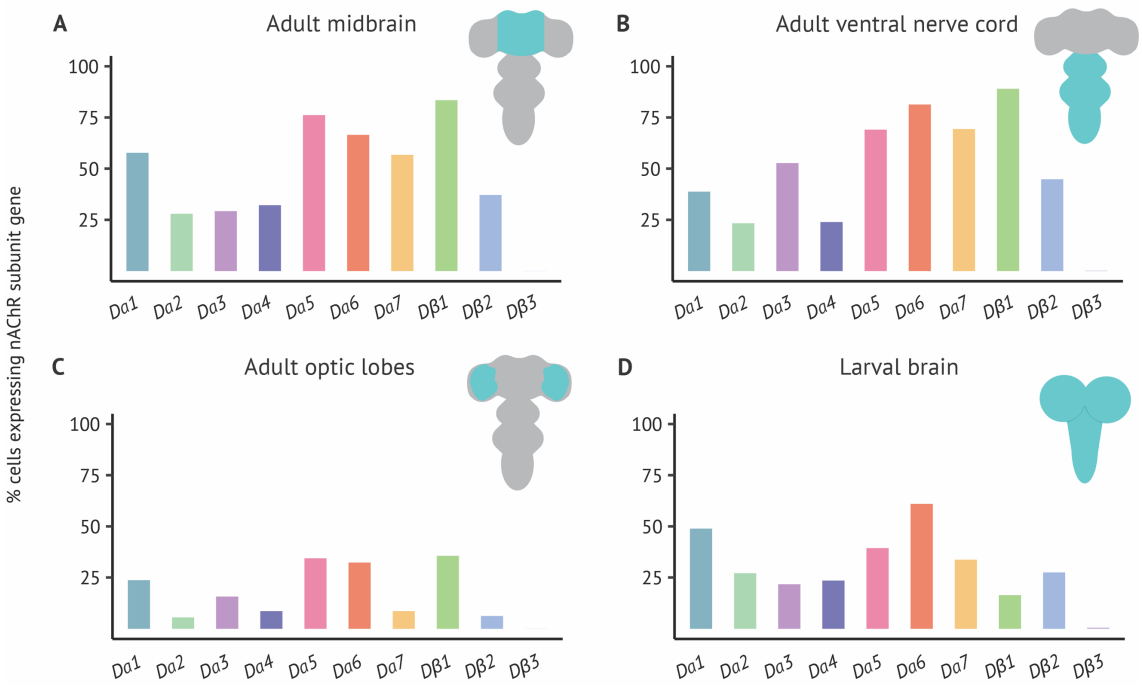


Figure 1.8 Expression of nAChR subunit genes in single-cell RNA-seq datasets

Percentage of cells expressing each of the *Drosophila* nAChR genes in (**A**) the adult midbrain, (**B**) the adult ventral nerve cord, (**C**) the adult optic lobes, and (**D**) the larval brain. Data were obtained from available single-cell RNA-seq datasets via Scope (https://scope.aertslab.org/) (Croset *et al.* 2018, Davie *et al.* 2018, Allen *et al.* 2020, Ravenscroft *et al.* 2020).

1.2.6 nAChRs as targets of insecticides

Herbivorous insects are estimated to be responsible for the destruction of up to 20% of crop production annually, making use of insecticides vital for food security (Sharma *et al.* 2017). In recent years, nAChRs have been the most popular molecular target for agricultural insecticides, with 28% of chemicals in use targeting this gene family (Sparks *et al.* 2019). An ongoing issue that threatens this practice is resistance, which can involve insects evolving mutations in targeted nAChR subunits (Baxter *et al.* 2010, Bao and Xu 2011, Bass *et al.* 2011, Perry *et al.* 2012, Puinean *et al.* 2013, Koo *et al.* 2014, Silva *et al.* 2016). Therefore, nAChRs have been the focus of work that aims to characterise insecticide modes of action and mechanisms of resistance in order to maximise the efficacy of modern agricultural pest control programs.

The most common nAChR-targeting insecticide classes are the neonicotinoids and spinosyns. Each of these classes has a unique mode of action and each target nAChR subtypes differently (**Table 1.4**) (Perry *et al.* 2021). The neonicotinoids are competitive modulators (Sparks *et al.* 2020). They share structural similarity with one of nature's original insecticides (nicotine) but, unlike nicotine, have higher binding affinity to insect nAChRs than to vertebrate nAChRs (Shimomura *et al.* 2006). They are thought to bind at a similar site to the natural ligand ACh; at the interface between two adjacent subunits (Ihara and Matsuda 2018, Matsuda *et al.* 2005, Shimomura *et al.* 2002). Unlike ACh, however, they are not degraded by acetylcholinesterase, and can keep the nAChR ion channel in an open conformation for longer than would normally occur during neurotransmission. If the concentration of neonicotinoid is high enough, this involuntary neuronal activation quickly leads to paralysis and death of the insect. Meanwhile, at sub-lethal doses (including concentrations that are likely to be widely present in the environment), chronic low levels of over-firing can instead lead to oxidative stress and a range of downstream consequences including mitochondrial dysfunction and glial cell damage (Martelli *et al.* 2020). Multiple lines of evidence indicate that *Dα1, Dα2, Dβ1*, and *Dβ2* are the major targets of neonicotinoids (Perry *et al.* 2008, Ihara *et al.* 2020, Perry *et al.* 2021). Mutations in any of these four subunits confer substantial (up to ~60-fold) levels of resistance.

Table 1.4 nAChR subunits involved in insecticide response

Subunit	Insecticide Class	Evidence	References
Dα1	Neonicotinoids	Radioligand binding	Lansdell and Millar 2000b
		Resistant allele	Perry *et al.* 2008
		RNAi knockdown	Mitchell 2012
		Genomic deletion	Somers *et al.* 2017
		Genomic deletion	Perry *et al* 2021
Dα2	Neonicotinoids	Radioligand binding	Lansdell and Millar 2000b
		Genomic deletion	Perry *et al.* 2021
	Sulfoximines	Electrophysiology	Watson *et al.* 2011
Dα3	Neonicotinoids	Radioligand binding	Lansdell and Millar 2000b
		RNAi knockdown	Mitchell 2012
Dα4			
Dα5			
Dα6	Spinosyns	Genomic deletion	Perry *et al.* 2007
		Resistant alleles, electrophysiology	Watson *et al.* 2010
Dα7			
Dβ1	Neonicotinoids	Electrophysiology	Yao *et al.* 2008
		RNAi knockdown	Mitchell 2012
		Genomic deletion	Perry *et al*. 2021
	Sulfoximines	Genomic deletion	Perry *et al*. 2021
Dβ2	Neonicotinoids	Resistant allele	Perry *et al.* 2008
		RNAi knockdown	Mitchell 2012
		Genomic deletion	Perry *et al.* 2021
Dβ3			

The spinosyns are marketed as an organic class, made during aerobic fermentation in the bacteria *Saccharopolyspora spinosa* (Sparks *et al.* 1998). These insecticides are allosteric modulators thought to bind near the C-terminal, specifically to Dα6 subunits (Perry *et al.* 2007, Watson *et al.* 2010, Somers *et al.* 2015). Initial evidence indicated that a conformational change opened the channel, causing death of the insect in a similar way to neonicotinoids (Salgado and Sparks 2005). However, more recently, electrophysiology experiments indicate that spinosyns binding to nAChRs may not increase the flow of Ca^{2+} (Martelli 2020). *Dα6* mutants are highly (>2000-fold) resistant to spinosyns and multiple insect species have evolved resistance to spinosyns in the field via mutation of *α6* subunits

(Baxter *et al.* 2010, Bao and Xu 2011, Puinean *et al.* 2013, Silva *et al.* 2016). Like many insecticides, chronic exposure to low doses of spinosyns also causes oxidative stress (Martelli 2020).

1.2.7 Endogenous roles of *Drosophila* nAChRs

Since early experiments that involved rearing flies on a choline-deprived diet, it has been known that cholinergic signalling is essential for development and viability in *Drosophila* (Geer 1967, Geer *et al.* 1968). But considering how many neurons have been described as cholinergic, relatively little is known about the roles the different nAChR subunits may play in different developmental and behavioural pathways. A range of techniques have been used over the years to knockdown or knockout each individual nAChR subunit, including EMS mutagenesis (Perry *et al.* 2008), ends-out gene targeting (Somers *et al.* 2017), p-element excision (Fayyazuddin *et al.* 2006, Mitchell 2012), RNAi (Mitchell 2012, Barnstedt *et al.* 2016), and most recently, CRISPR (Perry *et al.* 2021). Based on this work, we now know that only two subunits have severe loss of function phenotypes - Dα5 and Dβ1. Preliminary work on Dα5, using RNAi and deficiency strains, indicate Dα5 may be required during larval development (**Table 1.5**) (Mitchell 2012). Determining how loss of Dα5 might lead to death during larval development, and what neurons may require Dα5, will be the topic of investigation in *Chapter Two* of this thesis. The endogenous role of the Dβ1 subunit, which had not previously been associated with serious fitness effects, will then be the focus of *Chapter Three*.

The remaining eight subunits do not have severe loss of function phenotypes (Perry *et al.* 2021), revealing a level of functional redundancy in terms of viability. This redundancy makes evolutionary sense, considering how many neurons must rely on each individual subunit to fulfil all the various signalling roles required in a developing fly. However, for some of these subunits, dedicated behavioural assays have revealed more nuanced behavioural phenotypes that do not impact viability in an obvious way under laboratory conditions (**Table 1.5**). Multiple subunits have been shown to play a role in regulating sleep, with some promoting sleep (Dα1, Dα2, Dα*4*), and others promoting wakefulness (Dα3, Dα6,

Table 1.5 Endogenous roles of nAChR subunits

Subunit	Roles described in literature	References	Roles described in theses	References
Dα1	Sleep, mating, longevity Memory	Somers *et al.* 2017 Barnstedt *et al.* 2016		
Dα2			Sleep	Luong 2018
Dα3	Sleep	Wu *et al.* 2014	Sleep	Luong 2018
Dα4	Sleep Memory	Shi *et al.* 2014 Barnstedt *et al.* 2016	Sleep	Luong 2018
Dα5	Memory	Barnstedt *et al.* 2016	Larval development	Mitchell 2012
Dα6	Memory	Barnstedt *et al.* 2016	Sleep	Luong 2018
Dα7	Escape response	Fayyazuddin *et al.* 2006	Sleep	Luong 2018
Dβ1				
Dβ2				
Dβ3			Sleep	Luong 2018

Dα7, Dβ3) (Shi *et al.* 2014, Wu *et al.* 2014, Somers *et al.* 2017, Luong 2018). A consequence in some of these short-sleep mutants is slightly reduced longevity (Dα1, Dα2) (Somers *et al.* 2017, Luong 2018). Dα1 mutants have reduced mating success, with males taking up to 10 minutes longer to initiate courtship and copulation with females (Somers *et al.* 2017). Dα7 is required in the Giant Fibre, a neuron in the escape jump pathway, with mutants failing to show the normal jump response to sudden darkness (Fayyazuddin *et al*. 2006). Many subunits may also be required for memory formation (Dα1, Dα4, Dα5, Dα6), with RNAi knockdown specifically in the brain's memory centre (the mushroom body) causing flies to lose their negative response to aversive odours (Barnstedt *et al.* 2016).

1.3 Insect development

While investigating the endogenous roles of the Dα5 and Dβ1 subunits, several developmental processes were disrupted, and it is therefore important to introduce some fundamental aspects of insect development. All insects are encased in a rigid exoskeleton, or cuticle, and they need to periodically moult this cuticle in order to grow (Gilbert 2009). This moulting cycle, also known as ecdysis, is under complex hormonal control, and it occurs in the two major classes of insects: the holometabolous and the hemimetabolous insects.

1.3.1 The *Drosophila* life cycle

As holometabolous insects, *Drosophila* progress through multiple distinct developmental stages throughout their life cycle: embryo, first instar larva (L1), second instar larva (L2), third instar larva (L3), pupa, and adult (**Figure 1.9**) (Hartenstein 1993). Each of these stages is separated by a moult, and the duration of each stage is temperature and nutrient dependent, with development accelerated at higher temperatures.

Once a female has laid an egg, the embryo inside progresses through 17 sub-stages, lasting a total of approximately 24 hours (at 25°C) (Campos-Ortega and Hartenstein 1985). The larva that then emerges from the egg is specialised for feeding and growth. The L1 larva will spend one day feeding before moulting to become an L2 larva. The L2 larva then repeats this, feeding for one day before moulting to become an L3 larva. Throughout this thesis, the moults that occur at the L1-L2 and L2-L3 transitions will be referred to as M1 and M2, respectively.

It is during the L3 stage, which lasts three-four days, that the most feeding and growth occurs, with larval body weight increasing exponentially during this time (Edgar 2006). Once the L3 larva has reached a body weight threshold, the critical weight, it will soon wander away from its food source to find an appropriate site to initiate the next stage, pupation. The very start of this pupal stage is called pupariation, and is marked by eversion of the larval head. The larval cuticle then hardens to form the pupal case, and it is here in this

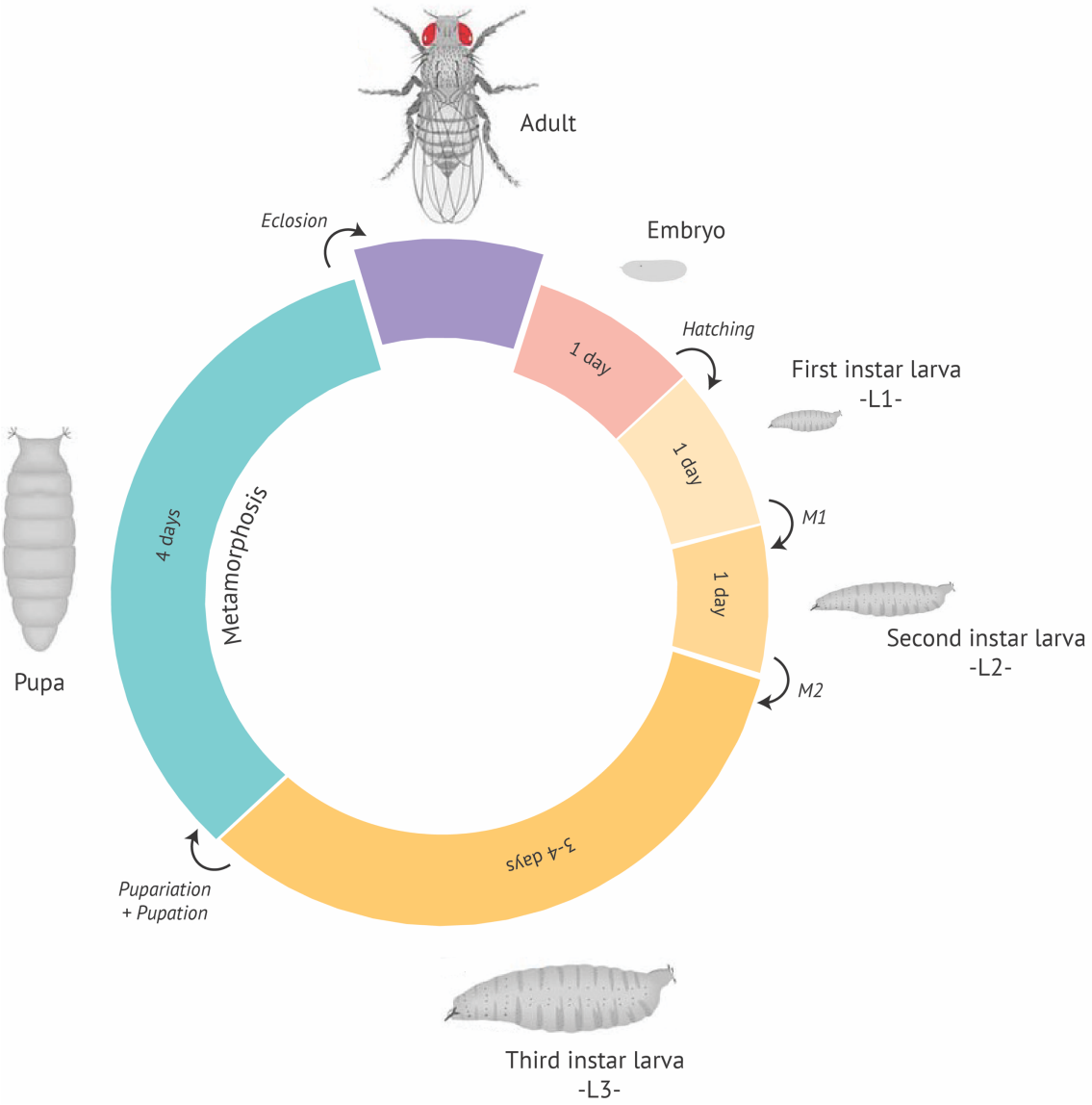


Figure 1.9 The *Drosophila* life cycle

Drosophila development involves multiple distinct stages, each of which is separated by a moulting event. Following the embryonic stage, larvae progress through three larval instar stages, then a pupal stage during which metamorphosis takes place. The fully formed adult then emerges from its pupal case via eclosion. The duration of each stage shown here is based on an ambient temperature of 25°C. Abbreviations: L1, first instar larva; L2, second instar larva; L3, third instar larva; M1, L1-L2 moult; M2, L2-L3 moult.

protective case that the pupa undergoes a four-day metamorphosis consisting of 24 defined sub-stages (Bainbridge and Bownes 1981). The transformed animal that exists within the pupal case at the end of metamorphosis is known as the pharate adult.

The final moult, in which the pharate adult emerges from the pupal case is known as eclosion (Hartenstein 1993). Following eclosion, during the early hours of adulthood, there are several more developmental processes that take place, including expansion of the wings and tanning of the cuticle. The fully formed adult reaches sexual maturity approximately 16 hours post-eclosion. From this time, adult males engage in an elaborate courtship ritual to make females more receptive to copulation (Greenspan 2000). Once mated, females can lay over 100 eggs per day (Shapiro 1932). Depending on the ambient temperature, both males and females can go on to live for up to several months.

1.3.2 Endocrine control of developmental transitions

The transitions between each of *Drosophila*'s developmental stages are subject to complex hormonal regulation (Di Cara and King-Jones 2013). Much of what we know about these hormones comes from earlier work on larger lepidopteran insects, such as the silkworm *Bombyx mori* and the tobacco hornworm *Manduca sexta* (Hanaoka and Ohnishi 1974, Nijhout 1975), but we now know these hormones and their respective roles are well conserved among holometabolous insects. Traditionally, the steroid ecdysone is known as *the* moulting hormone, but there are actually multiple hormones, produced in multiple different tissues, that are required before, during, and after each moult to ensure correct developmental progression.

The first of these is prothoracicotropic hormone (PTTH), a neuropeptide that is largely responsible for initiating the beginning of each moult (**Figure 1.10**) (McBrayer *et al.* 2007). PTTH is produced in the PTTH neurons, which integrate signals from circadian clock neurons and light. Prior to a moult, these neurons release a pulse of PTTH directly onto the prothoracic gland (PG), a small gland that is part of the ring gland complex adjacent to the

brain (Siegmund and Korge 2001). Here, PTTH triggers a pulse of production of the next hormone, ecdysone.

In the PG cells, Halloween enzymes convert dietary cholesterol into an inactive form of ecdysone that is secreted into the circulating haemolymph (Rewitz *et al.* 2006). Then, once ecdysone reaches peripheral tissues, it is converted into its active form, 20-hydroxyecdysone (20E) (Petryk *et al*. 2003). 20E is the hormone that causes many of the gene expression changes that are prerequisite to moulting (Ashburner 1990). Relatively small sized pulses of 20E are needed to stimulate the M1 and M2 moults, while much larger pulses of 20E precede hatching of the L1 larva, pupariation and metamorphosis (Riddiford 1993) (**Figure 1.11**). However, the nature of the moult is not entirely dependent on the size of the 20E pulse. Another hormone, juvenile hormone (JH), is present only until early in the L3 stage (Berger and Dubrovsky 2005). JH is synthesised in the corpus allatum, another gland in the ring gland complex. In the presence of JH, 20E only triggers hatching and larva-larva moults, while in its absence 20E can trigger the larva-pupa and pupa-adult transitions.

Just as the rise of 20E levels is vital for stimulating the moulting process, the fall of 20E is equally important for development to proceed. Once enzymes deactivate 20E, synthesis of two more hormones, ecdysis triggering hormone (ETH) and eclosion hormone (EH), can commence (Kingan and Adams 2000, Di Cara and King-Jones 2013). ETH is a peptide hormone produced in the Inka cells: seven pairs of cells located along the length of the larval body adjacent to the trachea. This hormone stimulates the pre-ecdysis program, a series of anterior-posterior contractions and waves of muscular squeezing that aid in preparing the old cuticle for detachment (Park *et al*. 2002). Unlike ETH, the physiological role of EH is not as well understood, but this neuropeptide is known to participate in a positive feedback loop with ETH to amplify production of both hormones and stimulate production of the next hormone, crustacean cardioactive peptide (CCAP) (Mesce and Fahrbach 2002).

CCAP, a neuropeptide produced in the 27 pairs of CCAP neurons, is responsible for the completion of ecdysis (Park *et al.* 2003). In larva-larva moults, CCAP stimulates the larva to plant its old mouthhooks (part of the old cuticle) into the substrate, and break forward through a gap in the old cuticle until that cuticle is fully shed. CCAP is equally important during eclosion, where it stimulates the pharate adult to break through the opening in the anterior end of the pupal case. One final hormone that is primarily required in the hours following eclosion is bursicon. Produced in a subset of the CCAP neurons, bursicon triggers tanning of the cuticle and expansion of the wings in the newly eclosed adult (Luan *et al.* 2006).

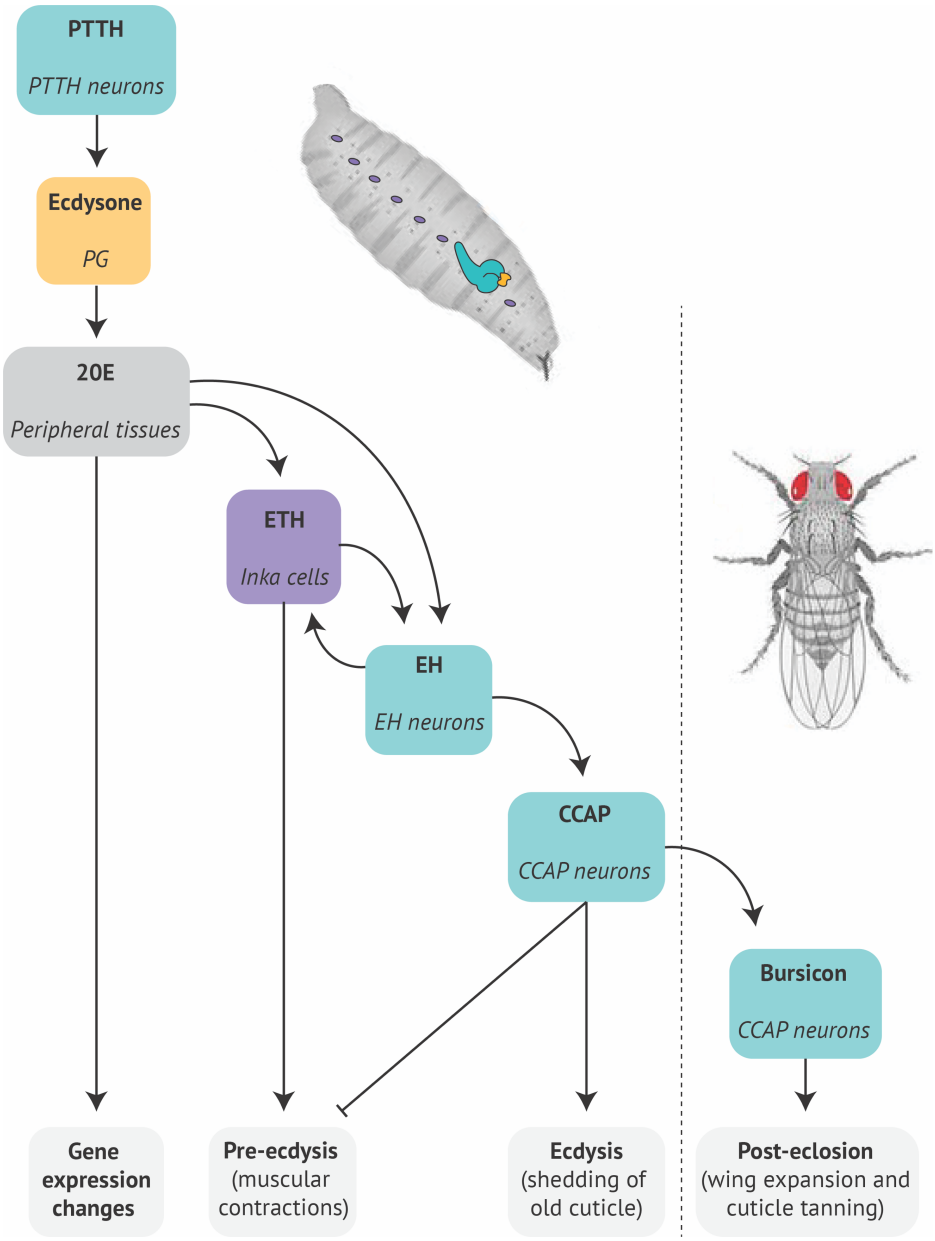


Figure 1.10 Endocrine control of moulting

A cascade of different hormones regulates the progression through each moult. Production of one hormone typically leads to production of the next hormone in the sequence. Tissues where these hormones are synthesized, which include the brain (green), the PG (orange), and the Inka cells (purple), are also shown. Abbreviations: PTTH, prothoracicotropic hormone; PG, prothoracic gland; 20E, 20-hydroxyecdysone; ETH, ecdysis triggering hormone; EH, eclosion hormone; CCAP, crustacean cardioactive peptide. (After Di Cara and King-Jones 2006).

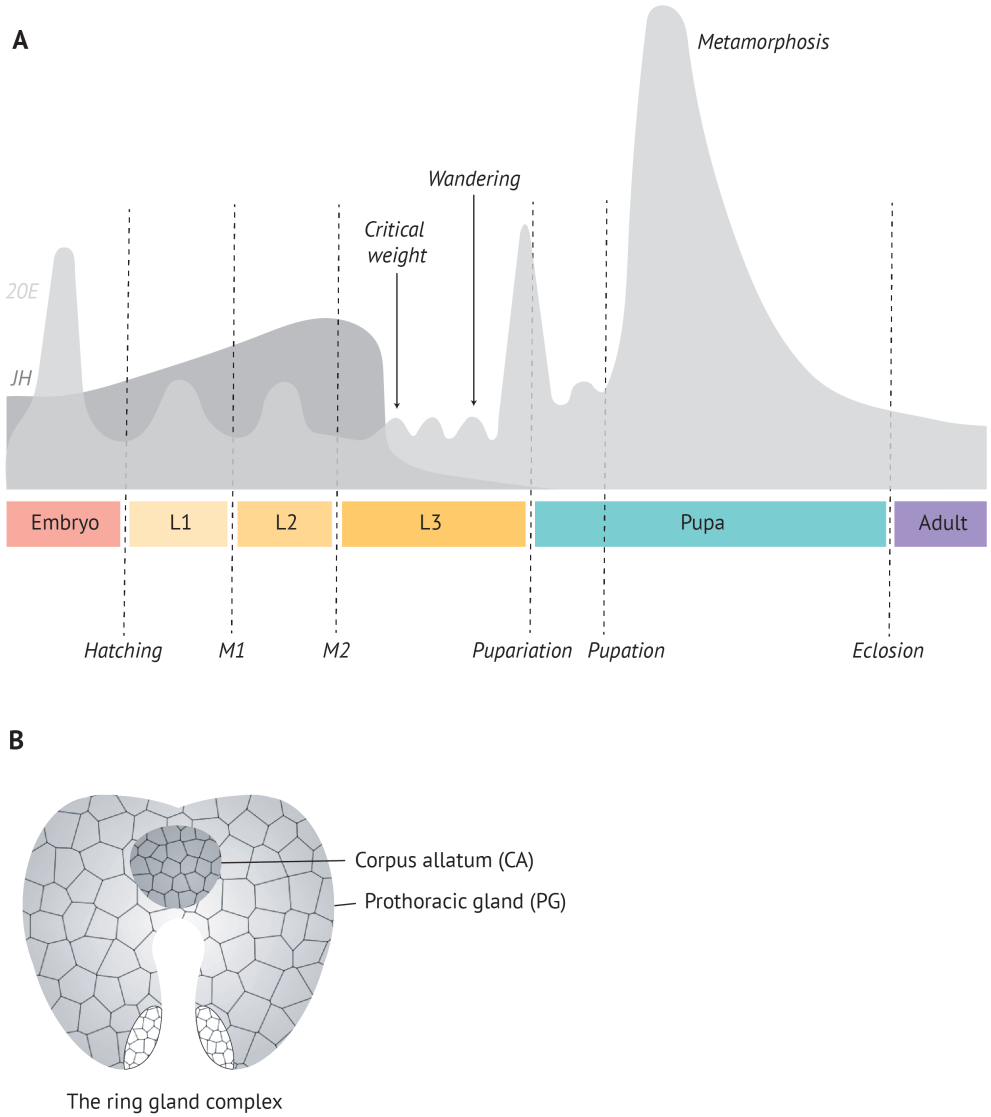


Figure 1.11 Pulses of 20E drive developmental transitions

(**A**) 20E titres reach a peak prior to each developmental transition, with the largest peak triggering metamorphosis. In the presence of JH, 20E can only trigger hatching and larva-larva moults. Once JH titres decline, 20E pulses can trigger the larva-pupa and pupa-adult transitions. (**B**) Both of these hormones are produced in the ring gland complex. The 20E precursor, ecdysone, is produced in the prothoracic gland. JH is produced in the corpus allatum. Abbreviations: 20E, 20-hydroxyecdysone; JH, juvenile hormone; L1, first instar larva; L2, second instar larva; L3, third instar larva; M1, L1-L2 moult; M2, L2-L3 moult. (After Edgar 2006 and Thummel 2001).

1.4 Aims of this thesis

This thesis aims to characterise developmental and behavioural phenotypes for flies carrying mutations in the two nAChR subunits reported to have the most severely reduced viability: Dα5 and Dβ1. The Dα5 subunit will be the focus of *Chapter Two*. With Dα5 as the only remaining *Drosophila* subunit to not have a CRISPR-generated genomic deletion (Perry *et al.* 2021), a priority will be to identify or generate mutant alleles of *Dα5*. These mutant strains will then be used to examine the role of Dα5 in larval development, including identification of any hormonal disruptions that may be causing larval death, and identification of cell types where *Dα5* expression may be required. The importance of Dα5's abnormally long N-terminal will also be investigated, as will the possibility for Dα5's role in insecticide response.

The focus of *Chapters Three* and *Four* will be Dβ1. *Chapter Three* will examine the role of Dβ1 in early adult development and adult viability. Preliminary observations indicate CRISPR-generated *Dβ1* deletion mutants can develop to adulthood but are plagued with pleiotropic consequences and limited lifespan. This chapter therefore aims to characterise the developmental and behavioural traits that are affected, identify any hormonal disruptions, and pinpoint specific neurons that may require Dβ1 for normal function. This chapter is presented as a manuscript, which was accepted for publication just prior to the completion of this thesis (Christesen *et al.* 2021).

Chapter Four will then extend the work performed in *Chapter Three* to examine β1 subunits in other insect species, by testing whether alternative *Dβ1* alleles, and a non-*Drosophila β1* subunit, can rescue the Dβ1 loss of function phenotypes. This will be done using a cDNA rescue system and will reveal whether specific amino acid replacements carry the same fitness costs as the deletion mutant, and whether there is functional conservation between β1 subunits from different species. Since Dβ1 is a known insecticide target, and Dβ1 mutants are known to confer resistance (Perry *et al.* 2021), the response of each of the β1 alleles to insecticide exposure will also be tested.

With Dβ1 and Dα5 as two of the most widely-expressed nAChR subunits (Croset *et al.* 2018, Allen *et al.* 2020), understanding their roles in development and viability will be essential information for completing the first functional wiring diagram of the *Drosophila* brain. This knowledge will also provide vital insight into the roles of similar nAChR subunits in pest and non-pest insect species. For any insect subunits that are the molecular targets of insecticides, knowing the phenotypes associated with loss of function may expose the fitness costs species might endure if they evolve resistance. It may also help us to predict which neuronal pathways might have the most potential to be impacted in insects exposed to the sub-lethal doses of insecticides that are often present in the environment.

Chapter Two

Investigating the role of the Dα5 subunit in larval development

2.1 Introduction

Dα5 was one of the last *Drosophila* nAChR subunits to be identified, being uncovered in a BLAST search on the then recently assembled *Drosophila* genome in 2002 (Grauso *et al.* 2002). This subunit is unusual in a number of ways. It has an abnormally large N-terminus of unknown function preceding the SP and LBD (Grauso *et al.* 2002) (**Figure 2.1**). This region spans 312 amino acids and it remains unclear whether it might be cleaved from the mature Dα5 subunit.

Dα5 also has an atypical phylogeny compared to other core nAChR subunits which, in turn, has resulted in confusing nomenclature. While most nAChR families contain a subunit in the insect α5 group, *Drosophila* does not (**Figure 1.7**). Instead, Dα5 appears to have arisen from an earlier duplication of a Dα5/Dα7 ancestor, and thus belongs in the insect α7 group (Jones and Sattelle 2010). This insect α7 group, together with the α6 and α5 groups, represent a superclade with relatively high similarly to the vertebrate α7 subunit (Grauso *et al.* 2002) (**Figure 2.2**), and subunits within this superclade (including Dα5) may share some unusual characteristics. Like vertebrate α7, which largely forms homomeric pentamers, Dα5 has only been reported to form homomeric pentamers or heteromeric pentamers with other α7-like subunits (Lansdell *et al.* 2012) (**Figure 2.3**). Vertebrate α7 also has high permeability to Ca^{2+}, priming it for roles in Ca^{2+}-dependent signalling cascades in non-neuronal and pre-synaptic membranes (Seguela *et al.* 1993, Wonnacott 1997, Lendvai and Vizi 2008). It is possible that Dα5 shares this capacity for non-post-synaptic signalling roles.

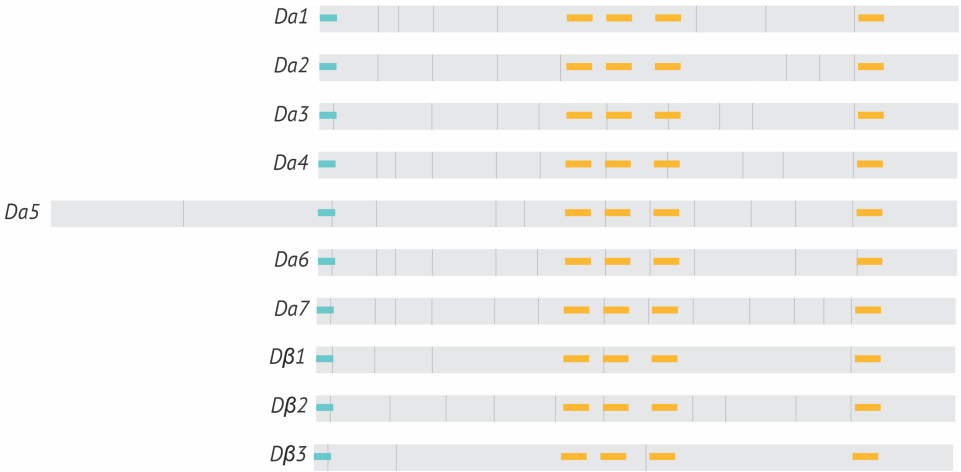


Figure 2.1 *Drosophila* nAChR subunit gene structure

Exon-intron structure of the *Drosophila* nAChR subunit genes. The signal peptides are shown in blue, and the TM domains are marked in orange. The abnormally long N-terminus can be seen for *Dα5*. (After Jones *et al.* 2005).

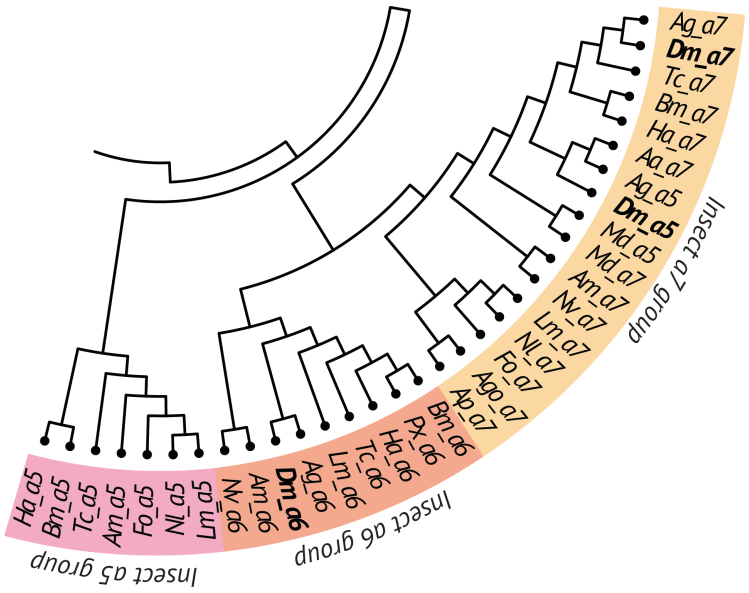


Figure 2.2 The α7-like superclade

A snapshot of the insect nAChR phylogenetic tree (Figure 1.7). Compared to other insect nAChR groups, the groups shown (insect α5, α6, α7) exhibit high amino acid similarity with each other and have the highest similarity with a vertebrate subunit (vertebrate α7). *D. melanogaster* subunits are featured in bold text.

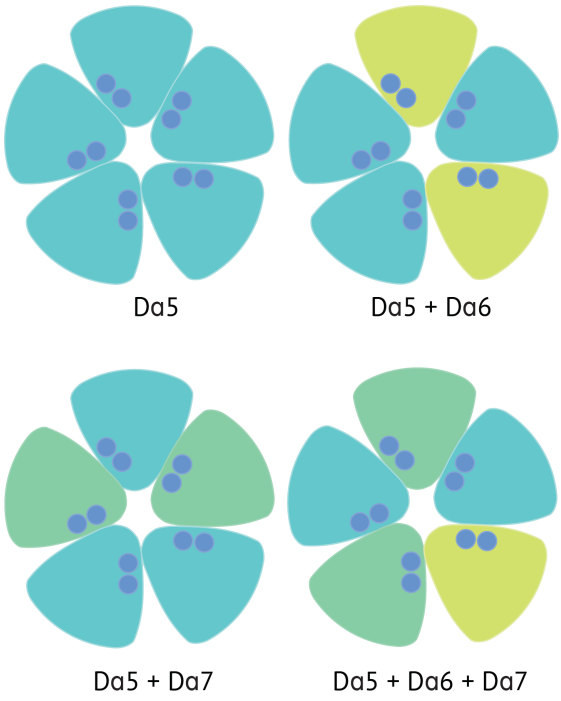


Figure 2.3 Known binding partners for Dα5

Dα5 can form functional homomeric pentamers, or heteromeric pentamers with Dα6 and/or Dα7 subunits. This is based on heterologous expression and radio ligand binding (Lansdell *et al.* 2012). Exact stoichiometries are unknown, and for all functional combinations, co-expression of the accessory protein, RIC3, was required.

2.1.1 Early descriptions of loss of Dα5 function

Despite its relatively recent evolution, preliminary work indicates Dα5 may be the only nAChR subunit in *Drosophila* with an essential role in larval development. Mitchell (2012) examined a deficiency strain which lacked a region of chromosome 2L containing the *Dα5* gene, plus the small gene within *Dα5*'s 5'UTR (*nimC4*), and six flanking genes. Individuals homozygous for this deficiency were reported to die early in the L3 stage. At the time of death these larvae were the size of L2 larvae, and had retained their old L2 mouthhooks and cuticle. This phenotype is indicative of incomplete moulting and has been described elsewhere as the "buttoned-up" phenotype (Park *et al.* 2002). Larvae were also reported to wander away from their food source prior to death (Mitchell 2012).

Mitchell (2012) also examined tissue-specific RNAi knockdown of *Dα5*. Given the moulting phenotype described above, focus was directed towards the tissues of the ring gland. Surprisingly, knockdown in the PG was sufficient to cause larval mortality, but knockdown in the CNS was not. This may point towards a non-neuronal role for Dα5, as is common for vertebrate α7-like subunits. However, evidence of Dα5 expression in the PG is inconsistent. Transcript expression was detected in fluorescent *in situ* hybridisation experiments (Ali 2012) but not in ring gland RNA-seq data (Christesen *et al.* 2017). Further work is required to determine if Dα5 is actually required in the PG, and how loss of Dα5 might be causing a disruption in moulting and precocious wandering.

2.1.2 Cues for moulting and wandering

Moulting and wandering are key events for developing larvae and both are intimately linked with feeding, growth and endocrine signalling. Wild type larvae feed continuously throughout the L1, L2 and L3 stages, accommodating their rapidly increasing body size by secreting a new, larger cuticle and moulting the old one. The hormone cascade that drives each of these moults involves an initial pulse of ecdysone from the PG, followed by sequential release of the peptidergic hormones ETH, EH, and CCAP (Di Cara and King-Jones 2013) (described in *section 1.3.2*). Disruptions in this moulting hormone cascade can have a wide range of phenotypic outcomes, from accelerated development (Ou *et al.* 2011) to embryonic lethality (Chavez *et al.* 2000), and can sometimes result in the buttoned-up double mouthhook phenotype. Multiple strains have been associated with this buttoned-up phenotype including, but not limited to, ecdysone receptor mutants (Li and Bender 2000), *ETH* mutants (Park *et al*. 2002), ecdysone-deficient strains (Freeman *et al.* 1999), and strains overexpressing the neuropeptide *hugin* (Meng *et al.* 2002).

Early in the L3 stage, the PG assesses whether larvae have attained a pre-determined critical weight (Mirth *et al.* 2005). If so, wild type larvae will wander away from their food source midway through the L3 stage and seek an appropriate site to pupariate. The endocrine cue that triggers this wandering behaviour is a mid-L3 pulse of ecdysone released from the PG. Precocious wandering has been observed in mutants with elevated ecdysone levels (Ou *et*

al. 2011) and can be induced with well-timed infusion of 20E (Dominick and Truman 1984). Some feeding mutants also exhibit precocious wandering behaviour, although this wandering is not followed by an attempt to pupariate and is associated with an inability to ingest food. These include *pumpless* mutants (Zinke *et al.* 1999) and, again, strains overexpressing the neuropeptide *hugin* (Melcher and Pankratz 2005, Schoofs *et al.* 2014).

2.1.3 Chapter aims

The overarching aim of this chapter is to more fully characterise what roles the Dα5 subunit may play during larval development. It will delve deeper into the moulting and wandering phenotypes first identified by Mitchell (2012), preferably using a *Dα5* genomic deletion that is specific to the *Dα5* locus and does not disrupt nearby genes. Newly available MiMIC strains and MiMIC-related tools such as T2A-GAL4 (TG4, Diao *et al.* 2015) and deGradFP (Caussinus *et al.* 2012) will also be used to build on existing work. A list of key questions is provided below.

1. Does larval mortality occur in a CRISPR-generated *Dα5* deletion strain (or in alternative *Dα5* null mutants)?
2. Do moulting and wandering phenotypes occur in a CRISPR-generated *Dα5* deletion strain (or in alternative *Dα5* null mutants)?
3. Are these phenotypes associated with underlying hormonal disruptions?
4. Is Dα5 required in the PG? Are there other neurons or cell types where Dα5 may be required?
5. Does Dα5 play a role in post-larval viability?
6. Is the abnormal N-terminus required for normal Dα5 function?
7. Does loss of Dα5 affect larval response to the Dα6-targetting insecticide, Spinosad?

2.2 Methods

2.2.1 Fly strains and maintenance

A summary of fly strains used throughout the chapter is provided in **Figure 2.4** and **Table 2.1**. Separate tables are provided for flies used in CRISPR (*Appendix 1*) and RNAi experiments (*section 2.2.1.2*). All flies were maintained on standard semolina fly media at 25°C under a 12:12 hour light: dark cycle unless otherwise stated. For larval experiments, embryos were collected for 3 hours on apple juice agar plates. L1 larvae were synchronised and selected for the absence of a fluorescent balancer chromosome within 2 hours of hatching then reared on apple juice agar plates smeared with yeast paste.

2.2.1.1 CRISPR strains

Multiple different CRISPR strategies became available over the course of this project. Since none of these strategies were successful in generating a *Dα5* deletion strain, detailed descriptions of each methodology, including sgRNA sequences, primer sequences, and fly strains, are provided in *Appendix 1*.

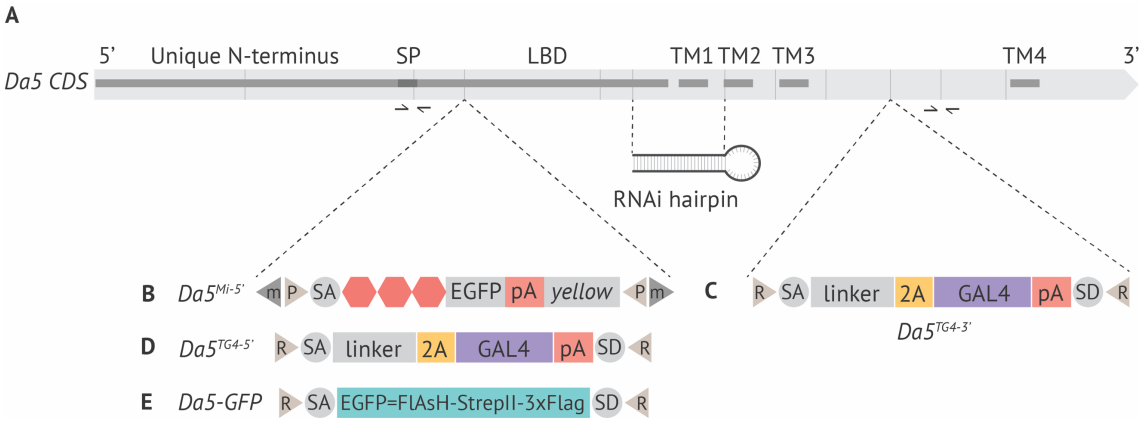


Figure 2.4 Key positions and insertion cassettes for fly strains used in *Chapter Two*

(**A**) Shows the 12 exons of the *Dα5* CDS (light grey) overlaid with domains present in the Dα5 protein (dark grey). These domains include the unique N-terminus, a signal peptide (SP), a ligand-binding domain (LBD), and 4 transmembrane domains (TM1-4). The hairpin in the fly strain *UAS-Dα5RNAi* shares homology with exon 6. qRT-PCR primer pairs are shown in exons 2, 3, 10 and 11 (black arrows). (**B**) The MiMIC cassette causes truncation of *Dα5* after exon 3. The splice acceptor (SA) ensures the cassette is incorporated into the *Dα5* mRNA. Stop codons in all three reading frames (red hexagons) and a polyadenylation signal (pA) ensure termination of transcription and translation. The cassette is flanked by two *Minos* inverted repeats (m) and two inverted *attP* sites (P). (**C, D**) The TG4 cassettes promote expression of GAL4 in the native *Dα5* expression pattern and cause truncation of *Dα5* after exon 3 ($D\alpha5^{TG4\text{-}5'}$) or exon 9 ($D\alpha5^{TG4\text{-}3'}$). The splice acceptors (SA) ensure the cassette is incorporated into the *Dα5* mRNA. A short linker maintains the reading frame, allowing contiguous transcription of a *Dα5::*GAL4 mRNA, and a polyadenylation signal (pA) ensures termination of transcription. The 2A sequence promotes "ribosomal skipping" during translation, resulting in a truncated Dα5 gene product and an independent GAL4 protein. The cassettes are flanked by two *attR* (R) sites. (**E**) The GFP cassette is inserted as an artificial exon between exons 3 and 4, without truncation of *Dα5*. The splice acceptor (SA) ensures the cassette is incorporated into *Dα5* mRNA and the splice donor (SD) ensures transcription continues after the cassette. The cassette is flanked by *attR* sites (R).

Table 2.1 Fly strains used throughout *Chapter Two*

Name	Origin	Genotype	Stock #	Reference
Dα5$^{Mi-5'}$	BDSC	*y[1] w[67c23]; Mi{y[+mDint2]=MIC}nAChRalpha5[MI05549]/GFP-CyO; +*	41424	Venken *et al*. 2011
yw isogenic (yw)	BDSC	*y[1] w[67c23]; +; +*	6599	
Dα5$^{TG4-5'}$	Lab stock	*y[1] w[67c23]; Mi[Trojan-GAL4.0]nAChRalpha5[MI05549-TG4.0]/GFP-CyO; +*		This study
Dα5$^{TG4-3'}$	BDSC	*y[1] w[*]; Mi{Trojan-GAL4.2}nAChRalpha5[MI13859-TG4.2]/GFP-CyO; +*	76755	
Dα5-GFP	BDSC	*y[1] w[67c23]; Mi{PT-GFSTF.0}nAChRalpha5[MI05549-GFSTF.0]; +*	59826	
da-GAL4 (daughterless-GAL4)	BDSC	*w[*]; +; P{w[+mW.hs]=GAL4-da.G32}UH1*	55849	
UAS-Dα5cDNA	Lab stock	*y[1] M{RFP[3xP3.PB] GFP[E.3xP3]=vas-int.Dm}ZH-2A w[*]; +; M{pUAST-Dα5cDNA}ZH-86Fb*		Perry *et al.* 2015
Dα5$^{Mi-5'}$/GFP-CyO; da-GAL4	Lab stock	*Mi{y[+mDint2]=MIC}nAChRalpha5[MI05549]/GFP-CyO; P{w[+mW.hs]=GAL4-da.G32}UH1*		This study
Dα5$^{Mi-5'}$/GFP-CyO; UAS-Dα5cDNA	Lab stock	*Mi{y[+mDint2]=MIC}nAChRalpha5[MI05549]/GFP-CyO; M{pUAST-Dα5cDNA}ZH-86Fb*		This study
Dα5-GFP/CyO; UAS-deGradFP_GAL80/TM6b	Lab stock	*Mi{PT-GFSTF.0}nAChRalpha5[MI05549-GFSTF.0]/CyO; P{w[+mC]=UAS-Nslmb-vhhGFP4}3, tubGAL80/TM6b*		This study
Df^{6075}	BDSC	*+; Df(2L)b75/CyO; +*	6075	
Df^{9061}	BDSC	*w[1118]; Df(2L)ED793, P{w[+mW.Scer\FRT.hs3]=3'.RS5+3.3'}ED793/SM6a; +*	9061	
Df^{25164}	BDSC	*w[1118]; Df(2L)ED8186, P{w[+mW.Scer\FRT.hs3]=3'.RS5+3.3'}ED8186/SM6a; +*	25164	
Dα6^{KO}	Lab stock	*W[1118]; Da6^{KO}; +*		Perry *et al.* 2021
w^{1118}	VDRC	*w[1118]; +; +*	60000	Dietzl *et al.* 2007
Armenia line 14 (L14)	Lab stock	*+; +; +*		Perry *et al.* 2008
Φ86fb	BDSC	*y[1] M{RFP[3xP3.PB] GFP[E.3xP3]=vas-int.Dm}ZH-2A w[*]; +; M{3xP3-RFP.attP}ZH-86Fb*	24749	Bischof *et al.* 2007
UAS-mCD8GFP	BDSC	*y[1] w[1118]; P{w[+mC]=UAS(FRT.stop)mCD8-GFP.H}11; +*	30125	
UAS-nGFP	BDSC	*w[1118]; P{w[+mC]=UAS-GFP.nls}14; +*	4775	
NetB-GFP	BDSC	*y[1] w[*] Mi{PT-GFSTF.1}NetB[MI10467-GFSTF.1] CG43088[MI10467-GFSTF.1-X]; +; +*	67644	

Abbreviations: BDSC (Bloomington *Drosophila* Stock Center), VDRC (Vienna *Drosophila* Resource Center

2.2.1.2 RNAi crosses

Fly strains used in RNAi crosses are provided in **Table 2.2**. Five virgin GAL4 females were crossed with 4 RNAi males and allowed to lay for 3 days. The F_1 were monitored for developmental phenotypes and adults scored on day 14. Crosses were replicated 4 times each at 18°C, 22°C and 25°C. Controls were obtained by crossing GAL4 virgin females to w^{1118} (for *Dα5*) or *36303* (for *ETH*).

2.2.1.3 Overexpression crosses

Five virgin *da-GAL4* females were crossed with 5 *UAS-Dα5cDNA* males and allowed to lay for 3 days. The F_1 were monitored for developmental phenotypes and adults scored on day 14. Crosses were replicated 4 times at 25°C.

Table 2.2 Fly strains used for RNAi

Name	Origin	Genotype	Stock #	Reference
UAS-Dα5RNAi	VDRC	*GD Collection*	10328	Dietzl *et al.* 2007
w^{1118}	VDRC	*w[1118]; +; +*	60000	Dietzl *et al.* 2007
UAS-ETHRNAi	BDSC	*y[1] v[1]; +; P{y[+t7.7] v[+t1.8]=TRiP.JF02141}attP2*	26242	
36303	BDSC	*y[1] v[1]; +; P{y[+t7.7]=CaryP}attP2*	36303	
5'phm-GAL4	Lab stock	*w[1118]; 5'phm-GAL4/GFP-CyO; +*		Christesen *et al.* 2017
Feb36-GAL4	BDSC	*w[*]; P{w[+mW.hs]=GawB}Feb36; +*	29968	
elav-GAL4	BDSC	*P{w[+mW.hs]=GawB}elav[C155]; +; +*	458	
5'6g2-GAL4	Lab stock	*w[1118]; 5'Cyp6g2-GAL4_2b/CyO; +*		Christesen *et al.* 2017
Akh-GAL4	BDSC	*y[1] w[*]; P{w[+mC]=Akh-gal4.L}2/CyO, y[+]; +*	25683	
ptth-GAL4	Gift from Michael O'Connor	*y[1] w[1118]; PTTH-HA-7aA3 ; +*		Rewitz *et al.* 2009
trh-GAL4	BDSC	*w[1118]; P{w[+mC]=Trh-GAL4.long}3; +*	38389	
hug-GAL4	BDSC	*w[*]; +; P{w[+mC]=Hug-GAL4.S3}3*	58769	
ETH-GAL4	BDSC	*w[1118]; P{w[+mC]=ETH-GAL4.TH}1M; +*	51982	
da-GAL4	BDSC	*w[*]; +; P{w[+mW.hs]=GAL4-da.G32}UH1*	55849	
tub-GAL4	BDSC	*y[1] w[*]; +; P{w[+mC]=tubP-GAL4}LL7/TM3, Sb[1] Ser[1]*	5138	
$D\alpha5\text{-}^{TG45'}$	Lab stock	*y[1] w[67c23]; Mi[Trojan-GAL4.0]nAChRalpha5[MI05549-TG4.0]/GFP-CyO; +*		This study
$D\alpha5\text{-}^{TG43'}$	BDSC	*y[1] w[*]; Mi{Trojan-GAL4.2}nAChRalpha5[MI13859-TG4.2]/GFP-CyO; +*	76755	

Abbreviations: BDSC (Bloomington *Drosophila* Stock Center), VDRC (Vienna *Drosophila* Resource Center

2.2.1.4 deGradFP crosses

Five virgin *Dα5Mi/GFP-CyO; da-GAL4* females were crossed with 4 *Dα5GFP/CyO; UAS-deGradFP_GAL80/TM6b* males under 3 different temperature protocols (**Figure 2.5**):

I) Flies were crossed and allowed to lay for 3 days at 28°C (restrictive temperature), then reared at 28°C until adulthood and scored on day 14.

II) Flies were crossed and allowed to lay for 5 days at 18°C (permissive temperature), then reared at 18°C until adulthood and scored on day 28.

III) Flies were crossed and allowed to lay for 5 days at 18°C, then shifted to 28°C upon pupariation and scored on day 24.

In each case, the F_1 were monitored for developmental phenotypes and adults scored for the presence of balancer chromosomes. Crosses were replicated 4 times under each temperature protocol.

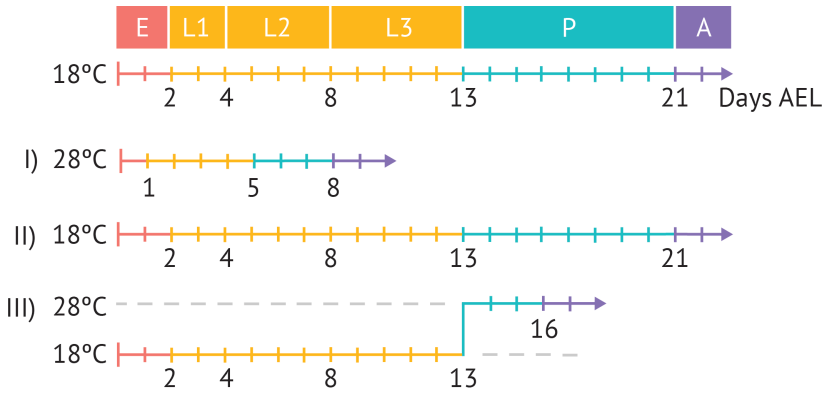


Figure 2.5 Timing of deGradFP experiments

deGradFP crosses were conducted under 3 different temperature protocols: I) reared at 28°C, II) reared at 18°C, and III) shifted from 18°C to 28°C upon pupariation on day 13. Timelines depict days AEL (after egg laying) and are coloured according to the developmental stages E (embryo), L1-3 (larval instars 1-3), P (pupa), and A (adult). (After Nagarkar-Jaiswal *et al*. 2015).

2.2.1.5 Complementation crosses

Five virgin females were crossed with 4 males and allowed to lay for 3 days. The F_1 were monitored for developmental phenotypes and adults scored on day 14. Crosses were replicated 4 times at 25°C. For *Dα5$^{Mi\text{-}5'}$/Dα5$^{TG4\text{-}3'}$ and Dα5$^{Mi\text{-}5'}$/Df^{9061}*, RNA was isolated from 10 pooled F_1 adults using *TRIsure Reagent* (Bioline) and quantified using the *Qubit RNA BR Assay Kit* (ThermoFisher). cDNA was then synthesised from 1µg RNA using the *GoScript Reverse Transcription Kit* (Promega). *Dα5* transcripts were detected by PCR using *Dα5_RT_ex10_F/Dα5_RT_ex11_R* primers (**Table 2.3**) and *GoTaq 2X Master Mix* (Promega).

Table 2.3 Primers used in complementation experiments

Name	Sequence
Dα5_RT_ex10_F	ATGATGACTTCCGGCACAA
Dα5_RT_ex11_R	GATGCACGTATGATGGGTGA

2.2.1.6 Genetic rescue crosses

Five virgin *Dα5$^{Mi\text{-}5'}$/GFP-CyO; da-GAL4* females were crossed with 4 *Dα5$^{Mi\text{-}5'}$/GFP-CyO; UAS-Dα5cDNA* males and allowed to lay for 3 days. The F_1 were monitored for developmental phenotypes and adults scored on day 14. Crosses were replicated four times at 25°C.

2.2.1.7 BAC clone strains

Three different 80kb Pacman clones (Venken *et al*. 2009) containing either a whole genomic copy of *Dα5* (CH321-64K12) or a partial genomic copy of *Dα5* (CH321-4M8, CH321-22L16) were each microinjected into attP (*Φ86Fb*) embryos (Bischof *et al.* 2007) (**Figure 2.6**). Injectees were self-crossed then the F_1 offspring were screened phenotypically for w^+ eye colour rescue.

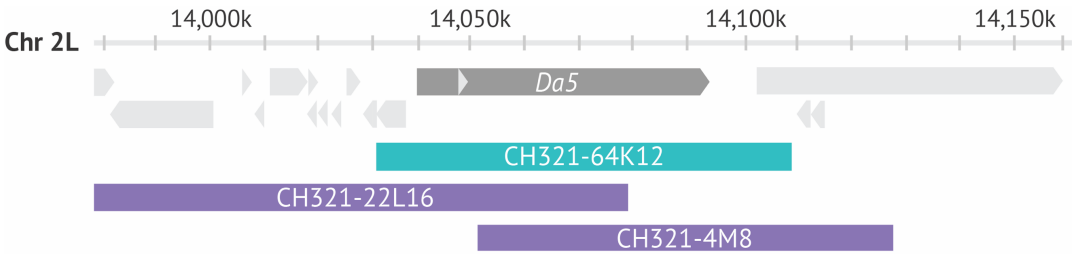


Figure 2.6 BAC clones

BAC clone CH321-64K12 (green) contains the entire *Dα5* gene region (dark grey) plus some flanking genes on chromosome 2L (light grey). BAC clones CH321-22L16 and CH321-4M8 (purple) contain these flanking genes but only part of the *Dα5* gene region.

2.2.1.8 "Mapping" lethality to the MiMIC insertion

Five $D\alpha5^{Mi\text{-}5'}$ virgins were crossed to 3 males of the *Armenia Line 14* (*L14*) wild type strain and F_1 heterozygous $D\alpha5^{Mi\text{-}5'}/D\alpha5^{L14}$ virgin females collected (**Figure 2.7**). Recombination took place in the germline of these females. They were then crossed back to $D\alpha5^{Mi\text{-}5'}$ males and F_2 individuals heterozygous for the intact $D\alpha5^{Mi\text{-}5'}$ and a $D\alpha5^{Mi\text{-}5'}$*: L14* recombinant chromosome (i.e. lacking the GFP-CyO balancer) were selected. Genomic DNA was extracted and individual flies were scored molecularly for the presence of a $D\alpha5^{L14}$ allele (i.e. the absence of a MiMIC insertion) using *Dα5_MiMIC_check_F* /*Dα5_MiMIC_check_R* primers (**Table 2.4**) which flank the cassette insertion site.

Table 2.4 Primers flanking the $D\alpha5^{Mi\text{-}5'}$ insertion site

Name	Sequence
Dα5_MiMIC_check_F	TCTCACGTTTTGCGGTTGTT
Dα5_MiMIC_check_R	TTCGTTTGACGCCACTAGGA

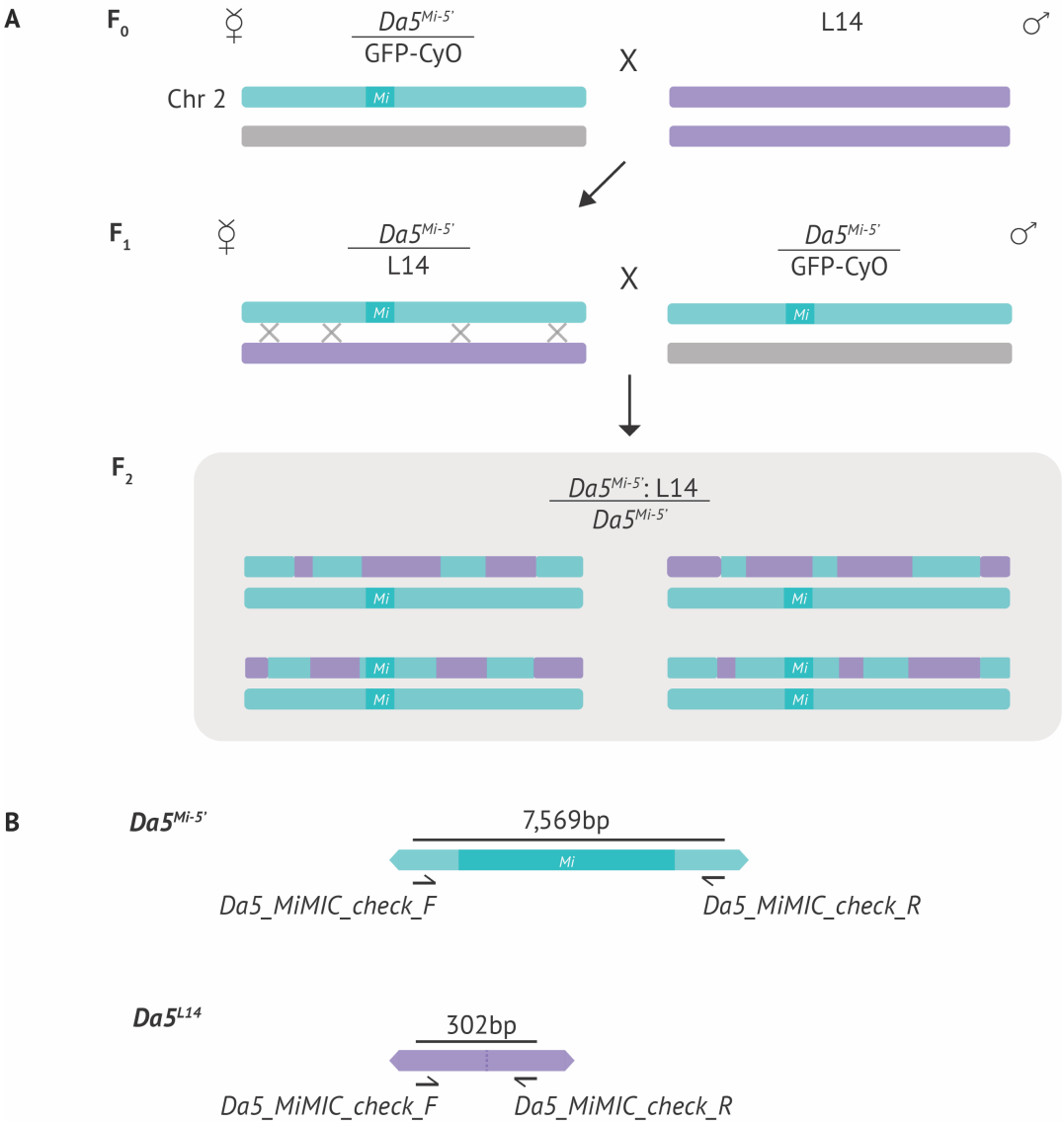


Figure 2.7 "Mapping" lethality on $D\alpha5^{Mi\text{-}5'}$ chromosome 2

(**A**) The crossing scheme used to generate F_2 offspring heterozygous for the intact $D\alpha5^{Mi\text{-}5'}$ chromosome and a recombinant $D\alpha5^{Mi\text{-}5'}$: L14 chromosome. Schematic depictions of chromosome 2 are provided for $D\alpha5^{Mi\text{-}5'}$ (green), L14 (purple), $D\alpha5^{Mi\text{-}5'}$: L14 (green/purple) and GFP-CyO (dark grey) and the MiMIC cassette (Mi) is labelled on $D\alpha5^{Mi\text{-}5'}$. Recombination occurred in F_1 females and F_2 offspring were screened for the absence of the fluorescent GFP-CyO balancer. Diagrams are not drawn to scale. (**B**) Molecular detection of the $D\alpha5^{L14}$ allele in F_2 offspring. When PCR extension time is limited to 30 seconds, primers flanking the MiMIC insertion site amplify the shorter $D\alpha5^{L14}$ allele, but not the longer $D\alpha5^{Mi\text{-}5'}$ allele.

2.2.2 Developmental mortality assays

Synchronised larvae were scored every 24 hours for developmental stage based on spiracle and mouthhook morphology (10 per plate, 5 independent plates, in some cases only 8/10 or 9/10 were recovered per plate so $n > 40$ for all genotypes). Upon pupariation, individuals were transferred to vials containing standard fly media.

2.2.3 Measuring body weight

Body weight was measured by pooling at least 50 larvae in 1.5mL Eppendorf tubes (3 replicates, $n > 150$ per instar). Significance was calculated using Student's *t*-test ($p < 0.05$).

2.2.4 Wandering assays

At 48 hours AEL (after egg laying), synchronised L2 larvae were transferred directly into 600mg of yeast paste on a large (85mm) apple juice agar plate (50 per plate, 5 replicates, $n = 250$). Plates were incubated in constant darkness and the number of larvae outside the yeast paste was scored at 56, 64 and 72 hours AEL. Significance was calculated at each timepoint using Tukey's honestly significant difference pair-wise test ($p < 0.05$).

2.2.5 Larval movement assays

Basal larval movement was measured using a modified Wiggle Index assay (Denecke *et al.* 2015). Briefly, L2 larvae were transferred into a 24-well plate (20 larvae per well, 8 wells per genotype, $n = 160$) containing 200µL 5% sucrose in distilled water. Thirty second videos were taken at 0, 30 and 60 minutes after the addition of larvae using a *Panasonic 3CCD Ultra-Compact Digital Palmcorder*. Raw videos were split into JPEG image sequences using the *DVDVideoSoft Converter*, and further processed as previously described (Denecke *et al.* 2015), generating heat maps and a numerical estimate of total motility (Wiggle Index). To calculate relative movement, Wiggle Index values were normalised to the background control mean. Significance was calculated

using a Student's *t*-test ($p < 0.05$).

The Wiggle Index assay was also used to measure larval response to a formulation containing the insecticide spinosad (Success®, Yates). Again, L2 larvae were transferred into a 24-well plate (20 larvae per well, 4 wells per genotype per treatment, $n = 80$) containing 200uL 5% sucrose in distilled water. After an initial 30 second recording (t_0), 50µL of 60ppm solution (spinosad in 5% sucrose) was added to wells, bringing the concentration to 12ppm, then 50µL removed to return the well volume to 200µL. Further 30 second videos were then taken at 15, 30, 60, 90 and 120 minutes after insecticide exposure. Videos were acquired and processed as described above. Wiggle Index values were normalised to the mean of each genotype at t_0. Significance was calculated using Tukey's test ($p < 0.05$).

2.2.6 Feeding assays

At 48 hours AEL, synchronised L2 larvae were starved for 1 hour in a petri dish containing paper towel dampened with tap water. Larvae were then transferred to yeast paste coloured with blue food dye (1g bakers' yeast, 300µL dye, 1500µL water) and incubated for 1 hour. At 50 hours AEL, larvae were dissected in 80% glycerol ($n > 10$). For analysis, larvae were imaged using a *Leica M205FA Microscope* and *DFC425 camera*. The percentage area of the midgut containing coloured yeast paste was measured using ImageJ (Fiji, version 2.0.0, Schindelin *et al.* 2012). Significance was calculated using Student's *t*-test ($p < 0.05$).

2.2.7 Longevity assays

Virgin $D\alpha5^{Mi\text{-}5'}$ and *yw* females were each crossed with w^{1118} males to obtain heterozygous $D\alpha5^{Mi\text{-}5'}/D\alpha5^{w1118}$ and $D\alpha5^{yw}/D\alpha5^{w1118}$ offspring. These heterozygotes were virgin collected over 48 hours then placed on standard semolina-based fly media (10 males and 10 females per vial, 4 vials per genotype, $n = 80$). Vials were maintained horizontally at 25°C under a 12:12 hour light: dark cycle. Heterozygotes were transferred to new vials and the number of dead flies recorded every 2-3 days (or

every 4-5 days from day ~30 onwards) until all were deceased. A Kaplan-Meier Survival Curve was constructed and significance was calculated using a Cox-Mantel test ($p < 0.05$).

2.2.8 Fertility assays

Vials used in longevity assays (*section 2.2.7*) were maintained at 25°C after removal of adult heterozygotes. Fertility was then estimated by scoring the number of viable offspring that eclose 2 weeks later. This number was divided by the number of parental females that were present in the vial (10 females per vial at the start of the experiment, 4 vials per genotype, $n = 40$) and the number of days females were present to lay eggs (2-5 days). Significance was calculated using Student's *t*-test ($p < 0.05$).

2.2.9 Climbing assays

Three-day-old flies were transferred without anaesthesia into clean empty vials, allowed to acclimate for 5 minutes, then tapped down 3 times on a fly pad to initiate the negative geotaxis response (Gargano *et al.* 2005). The vials were recorded for 10 seconds from a distance of 30cm on an *iPhone 8* (Apple Inc.). *QuickTime Player* (Apple Inc.) was used to capture the frame occurring 6 seconds (180 frames) post-third tap down. JPEGs were then imported into *Image J* (Fiji, version 2.0.0, Schindelin *et al.* 2012) and marked with a horizontal threshold 45mm from the bottom of the vials. The number of flies above this threshold was scored manually. Significance was calculated using Student's *t*-test ($p < 0.05$).

2.2.10 qRT-PCR

Quantitative real time PCR (qRT-PCR) was used to detect transcript levels for *Dα5, Dα6 and Dα7* in $D\alpha5^{Mi\text{-}5'}$ and *da-GAL4/UAS-Dα5RNAi*. Numerous additional genes, including many developmental hormones, were also measured in $D\alpha5^{Mi\text{-}5'}$. For at least 3 biological samples, 10 whole L2 larvae were collected, and RNA was isolated using

TRIsure Reagent (Bioline). RNA concentration was measured using the *Qubit Fluorometer*. cDNA was synthesised from 1µg RNA using the *GoScript Reverse Transcription Kit* (Promega). qRT-PCR reactions for each biological sample were carried out in triplicate using a *Quanti-fast SYBR Green PCR kit* (Qiagen) on the *CFX384 Touch Real-Time PCR Detection System* (Bio-Rad). The amount of target RNA was normalised to the geometric mean of the Ct values of two endogenous controls: *Rpl32* and *CG13220* (Van Hiel *et al.* 2009). mRNA levels were compared between samples using the ΔΔCt method (Bustin *et al.* 2009) and significance was calculated using Student's *t*-test ($p < 0.05$). All primer sequences are provided in **Table 2.5** and the MIQE checklist is provided in **Table 2.6**.

2.2.11 Semi-quantitative PCR

Semi-quantitative PCR was used to further test *da-GAL4/UAS-Dα5RNAi*. Using the same cDNA samples prepared above (*section 2.2.10*), full length *Dα5* cDNA was amplified using *Dα5_Clone_F/Dα5_Clone_R* primers (**Table 2.7**) and *GoTaq 2X Master Mix* (Promega). The amount of *Dα5* cDNA was normalised to the endogenous control *CG13220*. For *Dα5*, PCR cycles were repeated 32, 34, 36 and 38 times, and for *CG13220*, PCR cycles were repeated 20, 24, 28 and 32 times (**Table 2.8**). These conditions were chosen so that amplification reached, but did not pass, the exponential phase. Gel band intensities were quantified using *Image J* (Fiji, version 2.0.0, Schindelin *et al.* 2012).

Table 2.5 qRT-PCR primers

Name	Sequence	Amplicon size (bp)	PCR efficiency	Limit of Detection	Reference
Rp32_RT_F	CCAGTCGGATCGATATGCTAA	121	94%	24.14	
Rp32_RT_R	GTTCGATCCGTAACCGATGT				
CG13220_RT_F	TGGGCAGTGCCTTCTACATTT	71	95%	30.40	Van Hiel *et al.* 2009
CG13220_RT_R	CGTACGCACCTCGCTTGTT				
Dα5_RT_ex2_F	CAGCACGCAAATATTAAACGG	102	99%	29.71	
Dα5_RT_ex3_R	TTTTCATGATATCCTGCTAGGC				
Dα5_RT_ex10_F	ATGATGACTTCCGGCACAA	161	88%	26.48	
Dα5_RT_ex11_R	GATGCACGTATGATGGGTGA				
Dα6_RT_F	CAATATCTGGCTCCCAAACC	243	79%	29.03	
Dα6_RT_R	TCGTGAAGAGCGTGAAAACAA				
Dα7_RT_F	CCCACCAGCCCACATATTAC	218	77%	25.53	
Dα7_RT_R	AATGTCGCTTGTTTCGTCCT				
Lip3_RT_F2	TGGTTTTGGCCGGATCTCG	137	86%	31.40	
Lip3_RT_R2	TTTGGGGGAATACGGGATGC				
Hug_RT_F	CCTGCTCCTTCAAAAGCTACG	207	90%	34.50	
Hug_RT_R	TAGTCGCCAGGAGTCAATGC				
E75B_RT_F	CAACAGCAACAACACCCAGA	118	79%	33.12	Danielsen *et al.* 2016
E75B_RT_R	CAGATCGGCACATGGCTTT				
ETH_RT_F	ATGGGATTTGGAAACGAG	109	95%	32.32	Gauthier and Hewes 2006
ETH_RT_R	AAGGAGCGTATTCGAGTTG				
Eh_RT_F	TAGTCAGCTCCCCAAACA	99	92%	33.01	Gauthier and Hewes 2006
Eh_RT_R	ATTGCAACTGCCACAAAG				
CCAP_RT_F	TACAATGGAAGTACGAGAAGC	101	81%	32.11	Gauthier and Hewes 2006
CCAP_RT_R	GCGTTTGAATAGCGAGAAT				

Table 2.6 Minimum information required for publication of quantitative real time PCR experiments (MIQE)

Sample	**Details**
Source	*Drosophila melanogaster* whole 2nd instar larvae
Method of preservation	Liquid N_2
Storage time (if appropriate)	<2 months old
Handling	Frozen
Extraction method	TRIsure (Bioline)
RNA: DNA-free	Intron-spanning primers, DNaseI, PCR check
Concentration	Fluorometric quantitation (Qubit)
RNA: integrity	Agarose gel
Inhibition-free	Dilution curve, PCR efficiency <100%
Assay optimisation/validation	**Details**
Amplicon details	See **Table 2.5**
Primer sequence	See **Table 2.5**
In silico/empirical tests	Primer-BLAST, electrophoresis, melt curve
Primer conditions	10µM, 60°C
cDNA primer	oligo-dT
PCR efficiency	See **Table 2.5**
Linear dynamic range	7-fold serial dilution
Limits of detection	See **Table 2.5**
RT/PCR	**Details**
Protocols	12.5µl total reaction. 5µl SYBR green Master Mix, 0.25µl F, 0.25µl R, 4.5µl H2O and 2.5µl Template Initial denaturation: 95°C 5min Denaturation: 95°C 10sec Annealing: 60°C 30sec (x40 cycles)
Reagents	QuantiFast SYBR green PCR kit, Qiagen
Replicates	Triplicate
No template control	Ct value & melt curve not detected
No amplification control	N/A
Data analysis	**Details**
Specialist software	N/A
Statistical justification	3-4 biological replicates for each genotype
Transparent, validated normalisation	Target and housekeeper validated at the same life stage

Table 2.7 Semi-quantitative PCR primers

Name	**Sequence**	**Reference**
Dα5_Clone_F	GTAGAGAGCAGACAACATATCC	Perry *et al.* 2015
Dα5_Clone_R	CCATATGGCTACGAGACAATA	Perry *et al.* 2015
CG13220_RT_F	TGGGCAGTGCCTTCTACATTT	Van Hiel *et al.* 2009
CG13220_RT_R	CGTACGCACCTCGCTTGTT	Van Hiel *et al.* 2009

Table 2.8 Semi-quantitative PCR conditions

Target	Reaction step	Temperature (°C)	Time (s)	Number of cycles
Dα5	Denaturation	94	30	32, 34, 36 or 38
	Annealing	54	30	
	Extension	72	150	
CG13220	Denaturation	94	30	20, 24, 28 or 32
	Annealing	60	30	
	Extension	72	30	

2.2.12 Confocal microscopy

L3 brains and ring glands were dissected in 1X PBS, fixed with 3.7% formaldehyde for 15 minutes at room temperature, then washed in 1X PBS. Unstained samples were then mounted in *Vectashield* (Vector Labs) and imaged. Those samples that were stained with conjugated primary antibodies (**Table 2.9**) were incubated in 1X PBS-0.2% Triton X-100 (PBST) for 1 hour at room temperature, stained with primary antibodies overnight at 4°C, washed in PBST for 1 hour at room temperature, then mounted and imaged. For those samples that were stained with conjugated secondary antibodies, the fixed brains were incubated in PBST for 1 hour at room temperature, stained with primary antibodies overnight at 4°C (**Table 2.9**), washed in PBST for 1 hour at room temperature, stained with secondary antibodies for 2 hours at room temperature, washed in PBST for 2 hours at room temperature, then mounted and imaged. All samples were visualised on *Leica Sp5* or *Sp8* confocal microscopes. Images were processed using *Image J* (Fiji, version 2.0.0, Schindelin *et al.* 2012).

2.2.13 Protein alignments

Two BLASTp searches were performed on amino acid residues 1-312 of Dα5 (Altshul *et al.* 1990). This region spans the N-terminus up to, and including, the SP. The first search excluded the genus *Drosophila*. The second search was limited to the genus *Drosophila*, then narrowed down to species from the 12 genomes project (*Drosophila* 12 Genomes Consortium 2007). All other search parameters were default. *Geneious* was used for multiple protein alignments, with Dα5 nominated as the reference sequence (Geneious version 8.1.6, Kearse *et al.* 2012). *Signal P* was used to predict SPs (Petersen *et al.* 2011).

2.2.14 Western blotting

One hundred dissected L3 brains or adult heads were homogenised in 100µL lysis buffer. 10µL supernatant was then added to 10µL 2X loading buffer and boiled for 10 minutes at 100°C. Samples were run on *10% Mini-Protean TGX Precast Protein Gels* (Bio-Rad) for 1 hour at 100 volts in a *Bio-Rad Mini-PROTEIN NTM* system followed by blotting onto a nitrocellulose membrane using the *Trans-Blot Turbo Transfer* system (Bio-Rad). Membranes were blocked with blocking buffer (5% milk in 1X TBS-0.2% Tween (TBST)) for 2 hours at room temperature, probed with primary antibody overnight at 4°C (**Table 2.10**), washed in TBST for 45 minutes at room temperature, incubated with the secondary antibody for 2 hours at room temperature, and washed again in TBST for 45 minutes at room temperature. Membranes were imaged on the *Odyssey CLx Infrared Imaging System* (LI-COR Biosciences).

Table 2.9 Confocal microscopy antibodies

Antibody mix	Conjugated primary			Conjugated secondary		
	Component	Volume (µL)	Source	Component	Volume (µL)	Source
Primary	1XPBS-0.2% Triton X-100	1,900	-	1XPBS-0.2% Triton X-100	1,900	-
	Rabbit anti-GFP Alexa Fluor 488 (1:500)	4	Invitrogen	Chicken anti-GFP (1:1000)	2	Abcam
	HRP 649 Cy5 (1:500)	4	Jackson ImmunoResearch	Mouse anti-DLG (1:500)	4	DSHB Parnas *et al.* 2001
	NGS	100	-	NGS	100	-
Secondary				1XPBS-0.2% Triton X-100	2,000	-
				Donkey anti-chicken 488 (1:250)	8	Invitrogen
				Donkey anti-mouse Cy3 (1:250)	8	Invitrogen
				HRP 649 Cy5 (1:500)	4	Jackson ImmunoResearch

Abbreviations: DSHB (Developmental Studies Hybridoma Bank

Table 2.10 Western blotting antibodies

Antibody mix	Component	Quantity	Source
Primary	1XTBS-0.2% Tween	10mL	-
	Rabbit anti-GFP (1:5000)	2µL	LifeTechnologies
	Milk powder	0.5g	-
Secondary	1XTBS-0.2% Tween	10mL	-
	Goat anti-Rabbit 800 (1:5000)	2µL	LiCOR
	Milk powder	0.5g	-

2.3 Results

2.3.1 Attempts to generate *Dα5* genomic deletions

Multiple CRISPR strategies were adopted in an effort to generate a *Dα5* genomic deletion strain. These different approaches are summarised in **Figure 2.8** and **Table 2.11**. Three different regions were targeted for deletion: the entire coding sequence (5'UTR - exon 12), the transcription start site and N-terminus (5'UTR - exon 2), and the ligand binding domain (exon 2 - exon 6). Approaches also varied by the method of delivery for the CRISPR components. The Cas9 protein was always provided by a transgenic Cas9 fly strain: either the ubiquitously-expressed *actin-Cas9* (for optimising detection of genomic editing), or the germline-specific *nanos-Cas9* (for optimising recovery of heterozygous F_1 offspring). The sgRNAs were delivered either by injection of *in vitro* transcribed RNAs (Basset *et al.* 2013), pU6 plasmids (Gratz *et al.* 2013) or pCFD4 plasmids (Port *et al.* 2014) directly into the Cas9 strain, or by crossing the Cas9 strain to transgenic pCFD4 or pCFD5 strains (Port and Bullock 2016).

Despite countless efforts, no stable *Dα5* deletion strain could be generated. In many cases, genomic editing was not detected at all by PCR. In instances where promising bands were detected on gels, the same bands were not detected in subsequent generations (**Figure 2.9**) or were not detected in subsequent DNA extractions from the same fly (i.e. in single fly preps from individuals that had previously been wing-clipped) (**Figure 2.10**). It was also common for individuals yielding promising PCR results to not yield any viable offspring, thus discontinuing the line.

Given the failure to generate a *Dα5* deletion, *D. melanogaster* strains carrying a MiMIC insertion in the third intron of the *Dα5* gene were sourced (*BDSC #41424*, **Figure 2.4**) and $D\alpha5^{Mi\text{-}5'}$ homozygotes have been used as the primary *Dα5* null in all subsequent experiments unless otherwise specified. While this MiMIC insertion is designed to eliminate *Dα5* expression, it is important to note that truncated *Dα5* transcripts will still be expressed in this strain (up to exon 3) and expression of the full *Dα5* transcript remains possible in the event of exon-skipping (Nagarkar-Jaiswal *et al.* 2015).

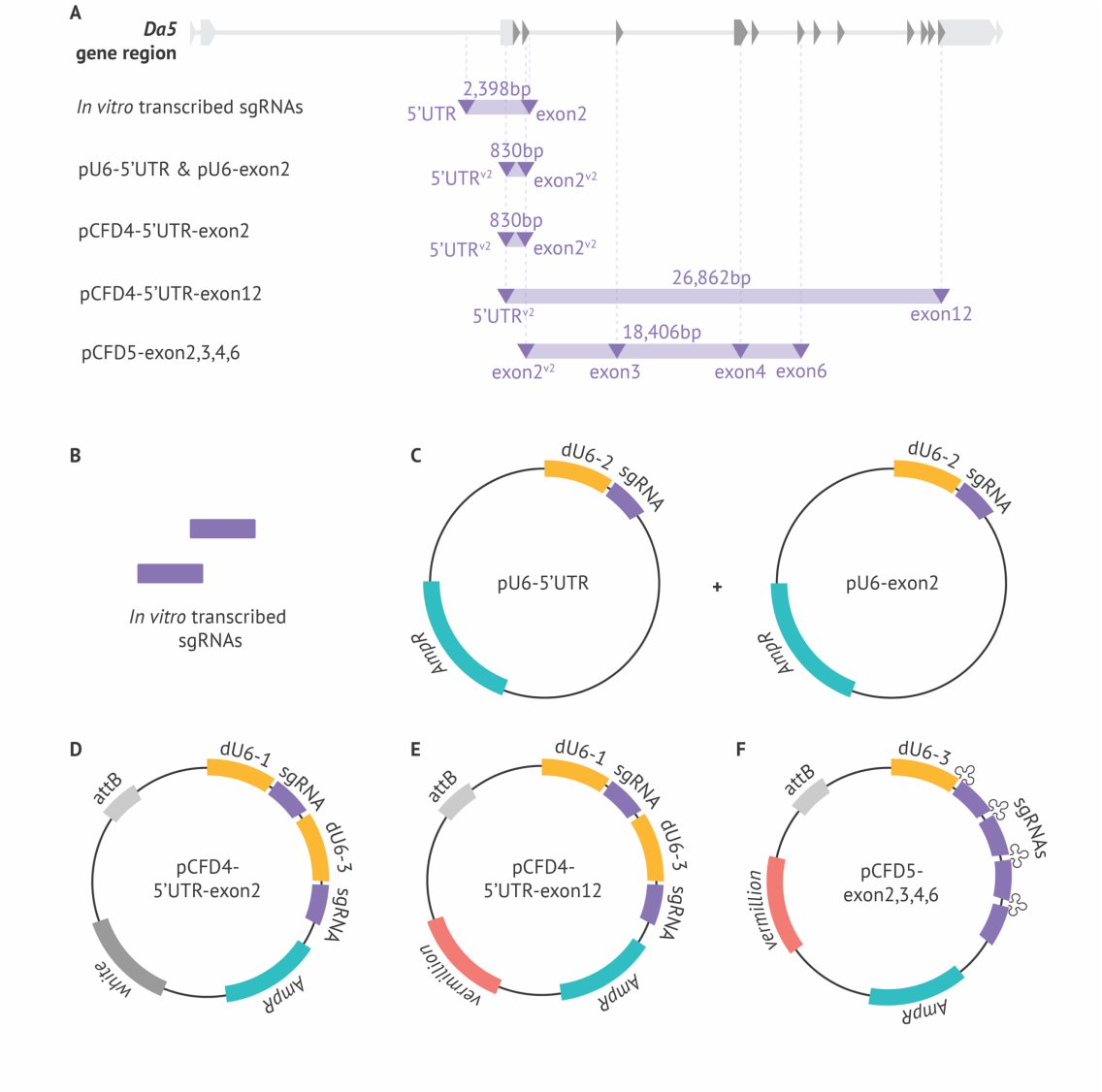


Figure 2.8 CRISPR target sites and plasmids

(**A**) The positions of sgRNA cut sites (purple triangles) and size of intended deletions (purple shading). The entire *Dα5* gene region is shown with exons (dark grey bars), untranslated regions (light grey bars), and introns (solid grey lines). (**B**-**F**) Schematic depiction of the delivery method for each set of sgRNAs shown in (A). (**B**) sgRNAs were transcribed *in vitro* and co-microinjected as RNA. (**C**) sgRNAs were incorporated into individual pU6 plasmids and co-microinjected. (**D**) sgRNAs were microinjected via a tandem pCFD4 plasmid and transgenics identified by *white* eye colour rescue. (**E**) sgRNAs were microinjected via a tandem pCFD4 plasmid and transgenics identified by *vermillion* eye colour rescue. (**F**) sgRNAs were microinjected via a tandem pCFD5 plasmid and transgenics identified by *vermillion* eye colour rescue.

Table 2.11 Attempted CRISPR strategies

Targeted regions	Source of sgRNAs	Source of Cas9	Size of intended deletion (bp)	Protocol
	Microinjection	**Microinjected strain**		
5'UTR, exon 2	*In vitro* transcribed RNA	*actin*-Cas9	2,398	Basset *et al.* 2013
5'UTR, exon 2	pU6	*actin*-Cas9	830	Gratz *et al.* 2013
5'UTR, exon 2	pU6	*nanos*-Cas9	830	Gratz *et al*. 2013
5'UTR, exon 2	pCFD4	*actin*-Cas9	830	Port *et al.* 2014
	Transgenic strain	**Crossed strain**		
5'UTR, exon 2	pCFD4	*actin*-Cas9	830	Port *et al*. 2014
5'UTR, exon 2	pCFD4	*nanos*-Cas9	830	Port *et al*. 2014
5'UTR, exon 12	pCFD4	*actin*-Cas9	26,862	Port *et al*. 2014
5'UTR, exon 12	pCFD4	*nanos*-Cas9	26,862	Port *et al*. 2014
Exons 2, 3, 4, 6	pCFD5	*actin*-Cas9	18,406	Port and Bullock 2016

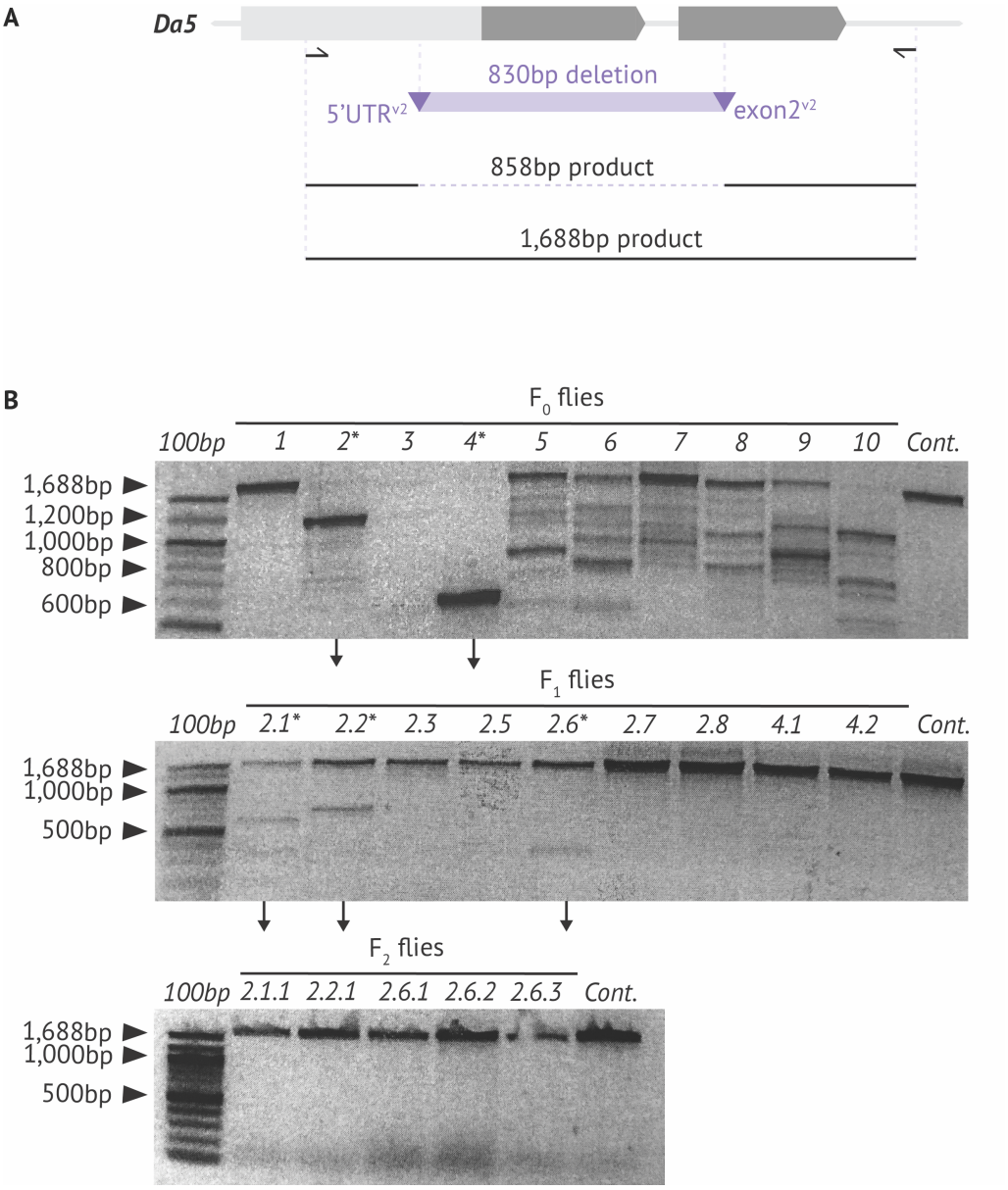


Figure 2.9 Evidence of CRISPR editing lost over subsequent generations

(**A**) Sizes of intended deletion and PCR products for pCFD4-5'UTR-exon2 CRISPR. The beginning of the *Dα5* gene is shown, including the 5'UTR (light grey bar), exons (dark grey bars) and introns (solid grey lines). Positions of sgRNAs (purple triangles) and PCR primers *Dα5_5'UTR_FC* and *Dα5_exon2_RD* (black arrows) are also shown. (**B**) Gel electrophoresis results for individual *actin-Cas9* flies injected with pCFD4-5'UTR-exon2 (F_0) and subsequent generations after crossing with *DbaI* (F_1 and F_2). Individuals giving rise to offspring in the next gel are marked (* and arrow). All PCR reactions are as per (A), with the wildtype 1,688bp product present in most samples and any shorter products representing possible CRISPR events. F_0 injectee *#2* gave rise to F_1 offspring with possible CRISPR products *(#2.1, #2.2, #2.6*), however only wildtype bands were then detected in their F_2 offspring. The control strain is *actin-Cas9*.

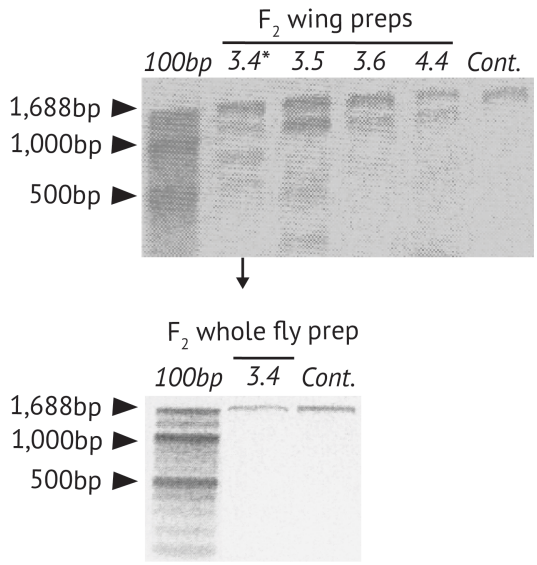


Figure 2.10 Evidence of CRISPR editing lost in subsequent DNA extractions

Gel electrophoresis results for individual F_2 offspring resulting from an initial F_0 cross between *nanos-Cas9* and the pCFD4-5'UTR-exon2 transgenic train. All PCR reactions are as per Figure 2.9, with the wildtype 1,688bp product present in all samples and any shorter products representing possible CRISPR events. DNA was first extracted from clipped wings and later from the whole fly. The wing prep for individual *#3.4* showed possible CRISPR products, however these were not detected in DNA extracted from the whole fly. The control strain is *nanos*-Cas9.

2.3.2 MiMIC insertions in *Dα5* disrupt larval development

2.3.2.1 Dα5$^{Mi-5'}$

All *Dα5$^{Mi-5'}$* homozygotes died by the early L3 stage. Most deaths occurred during larval moults, resulting in a buttoned-up phenotype (**Figure 2.11**). Thirty-four percent died during the first moult (M1) and 54% died during the second (M2). Many died early in the moult, as identified by the appearance of new mouthhooks. Others died late in the moulting process, with the old cuticle remaining attached to the posterior.

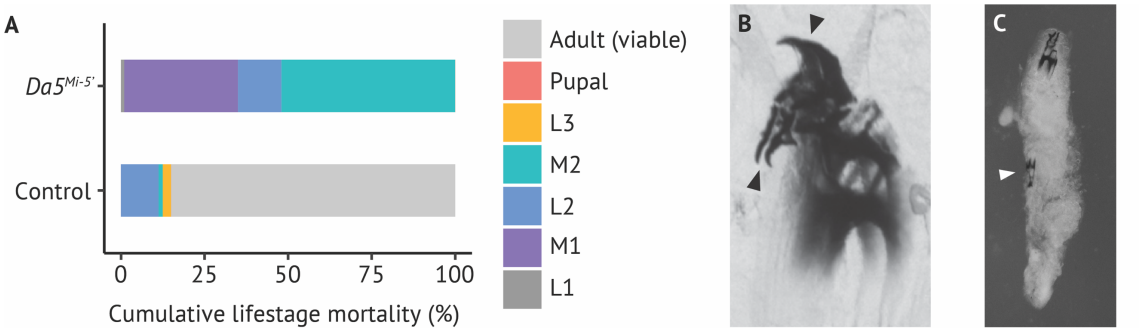


Figure 2.11 *Dα5*$^{Mi\text{-}5'}$ exhibits mid-moult mortality

(**A**) Cumulative percentage mortality at each lifestage. All *Dα5*$^{Mi\text{-}5'}$ larvae die by the early L3 stage, most commonly during larval moults (M1 and M2) (n = 330). Most *yw* control larvae survive through to adulthood (n = 80). (**B**) Many *Dα5*$^{Mi\text{-}5'}$ larvae die early during a moult, as indicated by two sets of mouthhooks (black arrowheads). (**C**) Some *Dα5*$^{Mi\text{-}5'}$ larvae die late during a moult with the old cuticle wrapped around the posterior (white arrowhead). Abbreviations: L1 (first larval instar), M1 (first-second instar moult), L2 (second larval instar), M2 (second-third instar moult), L3 (third larval instar).

Dα5$^{Mi\text{-}5'}$ larvae also exhibited impeded growth (**Figure 2.12**). While L1 mutant larvae are similar in body weight to background controls (*yw*), the average body weight of L2 and early L3 mutant larvae relative to control larvae was significantly lower, at 51% ($p < 0.01$, Student's t-test) and 9% ($p < 0.001$), respectively.

Truncation of *Dα5*$^{Mi\text{-}5'}$ transcripts was verified by qRT-PCR, which indicated no significant difference 5' of the truncation, and a significant 36-fold decrease in the presence of transcript 3' of the truncation ($p < 0.001$, Student's t-test) (**Figure 2.13**). Transcript levels for two of Dα5's binding partners, *Dα6* and *Dα7*, did not differ significantly between *Dα5*$^{Mi\text{-}5'}$ and the control. Another line, *Dα5*$^{Mi\text{-}3'}$ (*BDSC #59218*) was also available, however the MiMIC in this strain is inserted in the reverse direction. This means the cassette does not truncate the gene and the strain was therefore not examined.

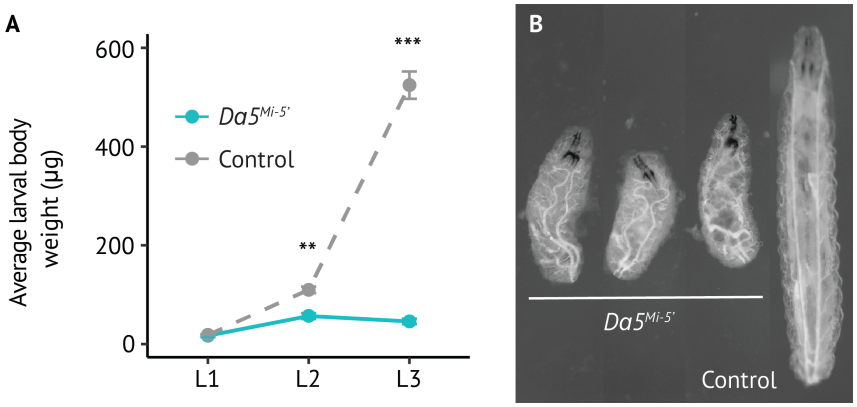


Figure 2.12 *Dα5*$^{Mi\text{-}5'}$ has low larval body weight

(**A**) Average body weight at each developmental stage. Body weight is significantly low in *Dα5*$^{Mi\text{-}5'}$ in the L2 and L3 stages. Error bars indicate SEM ($n \geq 50$, ** $p < 0.01$, *** $p < 0.001$, Student's *t*-test). (**B**) Representative *Dα5*$^{Mi\text{-}5'}$ larvae at time of death (M2), versus a time-matched early L3 *yw* control larva, to demonstrate difference in body size. Abbreviations: L1 (first larval instar), L2 (second larval instar), L3 (third larval instar).

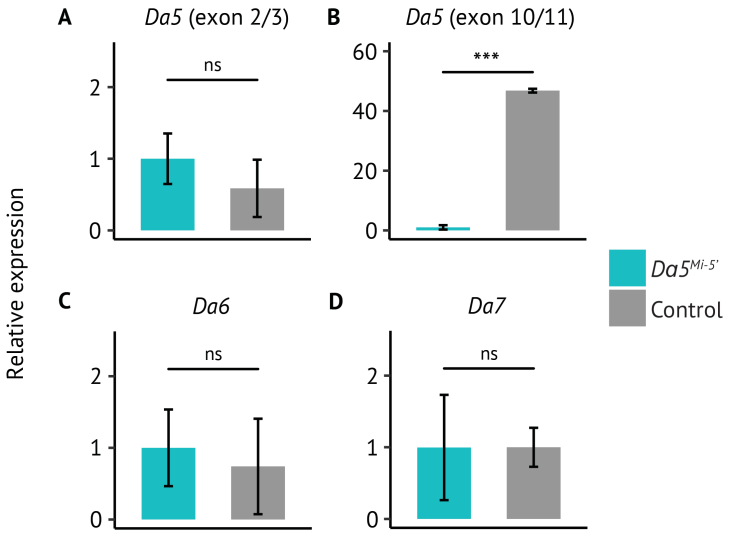


Figure 2.13 Relative expression of nAChR subunits in *Dα5*$^{Mi\text{-}5'}$ larvae

qRT-PCR was used to measure transcript levels for (**A**, **B**) *Dα5,* (**C**) *Dα6*, and (**D**) *Dα7* in L2 *Dα5*$^{Mi\text{-}5'}$ larvae versus *yw* control larvae. While no significant difference was detected for *Dα5* transcript upstream of the MiMIC cassette (**A**), a highly significant 36-fold reduction was detected in *Dα5* transcript downstream of the MiMIC cassette (**B**). Error bars indicate SD ($n \geq 3$ biological replicates, *** $p < 0.001$, Student's t-test).

2.3.2.2 Dα5$^{TG4\text{-}5'}$ and Dα5$^{TG4\text{-}3'}$

Developmental mortality was also examined in homozygotes for two alternative *Dα5* truncation lines (**Figure 2.14**). For *Dα5*$^{TG4\text{-}5'}$ (a line derived directly from *Dα5*$^{Mi\text{-}5'}$), the majority died during M2 (56%), with some escapers successfully moulting and dying later as L3 (19%). For *Dα5*$^{TG4\text{-}3'}$ (derived from *#59218*, but with the cassette in an orientation that truncated the gene), mortality occurred during L2 (40%) and M2 (52%). In both TG4 lines, an obvious difference in body size was observed (but not measured) in early L3 larvae relative to control larvae.

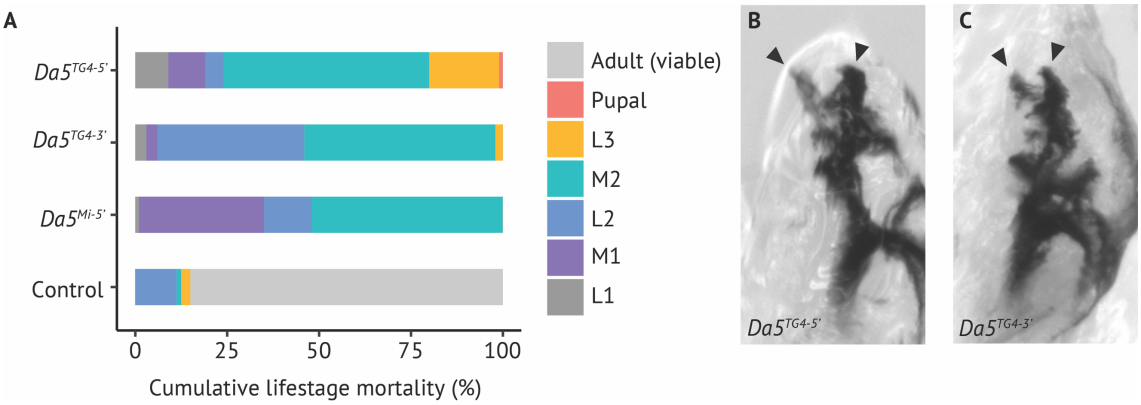


Figure 2.14 *Dα5*$^{TG4\text{-}5'}$ and *Dα5*$^{TG4\text{-}3'}$ exhibit mid-moult mortality

(**A**) Cumulative percentage mortality at each lifestage. Most *Dα5*$^{TG4\text{-}5'}$ larvae and all *Dα5*$^{TG4\text{-}3'}$ larvae die by the early L3 stage, most commonly during larval moults (M1 and M2) ($n > 40$). Results for *Dα5*$^{Mi\text{-}5'}$ and the *yw* control are repeated from Figure 2.10 for ease of comparison. (**B**) *Dα5*$^{TG4\text{-}5'}$ and (**C**) *Dα5*$^{TG4\text{-}3'}$ larvae often have two sets of mouthhooks at time of death (black arrowheads), indicative of mid-moult mortality. Abbreviations: L1 (first larval instar), M1 (first-second instar moult), L2 (second larval instar), M2 (second-third instar moult), L3 (third larval instar).

2.3.3 Larvae have abnormal wandering, movement and feeding behaviours

2.3.3.1 Wandering

In vials, $D\alpha5^{Mi\text{-}5'}$, $D\alpha5^{TG4\text{-}5'}$ and $D\alpha5^{TG4\text{-}3'}$ L2 larvae were frequently observed wandering away from their food source prior to M2 developmental arrest. This behaviour was quantified for $D\alpha5^{Mi\text{-}5'}$ and $D\alpha5^{TG4\text{-}3'}$ by placing synchronised L2 larvae into yeast paste in the centre of an arena and counting larvae outside the yeast paste at 8 hour intervals (56, 64, 72 hours AEL) (**Figure 2.15**). The percentage of $D\alpha5^{Mi\text{-}5'}$ larvae exhibiting precocious wandering behaviour reached 66% at 72 hours AEL. Larvae typically followed a direct path to the edges of the plate, with many crawling up the sides and onto the underside of the lid where they quickly became desiccated and did not attempt to pupariate. $D\alpha5^{TG4\text{-}3'}$ larvae exhibited a similar precocious wandering behaviour, reaching 52% at 72 hours AEL. At all timepoints, for $D\alpha5^{Mi\text{-}5'}$ and $D\alpha5^{TG4\text{-}3'}$, wandering was significantly higher than the control ($p < 0.001$, Tukey's test). Control larvae continued to feed throughout the experiment, with individuals occasionally venturing outside the yeast paste before quickly returning.

2.3.3.2 Movement

Total larval movement was measured in $D\alpha5^{Mi\text{-}5'}$ larvae using the Wiggle Index assay (Denecke *et al.* 2015). Despite the ability to disperse far from their food source, $D\alpha5^{Mi\text{-}5'}$ larvae exhibit significantly reduced net movement as L2 larvae ($p < 0.001$, Student's *t*-test) (**Figure 2.16**).

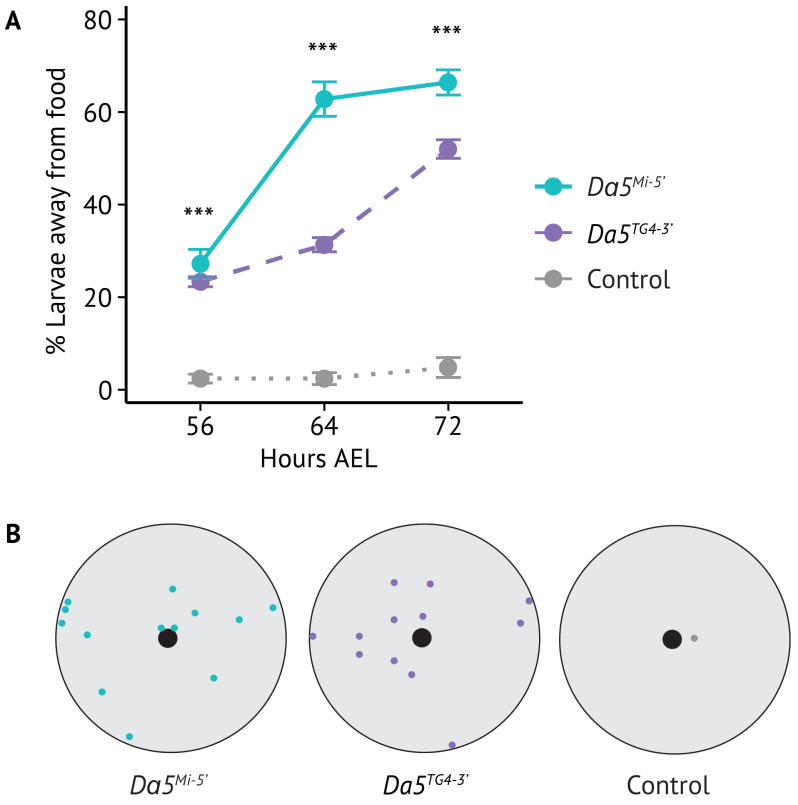


Figure 2.15 *Dα5*$^{Mi\text{-}5'}$ and *Dα5*$^{TG4\text{-}3'}$ exhibit precocious wandering behaviour

(**A**) A significant proportion of *Dα5*$^{Mi\text{-}5'}$ and *Dα5*$^{TG4\text{-}3'}$ larvae wander away from their food source during the L2 stage compared to *yw* control larvae. Error bars indicate SEM (n = 250, *** $p < 0.001$, Tukey's test). (**B**) Representative plates show the positions of larvae outside the food source (black dot) at 56 hours AEL. Abbreviations: AEL (after egg laying).

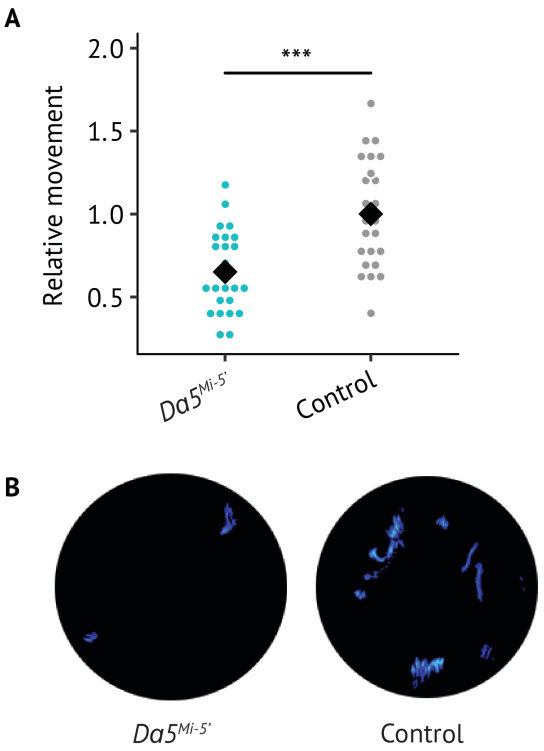


Figure 2.16 *Dα5*$^{Mi\text{-}5'}$ larvae have reduced basal movement

(**A**) Wiggle Index analysis at 48 hours AEL reveals significantly reduced movement in *Dα5*$^{Mi\text{-}5'}$ larvae relative to *yw isogenic* controls. Black diamonds indicate the mean (n = 360, *** $p < 0.001$, Student's t-test). (**B**) Representative Wiggle Index heat maps show larval movement inside a single well during a 30 second recording. Abbreviations: hours AEL (after egg laying).

2.3.3.3 Feeding

To determine if feeding ceased prior to wandering, food intake was measured in pre-wandering L2 *Dα5*$^{Mi\text{-}5'}$ larvae. At 50 hours AEL (following 1 hour starvation and 1 hour feeding) half of *Dα5*$^{Mi\text{-}5'}$ larvae had an empty midgut (**Figure 2.17**) ($p < 0.001$, Student's *t*-test). Remaining *Dα5*$^{Mi\text{-}5'}$ larvae had food occupying 2%-48% of the midgut (median = 6%). The positions of the boluses varied, with no apparent blockages along the alimentary canal. Control larvae continued feeding throughout the 1 hour session, with food occupying 58% of the midgut on average. To test whether the cessation of feeding might be associated with satiation, the expression level of the starvation response gene *Lip3* was measured in pre-wandering L2 larvae using qRT-PCR (Zinke *et*

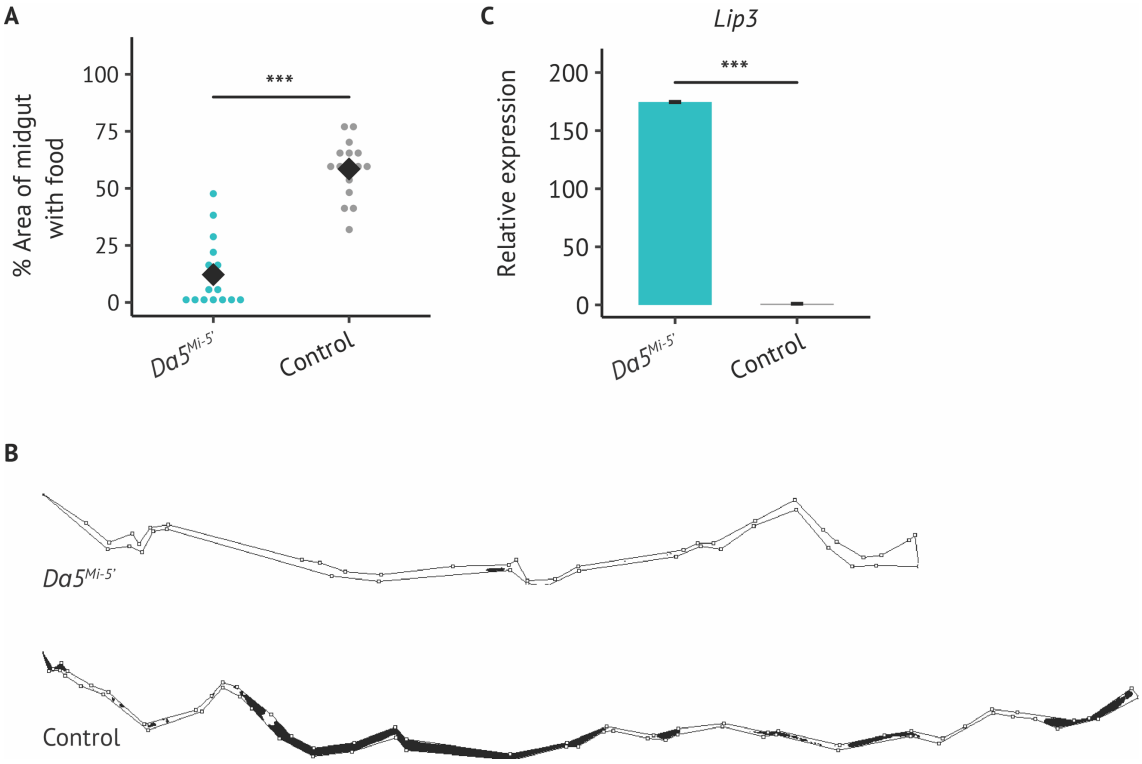


Figure 2.17 *Dα5*$^{Mi\text{-}5'}$ larvae stop feeding during the second instar stage

(**A**) Midguts dissected at 50 hours AEL contain significantly less food in *Dα5*$^{Mi\text{-}5'}$ larvae compared to *yw* controls. Black diamonds indicate the mean ($n \geq 10$, *** $p < 0.001$, Student's t-test). (**B**) Representative dissections show the amount of food (black) in the midgut (outlined) at 50 hours AEL. (**C**) qRT-PCR reveals highly significant 174-fold upregulation of the starvation response gene *Lip3* in *Dα5*$^{Mi\text{-}5'}$ larvae at 48 hours AEL. Error bars indicate SD ($n \geq 3$ biological replicates, *** $p < 0.001$, Student's t-test). Abbreviations: AEL (after egg laying).

al. 1999). A highly significant 174-fold up-regulation of *Lip3* transcripts was detected in *Dα5*$^{Mi\text{-}5'}$ larvae, indicating a severely starved state prior to wandering ($p < 0.001$, Student's *t*-test). A schematic depicting the timing of cessation of feeding relative to wandering, *Lip3* detection and other key observations is provided in **Figure 2.18**.

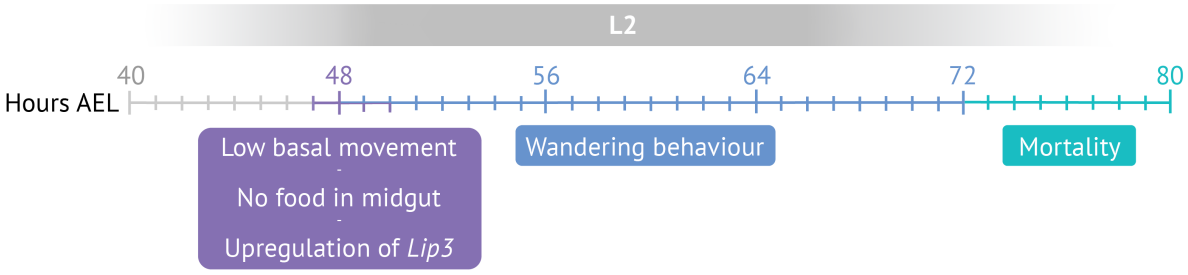


Figure 2.18 Timing of observations for $D\alpha5^{Mi\text{-}5'}$

A summary of the events leading up to mortality, mostly occurring during the L2 (second larval instar stage). The timeline shows hours AEL (after egg laying).

2.3.4 Loss of Dα5 disrupts a hormone pathway

2.3.4.1 Comparison with existing literature

Based on existing literature, it appears loss of Dα5 phenocopies altered signalling of the neuropeptide hugin or the hormone ETH (**Table 2.12**). Increased hugin signalling leads to mid-moult mortality, a buttoned-up cuticle, precocious wandering and precocious cessation of feeding (Meng *et al.* 2002, Schoofs *et al.* 2014). Deletion or misexpression of ETH has the same effects, although no wandering phenotypes were previously described (Park *et al*. 2002). Using a wandering assay, I have shown that disruption of *ETH* via RNAi also results in precocious wandering (**Figure 2.19**). At all timepoints, significantly more *ETH* RNAi larvae (w^{1118}*; +; tub-GAL4/UAS-ETHRNAi*) were found outside their food source compared to GAL4-only controls (w^{1118}*; +; tub-GAL4/+)* ($p < 0.01$, $p < 0.001$, Student's *t*-test).

Table 2.12 Comparison of *Dα5*$^{Mi\text{-}5'}$ with previously-reported phenotypes

Phenotype	***Dα5*$^{Mi\text{-}5'}$**	***hugin***		***ETH***		
	MiMIC truncation	**overexpression**	**neuron activation**	**deletion mutant**	**ectopic injection**	**RNAi**
	Present study	*Meng et al. 2002*	*Schoofs et al. 2014*	*Park et al. 2002*	*Park et al. 2002*	*Present study*
Mortality	M1 / M2	M2	n/a	M1 / M2	M1 / M2	M1 / M2
Buttoned-up cuticle	✔	✔	n/a	✔	✔	✔
L2 wandering	✔	n/a	✔	n/a	n/a	✔
L2 cessation of feeding	✔	n/a	✔	✔	✔	n/a

Abbreviations: L2 (second larval instar), M1 (first-second instar moult), M2 (second-third instar moult), ETH (ecdysis triggering hormone)

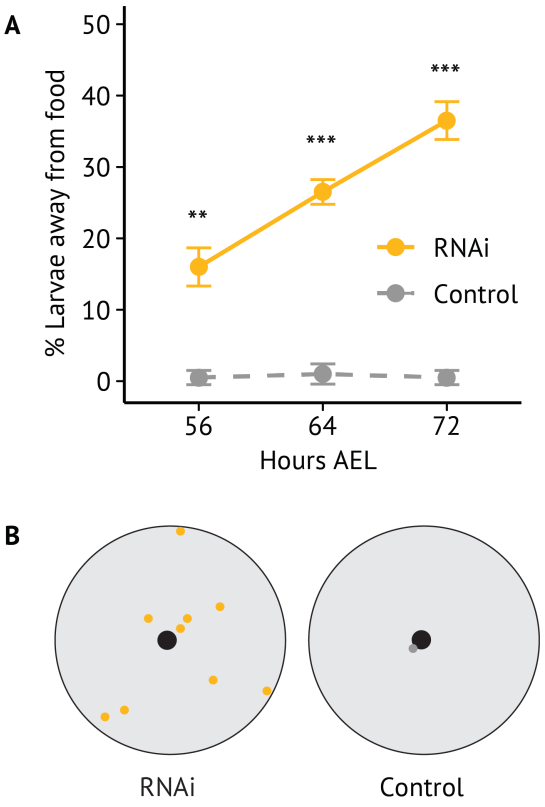


Figure 2.19 Knockdown of *ETH* causes precocious wandering behaviour

(**A**) A significant proportion of *ETH* RNAi larvae wander away from their food source during the L2 stage compared to GAL4-only control larvae. Error bars indicate SEM (n = 250, *** $p < 0.001$, Student's t-test). (**B**) Representative plates show the positions of larvae outside the food source (black dot) at 56 hours AEL. Abbreviations: AEL (after egg laying).

2.3.4.2 Hormone qRT-PCR

To test if the $D\alpha5^{Mi\text{-}5'}$ phenotype was associated with a change in expression of *hugin* or *ETH*, qRT-PCR was used to measure transcript levels in L2 larvae (**Figure 2.20**). Other hormones in the moulting hormone cascade were also measured, including *EH* and *CCAP*. The 20E response gene *E75B* was measured as a proxy for the steroid hormone 20E. The only significant result observed was for *ETH*, with a 32-fold reduction in $D\alpha5^{Mi\text{-}5'}$ L2 larvae relative to the control ($p < 0.001$, Student's t-test).

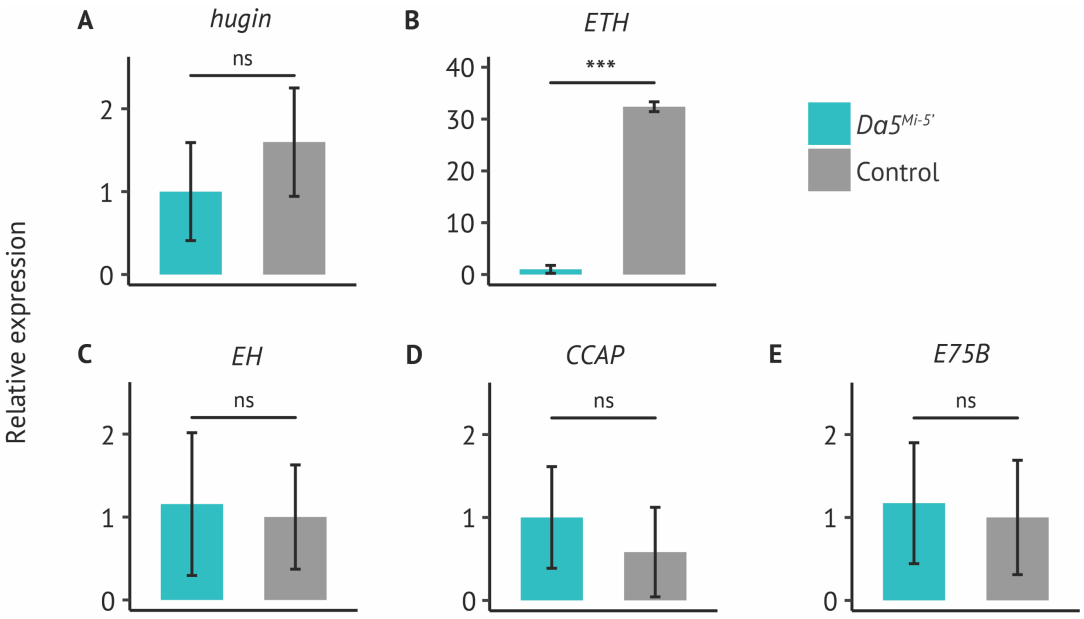


Figure 2.20 Hormone levels in $D\alpha5^{Mi\text{-}5'}$ larvae

qRT-PCR was used to measure transcript levels for the neuropeptide hormones (**A**) *hugin,* (**B**) *ETH* (ecdysis triggering hormone), (**C**) *EH* (eclosion hormone), and (**D**) *CCAP* (*crustacean cardioactive peptide*) in $D\alpha5^{Mi\text{-}5'}$ L2 larvae versus *yw* control larvae. (**E**) The ecdysone-induced gene *E75B* (*ecdysone-induced protein 75B*) was measured as a proxy for the steroid hormone ecdysone. (**B**) A highly significant 32-fold reduction was detected for *ETH*. Error bars indicate SD ($n \geq 3$ biological replicates, *** $p < 0.001$, Student's *t*-test).

2.3.5 Dα5 may be required in the PG or PG neurons

2.3.5.1 Tissue-specific RNAi knockdown

To identify tissues where Dα5 may be required, the GAL4-UAS system was used to achieve tissue-specific RNAi knockdown (Brand and Perrimon 1993). The most frequent stage of developmental mortality was recorded for each knockdown with a range of stages observed (**Table 2.13**). Of all tissue-specific drivers tested, only PG knockdown phenocopied $D\alpha5^{Mi\text{-}5'}$. Knockdown using two independent PG drivers, *5'phm-GAL4* and *Feb36-GAL4*, resulted in developmental mortality predominantly during M2. Precocious wandering and buttoned-up cuticles were also observed. Pan-

Table 2.13 Most frequent stage of mortality for tissue-specific RNAi knockdown

Tissue	GAL4 driver	18°C	22°C	25°C
PG	5'*phm*	L3-Ph	M2	M2
PG + CA	*Feb36*	L3-Ph	M2-Ph	M2
CNS	*elav*	viable (weak)	viable (weak)	Ph
CA	5'*6g2*	viable	viable	viable
CC	*Akh*	viable	viable	viable
PTTH neurons	*ptth*	viable	viable	viable
serotonergic neurons	*trh*	viable	viable	viable
hugin neurons	*hugin*	viable	viable	viable
Inka cells	*ETH*	viable	viable	viable
Dα5-expressing cells	$D\alpha5^{TG4\text{-}5'}$	viable	viable	viable
Dα5-expressing cells	$D\alpha5^{TG4\text{-}3'}$	viable	viable	viable
ubiquitous	*da*	viable	L3-Ph	embryo
ubiquitous	*tub*	embryo	embryo	embryo

Abbreviations: PG (prothoracic gland), CA (corpus allatum), CC (corpora cardiaca), PTTH (prothoracicotropic hormone), L3 (third larval instar), M2 (second-third instar moult), Ph (pharate adult).

neuronal knockdown was less severe, with mortality predominantly in pharate and newly eclosed adults. These adults exhibited weak movement and all had abnormal eye morphology (**Figure 2.21**).

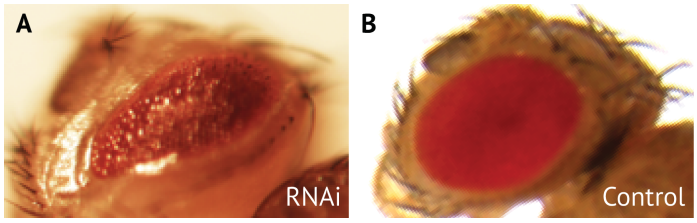


Figure 2.21 Pan-neuronal RNAi knockdown of *Dα5* causes eye phenotype

(**A**) At all temperatures, *elav-GAL4* RNAi (*elav-GAL4/+; +; UAS-Dα5RNAi/+*) adults exhibit abnormal eye morphology. (**B**) Wildtype eye morphology in a control adult (*elav-GAL4/+; +; +*).

Knockdown in other RG tissues (the corpus allatum, CA, and corpora cardiaca, CC), in neurons innervating the PG (PTTH and serotonergic neurons), in hugin neurons, and in ETH-producing Inka cells each had no effect on viability. Particularly noteworthy, knockdown driven by $D\alpha5^{TG4\text{-}5'}$ or $D\alpha5^{TG4\text{-}3'}$ also had no effect on viability, potentially revealing an incomplete expression profile in these *Dα5*-specific drivers.

Ubiquitous knockdown using the *da-GAL4* driver phenocopied $D\alpha5^{Mi\text{-}5'}$ at 22°C, but was embryonic lethal at 25°C (**Table 2.13**). *tub-GAL4* ubiquitous knockdown was embryonic lethal at all temperatures. qRT-PCR indicates the increased severity of these ubiquitous knockdowns (versus the $D\alpha5^{Mi\text{-}5'}$ truncation) was not due to simultaneous off-target knockdown of the *Dα6* or *Dα7* transcripts (**Figure 2.22**). qRT-PCR results for *Dα5* were inconsistent, with no significant difference 5' (upstream) of the RNAi hairpin, and a significant increase 3' of the RNAi hairpin (484 fold, $p < 0.001$, Student's *t*-test). However, semi-quantitative PCR for the entire *Dα5* cDNA indicated knockdown was successful (-3.5 fold, $p < 0.001$, Student's *t*-test) (**Figure 2.23**). Moreover, ubiquitous overexpression of *Dα5* cDNA (*+; +; da-GAL4/UAS-Dα5cDNA*) does not have an effect on viability, indicating the RNAi results are unlikely to be caused by inadvertent overexpression in RNAi individuals.

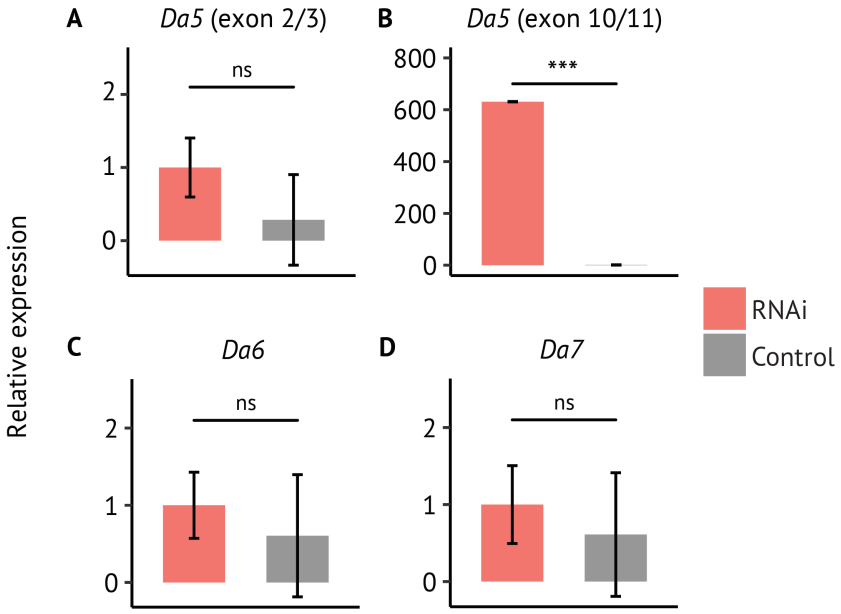


Figure 2.22 Relative expression of nAChR subunits in *da-GAL4* RNAi larvae

qRT-PCR was used to measure transcript levels for (**A**, **B**) *Dα5,* (**C**) *Dα6*, and (**D**) *Dα7* in L2 *da-GAL4* RNAi larvae (w^{1118}*; +; da-GAL4/UAS-Dα5RNAi*) versus control larvae (w^{1118}*; +; da-GAL4/+*) reared at 22°C. Results for *Dα5* were inconsistent and unexpected, with no significant difference detected with *Dα5_RT_ex2_F/Dα5_RT_ex3_R* primers (**A**), and a highly significant 484-fold increase detected using *Dα5_RT_ex10_F/Dα5_RT_ex11_R* primers (**B**). Error bars indicate SD ($n \geq 3$ biological replicates, *** $p < 0.001$, Student's t-test).

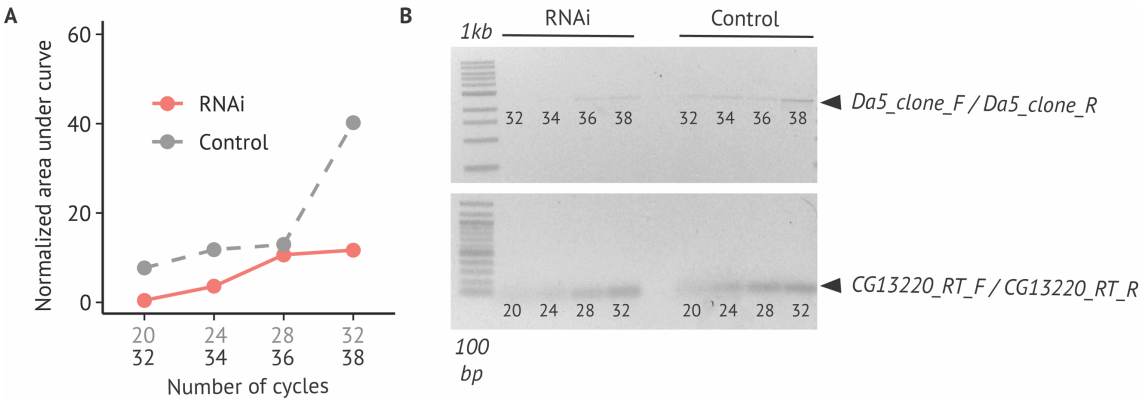


Figure 2.23 Semi-quantitative PCR analysis of *Dα5* in *da-GAL4* RNAi larvae

(**A**) Gel band intensities (area under curve) for *Dα5* after increasing number of PCR cycles, normalised to *CG13220* band intensities. Indicates *Dα5* transcript levels are reduced in *da-GAL4* RNAi larvae (w^{1118}*; +; da-GAL4/UAS-Dα5RNAi*) relative to control larvae (w^{1118}*; +; da-GAL4/+*) reared at 22°C. The x-axis shows the number of PCR cycles for *Dα5* (black) and *CG13220* (grey). (**B**) The gel used to calculate band intensities in (A). The number of PCR cycles is noted under each band. *ImageJ* was used to quantify area under curve (Fiji, version 2.0.0, Schindelin *et al.* 2012).

2.3.5.2 TG4 expression patterns

To visualise the expression pattern of *Dα5* in larval tissues, the *UAS-mCD8GFP* reporter was driven by $Dα5^{TG4\text{-}5'}$ and $Dα5^{TG4\text{-}3'}$ (**Figure 2.24**). For both drivers, a strong signal was only detected in the CNS. Expression was not detected in PG cells, despite convincing results for PG-specific RNAi knockdown. Instead, GFP was detected in the PG-innervating neurons (PGNs). Expression of *Dα5* in PGNs was also supported by single-cell RNA-seq data, with *Dα5* transcripts detected in 41% of *ptth*-expressing cells, and in 64% of *trh*-expressing cells (Ravenscroft *et al.* 2021).

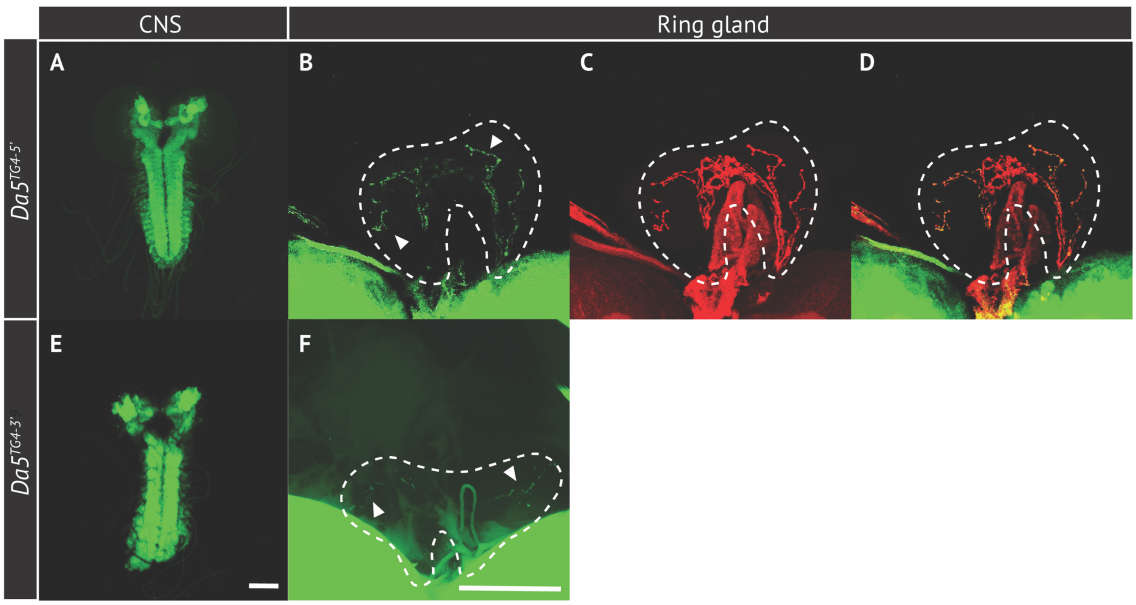


Figure 2.24 $D\alpha5^{TG4\text{-}5'}$ and $D\alpha5^{TG4\text{-}3'}$ are expressed in the CNS and PGNs

The expression patterns for $D\alpha5^{TG4\text{-}5'}$ and $D\alpha5^{TG4\text{-}3'}$ were observed in L3 larvae using the *UAS-mCD8GFP* reporter. (A) Expression from $D\alpha5^{TG4\text{-}5'}$ was detected in the CNS, and (**B**) the PGNs (white arrow heads). (**C**) HRP staining highlights neuronal membranes in the ring gland. (**D**) Merge. (**E**) Expression from $D\alpha5^{TG4\text{-}3'}$ was also detected in the CNS, and (**F**) the PGNs (white arrow heads). Dashed white lines mark the outline of the ring gland. Scale bars are 100µm. Abbreviations: CNS (central nervous system), PGNs (prothoracic gland neurons).

As noted above (*section 2.3.5.1*), knockdown in these two sets of known PGNs had no effect on viability. There are several theories that explain these incongruent results (fully discussed in *section 2.4.4*). One possibility is neuronal expression from "PG-specific" GAL4s, resulting in simultaneous PG-and-neuronal knockdown. The observation of reporter expression in a similar subset of neurons for both PG drivers used supports this (**Figure 2.25**). *Dα5* expression was not detected in the Inka cells, the eye imaginal disks, nor elsewhere in the larval body.

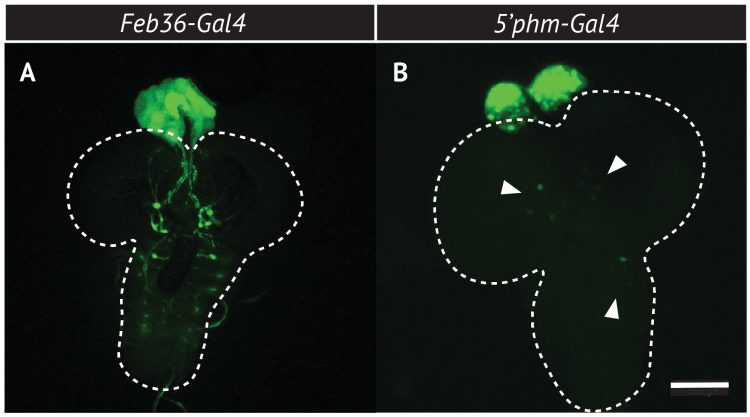


Figure 2.25 PG driver expression in the CNS

The expression patterns for (**A**) *Feb36-GAL4* and (**B**) *5'phm-GAL4* were observed in L3 larvae using the *UAS-nGFP* reporter. Both exhibit strong expression in the PG (prothoracic gland) and limited expression in a similar region of the CNS (central nervous system). Dashed white lines mark the outline of the CNS and white arrow heads highlight less visible neuronal GFP expression. Scale bar is 100µm.

2.3.6 Loss of Dα5 in adults

2.3.6.1 Post-larval deGradFP knockdown

The temperature-sensitive deGradFP protein knockdown system was used in an attempt to investigate post-larval knockdown of Dα5 (Caussinus *et al.* 2012, Nagarkar-Jaiswal *et al.* 2015). deGradFP works by targeting any GFP-tagged protein for ubiquitination, resulting in that protein being degraded by proteasomes. Driving *UAS-deGradFP* in a $D\alpha5^{Mi\text{-}5'}/D\alpha5\text{-}GFP$ background ensures the GFP-tagged Dα5 is the only available Dα5 protein, and pairing this with GAL80 provides temporal control of *UAS-deGradFP* expression.

To test the efficiency of this system with Dα5, deGradFP animals ($D\alpha5^{Mi\text{-}5'}/D\alpha5\text{-}GFP$; *da-GAL4/UAS-deGradFP-GAL80*) were first reared at the restrictive temperature (28°C) from the embryonic stage. This caused no obvious phenotypes and no change in adult viability compared to controls reared at the permissive temperature (18°C). This result indicates the deGradFP system may not be sufficiently knocking down Dα5. Consistent

with this result, when deGradFP animals were shifted to the restrictive temperature later upon pupariation, this also had no effect on viability.

A benefit of the deGradFP system is that knockdown can usually be visualised by loss of GFP signal (Nagarkar-Jaiswal *et al.* 2015). This is because many stained GFP-tagged MiMIC lines provide a well-defined expression pattern. Unfortunately, the tagged *Dα5-GFP* line produced a weak signal, and although this could be enhanced with primary or secondary staining, fluorescence levels were inconsistent between stained samples (**Figure 2.26**). Furthermore, staining appeared to disproportionately increase background fluorescence, and did not enhance the more defined TG4-like expression pattern through the mushroom bodies and ventral nerve cord. Detecting GFP using western blotting also proved challenging (see *section 2.3.8.2*) so neither method of detecting GFP knockdown was pursued further.

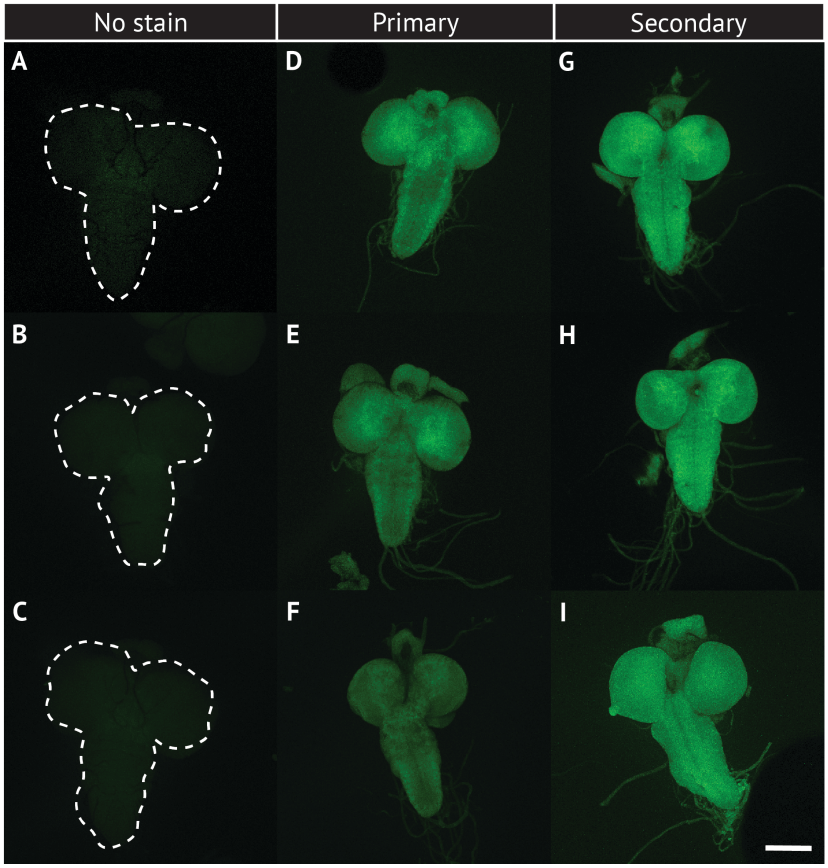


Figure 2.26 *Dα5-GFP* expression in the CNS

The expression pattern of the tagged *Dα5-GFP* protein was observed in L3 larvae using three levels of staining. Three replicates are shown for each staining protocol. (**A, B, C**) Without staining, only a weak GFP signal is detected. Dashed white lines mark the outline of the CNS (central nervous system). (**D, E, F**) The GFP signal is stronger and more defined after staining with conjugated primary antibody. Expression can be seen in the mushroom bodies and ventral nerve cord. However, there is inconsistency in the intensity between samples, with a stronger signal shown in (D) and (E) relative to (F). (**G, H, I**) More GFP is detected after staining with conjugated secondary antibody, however this is largely due to increased background fluorescence. The signal in the mushroom bodies and ventral nerve cord as seen in (D, E, F) was not enhanced here. Scale bar is 100µm.

2.3.6.2 Longevity, fertility, and climbing performance in heterozygous adults

To investigate any fitness costs associated with dosage in heterozygous $D\alpha5^{Mi\text{-}5'}$ adults, $D\alpha5^{Mi\text{-}5'}$ and the *yw* control were each crossed to the independent background line w^{1118}. F_1 adult offspring were then examined for longevity, fertility and climbing performance. No significant difference in longevity was observed, with both heterozygous genotypes exhibiting a median survival of 68 days and a similar survival curve ($p > 0.05$, Cox-Mantel test) (**Figure 2.27**). $D\alpha5^{Mi\text{-}5'}/D\alpha5^{w1118}$ exhibited significantly reduced fertility over the first 12 days of sexual maturity (day 4, day 7, day 12 $p < 0.01$, Student's *t*-test) but for the remainder of their lifespan, females laid a similar number of viable eggs as the control (**Figure 2.27**). Negative geotaxis assays performed on three-day-old adults revealed no significant difference in climbing performance ($p > 0.05$, Student's *t*-test) (**Figure 2.27**).

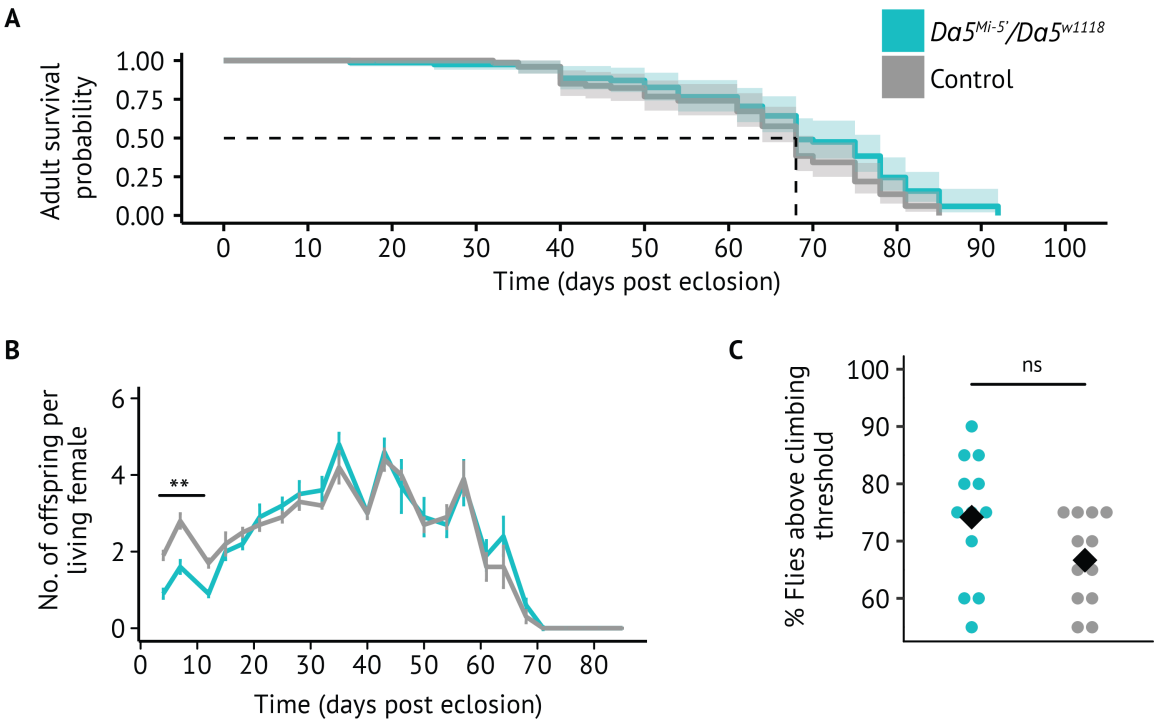


Figure 2.27 Fitness of heterozygous $D\alpha5^{Mi\text{-}5'}/D\alpha5^{w1118}$ adults

$D\alpha5^{Mi\text{-}5'}$ and the *yw* control strain were each crossed to w^{1118} and the F_1 adult offspring were used to investigate any fitness costs associated with dosage in adult heterozygotes. (**A**) A Kaplan-Meier survival plot with black dashed lines marking median longevity. Median longevity was 68 days for both groups and there was no significant difference in the survival curve ($n = 80$, $p > 0.05$, Cox-Mantel test). (**B**) Number of viable eggs laid per female per day, throughout lifespan. $D\alpha5^{Mi\text{-}5'}/D\alpha5^{w1118}$ females lay significantly fewer viable eggs over the first 12 days ($n = 40$, ** $p < 0.01$, Student's *t*-test) but for the remainder of their lifespan, females laid a similar number of viable eggs as the control. (**C**) Negative geotaxis performance was not significantly different to the control ($n = 80$, $p > 0.05$, Student's *t*-test).

2.3.7 Attempts to verify loss of Dα5 as the cause of mortality

Up to this point, it has been assumed that loss of Dα5 was causing the lethal phenotype observed in $D\alpha5^{Mi\text{-}5'}$, $D\alpha5^{TG4\text{-}5'}$, $D\alpha5^{TG4\text{-}3'}$, ubiquitous RNAi and PG-specific RNAi. However, the lack of any phenotype observed in $D\alpha5^{TG4\text{-}5'}$ RNAi, $D\alpha5^{TG4\text{-}3'}$ RNAi or deGradFP crosses was concerning. Furthermore, many of the Dα5 strains exhibit unexpected results in complementation (*section 2.3.7.1*) and rescue experiments (*section 2.3.7.2*), hence the additional experiments to verify loss of Dα5 as the cause of mortality.

2.3.7.1 Complementation crosses

Various Dα5 strains became available over the course of the project, including the MiMIC lines and several deficiencies. All those that disrupt *Dα5* expression (i.e. all except *Dα5-GFP*) were homozygous lethal. Theoretically, when any of these strains are crossed together, if loss of Dα5 is the underlying cause of mortality, then the F_1 transheterozygous offspring would be expected to also exhibit mortality (i.e. they will fail to complement each other). Alternatively, if a second-site mutation is the cause of mortality, complementation should occur between the strains that possess different genetic backgrounds, resulting in viable F_1 transheterozygous offspring.

Complementation crosses between available Dα5 strains produced unexpected and inconsistent results (**Figure 2.28**). All crosses between different MiMIC lines, and between MiMIC lines and deficiencies, yielded viable F_1 offspring, indicating loss of Dα5 may not be the cause of mortality. However, it is also important to note that for crosses between different MiMIC lines which share the same genetic background, that these also yielded viable F_1 offspring, indicating a second-site mutation is also unlikely to be the cause of lethality. The only combination that failed to complement was Df^{6075}/Df^{9061} which exhibited embryonic lethality like its homozygous parental strains, however this combination of deficiencies also encompasses deletions of genes flanking Dα5.

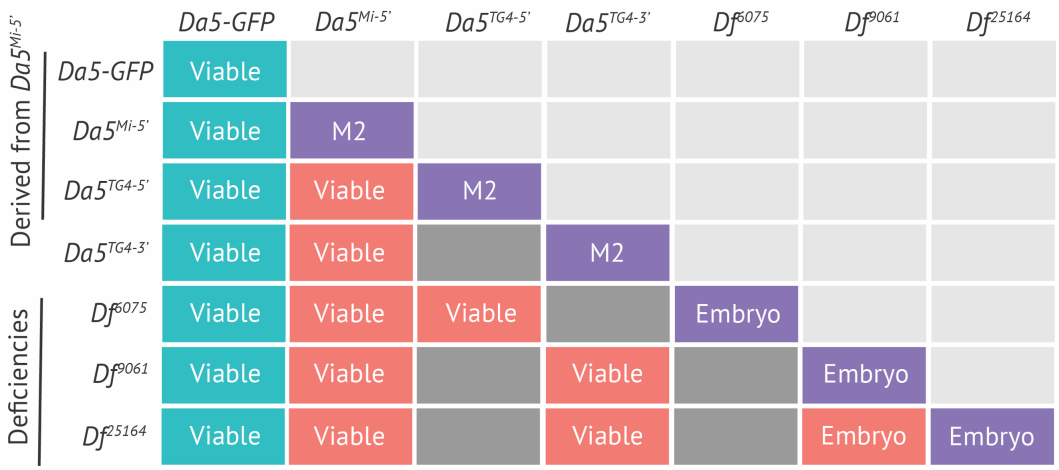


Figure 2.28 Complementation between different *Dα5* strains

Available MiMIC lines and deficiency lines were crossed, and the viability of F_1 transheterozygotes was recorded. In green are the F_1 that were expected to be viable – all possess the *Dα5-GFP* allele which itself is homozygous viable and expected to complement the other strains. In red are the F_1 that were expected to be inviable – all possess alleles that are themselves homozygous lethal (purple) and are not expected to complement. Only the Df^{6075}/Df^{9061} transheterozygotes showed the expected mortality. Some combinations were not tested (dark grey) as not all strains were available at the same times during the project. Abbreviations: M2 (second-third instar moult).

To investigate whether unexpected expression of Dα5 might be permitting these transheterozygotes to survive, cDNA was extracted from $Dα5^{Mi\text{-}5'}/ Dα5^{TG4\text{-}3'}$ and $Dα5^{Mi\text{-}5'}/Df^{9061}$ adults and tested for *Dα5* transcripts using a PCR with *Dα5_RT_ex10_F/Dα5_ex1_R* primers (**Figure 2.29**). A band corresponding to *Dα5* cDNA was detected in all samples tested, rendering complementation crosses inconclusive. Attempts were also made to detect a full-length *Dα5* cDNA using *Dα5_Clone_F/Dα5_Clone_R primers*, however technical issues prevented any products being detected in transheterozygote or control samples.

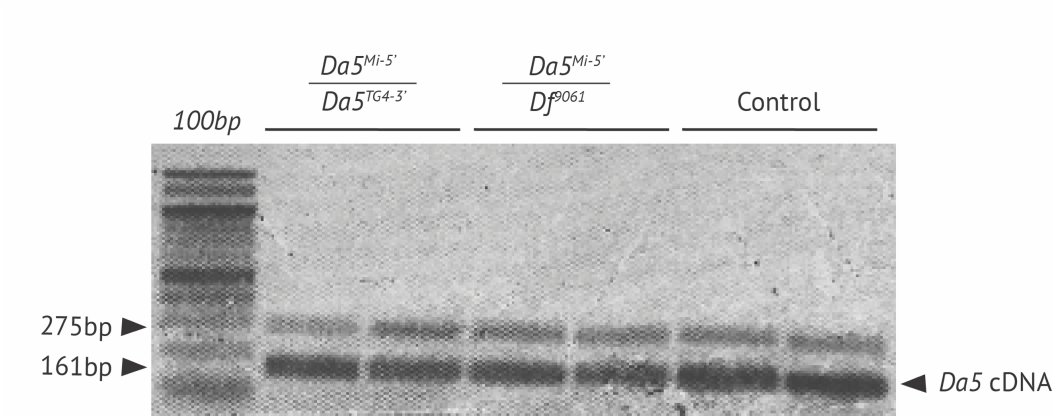


Figure 2.29 *Dα5* cDNA is detectable in transheterozygotes

cDNA was prepared from pooled adult F_1 offspring arising from $D\alpha5^{Mi\text{-}5'}/D\alpha5^{TG4\text{-}3'}$ and $D\alpha5^{Mi\text{-}5'}/Df^{9061}$ complementation crosses, and the *yw* control (two pools per genotype). Intron-spanning primers *Dα5_RT_ex10_F/Dα5_RT_ex11_R* were then used to detect *Dα5*. Notably, these primers are located downstream of the intended truncation points in $D\alpha5^{Mi\text{-}5'}$ and $D\alpha5^{TG4\text{-}3'}$. A 161bp band corresponding to intron-less *Dα5* cDNA was detected in all samples. The presence of a weaker 275bp band indicates some gDNA remained after DNase treatment of the extracted RNA.

2.3.7.2 Genetic rescue

Developmental mortality was examined in *Dα5*$^{Mi\text{-}5'}$ larvae ubiquitously expressing *UAS-Dα5cDNA* (*Dα5*$^{Mi\text{-}5'}$*; da-GAL4/UAS-Dα5cDNA*) (**Figure 2.30**). Only a minor improvement in survival was observed relative to non-rescued *Dα5*$^{Mi\text{-}5'}$. Like non-rescued *Dα5*$^{Mi\text{-}5'}$, 100% developmental mortality was observed and the majority died during M2 (50%). However, 10% of individuals were able to survive longer than non-rescued *Dα5*$^{Mi\text{-}5'}$, into the L3 stage.

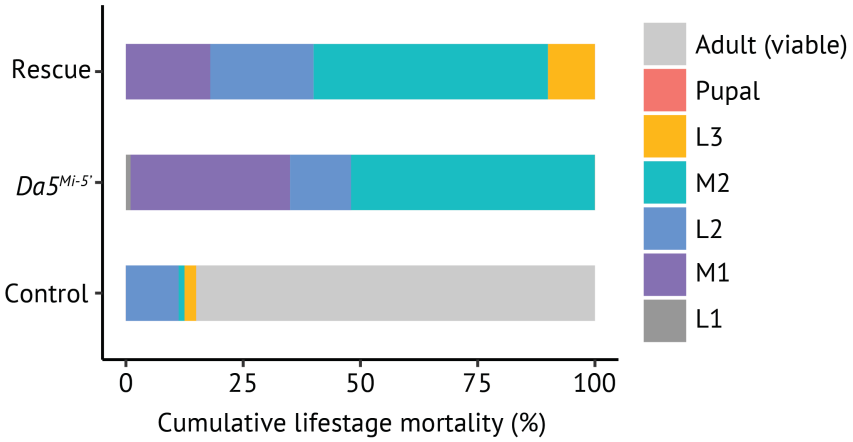


Figure 2.30 Ubiquitous expression of *UAS-Dα5cDNA* does not rescue *Dα5*$^{Mi\text{-}5'}$

Cumulative percentage mortality at each lifestage. When *UAS-Dα5cDNA* is driven by the ubiquitous *da-GAL4* driver in the *Dα5*$^{Mi\text{-}5'}$ background ('Rescue'), all larvae die by the early L3 stage, indicating rescue is inefficient ($n > 40$). Results for *Dα5*$^{Mi\text{-}5'}$ and the *yw* control are repeated from Figure 2.10 for ease of comparison. Abbreviations: L1 (first larval instar), M1 (first-second instar moult), L2 (second larval instar), M2 (second-third instar moult), L3 (third larval instar).

2.3.7.3 BAC clone rescue

Attempts were made to insert an 80kb BAC clone containing the full *Dα5* genomic region onto the third chromosome (**Figure 2.6**). This would have been crossed into the $D\alpha5^{Mi\text{-}5'}$ background to test for rescue of the $D\alpha5^{Mi\text{-}5'}$ phenotype, however injections did not produce any transgenic flies. Injections of two adjacent 80kb BAC clones containing a partial *Dα5* sequence were also attempted. These would have ruled out the possibility that rescue could be achieved by a flanking gene. These injections were also unsuccessful.

2.3.7.4 "Mapping" lethality to the MiMIC insertion

The $D\alpha5^{Mi\text{-}5'}$ chromosome was allowed to recombine with wild type L14 in heterozygous females, then crossed back over the intact $D\alpha5^{Mi\text{-}5'}$ chromosome. The surviving F_2 adult offspring were then scored molecularly for the presence of the $D\alpha5^{L14}$ allele (**Figure 2.7**). If flies homozygous for the MiMIC insertion are viable, all surviving offspring should be $D\alpha5^{L14}$-positive. Alternatively, if a second-site mutation on the $D\alpha5^{Mi\text{-}5'}$ chromosome is the cause of mortality, and there has been recombination between the cassette and the other locus, some offspring homozygous for the $D\alpha5^{Mi\text{-}5'}$ insertion allele should be able to survive. In all surviving F_2 offspring, the $D\alpha5^{L14}$ allele was detected (n = 50) (**Figure 2.31**), indicating individuals homozygous for the $D\alpha5^{Mi\text{-}5'}$ insertion likely died during development. This is convincing preliminary evidence that the MiMIC insertion, not a second-site mutation, is the cause of mortality.

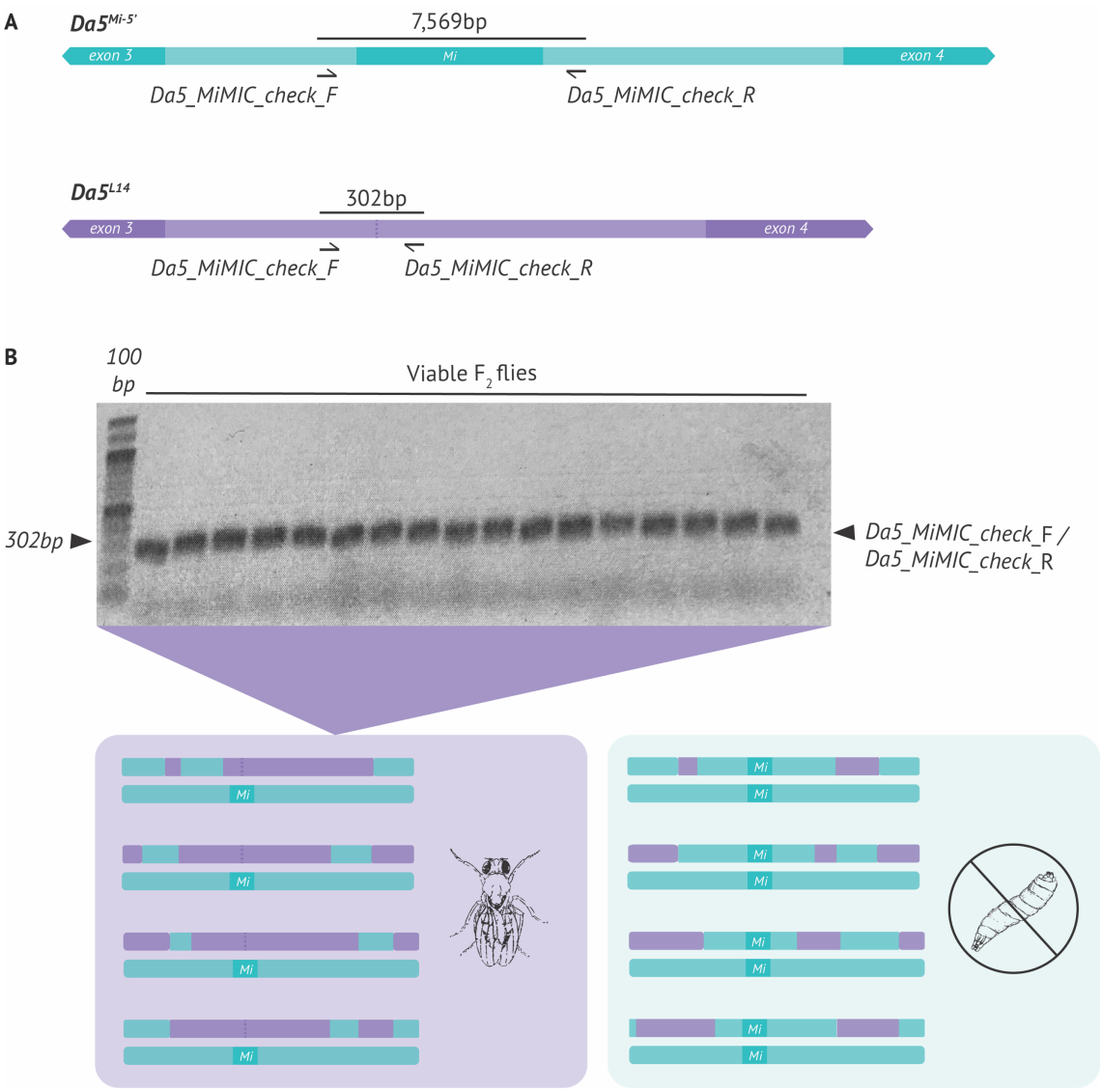


Figure 2.31 Lethality is associated with the MiMIC cassette

$D\alpha5^{Mi\text{-}5'}$ was allowed to recombine with Armenia Line 14 (L14) in a heterozygous female and then crossed back over the intact $D\alpha5^{Mi\text{-}5'}$ chromosome. (**A**) The F_2 offspring were then scored molecularly for the presence of the $D\alpha5^{L14}$ allele. When PCR extension time is limited to 30 seconds, primers flanking the MiMIC insertion site amplify the shorter $D\alpha5^{L14}$ allele, but not the longer $D\alpha5^{Mi\text{-}5'}$ allele. (**B**) Gel electrophoresis results for individual F_2 offspring. The $D\alpha5^{L14}$ allele was detected in all viable offspring, indicating individuals homozygous for the MiMIC cassette remain inviable. Schematic depictions of chromosome 2 are provided for $D\alpha5^{Mi\text{-}5'}$ (green), $D\alpha5^{Mi\text{-}5'}$:L14 (green/purple) and the MiMIC cassette (Mi) is labelled on $D\alpha5^{Mi\text{-}5'}$. Diagrams are not drawn to scale.

2.3.8 Analysis of Dα5's abnormal N-terminus

2.3.8.1 Bioinformatic analyses

Excluding the genus *Drosophila* and ignoring isoforms, BLASTp analysis of the first 312 amino acid residues of Dα5 yielded hits from six Dipteran species (**Figure 2.32, Table 2.14**). All six of these nAChR subunits have a large N-terminus upstream of their SP, ranging from 121 amino acids in *Bacterocera dorsalis* to 495 amino acids in *Ceratitis capitata*. However, sequence identity within these N-termini is minimal, with all BLASTp hits arising due to the 23 amino acid region surrounding the SP of Dα5 (KHSWIFLLIYLNLSAKVCLAGYH, SP underlined). Further BLASTp searches with these unique N-termini failed to return any significant hits, providing no new insight into their possible function. Full protein sequence alignments with Dα5 have a relatively low percentage identity (average 64%) but removal of all N-termini boosts identity in most cases to > 95%. The identity with Dα7 (Dα5's closest *Drosophila* orthologue) remains relatively low upon removal of all N-termini (average 77%). Thus, although all six Diptera subunits are labelled as α7 subunits, or as uncharacterised proteins, they in fact bear more similarity with Dα5 than with other insect α7 subunits. Nomenclature becomes problematic at this point, as they are clearly related to Dα5, but other insect α5s belong in a more distant group (**Figure 2.2**). It is also noteworthy that all hits originate from species classed as pests, either for their impact on crops (*Rhagoletis zephyria, C. capitata, B. latifrons, Zeugodacus cucurbitae, B. dorsalis*), or as vectors of human pathogens (*Musca domestica*). However, this is likely influenced by the bias towards sequencing pests versus non-pest species.

Within the *Drosophila* genus, the LBD and TM protein domains are highly conserved (99-100% identity) but significant variation is found in the N-terminus. N-terminus length varies from 269 amino acids in *D. sechelia*, to 309 amino acids in *D. erecta* and *D. willistoni*. Conservation is highest within the melanogaster subgroup (*D. simulans, D. sechelia, D. melanogaster, D. yakuba, D. erecta*). Outside the melanogaster group, full protein alignments of the N-terminus fall below 80% identity. It is worth noting that the *D. sechelia* sequence used is a concatenation of two predicted peptides (GM15476

and GM15477), each corresponding to the N-terminus and core nAChR receptor, respectively.

The long N-terminus was not found in seven other species investigated, which included representatives from Diptera, Lepidoptera, Hemiptera, Hymenoptera and Coleoptera. With the exception of *A. gambiae*, these non-*Drosophila* subunits belong in a different phylogenetic group (the insect α5 group) than Dα5 (which belongs in the insect α7 group) (**Figure 2.2**), so low overall levels of similarity were to be expected, regardless of the N-terminus (Jones and Sattelle 2010). The presence of a long N-terminus in *Drosophila*, houseflies and tephritids, and the absence in mosquitoes, suggests that this feature arose within the Diptera lineage before the divergence of Schizophora.

Figure 2.32 (over page) Abnormal N-terminus is restricted to the *Drosophila* genus and select dipterans

Protein alignments of the N-terminus of Dα5 with (i) Dα6 and Dα7, (ii) non-*Drosophila* N-terminus BLASTp hits, (iii) *Drosophila* genus N-terminus BLASTp hits, and (iv) representative α5s from various insect orders. Identity with Dα5 is represented by black rectangles, and mismatches by grey rectangles. Black lines represent gaps in the alignment with Dα5. Predicted signal peptides are underlined in green. The *D. sechelia* sequence is a concatenation of two predicted peptides and the concatenation site is marked with a green arrowhead.

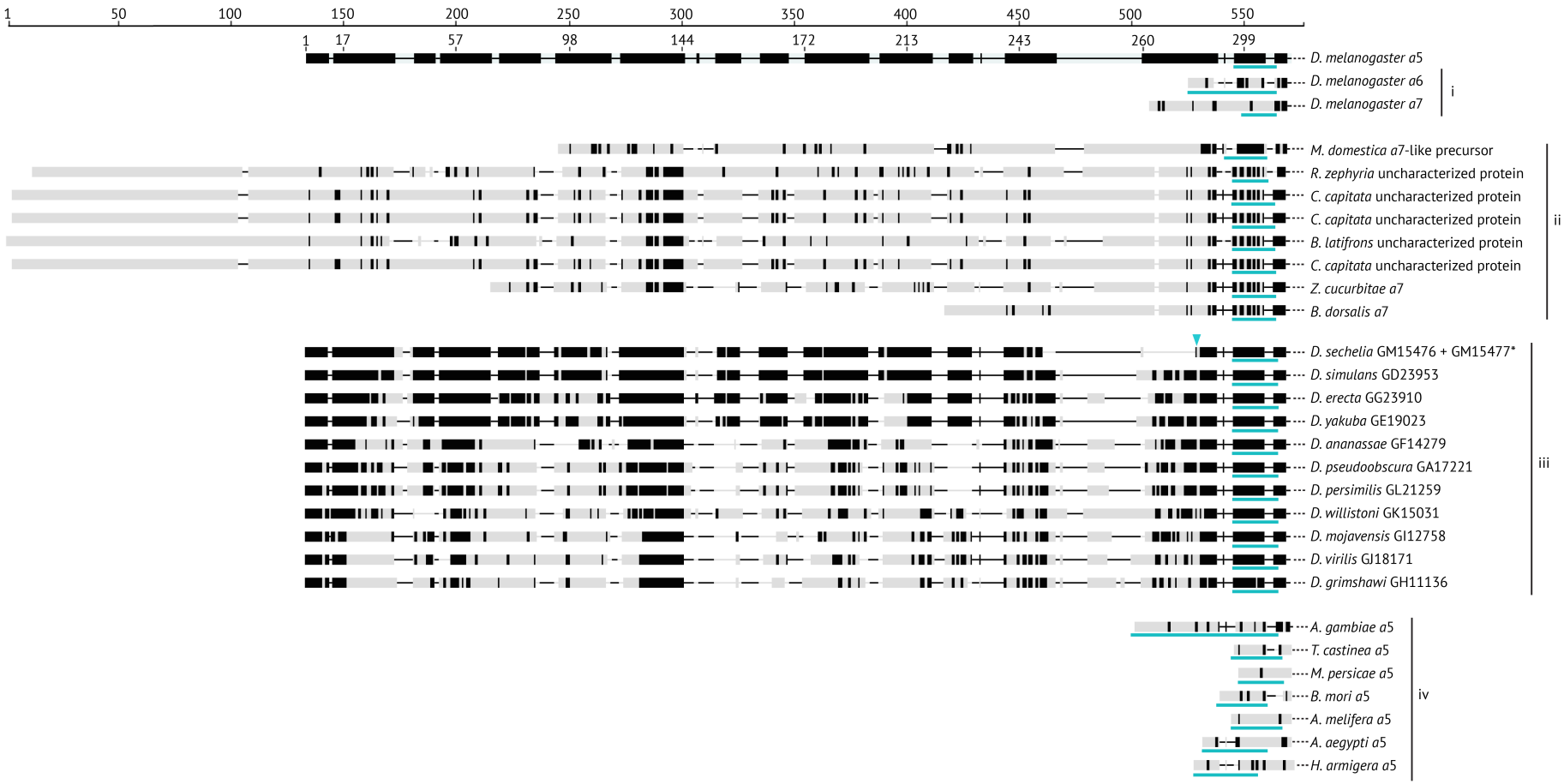

1
50
100
150
200
250
300
350
400
450
500
550
1
17
57
98
144
172
213
243
260
299
D. melanogaster a5
D. melanogaster a6
D. melanogaster a7
i
M. domestica a7-like precursor
R. zephyria uncharacterized protein
C. capitata uncharacterized protein
C. capitata uncharacterized protein
B. latifrons uncharacterized protein
C. capitata uncharacterized protein
Z. cucurbitae a7
B. dorsalis a7
ii
D. sechelia GM15476 + GM15477*
D. simulans GD23953
D. erecta GG23910
D. yakuba GE19023
D. ananassae GF14279
D. pseudoobscura GA17221
D. persimilis GL21259
D. willistoni GK15031
D. mojavensis GI12758
D. virilis GJ18171
D. grimshawi GH11136
iii
A. gambiae a5
T. castinea a5
M. persicae a5
B. mori a5
A. melifera a5
A. aegypti a5
H. armigera a5
iv

Table 2.14 Sequence conservation amongst insect α5 and α7 subunits

Protein	Species	Order	Protein Length (aa)	N-term length (5' of SP)	% Identity Dα5 (full)	% Identity Dα5 (N-term deleted)	% Identity Dα7 (N-term deleted)	Insect clade*
***Drosophila* α7-like subunits**								
Dα5	*D. melanogaster*	Diptera	808	294	100	100	79.35	α7
Dα6	*D. melanogaster*	Diptera	523	0	62.7	62.2	59.78	α6
Dα7	*D. melanogaster*	Diptera	560	41	73.67	78.78	100	α7
BLASTp hits for Dα5 N-terminus (residues 1-312)								
neuronal acetylcholine receptor subunit alpha-7-like precursor // nicotinic acetylcholine receptor alpha 5 subunit	*Musca domestica*	Diptera	781	263	65.83	▲94.81	76.85	α7
PREDICTED: uncharacterized protein	*Rhagoletis zephyria*	Diptera	644	473	41.68	▲96.49	83.63	α7
uncharacterized protein LOC101453167 isoform X2	*Ceratitis capitata*	Diptera	961	495	63.85	▲97.44	77.57	α7
uncharacterized protein LOC101453167 isoform X3	*Ceratitis capitata*	Diptera	960	495	63.93	▲97.64	77.73	α7
PREDICTED: uncharacterized protein	*Bactrocera latifrons*	Diptera	927	449	61.75	▲95.21	75.87	α7
uncharacterized protein LOC101453167 isoform X1	*Ceratitis capitata*	Diptera	1009	495	65.97	▲98.44	78.39	α7
PREDICTED: LOW QUALITY PROTEIN: neuronal acetylcholine receptor subunit alpha-7	*Zeugodacus cucurbitae*	Diptera	771	230	67.32	▲89.46	70.67	α7
PREDICTED: neuronal acetylcholine receptor subunit alpha-7	*Bactrocera dorsalis*	Diptera	635	121	81.53	▲98.44	78.39	α7
Dα5-like subunits in 12 *Drosophila* species								
GM15476 + GM15477**	*D. sechelia*	Diptera	259 + 524*	269	93.38	▲100	79.35	α7
uncharacterized protein Dsimw501_GD23953	*D. simulans*	Diptera	815	296	95.38	▲100	79.35	α7
uncharacterized protein Dere_GG23910, isoform C	*D. erecta*	Diptera	823	309	92.17	▲100	79.35	α7
uncharacterized protein Dyak_GE19023	*D. yakuba*	Diptera	810	296	92.08	▲100	79.35	α7

Table continued over page

Table 2.14 (*continued*) Sequence conservation amongst insect α5 and α7 subunits

Protein	Species	Order	Protein Length (aa)	N-term length (5' of SP)	% Identity Dα5 (full)	% Identity Dα5 (N-term deleted)	% Identity Dα7 (N-term deleted)	Insect clade*
Dα5-like subunits in 12 *Drosophila* species (continued)								
uncharacterized protein Dana_GF14279	*D. ananassae*	Diptera	789	275	79.18	▲100	79.35	α7
uncharacterized protein Dpse_GA17221, isoform A	*D. pseudoobscura*	Diptera	806	292	78.83	▲99.61	79.54	α7
GL21259	*D. persimilis*	Diptera	686	296	74.37	▲98.21	83.46	α7
uncharacterized protein Dwil_GK15031	*D. willistoni*	Diptera	823	309	74.17	▲99.42	79.54	α7
uncharacterized protein Dmoj_GI12758	*D. mojavensis*	Diptera	793	279	74.07	▲99.42	79.35	α7
uncharacterized protein Dvir_GJ18171	*D. virilis*	Diptera	692	291	74.61	▲99.61	79.54	α7
GH11136	*D. grimshawi*	Diptera	799	285	73.6	▲99.61	79.35	α7
Other non-*Drosophila* α5s								
nicotinic acetylcholine receptor subunit alpha 5	*Anopheles gambiae*	Diptera	552	0	80.54	▲83.88	78.75	α7
nicotinic acetylcholine receptor subunit alpha5	*Tribolium castinea*	Coleoptera	363	0	40.82	40.16	39.89	α5
nicotinic acetylcholine receptor, alpha5 subunit	*Myzus persicae*	Hemiptera	549	0	35.37	35.26	37.06	α5
nicotinic acetylcholine receptor subunit alpha 5 isoform A precursor	*Bombyx mori*	Lepidoptera	499	0	31.61	31.39	30.66	α5
nicotinic acetylcholine receptor alpha5 subunit	*Apis melifera*	Hymenoptera	481	0	33.88	32.23	33.33	α5
neuronal acetylcholine receptor subunit alpha-5	*Aedes aegypti*	Diptera	434	0	20.35	19.12	18.76	α5
neuronal acetylcholine receptor subunit alpha-5-like	*Helicoverpa armigera*	Lepidoptera	422	0	17.92	19.04	17.59	α5

*Based on classification of insect nAChR subunits from Jones and Sattelle 2010.

**Adjacent annotated transcripts were concatenated to form a complete Dα5-like subunit.

▲ Highlights higher identity with Dα5 than Dα7 when N-termini are omitted.

2.3.8.2 Western blotting

The size of the tagged Dα5-GFP protein was investigated using Western blotting with anti-GFP staining (**Figure 2.33**). If the Dα5 N-terminus is retained in the mature protein, a band of 126kDa would be expected (91kDa Dα5 + 35kDa GFP). However, if the N-terminus is cleaved, a band of ~92kDa would be expected, similar to the size of Dα6-GFP (57kDa Dα5 + 35kDa GFP). In samples collected from Dα5-GFP L3 brains, the 126kDa and 92kDa bands were both detected, suggesting uncleaved and cleaved versions may both be present. Meanwhile, samples collected from whole adult heads produced only the 95kDa band, suggesting a cleaved Dα5 protein lacking the N-terminus could be the main form present in adults. A similar sized band was detected in adult heads collected from the Dα6-GFP strain.

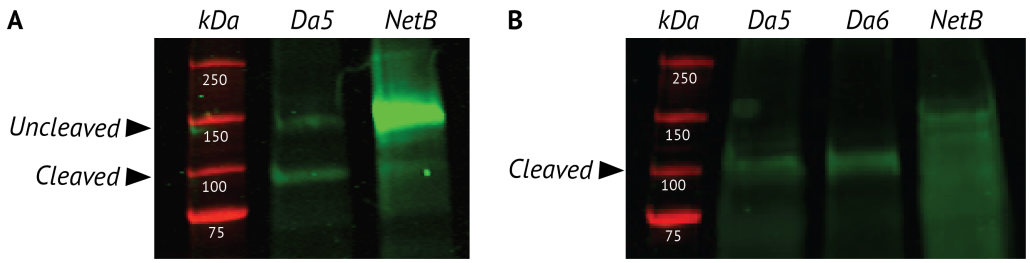


Figure 2.33 Western blotting indicates the abnormal N-terminus may be cleaved

Anti-GFP staining was used to detect GFP-tagged proteins in *Dα5-GFP, Dα6-GFP*, and *NetB-GFP.* (**A**) Samples collected from L3 brains. Two bands were detected for *Dα5-GFP*; one corresponding to the predicted size of the full-length Dα5-GFP (uncleaved), and one corresponding to the predicted size of Dα5-GFP if the large N-terminus was removed (cleaved). (**B**) Samples collected from adult heads. A single band was detected for *Dα5-GFP* and *Dα6-GFP.* Both bands are similar in size and correspond to the size of a subunit lacking a large N-terminus (cleaved). Ladders are *Odyssey® One-Color Protein Molecular Weight Marker* (LiCOR). The *NetB-GFP* strain was included as it has the same GFSTF tag as *Dα5-GFP* and *Dα6-GFP*, is highly expressed in the brain, and was known to respond well to the chosen staining protocol (Nagarkar-Jaiswal *et. al.* 2015).

2.3.9 The role of Dα5 in insecticide response

A Wiggle Index assay was used to measure relative larval movement following exposure to the insecticide spinosad (12ppm) (**Figure 2.34**). A rapid reduction in movement was observed in $D\alpha5^{Mi\text{-}5'}$ larvae, with relative movement dropping to 0.8 by t_{15}, 0.3 by t_{30}, and finally 0.2 from t_{60}-t_{120}. Unlike $D\alpha5^{Mi\text{-}5'}$, spinosad-resistant $D\alpha6^{KO}$ larvae and spinosad-sensitive *yw* control larvae both exhibited an initial increase in movement at t_{15}, although this was not significantly different to $D\alpha5^{Mi\text{-}5'}$ at the same timepoint ($p > 0.05$, Tukey's Test). For the remainder of the experiment, $D\alpha6^{KO}$ relative movement remained above 1.0, significantly higher than $D\alpha5^{Mi\text{-}5'}$ at all remaining timepoints (t_{30}, t_{60}, t_{120}, $p < 0.001$; t_{90}, $p < 0.01$). Meanwhile, in *yw* larvae an overall reduction in relative movement similar to $D\alpha5^{Mi\text{-}5'}$ was observed.

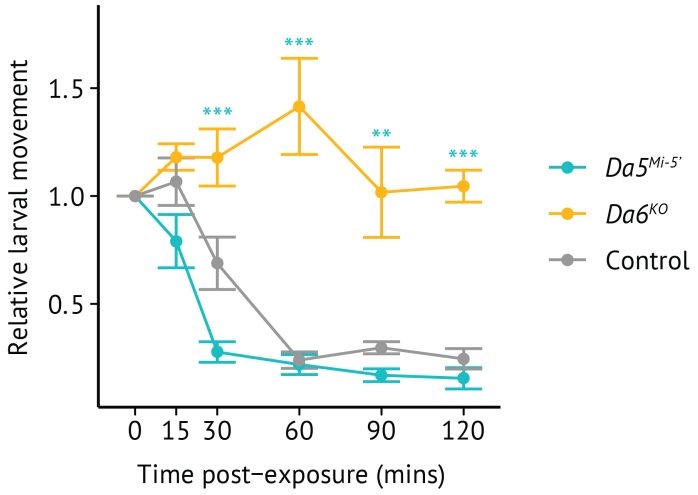


Figure 2.34 Wiggle Index analysis following exposure to spinosad

Exposure to 12ppm spinosad leads to an overall reduction in movement for $D\alpha5^{Mi\text{-}5'}$ and *yw* control larvae. In contrast, spinosad-resistant $D\alpha6^{KO}$ larvae exhibit an overall increase in movement relative to t_0. Error bars indicate 95% confidence intervals and significance levels relative to $D\alpha5^{Mi\text{-}5'}$ are shown ($n = 80$, ** $p < 0.01$, *** $p < 0.001$, Tukey's test).

2.4 Discussion

The primary goal of this chapter was to investigate Dα5's potential role in larval development, preferably using a CRISPR-generated deletion mutant. Unfortunately, several efforts to generate this mutant were unsuccessful (*Appendix 1*). A different approach was taken to address this question, making use of other available strains. The results, while requiring further validation, bring us significantly closer to understanding the role of Dα5 and how the loss of Dα5 function might lead to larval death.

2.4.1 A deeper look at the lethal phenotype

Early descriptions of a *Dα5* deficiency line and *Dα5* RNAi knockdown indicated that this subunit was essential for larval development (Mitchell 2012). In these preliminary experiments, larvae were described as being small and having two sets of mouthhooks (i.e. a buttoned-up phenotype). They were also observed wandering away from their food in vials, dying without progressing to pupation. I have now shown that these same phenotypes exist in three alternative *Dα5* strains ($D\alpha5^{Mi\text{-}5'}$, $D\alpha5^{TG4\text{-}5'}$ and $D\alpha5^{TG4\text{-}3'}$) and have further characterised the phenotypes, primarily using $D\alpha5^{Mi\text{-}5'}$.

A closer look at the dead $D\alpha5^{Mi\text{-}5'}$ larvae revealed that the majority die during the M1 or M2 moults. The exact timing of death relative to the moulting process varied, with the positions of old mouthhooks ranging from anterior (adjacent to the new mouthhooks) to posterior (almost completely shed). These patterns are typical of other mutants that also display the buttoned-up phenotype (Meng *et al.* 2002, Park *et al.* 2002).

Measuring larval mass revealed that $D\alpha5^{Mi\text{-}5'}$ larvae fail to grow during the L2 stage, and we now know that this is correlated with cessation of food intake at the same stage. This represents a stark contrast to wild type larvae, which continue to feed and grow substantially for several more days as L3. Whether the absence of food in $D\alpha5^{Mi\text{-}5'}$ L2 midguts was perhaps due to behavioural avoidance of food, or a physical inability to ingest food is yet to be determined. However, the significant 174-fold upregulation of *Lip3*

suggests the normal starvation response is being induced and indicates that they are not avoiding food as a result of perceived satiety (Zinke *et al.* 1999). Further, there was no blockage observed in the midgut making it unlikely there is an issue pumping food through this region of the alimentary canal (Zinke *et al.* 1999).

Investigation of the precocious wandering behaviour showed that it was not a completely penetrant phenotype, only observed in up to 65% of $D\alpha5^{Mi\text{-}5'}$ larvae, however similar proportions are reported in other buttoned-up mutants (Schoofs *et al*. 2014). Curiously, an overall reduction in basal movement was observed in larvae assayed just hours prior, and yet they were able to wander relatively far. It was also interesting to find that wandering occurred after feeding had already ceased, and thus that the absence of food in the midgut was not merely a side effect of larvae leaving the food. Together, these observations suggest the larvae could have an active aversion to their food, although additional behavioural assays would be needed to conclude if there is a negative or neutral valence.

2.4.2 An underlying cause for the lethal phenotype

With a more complete picture of the lethal phenotype, we can now consider what might be causing the larvae to die in this manner. The buttoned-up phenotype has previously been associated with a number of mutants (Park *et al.* 2002), but it is only known to be coupled with precocious wandering for mutant alleles of two genes - *ETH* and *hugin* (Schoofs *et al.* 2014).

Having tested transcript levels for these two genes in $D\alpha5^{Mi\text{-}5}$, it appears *ETH* levels are severely reduced, while *hugin* levels are unchanged. ETH plays a key role during moulting, triggering specific anterior-posterior contractions and squeezing waves during the pre-ecdysis phase of each moult (Park *et al.* 2002). In the absence of this hormone, *ETH* mutant larvae fail to execute these pre-ecdysis behaviours before attempting ecdysis. This reduces moulting success, leading to buttoned-up larvae that typically die mid-moult. It seems highly likely that the *ETH* deficiency is what causes this phenotype to arise in $D\alpha5^{Mi\text{-}5'}$.

The reduction in *ETH* is also a likely cause of *Dα5*$^{Mi\text{-}5'}$s feeding and wandering phenotypes. Like *Dα5*$^{Mi\text{-}5'}$, *ETH* mutants fail to ingest food (Park *et al*. 2002), and I have now shown that RNAi knockdown of *ETH* also results in the wandering phenotype. In contrast to ETH's well-defined role in moulting, the mechanism by which ETH affects feeding and wandering is yet to be described. Thus, for now, the questions raised above (*section 2.4.1*) regarding why these mutants stop feeding and what drives them to wander away from their food, remain unanswered.

So far, I have shown that loss of *ETH* is occurring in *Dα5*$^{Mi\text{-}5'}$, but further work will be required to verify the role of ETH in *Dα5*$^{Mi\text{-}5'}$'s moulting, feeding and wandering phenotypes. It will be important to attempt to rescue these phenotypes with ETH and this could be done via expression of *ETH* cDNA in the *Dα5*$^{Mi\text{-}5'}$ background, preferably from an *ETH-GAL4* driver to ensure accurate timing. Feeding or injection of ETH are also viable options, although more difficult to perform with temporal accuracy. *ETH* transcripts should also be measured in other Dα5 strains to test if this ETH deficiency is replicable.

2.4.3 Linking loss of Dα5 and loss of ETH

How might loss of Dα5 lead to a reduction in *ETH* transcripts? Based on the literature and results presented here, there is no direct link between Dα5 and the ETH-producing Inka cells. I have observed that Dα5 is not expressed in Inka cells, I have shown that *Dα5* knockdown in Inka cells has no effect, and previous reports indicate that Inka cells are not innervated (O'Brien and Taghert 1997, Clark *et al.* 2004).

The simplest way that Dα5 could affect ETH production in the Inka cells is by influencing ecdysone signalling from the PG. Two experiments indicate Dα5 could have a role in the PG; the PG was the only tissue where tissue-specific RNAi knockdown was able to phenocopy *Dα5*$^{Mi\text{-}5'}$, and while expression of the TG4 drivers was not detected in the PG itself, it was detected in the PGNs. Ecdysone signalling leads (indirectly) to ETH production in the Inka cells via the moulting hormone cascade (*section 1.3.2*), and mistimed release of ecdysone

from the PG can disrupt ETH levels downstream (Kingan and Adams 2000). If loss of Dα5 were to disrupt ecdysone signalling, this too could have downstream consequences for ETH levels.

Unfortunately, the proxy gene (*E75B*) used to detect levels of the active form of ecdysone (20E) indicated no significant change in 20E in $D\alpha5^{Mi\text{-}5'}$ larvae. However, we can't exclude the involvement of 20E based on this single result. While *E75B* is regularly used as a reliable 20E response gene (Segraves and Hogness 1990), hormone levels are constantly fluctuating and therefore very sensitive to the timing of sample collection, so it could be that a disruption in 20E levels was simply not detected in our samples. The PG is sensitive to a wide range of inputs (Marchal *et al.* 2010), including signals from innervating neurons (Siegmund and Korge 2001, Shimada-Niwa and Niwa 2014), so it is possible that Dα5-containing receptors facilitate one of these incoming signals that regulate ecdysone production or release. Dα5-containing receptors could also facilitate formation of the correct innervation pattern.

Using an ELISA test to directly measure 20E levels, preferably at a range of time points, and using haemolymph extracted from tightly time-controlled larvae would be ideal for testing the involvement of 20E in the $D\alpha5^{Mi\text{-}5'}$ phenotypes. While difficult to perform given the size and fragility of $D\alpha5^{Mi\text{-}5'}$ larvae, it would also be worth examining the innervation pattern of PGNs in $D\alpha5^{Mi\text{-}5'}$.

2.4.4 Hypotheses on which cells need Dα5

I have three hypotheses that explain which cells might require Dα5 such that loss of Dα5 leads to loss of ETH. It must be noted that all three hypotheses are centred on the PG, which makes sense based on the available results, but they therefore depend on the assumption that there is some sort of disruption in 20E signalling that leads to the ETH disruption. This remains the simplest explanation for loss of ETH in the absence of a clear link between Dα5-expressing cells and the ETH-producing Inka cells.

2.4.4.1 Dα5 may be required in the PG cells

The first possibility is that Dα5 is required in PG cells. The key evidence for this hypothesis is RNAi knockdown. While RNAi technology has its flaws, the fact that knockdown using two independent PG drivers, but not a pan-neuronal driver, is able to phenocopy $D\alpha5^{Mi\text{-}5'}$, $D\alpha5^{TG4\text{-}5'}$ and $D\alpha5^{TG4\text{-}3'}$ is strong evidence that Dα5 may be required not in the brain, but in the PG itself.

While these PG cells are non-neuronal, there is a precedent for Dα5-like subunits functioning in non-excitable cells outside the nervous system. Dα5's closest vertebrate relative, vertebrate α7, is found in non-neuronal cell types such as skin cells and testes (Beckman and Lips 2013), where it forms homomeric receptors that facilitate Ca^{2+} flux. Thus, if Dα5 is required in the PG, a likely role would be upstream of a Ca^{2+}-dependent signalling cascade, of which there are several that regulate ecdysone output (Henrich 1995; Marchal *et al.* 2010; Yamanaka *et al.* 2015).

Inconsistent expression data does add a degree of uncertainty to this hypothesis. While Dα5 has been detected in the L3 PG using fluorescent *in situ* hybridisation (Ali 2012), only low expression is reported in L3 ring gland RNA-seq data (Christesen *et al.* 2017), and zero expression was detected when $D\alpha5^{TG4\text{-}5'}$ or $D\alpha5^{TG4\text{-}3'}$ were used to drive reporter expression. The TG4 Trojan Exon is large (4 kb), and its integration into Dα5 could cause regulatory disruption, potentially resulting in an unfaithful representation of Dα5's native expression pattern. The fact that neither of these TG4 strains were able to produce an RNAi phenotype supports the possibility that the expression pattern of these TG4s is modified or incomplete compared to native Dα5 expression.

2.4.4.2 Dα5 may be required in the PGNs

The second possibility is that Dα5 is required in the PGNs. The key evidence for this hypothesis is the expression pattern detected in both TG4 drivers, which resembles that of known PGNs, the PTTH neurons and serotonergic neurons (Siegmund and Korge 2001, Shimada-Niwa and Niwa 2014). Inspection of a larval brain single-cell RNA-seq dataset also revealed substantial co-expression between *Dα5* and the markers for these two sets of neurons (*ptth* and *trh*) (Ravenscroft *et al.* 2021). This hypothesis places Dα5 in a position that could still affect PG function, whilst keeping it in a typical neuronal role, without assuming that it might be able to facilitate calcium signalling in non-neuronal cells like its vertebrate relative α7. The *UAS-mCD8GFP* reporter used to detect TG4 expression does not reveal the subcellular localisation of Dα5, so any Dα5 receptors present in PGNs could function at either end of the neuron, in either pre-synaptic or post-synaptic roles.

The main evidence against this hypothesis is that neuronal RNAi knockdown - using the pan-neuronal *elav-GAL4* driver or the two PGN drivers (*ptth-GAL4* or *trh-GAL4*) - does not result in the $D\alpha5^{Mi\text{-}5'}$ lethal phenotype. Notably, *elav-GAL4* does not appear to be expressed in PGNs (Setiawan *et al.* 2018), so even a "pan-neuronal" knockdown may not necessarily knockdown *Dα5* in every neuron. As for the *ptth-GAL4* and *trh-GAL4* drivers, while they are expressed in the PGNs, expression from these drivers may be too specific to knockdown *Dα5* in all cells where it is required, and therefore insufficient to achieve a phenotype. Alternatively, there may be some additional PGNs that are yet to be characterised and are not covered by these drivers.

Moving forward, it will be important to determine the identity of the PGNs where both TG4s are expressed. The split-GAL4 system could be used to determine which cell markers (e.g. *ptth*) are co-expressed with the TG4s in these neurons.

2.4.4.3 Dα5 may be required in the PG driver neurons

The third possibility is that Dα5 is required in neurons where *5'phm-GAL4* and *Feb36-GAL4* expression was detected. For both of these "PG-specific" drivers, fluorescence was detected in a small number of neurons in the CNS. Although the expression patterns were not completely identical, some neurons were certainly located in similar positions in the CNS. If Dα5 were required in these neurons, this would explain the lethality of RNAi knockdown using these drivers and the apparent absence of Dα5 expression in PG cells.

It is difficult to visualise whether these *5'phm-GAL4* and *Feb36-GAL4* neurons might be PGNs, as the fluorescent signal from the PG itself is too high with these drivers. At the CNS end, these neurons do not have an expression pattern resembling known PGNs (Siegmund and Korge 2001, McBrayer *et al.* 2007, Shimada-Niwa and Niwa 2014). Inspection of the online *FlyLight* collection of larval CNS GAL4s is also unhelpful in narrowing down the identity of these neurons, as there are numerous drivers possessing a very similar expression pattern (Jenett *et al.* 2012). Notably however, one of these similar *FlyLight* GAL4s uses the *Dα5* promotor region (*CG32975*), indicating the neurons where *5'phm-GAL4* and *Feb36-GAL4* were driving could indeed be Dα5-positive neurons.

2.4.4.4 Next steps for narrowing down cells of interest

For now, the exact cells where Dα5 is required remains in contention. As previously mentioned, co-expression work using split-GAL4 lines and available antibodies will enable us to check for co-expression of *Dα5* and key markers in different cell types. Similarly, continual development of single-cell RNA-seq databases will aid in identifying which cell types express *Dα5*. Since Dα5 subunits require numerous accessory proteins to form functional receptors, it will be worth examining whether any cells of interest express these accessory proteins (e.g. *nacho*), and whether knockdown or knockout of such accessory proteins can phenocopy $D\alpha5^{Mi\text{-}5'}$. Once an efficient CRISPR protocol has been established for

Dα5 (*section 2.4.9.4*), a somatic CRISPR approach should also be adopted as an alternative to tissue-specific RNAi work.

2.4.5 Adult heterozygotes are healthy, or are they?

In the absence of an effective temperature-sensitive protein knockdown system for Dα5, I resorted to testing adult heterozygotes for any dosage effects associated with having a single copy of *Dα5*. On the whole, the heterozygotes appeared relatively fit, with no effects on longevity or climbing performance, and only a minor reduction in egg laying early in adult life. While the reduction in fertility was mild, and recovered to control-like levels after two weeks, it could indicate an underlying courtship or copulation issue. If, for instance, there is reduced courtship success, fewer females would be expected to lay fertilised eggs in the early days of adulthood, however this would presumably "catch up" to control levels as the number of mated females gradually increases in the vial. Other nAChR subunit knockouts have already been shown to have courtship and copulation phenotypes (Somers *et al.* 2017, *Chapter Three*), indicating some mating pathways must use cholinergic signalling.

It is also important to keep in mind that only three assays have been performed here. Other nAChR subunits have been reported with more nuanced behavioural roles that are less obvious without performing intentional assays. For example, *Dα7* nulls appear healthy but fail to demonstrate the normal escape behaviour in response to sudden changes in light levels (Fayyazuddin *et al*. 2006). Dα1, Dα3 and Dα4 have been shown to play a role in sleep (Shi *et al.* 2014, Wu *et al.* 2014, Somers *et al.* 2017) and multiple subunits including Dα5 have been reported to have a role in adult learning and memory (Barnstedt *et al.* 2006). Therefore, further behavioural assays could reveal some more subtle underlying behavioural problems.

The broad expression of *Dα5* throughout the adult *Drosophila* midbrain (Croset *et al.* 2018) suggests this subunit is probably important for adult brain function. It is the second highest expressed nAChR subunit after Dβ1, which itself is essential for adult survival (*Chapter Three*). It is therefore highly likely that performing many of these adult assays not with

heterozygotes, but with a null would result in more obvious and severe phenotypes. This will of course require a delay in knockdown or knockout, given the highly penetrant larval mortality. An efficient deGradFP system remains an ideal option for delayed knockdown as it removes pre-existing protein, however temperature-controlled somatic CRISPR may also become a useful system if current issues with Dα5 deGradFP can't be resolved (*section 2.4.9.3*).

2.4.6 Is Dα5's essential role conserved among insects?

Dα5-like subunits are not present in all insect species. While Dα5 belongs in the insect α7 phylogenetic group, insects outside the Dipteran lineage (plus some Dipterans, e.g. *A. aegypti*) do not have a second subunit in the α7 group and instead have a more distantly related α5 subunit that belongs in a separate α5 group (**Figure 2.2**). This limited conservation of "true" Dα5-like subunits, combined with the severe lethality of *Dα5* mutants, provides a fascinating case in terms of evolution. How could a subunit come to have a specialised and essential role in potentially only a subset of Dipterans?

A possible answer is that one or multiple other nAChR subunits perform this essential role in other insects. Given that Dα5 shares an ancestor with α6 and α7 subunits, it is theoretically possible that other insects might have an essential subunit in the α7-like superclade that performs the same developmental role as Dα5. Such a severe developmental phenotype has not yet been reported for any other insect nAChR gene, however few nAChR nulls have actually been described in other species. Most nulls have been obtained from the field or from lab-selection studies, and in both cases have been selected for their relative fitness in the presence of insecticides (Baxter *et al.* 2010, Silva *et al.* 2016), making them unlikely to possess severe developmental phenotypes. Laboratory-generated nAChR knockouts are starting to emerge in pest species, but so far those have been homozygous viable (Wang *et al.* 2020). Ultimately, it's not that an essential nAChR subunit doesn't exist in other insects, one simply hasn't been discovered yet. Now that CRISPR is being used in a broad range of species, it will be intriguing to see whether knockout of any of the other subunits, or groups

of subunits, particularly those in the α7 superclade, leads to similar phenotypes outside the *Drosophila* lineage.

2.4.7 How important is the abnormal N-terminus?

Despite the huge size of Dα5's N-terminus, the results here indicate that it may not be important to Dα5's function after all. Phylogenetic analysis of this region revealed no similarity with any known protein domains and a lack of sequence conservation even within the closely related *Drosophila* sub-group. This indicates the N-terminus has been able to mutate more freely over evolutionary time than functionally-restricted domains of importance in the core regions of the subunit. Furthermore, when an anti-GFP stain was used to detect Dα5-GFP in western blots, in both larval and adult brains a protein was detected corresponding to a potentially cleaved Dα5 subunit. Cleaving of the N-terminus from the mature subunit would make sense, given that it is upstream of the SP sequence which would itself be cleaved after export to the cell membrane from the ER (von Heijne 1990).

These results do not definitively rule out a role for the N-terminus so further investigation will be necessary. Even if the N-terminus is not present in the mature subunit, it is possible the N-terminus could have an effect on protein trafficking prior to potential cleavage. Once CRISPR is working efficiently for *Dα5*, it would make sense to test the effect of specifically deleting the region from *Dα5* using CRISPR, preferably from a tagged subunit to visualise localisation and trafficking. Likewise, it would also be fascinating to overexpress the N-terminus alone, and to generate chimeric tagged subunits possessing the Dα5 N-terminus attached to the Dα6 and Dα7 cores to see how the domain affects the function and localisation of these subunits.

2.4.8 The *Dα5*$^{Mi\text{-}5'}$ response to spinosad

Previous heterologous expression work has shown that formation of spinosad-sensitive receptors requires co-expression of Dα5 with the primary spinosad target, Dα6 (Watson *et*

al. 2009). Loss of Dα6 function is already known to confer high levels of resistance to this insecticide (Perry *et al.* 2007, Watson *et al.* 2010), however the effect of disrupting Dα5 had not yet been reported. Since $D\alpha5^{Mi\text{-}5'}$ larvae already have a lethal phenotype, a standard toxicology assay was unsuitable for testing insecticide response. Instead, a Wiggle Index assay (Denecke *et al.* 2015) was used to measure the change in relative L2 movement upon exposure.

During this Wiggle Index analysis, $D\alpha5^{Mi\text{-}5'}$ larvae showed a sharp reduction in relative movement. This response is typical of a sensitive genotype, indicating that, unlike Dα6, loss of Dα5 does not confer any resistance. While this may seem surprising given Dα5's requirement in forming a spinosad-sensitive receptor *in vitro* (Watson *et al.* 2009), it remains possible that spinosad-sensitive receptors do not require Dα5 *in vivo*. It is interesting to note, however, that the initial increase in relative movement, seen within the first 15 minutes in control and $D\alpha6^{KO}$ larvae, was absent in $D\alpha5^{Mi\text{-}5'}$. This could indicate that Dα5-containing receptors *are* responding to spinosad and could be partially or wholly responsible for the early spike in movement sometimes seen in spinosad-exposed larvae (Ghazali 2020, Martelli 2020, Nguyen *et al.* 2021). The absence of this movement peak could also be due to the reduced fitness and lower basal movement of the $D\alpha5^{Mi\text{-}5'}$ larvae.

2.4.9 Addressing issues with Dα5 strains

While multiple strains indicate that *Dα5* is an essential gene, there were issues validating some strains, and attempts to generate a genomic deletion of *Dα5* were also unsuccessful. Until a genomic deletion is characterised, or an efficient rescue system is developed, there remains some uncertainty that *Dα5* is the gene responsible for the observed phenotypes. Up to this point, I have assumed that *Dα5 is* responsible, enabling me to hypothesise about how loss of Dα5 might be causing larval mortality. A discussion of why certain strains may be unreliable, and why *Dα5* seems refractory to CRISPR editing is provided here.

2.4.9.1 Complementation between Dα5 strains

Complementation crosses yielded multiple unexpected results. Homozygous lethal $D\alpha5^{Mi\text{-}5'}$ and $D\alpha5^{TG4\text{-}3'}$ strains were able to complement a strain derived from the same background (*Dα5-GFP*), indicating second-site mutations are unlikely to be contributing to the lethal phenotype. However, these homozygous lethal strains were also able to complement each other and large deficiencies, casting doubt on whether loss of Dα5 was the cause of mortality. We now know that *Dα5* cDNA could be detected in the viable offspring from at least two of these complementation crosses. This restores some confidence in *Dα5* being an essential gene, but also raises a new question - where are these *Dα5* transcripts coming from?

Exon skipping is a possible explanation for *Dα5* expression in the offspring of complementation crosses. The ability of the MiMIC and TG4 cassettes to truncate *Dα5* relies upon the cassette's splice acceptor site being used by the pre-mRNA splicing machinery in preference to the endogenous exon four splice acceptor site. When the cassette has been successfully spliced in, the *polyA* signal and stop codons will ensure transcription and translation are terminated. However, if the cassette is skipped, the normal full length Dα5 product may be expressed in these flies. The team that developed the MiMIC system acknowledge that exon skipping is rare but does occur in these strains (Nagarkar-Jaiswal *et al*. 2015). The question that now remains is why this would be occurring consistently in transheterozygotes and never in homozygotes.

2.4.9.2 Failed genetic rescue

If loss of Dα5 were the cause of mortality for $D\alpha5^{Mi\text{-}5'}$, then expression of *UAS-Dα5cDNA*, driven by the ubiquitous promotor *da-GAL4*, should have been able to rescue the lethal phenotype. While this experiment was not successful, there are a few things to consider before concluding that a different locus is the cause of mortality.

The first thing to consider is the functionality of the *UAS-Dα5cDNA*. Even if the cDNA was being efficiently overexpressed, which could be verified by qRT-PCR, we would also need to be sure that the expressed product is actually able to form functional receptors. For instance, it would be interesting to test whether heterologous expression of this cDNA in *Xenopus* oocytes (with the appropriate co-factors) could result in a positive electrophysiological response to ACh.

The other consideration is the suitability of the *da-GAL4 driver*. Although *da-GAL4* is a ubiquitous driver, and would presumably restore *Dα5* expression in the correct cells, use of a *Dα5*-specific driver such as $D\alpha5^{TG4\text{-}5'}$ or $D\alpha5^{TG4\text{-}3'}$ would be ideal. While these drivers were available during the present study, the complementation observed between each TG4 and $D\alpha5^{Mi\text{-}5'}$ would have rendered a cross with $D\alpha5^{Mi\text{-}5'}$*; UAS-Dα5cDNA* useless for testing rescue. Generating a $D\alpha5^{TG4\text{-}3'}$*/GFP-CyO; UAS-Dα5cDNA* strain will be useful for future rescue attempts.

2.4.9.3 A poorly visible GFP tag and ineffectual deGradFP

Fluorescent tagging of proteins is a fantastic tool for visualising the expression pattern and subcellular localisation of a protein of interest, also allowing the protein to be targeted for staining, immunoprecipitation and other techniques that would otherwise require a protein-specific antibody. Unfortunately, the *Dα5-GFP* strain did not prove as useful as hoped, with a weak and ill-defined expression pattern that did not respond well to anti-GFP staining. Investigation of the expression pattern of other GFP-tagged MiMIC lines (e.g. *Beat-IIb* and *drp12*, Nagarkar-Jaiswal *et al.* 2015) that are expressed at a similar level in the L3 brain as *Dα5* (Christesen *et al.* 2017) reveals that the expression level is probably not limiting the visibility of Dα5-GFP, as these other strains are capable of producing a strong GFP signal.

Exon skipping could explain the weak signal in *Dα5-GFP*, such that the GFP tag is not incorporated into every Dα5 protein. The position of the GFP tag may also be less than ideal. According to recommended positions for fluorescent tags (Snapp 2005), the Dα5 tag

is in a good position; it is at the N-terminus between the SP and the LBD. This means it should be visible and not disrupt subunit assembly or function. Despite this, the clear fluorescent signal visible in the *Dα6-YFP* strain (Nguyen *et al.* 2021) indicates tagging of nAChR subunits in the large intracellular loop could be superior to N- or C-terminal tagging. The $D\alpha5^{Mi\text{-}3'}$ (*BDSC #59218*) cassette is already positioned in the intracellular loop, and could be converted to a GFP tag via recombinase-mediated cassette exchange (RMCE) for future work.

The position of the Dα5-GFP tag may also have restricted deGradFP knockdown of Dα5. No phenotype was observed for deGradFP protein knockdown experiments, even when knockdown was initiated from the time of egg-laying, suggesting knockdown of Dα5 may not have be efficient. One possible reason is that the *Dα5-GFP* strain used in deGradFP experiments, as described above, contains an extracellular tag. This means the deGradFP machinery may only have access to the GFP tag during trafficking of the protein from the ER to the cell membrane, and any Dα5 subunits already present in the membrane may not be degraded, thus resulting in incomplete knockdown. The deGradFP system remains the primary tool for achieving protein knockdown, so generation of an intracellularly-tagged Dα5-GFP, whether by RMCE of $D\alpha5^{Mi\text{-}3'}$ or CRIMIC, should be prioritised before further deGradFP experiments are attempted for Dα5.

2.4.9.4 Dα5's aversion to CRISPR

A priority in this project was to use CRISPR to generate a full genomic deletion of *Dα5*. Such a strain would enable us to examine the consequences of loss of Dα5, without complications like the presence of a truncated product or potential mis-splicing of the cassette. Different strategies with varying ease and efficiency became available over the course of the project, and yet none were successful in generating a stable *Dα5* deletion strain. *Dα5* is now the only gene missing from the complete collection of CRISPR-generated nAChR subunit knockouts (Perry *et al.* 2021). Here, I cover some issues that may have hampered efforts to delete *Dα5*.

A recurring issue for *Dα5* CRISPR was inconsistency in diagnostic PCRs. Promising PCR bands were sometimes lost when molecular testing was repeated on the same fly, plus individuals that were apparently heterozygous often gave rise entirely to offspring that tested negative for a deletion. One possibility is that some or all PCR bands were false positives. Indeed, some sequenced PCR products revealed unrelated sequences from the X chromosome despite the lack of off targets predicted during primer design. If this is true, it would indicate that there is an underlying issue that reduces the efficiency of cutting. It is also possible that some negative PCRs were false negatives, as there was no suitable positive control for ensuring the PCRs had worked. However, given the number of technical variations attempted, and the number of different primer sets used, it seems unlikely that diagnostic issues are entirely responsible for the failure to generate a deletion line.

The size of the attempted *Dα5* deletions may contribute to reduced cutting efficiency. Using multiple sgRNAs is ideal for generating a large deletion but does depend on roughly simultaneous cutting at both sites, such that non-homologous end-joining mechanisms do not make any repairs until the intervening sequence has "dropped out" (Song *et al.* 2017). If the attempted deletion is very large, this process is less efficient and smaller mutations not detected by PCR may be more likely to occur (Canver *et al.* 2014, Song *et al*. 2014). Nevertheless, large deletions of up to 83kb, far larger than the largest region attempted for *Dα5* (27kb), have been generated in our own lab using the same conditions (Perry *et al*. 2021) and with far less difficulty. Thus, while the size of the deletion may be a contributing factor, it does not wholly explain the lack of success.

The state of the chromatin can also affect the efficiency of CRISPR editing. For instance, in regions of the genome that are not being actively transcribed, the formation of densely assembled heterochromatin can greatly impede accessibility for the Cas9 protein (Verkuiji and Rots 2019). While *Dα5* expression in the embryo is relatively low compared to many other genes (modENCODE, Contrino *et al.* 2012), the *Dα5* gene is not inactive. Further, the gene within *Dα5's* 5'UTR, *nimC4*, is very highly expressed at this time, making it highly

unlikely that this genomic region would be heterochromatic, and therefore inaccessible for CRISPR editing, in the cells of the embryo.

Finally, there could be issues with the chosen target sites. Different sgRNAs show different mutagenesis efficiencies (Bassett *et al.* 2013), and SNPs and additional internal PAM sites can render sgRNAs even less effective (Malina *et al.* 2015). Sequencing of the *actin-Cas9* strain indicates there should not be SNPs in the sgRNAs, and none of the sgRNAs have enough internal PAM sites that reduced cutting would be expected. While it would seem incredibly unlucky to have chosen eight independent sgRNAs that all inherently have poor efficiency, it remains possible that this is contributing to the difficulty in generating a *Dα5* deletion.

Many new CRISPR variations are now emerging and these may improve the efficiency of generating a stable *Dα5* deletion line. For instance, briefly inhibiting non-homologous end-joining using small molecules could increase the chance that "dropouts" are successful (Bischoff *et al.* 2020), use of chromatin-modulating peptides could improve Cas9 access in refractory target sites (Ding *et al*. 2019), and modifications to the core sgRNA design may also improve efficiency (Filippova *et al*. 2019). Without knowing the underlying cause for *Dα5*'s CRISPR difficulties, it is hard to predict whether adopting any particular strategy will improve the chances of generating a deletion, but pursuing this task remains a priority for enabling further work on this subunit.

2.4.10 Final comments

While we are a few steps closer to understanding Dα5's role in larval development, it is clear that further validation of the true nature of the role of Dα5 is required. The generation of a genomic deletion will be crucial for verifying that the phenotypes described in this chapter are actually due to loss of Dα5, and should clarify the lingering uncertainties associated with some of the results obtained from the several strains used here. From there, dissecting the mechanism by which Dα5 might affect ETH signalling represents the most enticing step forward. Looking further, the emerging interest in chemoconnectomics (Deng *et al.* 2019), and the ongoing efforts to generate a functional wiring diagram of the *Drosophila* brain, may mean we see more of Dα5 in the literature. It will be fascinating to see just how many larval and adult neuronal pathways require this ubiquitous subunit.

Chapter Three*

Loss of the Dβ1 nicotinic acetylcholine receptor subunit disrupts bursicon-driven wing expansion and diminishes adult viability in *Drosophila melanogaster*

*This chapter is a manuscript that was accepted for publication in the journal *Genetics* in June 2021.

3.1 Abstract

Cholinergic signaling dominates the insect central nervous system, contributing to numerous fundamental pathways and behavioral circuits. However, we are only just beginning to uncover the diverse roles different cholinergic receptors may play. Historically, insect nicotinic acetylcholine receptors have received attention due to several subunits being key insecticide targets. More recently, there has been a focus on teasing apart the roles of these receptors, and their constituent subunits, in native signaling pathways. In this study, we use CRISPR-Cas9 genome editing to generate germline and somatic deletions of the *Dβ1* nicotinic acetylcholine receptor subunit and investigate the consequences of loss of function in *Drosophila melanogaster*. Severe impacts on movement, male courtship, longevity, and wing expansion were found. Loss of *Dβ1* was also associated with a reduction in transcript levels for the wing expansion hormone *bursicon*. Neuron-specific somatic deletion of *Dβ1* in *bursicon*-producing neurons (*CCAP*-GAL4) was sufficient to disrupt wing expansion. Furthermore, *CCAP*-GAL4-specific expression of *Dβ1* in a germline deletion background was sufficient to rescue the wing phenotype, pinpointing CCAP neurons as the neuronal subset requiring *Dβ1* for the wing expansion pathway. Dβ1 is a known target of multiple commercially important insecticides, and the fitness costs exposed here explain why field-isolated target-site resistance has only been reported for amino acid replacements and not loss of function. This work reveals the importance of Dβ1-containing nicotinic acetylcholine receptors in CCAP neurons for robust *bursicon*-driven wing expansion.

3.2 Introduction

The nicotinic acetylcholine receptors (nAChRs) are the most abundant neuronal receptor in the insect brain, responding to the native neurotransmitter acetylcholine to facilitate fast excitatory synaptic neurotransmission (Florey 1963, Croset *et al.* 2018). Their ubiquity in the insect nervous system, combined with their pharmacological sensitivity, also makes them ideal targets for neuroactive insecticides. Interactions between nAChRs and insecticides, and the role of nAChRs in insecticide resistance, are well-covered in the literature (Lansdell and Millar 2000b, Tomizawa and Casida 2005 Millar and Denholm 2007 Perry *et al.* 2012

Crossthwaite *et al.* 2017 Homem *et al.* 2020). Now, unravelling the endogenous signaling roles of nAChRs across many cholinergic pathways will enhance our understanding of contributions to insect life history traits, also offering insights into potential fitness costs underlying insecticide resistance.

nAChRs are pentameric ligand-gated ion channels, formed by five subunits arranged symmetrically around a central cation-selective pore (Coringer *et al.* 2000, Karlin 2002). In *Drosophila melanogaster,* there are 10 genes encoding nAChR subunits (Sattelle *et al.* 2005). Seven of these encode α subunits (*Dα1-Dα7*) which contain a motif (YXCC) that coordinates acetylcholine binding (Kao *et al.* 1984, Karlin and Akabas 1995). Three genes encode β subunits (*Dβ1-Dβ3*). These lack the di-cysteine motif. The subunit composition defines the pentamer "subtype" and determines the receptor pharmacology (Millar 2003, Sattelle *et al.* 2005, Thany *et al.* 2007, Lansdell *et al.* 2012, Ihara *et al.* 2020). Single-cell sequencing analysis reveals different levels of expression of individual subunit genes across the brain, suggesting that the spectrum of subtypes present may vary between different neurons and synapses (Croset *et al.* 2018). This variability in subtype distribution and pharmacology means that a given subunit may have specialized roles in different biological processes. Six *Drosophila* subunits (Dα1, Dα3, Dα4, Dα5, Dα6, Dα7) have been briefly described for their roles in behaviors such as sleep (Shi *et al*. 2014, Wu *et al.* 2014, Somers *et al.* 2017), courtship (Somers *et al.* 2017), learning and memory (Barnstedt *et al*. 2016), and escape (Fayyazuddin *et al.* 2006). Meanwhile, five subunits (Dα1, Dα2, Dα6, Dβ1, Dβ2) are known to have insecticide interactivity, based on heterologous expression (Watson *et al.* 2010, Ihara *et al.* 2020) and strong resistance phenotypes seen in individual loss of function mutants (Perry *et al.* 2008, Watson *et al.* 2010, Perry *et al.* 2012).

The Dβ1 subunit is well overdue for investigation. In 2011, a field population of the global agricultural pest, *Myzus persicae*, the peach-potato aphid, was found to harbor a non-synonymous mutation in the *β1* nAChR subunit (*Mpβ1*^{R81T}) that conferred resistance to neonicotinoids (Bass *et al.* 2011). The potential impact on *M. persicae* control could have been devastating, especially given the species' capacity to vector hundreds of plant viruses

to a huge range of host plants worldwide (Blackman and Eastop 2000). Fortunately, there has only been one other report of a field-evolved resistant *β1* allele (*Aphis gossypii Agβ1*^{R81T}, Koo *et al.* 2014) despite over 20 years of ongoing neonicotinoid usage. *In vivo* and *in vitro* studies identify β1 as a neonicotinoid target in multiple insect species (Li *et al.* 2010, Shi *et al.* 2012, Homem *et al.* 2020), so why haven't more insects evolved resistance via disruption of the β1 subunit?

The simplest explanation for the absence of naturally occurring loss of function alleles is that nAChRs containing β1 subunits may have an essential role(s) in the brain. β1 is the most highly conserved nAChR subunit among insects (Jones and Sattelle 2010). It is also the most highly and broadly expressed of all nAChR subunits in the *D. melanogaster* nervous system (Graveley *et al*. 2011, Croset *et al*. 2018, Allen *et al.* 2020), suggesting loss of β1 subunits could be quite detrimental to viability. Indeed, Homem *et al.* (2020) recently generated a *D. melanogaster Dβ1*^{R81T} strain and observed significant reductions in fertility, male longevity, larval crawling, and adult climbing performance in individuals homozygous for the R81T allele. The R81T amino acid replacement only slightly alters acetylcholine binding affinity (Shimomura *et al.* 2006, Ihara *et al*. 2020), so it is probable that complete loss of the Dβ1 subunit would have more severe consequences for viability.

Here, we have used the CRISPR-Cas9 system to investigate complete loss of the Dβ1 subunit in *D. melanogaster*. We describe the pleiotropic consequences of germline genomic deletion, which include a prominent disruption in wing expansion and severely reduced adult viability. By generating GAL4-driven somatic deletions, we have also pinpointed a neuronal subset, the CCAP neurons, that require Dβ1 to execute timely release of the wing expansion hormone, bursicon. This represents the first association of a specific nAChR subunit with hormone-driven developmental cues and suggests many roles in a variety of life history traits are yet to be uncovered for this important gene family.

3.3 Methods

3.3.1 Fly strains and maintenance

All fly strains used and generated are described in **Tables S1** and **S2** (*Appendix 2*). The wAC9 control is a strain we previously generated for a collection of nAChR CRISPR mutants (Perry *et al*. 2021). It contains the autosomes of the *actin*-Cas9 strain, with a substituted *w*- X chromosome (and therefore lacks an *actin*-Cas9 element).

All flies were maintained on standard semolina fly media at 25°C under a 12:12h light: dark cycle unless otherwise stated. Due to the low viability of *Dβ1Δex5*, *Dβ1Δex3* and *Dβ1*-TG4, any strains containing these alleles were maintained over the TM3.GFP fluorescent balancer chromosome. In preparation for all adult experiments, embryos were collected for 24 hours on apple juice agar plates and first instar larvae lacking the fluorescent balancer chromosome were transferred to standard semolina fly media where they were reared until adulthood. For larval experiments, embryos were collected for three hours on apple juice agar plates and first instar larvae lacking the fluorescent balancer chromosome were synchronized within three hours of hatching then reared on apple juice agar plates supplemented with yeast paste.

3.3.2 Generating *Dβ1* genomic deletions using CRISPR-Cas9

Generation of *Dβ1Δex5* is described elsewhere (Perry *et al.* 2021), and we have used the same methods to generate the smaller deletion, *Dβ1Δex3*. Briefly, sgRNAs targeting the *Dβ1* 5' region (77bp upstream of the 5'UTR; *Dβ1_5'UTR_sgRNA*), exon 3 (*Dβ1_sgRNA1*), and exon 5 (*Dβ1_sgRNA2*) were designed using the *crisprflydesign.org* online tool and integrated in pairs into the pCFD4 plasmid (Addgene: 49411) using the recommended protocol (Port *et al.* 2014) (sgRNA positions in **Figure 3.1**, primer sequences in **Table S3**, *Appendix 2*). Plasmids were microinjected into attP40 (25709 v^-) embryos then transgenics were identified both phenotypically (v^+ eye colour rescue) and molecularly (*Vermillion_F* and *25709_External_R1* primers). Homozygotes were recovered by self-crossing the

heterozygous offspring of injectees (crossing scheme in **Figure S1**, *Appendix 2*). Homozygotes were then crossed to *nanos*-Cas9 flies, producing F_1 offspring with all components required for CRISPR (crossing scheme in **Figure S2***, Appendix 2*). Genomic cutting was detected molecularly using *Dβ1_5'UTR_sgRNA_HMA_F/ Dβ1_sgRNA1_HMA_R*, or *Dβ1_5'UTR_sgRNA_HMA_F/Dβ1_sgRNA2_HMA_R*, and sequenced using the *Dβ1_5'UTR_sgRNA_HMA_F* primer. Successful genomic deletions were crossed to incorporate the X chromosome and chromosome 2 from the wAC9 strain, and the TM3.GFP balancer on chromosome 3 (crossing scheme in **Figure S2,** *Appendix 2*). sgRNA homozygotes containing the *Dβ1_5'UTR_sgRNA/Dβ1_sgRNA2* pair were also crossed into GAL4 backgrounds to enable tissue-specific somatic CRISPR crosses with UAS-Cas9 (final crosses outlined in **Figure S3***, Appendix 2*) (Meltzer *et al.* 2019). Genomic cutting was detected in these somatic CRISPR mosaics using *Dβ1_5'UTR_sgRNA_HMA_F/Dβ1_sgRNA2_HMA_R.*

3.3.3 Generating *Dβ1*-TG4 using CRIMIC

An sgRNA targeting *Dβ1* intron one was designed using the *crisprflydesign.org* online tool and integrated into the pU6-BbsI-chiRNA plasmid (Addgene: 45946) using the recommended protocol (Gratz *et al.* 2013). Homology arms of approximately 1kb adjacent to the sgRNA were amplified using Q5 PCR (NEB) from genomic DNA of the *actin*-Cas9 strain and ligated into the pT-GEM(attP2-SA(1)-T2A-GAL4-Hsp70-lox2-3XP3-RFP) plasmid (Addgene: 62893) using the recommended protocol (Diao *et al.* 2015). The *Dβ1*-TG4 strain was made by microinjection of pU6-BbsI-chiRNA and pT-GEM plasmid DNA into *actin*-Cas9 embryos. Transgenic adults were selected by the eye-specific RFP marker and crossed to incorporate the X chromosome and chromosome 2 from the wAC9 strain, and the TM3.GFP balancer on chromosome 3 (crossing scheme in **Figure S4***, Appendix 2*).

3.3.4 Generating cDNA rescue constructs

Total RNA was extracted from the wild type line Armenia[14]. The *Dβ1* open reading frame was then PCR amplified using *Dβ1_clone_F* and *Dβ1_clone_R* primers (**Table S3***, Appendix 2*) and cloned into pGEM-T Easy (Promega). Clones were sequenced, sub-cloned into the *Not*I

site of the pUAST-attB vector (Bischof *et al.* 2007), and microinjected into attP40 (25709 w^-) embryos. Successful transgenics were screened phenotypically for w^+ eye colour rescue, and molecularly using *SV40* and *25709_External_R1* primers. Homozygotes were recovered by self-crossing the heterozygous offspring of injectees. Homozygotes were then crossed to incorporate the *Dβ1Δex5* deletion and the TM3.GFP balancer on chromosome 3 for use in rescue experiments (rescue crosses outlined in **Figure S3***, Appendix 2*). For the chromosome 3 driver *CCAP*-GAL4, a recombined *CCAP-GAL4*, *Dβ1Δex5* line was generated.

3.3.5 Developmental mortality assays

First instar larvae were transferred from apple juice agar plates to standard semolina fly food, reared for 2 weeks, then scored for stage of mortality (50 per vial, 5 independent vials, n = 250). Individuals that died during pupal stages P1-P11 or P12-P15 (Bainbridge and Bownes 1981) were scored as "pupal" and "eclosing" respectively.

3.3.6 Wing morphology scoring

Adults were scored for wing morphology (n = 250) using nomenclature established by Luan *et al.* (2006) as a guide. Unexpanded (UE) wings had an angle ≤90º between the distal and proximal portions of the folded wing, and fully expanded (FE) wings were completely straight or only slightly curled, resembling wild type morphology. Partially expanded (PE) wings had intermediate phenotypes, often with unfolded costal elbows.

3.3.7 Longevity and fertility assays

Virgin males and females were collected over 48 hours then placed on standard semolina-based fly media (10 males and 10 females per vial, 4 vials per genotype, n = 80). Vials were maintained horizontally at 25°C under a 12:12h light: dark cycle. Flies were transferred to new vials and the number of dead flies recorded every 2-3 days (or every 4-7 days late in the experiment for long-lived genotypes) until all were deceased. A Kaplan-Meier Survival Curve was constructed and significance was calculated using a Cox-Mantel test ($p < 0.05$). To

estimate fertility, these vials were then maintained for 2 weeks at 25°C and scored for the number of eclosing adult offspring relative to the number of surviving parental females present at time of egg-laying (n = 40). Significance was calculated for each timepoint using Tukey's honestly significant difference pair-wise test ($p < 0.05$).

3.3.8 Mating assays

Virgin males and females were collected and stored individually for 3 days. For single pair crosses, an individual male and female were placed in a standard semolina fly media vial with the stopper pushed down to ~20mm from the surface of the food. This was repeated for all 4 possible combinations of wAC9 and *Dβ1Δex5* flies (n = 20 per combination). Pairs were allowed to mate for 3 days, then removed from the vial, and the presence of F_1 offspring recorded 2 weeks later. For filmed assays, an individual male was gently aspirated without anesthesia into a mating chamber (12mm x 4mm) and allowed to acclimate for 3 minutes. A single female was then introduced and video recording initiated. Mating pairs were recorded using a Panasonic 3CCD Ultra-Compact Digital Palmcorder for 30 minutes or until copulation commenced. This was repeated with wAC9 males and *Dβ1Δex5* males, each of which were only paired with a wAC9 female (n = 20 per combination). Videos were inspected manually for courtship behaviour and copulation. The Courtship Index was measured using only the first 10 minutes of the recording (or only the time prior to copulation for pairs that commenced copulation within 10 minutes) and was defined as the proportion of time males spent exhibiting the following courtship behaviours: wing extension, following, tapping, and attempted copulation. Significance was calculated using Student's t-test ($p < 0.05$).

3.3.9 Adult climbing assays

Three-day-old flies were transferred without anesthesia into clean empty vials, allowed to acclimate for 5 minutes, then tapped down 3 times on a fly pad to initiate the negative geotaxis response (Gargano *et al.* 2005) (10 males and 10 females per vial, 4 vials per genotype, n = 80). The vials were recorded for 10 seconds from a distance of 30cm on an

iPhone 8 (Apple Inc.). QuickTime Player (Apple Inc.) was used to capture the frame occurring 6 seconds (180 frames) post-third tap down. JPEGs were then imported into Image J (Fiji, version 2.0.0, Schindelin et al. 2012) and marked with a horizontal threshold 35mm from the bottom of the vials. The number of flies above this threshold was scored manually. Significance was calculated using Tukey's test ($p < 0.05$).

3.3.10 Larval movement assays

Basal larval movement was measured using a modified Wiggle Index (WI) Assay (Denecke *et al.* 2015). Briefly, second or third instar larvae were transferred into a 24-well plate (25 larvae per well, 4 wells per genotype, $n = 100$) containing 200µL 5% sucrose in distilled water. Thirty second videos were taken at 0, 15, 30, 60, 90, and 120 minutes after the addition of larvae using a Panasonic 3CCD Ultra-Compact Digital Palmcorder. Raw videos were split into JPEG image sequences using the DVDVideoSoft Converter, and further processed as previously described (Denecke *et al.* 2015), generating heat maps and a numerical estimate of total motility (WI). To calculate relative movement, WI values were normalized to the wAC9 WI mean. Significance was calculated using Student's t-test ($p < 0.05$).

3.3.11 qRT-PCR

Quantitative real time PCR (qRT-PCR) was used to measure transcript levels of *Dβ1* and peptide hormones in *Dβ1Δex5* and *Dβ1Δex3* relative to the wAC9 control. For each of 4 biological samples, 10 pharate pupae or 10 one-day-old adults were collected in liquid nitrogen. RNA was isolated using TRIsure Reagent (Bioline) and the concentration measured using the Qubit Fluorometer. cDNA was synthesized from 1µg RNA using the GoScript Reverse Transcription Kit (Promega). qRT-PCR reactions for each biological sample were carried out in triplicate using a Quanti-fast SYBR Green PCR kit (Qiagen) on the CFX384 Touch Real-Time PCR Detection System (Bio-Rad). The amount of target RNA was normalized to the geometric mean of two endogenous controls: *Rpl32* and *CG13220* (Van Hiel *et al*. 2009). mRNA levels were compared between samples using the $\Delta\Delta C_T$ method

(Bustin *et al.* 2009) and significance was calculated using Student's t-test ($p < 0.05$). All primer sequences used are provided in **Table S3** (*Appendix 2*) and the Minimum Information for publication of Quantitative Real-time PCR Experiments (MiQE) checklist is also provided (**Table S4***, Appendix 2*).

3.3.12 Data availability

The authors affirm that all data necessary for confirming the conclusions of this article are represented fully within the article and its tables and figures. All fly strains are available upon request.

3.4 Results

3.4.1 *Dβ1* genomic deletions and *Dβ1*-TG4

Two *Dβ1* genomic deletions were used in this study (**Figure 3.1 A**). The larger deletion, *Dβ1Δ*ex5, removes 5,484bp spanning the region from the 5'UTR to exon 5 (Perry *et al.* 2021). Most of the receptor, up to and including transmembrane domain 3, is deleted. The smaller deletion, *Dβ1Δex3,* removes 4,148bp, removing the region from the 5'UTR to exon 3. The beginning of the ligand-binding domain (LBD), up to and including loop D is deleted. For both deletions, loss of *Dβ1* transcripts in homozygotes was confirmed with qRT-PCR (**Figure 3.1 B**). Unless otherwise specified, the larger deletion, *Dβ1Δex5,* was used in all subsequent experiments. A *Dβ1* T2A-GAL4 strain was also generated in this study (*Dβ1*-TG4). This strain contains a Trojan GAL4 exon in intron 1, resulting in truncation of the *Dβ1* gene product and expression of GAL4 in *Dβ1*'s native pattern (expression pattern provided in **Figure S5***, Appendix 2*). It was thus used as both a null allele and a *Dβ1*-specific GAL4 driver (Diao and White, 2012).

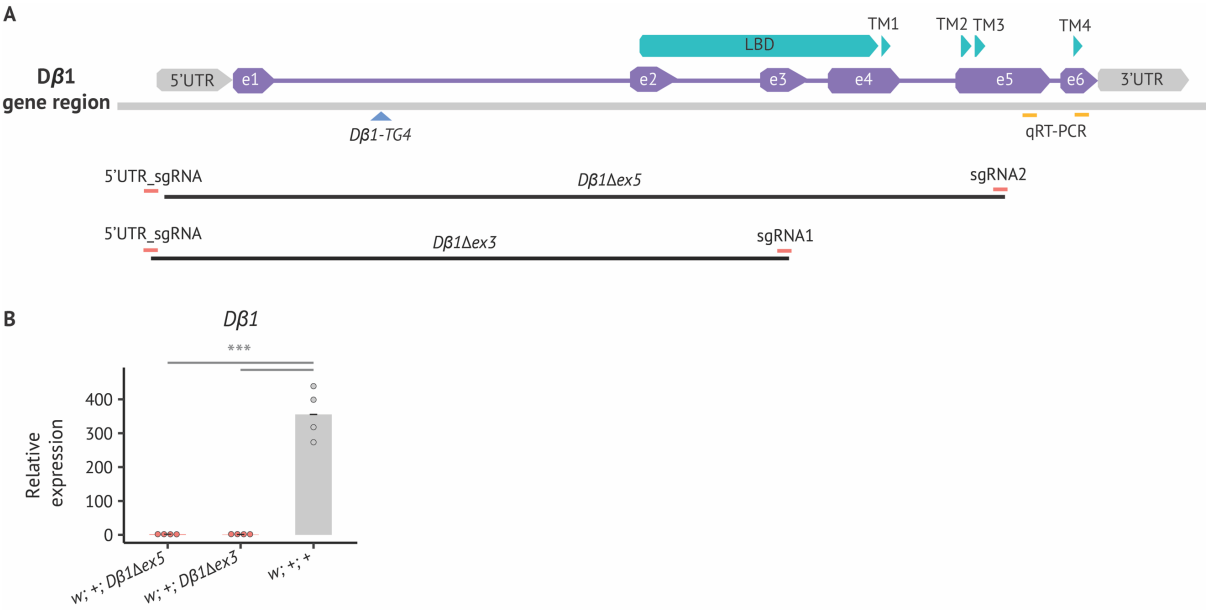


Figure 3.1 Genomic deletion of the *Dβ1* nAChR subunit gene

(**A**) Two deletions were used in this study: *Dβ1Δex5* and *Dβ1Δex3*. The deleted regions are shown flanked by synthetic guide RNAs (sgRNA, red). The positions of the *Dβ1* ligand binding domain (LBD, green), transmembrane domains (TM1-4, green), exons (e1-6, purple), and qRT-PCR primers (orange) are shown above. The position of the T2A-GAL4 insertion in intron 1 is also indicated (*Dβ1*-TG4, blue). (**B**) qRT-PCR indicates loss of *Dβ1* transcripts in both deletion strains. Error bars indicate SEM (n = 4 biological replicates, *** $p < 0.001$, Student's t-test).

3.4.2 Loss of *Dβ1* decreases fitness and disrupts wing expansion

The deletion of *Dβ1* incurs severe fitness costs. When reared in non-competitive conditions (i.e. in the absence of heterozygous siblings), *Dβ1Δex5* homozygotes exhibited reduced survival to adulthood (83%) compared to wAC9 controls (98%) (**Figure 3.2 A**). One distinctive stage of mortality was mid-eclosion (**Figure 3.2 B**). For those flies that developed to adulthood, median longevity was shortened significantly from 40 days (wAC9) to 6 days ($D\beta1\Delta^{ex5}$) ($p < 0.001$, Cox-Mantel test) (**Figure 3.2 C**) and these adults failed to produce any viable offspring ($p < 0.001$, Tukey's test, **Table S5,** *Appendix 2*) (**Figure 3.2 D**). Adults exhibited varying disruptions in wing expansion. Only 26% attained the FE (fully expanded) morphology, whilst 19% presented with the intermediate PE (partially expanded) wings and 55% had the severe UE (unexpanded) morphology (**Figure 3.2 E, F**).

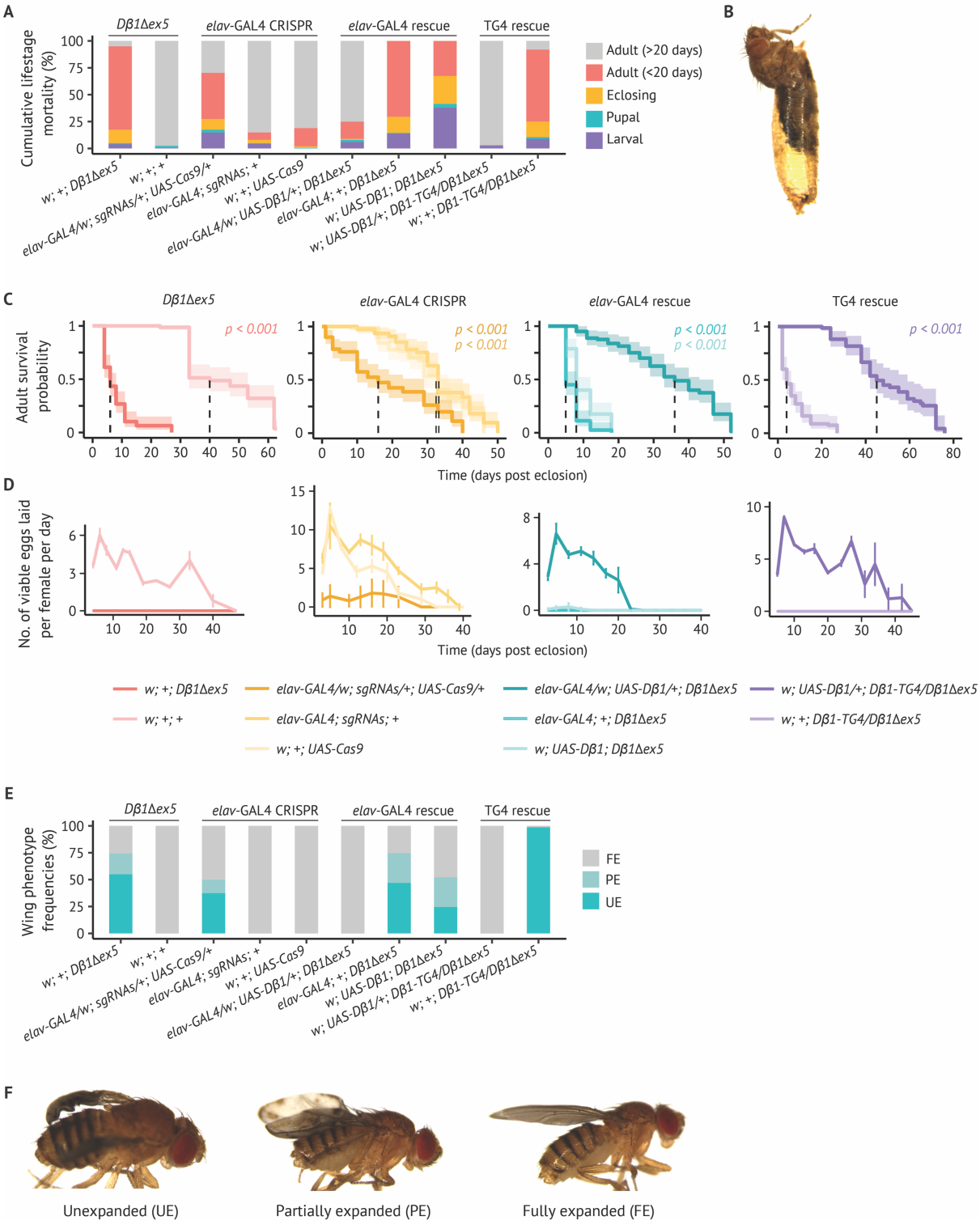
We were able to replicate these phenotypes using pan-neuronal somatic CRISPR. In *elav*-GAL4 CRISPR mosaics (*elav-GAL4/w; sgRNAs/+; UAS-Cas9/+*), genomic deletion of *Dβ1* is restricted to neurons by expressing UAS-Cas9 under the control of *elav*-GAL4 in the presence of two ubiquitously expressed *Dβ1*-targeting sgRNAs. Like *Dβ1Δex5* flies, *elav*-GAL4 CRISPR mosaics exhibited 79% survival to adulthood (**Figure 3.2 A**). Longevity and fertility were both affected, with median adult survival shortened significantly to 16 days ($p < 0.001$, Cox-Mantel test) (**Figure 3.2 C**) and no viable offspring produced in all but one vial (**Figure 3.2 D**). Wing expansion was disrupted, although in slightly less severe proportions (50% FE, 13% PE, 37% UE) (**Figure 3.2 E, F**). The general concordance of *elav*-GAL4 CRISPR and *Dβ1Δex5* results indicate that loss of Dβ1 function in the neurons is responsible for the fitness and wing phenotypes observed.

We further verified that loss of *Dβ1* function was responsible for these phenotypes using two approaches. First, expression of *Dβ1* cDNA in a *Dβ1* null background was sufficient to rescue all elements of the phenotype. Full phenotypic rescues were achieved when using the *Dβ1*-TG4 driver ("TG4 rescue") (**Figure 3.2 A, C, D, E**). When using the pan-neuronal *elav*-GAL4 driver ("*elav*-GAL4 rescue"), full rescues were achieved for longevity (**Figure 3.2**

C) and wing expansion (**Figure 3.2 E**), while partial rescues were observed for developmental mortality (**Figure 3.2 A**) and production of viable offspring (**Figure 3.2 D**). No overexpression phenotypes were observed. Second, *Dβ1Δex5* failed to complement two independent *Dβ1* mutant alleles: the *Dβ1Δex3* genomic deletion and the *Dβ1*-TG4 truncation allele (**Figure S6,** *Appendix 2*).

Figure 3.2 (opposite) *Dβ1* deletion reduces adult fitness

Dβ1Δex5 homozygotes have low fitness levels for several traits. This reduced fitness is replicated by neuron-specific somatic deletion of *Dβ1* (*elav*-GAL4 CRISPR) and it is rescued by expression of *Dβ1* cDNA in neurons (*elav*-GAL4 rescue) or in *Dβ1*-expressing cells (*Dβ1*-TG4 rescue). Results for *Dβ1Δex5* homozygotes are shown alongside their background control, wAC9 (*w; +; +*). For *elav*-GAL4 CRISPR, *elav*-GAL4 rescue, and TG4 rescue, results for experimental animals are followed by results for parental controls. (**A**) Deaths during early adulthood (<20 days) and the "Eclosing" phase were most common for *Dβ1Δex5* and other strains lacking *Dβ1* (*n* = 250). (**B**) Depicts a fly arrested during the "Eclosing" phase. (**C**) Kaplan-Meier survival plots with black dashed lines marking median longevity. Median longevity was shortened significantly to 6 days in *Dβ1Δex5.* Shading represents 95% confidence intervals (*n* = 80, Cox-Mantel test). (**D**) Number of viable eggs laid per female per day, throughout lifespan. Error bars indicate SEM and *p* values for each time point are provided in **Table S5** *Appendix 2* (*n* = 40, Student's t-test). (**E**) *Dβ1Δex5* and other strains lacking *Dβ1* are afflicted with unexpanded (UE) and partially expanded (PE) wings, with fewer achieving fully expanded (FE) wings (*n* = 250). (**F**) Images of representative individuals from each wing phenotype category.


A
Dβ1Δex5
elav-GAL4 CRISPR
elav-GAL4 rescue
TG4 rescue
Cumulative lifestage mortality (%)
Adult (>20 days)
Adult (<20 days)
Eclosing
Pupal
Larval
w; +; Dβ1Δex5
w; +; +
elav-GAL4/w; sgRNAs/+; UAS-Cas9/+
elav-GAL4; sgRNAs; +
w; +; UAS-Cas9
elav-GAL4/w; UAS-Dβ1/+; Dβ1Δex5
elav-GAL4; +; Dβ1Δex5
w; UAS-Dβ1; Dβ1Δex5
w; UAS-Dβ1/+; Dβ1-TG4/Dβ1Δex5
w; +; Dβ1-TG4/Dβ1Δex5
B
C
Adult survival probability
p < 0.001
Time (days post eclosion)
D
No. of viable eggs laid per female per day
Time (days post eclosion)
E
Wing phenotype frequencies (%)
FE
PE
UE
F
Unexpanded (UE)
Partially expanded (PE)
Fully expanded (FE)

3.4.3 Loss of *Dβ1* affects locomotor performance

Having casually observed reduced movement in *Dβ1Δex5* larvae, relative larval movement was quantified in second and third instar larvae using a modified WI Assay (Denecke *et al.* 2015). This plate-based assay involves filming larvae crawling in a shallow pool of sucrose solution. Thirty-second videos were converted to heat maps and numerical estimates of total motility (WI). Compared to the wAC9 control, *Dβ1Δex5* homozygotes displayed 40% and 85% relative basal movement in second and third instar larvae, respectively. Both differences were highly significant ($p < 0.001$, Student's t-test) (**Figure 3.3 A**).

In adults, severe overall movement deficiencies were observed, however we chose to limit our investigation to climbing assays (**Figure 3.3 B**). Individuals that climbed beyond a 35mm checkpoint within six seconds were deemed to have a successful climbing response. Almost all *Dβ1Δex5* homozygotes failed (2%), whilst 93% of wAC9 controls were successful ($p < 0.001$, Tukey's test). *elav*-GAL4 CRISPR mosaics were also unable to climb (2%) ($p < 0.001$). Climbing response was only partially rescued (20%) in the *elav*-GAL4 rescue, however this was a statistically significant improvement in performance compared to non-rescued parental controls (both 0%, $p < 0.001$). Full rescue was achieved using the *Dβ1*-TG4 driver ($p < 0.001$).

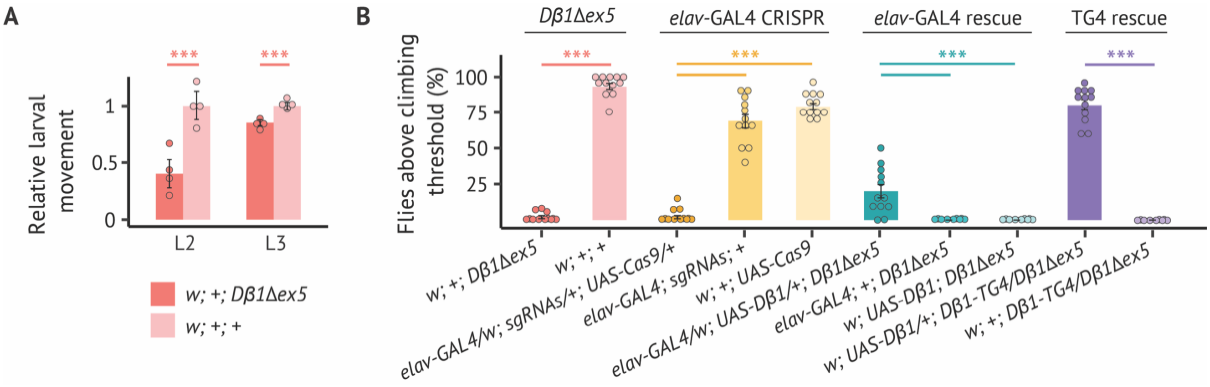


Figure 3.3 *Dβ1* deletion affects larval crawling and adult climbing performance

Results for *Dβ1Δex5* homozygotes are shown alongside their background control, wAC9 (*w; +; +*). For *elav*-GAL4 CRISPR, *elav*-GAL4 rescue, and TG4 rescue, results for experimental animals are followed by results for parental controls. (**A**) A Wiggle Index assay measuring relative larval movement reveals significantly reduced crawling in second (L2) and third (L3) instar larvae. Error bars indicate SEM (n = 100, p *** < 0.001, Student's t-test). (**B**) Adult climbing performance was significantly low in all genotypes lacking *Dβ1*. Error bars indicate SEM (n = 80, p ** < 0.01, *** < 0.001, Tukey's test).

3.4.4 Males lacking *Dβ1* spend less time courting and fail to initiate copulation

Given the failure to produce offspring, and the reduced locomotor performance observed in previous assays, we were curious if *Dβ1Δex5* adults exhibited normal mating behaviours. First, we crossed individual *Dβ1Δex5* and wAC9 males and females in all four possible combinations and recorded the presence of F_1 offspring (**Figure 3.4 A**). Offspring were observed in almost all crosses between wAC9 males and *Dβ1Δex5* females, indicating *Dβ1Δex5* females are fertile. Meanwhile, crosses involving *Dβ1Δex5* males never gave rise to offspring, indicating a male issue. Males were therefore investigated further in filmed 30-minute mating assays. All pairs consisting of a wAC9 male and wAC9 female initiated copulation within the 30-minute recording, while no copulation was observed when wAC9 females were paired with *Dβ1Δex5* males (**Figure 3.4 B**). The first ten minutes of the recording was also used to calculate a Courtship Index, defined as the proportion of time males spent exhibiting any of the following behaviours: wing extension, following, tapping, and attempted copulation (**Figure 3.4 C**). On average, *Dβ1Δex5* males spent only 2% of their time courting, compared to 39% in wAC9 males ($p < 0.001$, Student's t-test). The only behaviours observed in *Dβ1Δex5* males were weak attempts at wing extension and brief bouts of following.

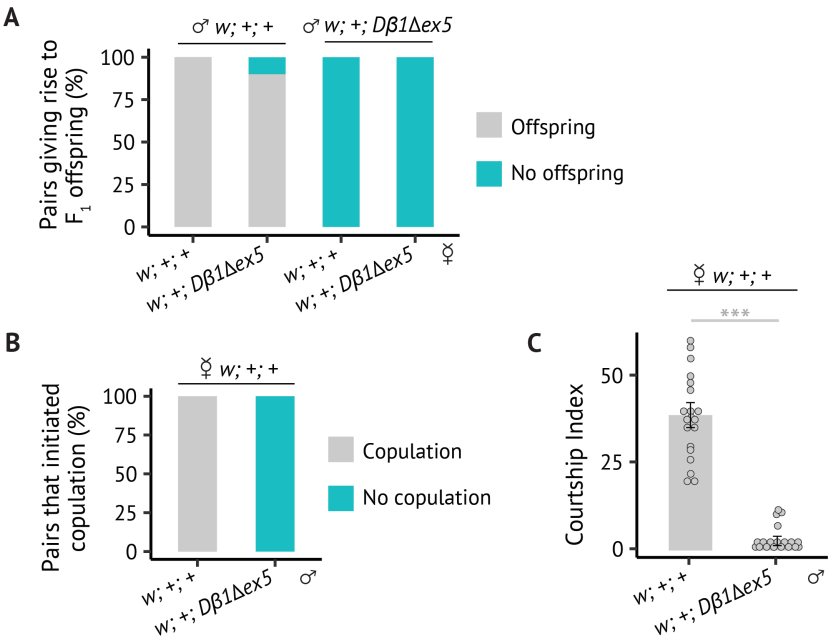


Figure 3.4 Males lacking *Dβ1* fail to mate

(**A**) For crosses between single mating pairs, the presence of F_1 offspring was recorded. The male genotype is indicated above and the female genotype indicated below. Crosses involving *Dβ1Δex5* males gave never gave rise to offspring, while *Dβ1Δex5* females were shown to be fertile (*n* = 20 pairs per mating combination). (**B**) Percentage of pairs that initiated copulation within 30 minutes of a female being introduced. The female genotype is indicated above and the male genotype indicated below. *Dβ1Δex5* males do not initiate copulation (*n* = 20 pairs per mating combination). (**C**) *Dβ1Δex5* males spend significantly less time courting females than wAC9 control (*w; +; +*) males. The female genotype is indicated above and the male genotype indicated below. Error bars indicate SEM (*n* = 20 pairs per mating combination, *** $p < 0.001$, Student's t-test).

3.4.5 Pinpointing a neuronal subset that requires *Dβ1*

Having observed disruptions in eclosion and wing expansion, we chose to investigate the role of Dβ1 in the CCAP neurons. These neurons secrete the neuropeptide hormones CCAP, required for eclosion (and other ecdyses) (Park *et al.* 2003), and bursicon, required for wing expansion and cuticle tanning (Luan *et al.* 2006).

We used somatic CRISPR to generate mosaics with a genomic deletion of *Dβ1* specifically in CCAP neurons ("*CCAP*-GAL4 CRISPR") of which there are approximately 27 pairs in the larval brain (Park *et al.* 2003, Karsai *et al.* 2013) (**Figure 3.5 A**). This CCAP-specific deletion of *Dβ1* was sufficient to cause the wing expansion phenotype only (**Figure 3.5 B**). Wing morphology was severely affected, with 60%, 29%, and 12% displaying the UE, PE, and FE phenotypes, respectively. Meanwhile, developmental mortality, adult longevity, fertility, and climbing performance were comparable to the parental controls (**Figure S7***, Appendix 2*). We performed the same somatic CRISPR experiment using the more restrictive *bursicon*-GAL4 driver. *Bursicon* has a later temporal expression pattern than *CCAP* (Kim *et al.* 2006, Di Cara and King-Jones 2013), and its expression is limited to a subset of the CCAP neurons (Luan *et al.* 2006, Kim *et al.* 2006). No phenotypes were observed, so we extracted genomic DNA from these *bursicon*-GAL4 CRISPR flies. We were not able to detect any CRISPR editing in pooled samples (**Figure S8***, Appendix 2*), so we concluded that the lack of phenotype was actually due to inefficient CRISPR in these flies and they were not examined further.

Having evidence that *Dβ1* plays a key role in CCAP neurons, we moved on to consider whether expression of *Dβ1* in CCAP neurons alone is *sufficient* for viability. To test this, *CCAP*-GAL4 and *bursicon*-GAL4 were used to drive expression of UAS-*Dβ1* cDNA in a *Dβ1Δex5* homozygous background. For *CCAP*-GAL4, full rescue was achieved for developmental mortality (**Figure 3.5 C**) and wing morphology (**Figure 3.5 F**). This suggests *Dβ1* is required almost exclusively in CCAP neurons to fulfil its roles in wing expansion and survival through development. Partial rescue was achieved for *CCAP*-GAL4 for adult longevity (28 days) (**Figure 3.5 D**), and to a lesser extent, fertility (**Figure 3.5 E**) and climbing

performance (14%) (**Figure 3.5 G**), indicating *Dβ1* also plays critical roles in other neuronal subsets affecting ageing, mating, and climbing ability.

bursicon-driven expression of UAS-*Dβ1* was slightly less efficient in its capacity to rescue these phenotypes. For *bursicon*-GAL4, full rescue was achieved only for wing morphology (**Figure 3.5 F**). Partial rescue was achieved for *bursicon*-GAL4 for developmental mortality (86%) (**Figure 3.5 C**) and adult longevity (29 days) (**Figure 3.5 D**) and to a lesser extent, fertility (**Figure 3.5 E**) and climbing performance (4%) (**Figure 3.5 G**). No phenotypes were observed from overexpression of *Dβ1* with *CCAP*-GAL4 or *bursicon*-GAL4.

To test whether loss of Dβ1 disrupts peptide hormone expression in CCAP neurons, we used qRT-PCR to measure hormone transcripts in *Dβ1Δex5* relative to the wAC9 control. Transcripts were measured in a lifestage where the respective hormone is known to be active (Di Cara and King-Jones 2013); *CCAP* transcripts where measured in pharate pupae, whilst *bursicon* and its heterodimer partner, *partner of bursicon,* were measured in newly eclosed adults. A significant 21-fold reduction in *bursicon* transcripts was detected in *Dβ1Δex5* ($p < 0.01$), as was a significant 4-fold reduction in *partner of bursicon* ($p < 0.05$) (**Figure 3.5 H**). A small reduction in *CCAP* was also detected in *Dβ1Δex5* however this was not statistically significant due to variation between biological replicates.

Finally, given that bursicon plays an important role in cuticle tanning, the cuticles of *Dβ1Δex5* and wAC9 adults were also compared, however only a subtle difference in pigmentation was observed (**Figure 3.5 I**).

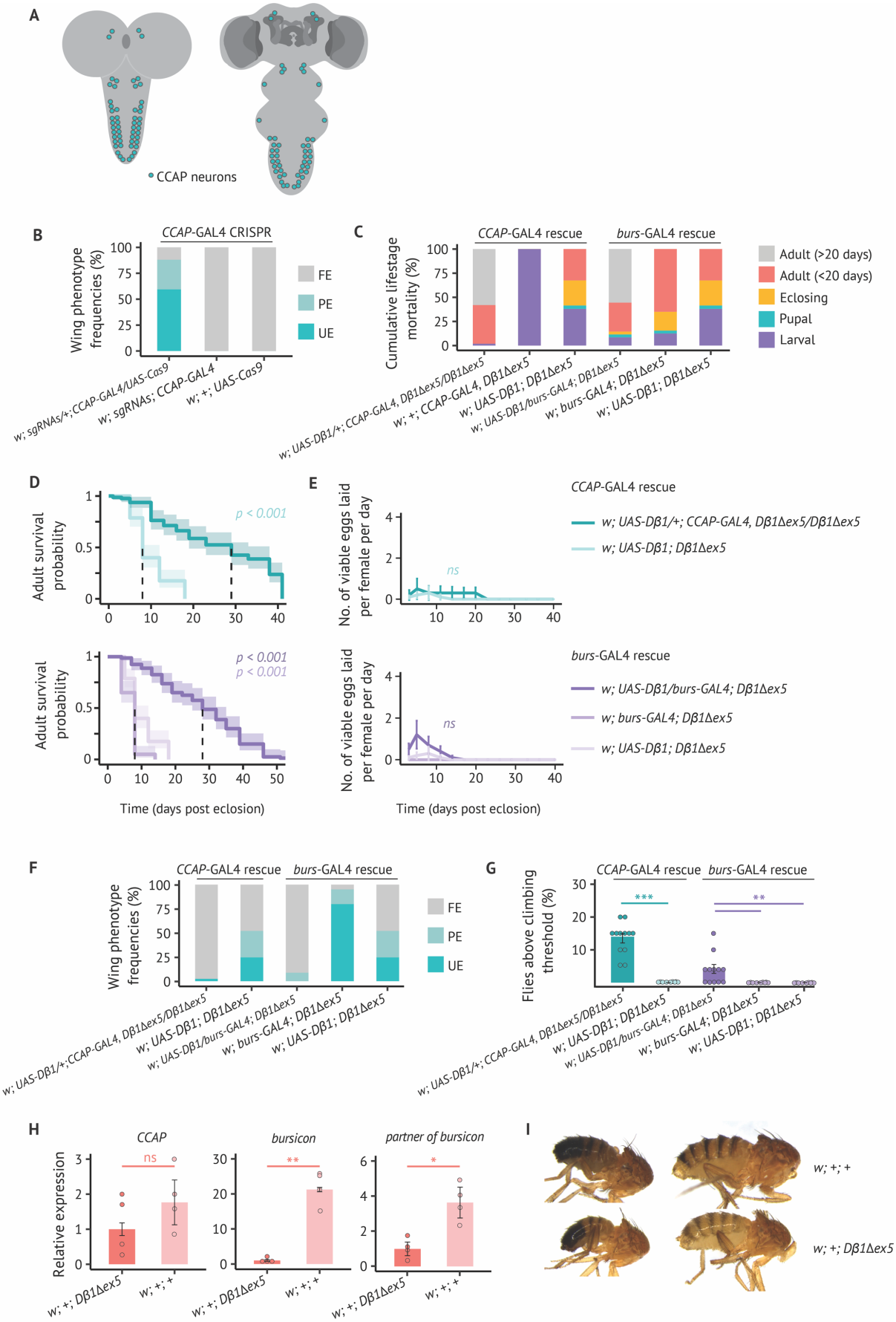

A
CCAP neurons
B
CCAP-GAL4 CRISPR
Wing phenotype frequencies (%)
FE
PE
UE
w; sgRNAs/+;CCAP-GAL4/UAS-Cas9
w; sgRNAs; CCAP-GAL4
w; +; UAS-Cas9
C
CCAP-GAL4 rescue
burs-GAL4 rescue
Cumulative lifestage mortality (%)
Adult (>20 days)
Adult (<20 days)
Eclosing
Pupal
Larval
w; UAS-Dβ1/+; CCAP-GAL4, Dβ1Δex5/Dβ1Δex5
w; +; CCAP-GAL4, Dβ1Δex5
w; UAS-Dβ1; Dβ1Δex5
w; UAS-Dβ1/burs-GAL4; Dβ1Δex5
w; burs-GAL4; Dβ1Δex5
w; UAS-Dβ1; Dβ1Δex5
D
Adult survival probability
p < 0.001
p < 0.001
p < 0.001
Time (days post eclosion)
E
No. of viable eggs laid per female per day
ns
ns
CCAP-GAL4 rescue
w; UAS-Dβ1/+; CCAP-GAL4, Dβ1Δex5/Dβ1Δex5
w; UAS-Dβ1; Dβ1Δex5
burs-GAL4 rescue
w; UAS-Dβ1/burs-GAL4; Dβ1Δex5
w; burs-GAL4; Dβ1Δex5
w; UAS-Dβ1; Dβ1Δex5
Time (days post eclosion)
F
CCAP-GAL4 rescue
burs-GAL4 rescue
Wing phenotype frequencies (%)
FE
PE
UE
w; UAS-Dβ1/+;CCAP-GAL4, Dβ1Δex5/Dβ1Δex5
w; UAS-Dβ1; Dβ1Δex5
w; UAS-Dβ1/burs-GAL4; Dβ1Δex5
w; burs-GAL4; Dβ1Δex5
w; UAS-Dβ1; Dβ1Δex5
G
CCAP-GAL4 rescue
burs-GAL4 rescue
Flies above climbing threshold (%)
***
**
w; UAS-Dβ1/+; CCAP-GAL4, Dβ1Δex5/Dβ1Δex5
w; UAS-Dβ1; Dβ1Δex5
w; UAS-Dβ1/burs-GAL4; Dβ1Δex5
w; burs-GAL4; Dβ1Δex5
w; UAS-Dβ1; Dβ1Δex5
H
CCAP
bursicon
partner of bursicon
Relative expression
ns
**
*
w; +; Dβ1Δex5
w; +; +
I
w; +; +
w; +; Dβ1Δex5

Figure 3.5 (opposite) *Dβ1* is required in CCAP neurons for bursicon-driven wing expansion

(**A**) Cartoon depicting CCAP neurons in a larval and pupal brain (modified from Veverytsa and Allan 2012, Moris-Sanz *et al*. 2015). (**B**) Somatic CRISPR deletion of *Dβ1* specifically in CCAP neurons is sufficient to impair wing expansion (*n* = 250). Results for experimental animals are followed by results for parental controls. (**C-H**) Expression of *Dβ1* driven by *CCAP*-GAL4 or *bursicon*-GAL4, in a *Dβ1Δex5* background, can fully or partially rescue some *Dβ1Δex5* phenotypes. Results for each rescue are followed by results for non-rescued parental controls. (**C**) *CCAP*-GAL4 rescue and *bursicon*-GAL4 rescue largely eliminate developmental mortality (*n* = 250). Given the high rate of larval mortality observed in the parental control *w; +; CCAP-GAL4, Dβ1Δex5*, this strain is absent from subsequent adult experiments. (**D**) Kaplan-Meier survival plot with black dashed lines marking median longevity. *CCAP*-GAL4 and *bursicon*-GAL4 rescue median longevity to 29 and 28 days, respectively. This is significant compared to parental controls, but less efficient than restoring *Dβ1* expression in all *Dβ1*-expressing cells (**Figure 3.2**). Shading represents 95% confidence intervals (*n* = 80, $p < 0.001$, Cox-Mantel test). (**E**) Number of viable eggs laid per female per day, throughout lifespan. *CCAP*-GAL4 rescue and *bursicon*-GAL4 rescue do not significantly improve egg counts. Error bars indicate SEM (*n* = 40, Student's t-test performed for each time point). (**F**) *CCAP*-GAL4 rescue and *bursicon*-GAL4 rescue almost completely restore normal wing expansion (*n* = 250). UE, unexpanded; PE, partially expanded; FE, fully expanded. (**G**) *CCAP*-GAL4 rescue and *bursicon*-GAL4 rescue partially but significantly improved adult climbing performance. Error bars indicate SEM (*n* = 80, p *** < 0.001, Tukey's test). (**H**) qRT-PCR indicates 21-fold reduction in *bursicon* transcripts and 4-fold reduction in *partner of bursicon* transcripts in newly-eclosed *Dβ1Δex5* homozygous adults. A non-significant reduction was observed for *CCAP* transcripts in pharate pupae. Error bars indicate SD (*n* = 4 biological replicates, * $p < 0.05$, ** $p < 0.01$, Student's t-test). (**I**) Male and female *Dβ1Δex5* homozygotes have a slight reduction in cuticle pigmentation compared to wAC9 controls.

3.5 Discussion

Understanding nAChR biology is a vital step in dissecting the cholinergic circuits of the insect brain. It also provides valuable insight into how nAChR-targeting chemicals used for pest control may affect insect development, physiology and behavior. In the present study, we provide the first functional description of a deletion of the *Dβ1* nAChR subunit, a known insecticide target, and the most highly expressed nAChR subunit in the *Drosophila* brain. As expected, loss of Dβ1 was highly disruptive, with individuals having a shortened lifespan, reduced mating success, limited larval and adult movement, and unexpanded wings. This reduction in viability was partially attributed to CCAP neurons requiring *Dβ1* expression and linked to loss of the peptide hormone bursicon. These are by far the most severe pleiotropic consequences described for an nAChR mutant so far (Somers *et al.* 2017, Homem *et al.* 2020, Perry *et al.* 2021). Deletion mutants for nine of the ten *Drosophila* nAChR subunits have now been described, and while not all the traits examined here have been analyzed in these other mutants, no subunits aside from *Dβ1* have been observed with a wing expansion phenotype (Perry *et al.* 2021).

Our findings follow recent work on a resistance-conferring mutation in *Dβ1*, the R81T amino acid replacement (Homem *et al.* 2020). Homem and colleagues describe similar fitness costs in their CRISPR-generated $D\beta1^{R81T}$ allele. Like the *Dβ1Δex5* deletion, $D\beta1^{R81T}$ mutant flies were infertile and had poor larval crawling performance. Reduced longevity and climbing performance were also described, albeit with sex-specific differences that we did not observe in our own lines. Notably, the authors did not describe any disruptions in wing expansion in either sex, but it is important to keep in mind the nature of the alleles when comparing these sets of results. Our deletions, *Dβ1Δex5* and *Dβ1Δex3*, result in complete loss of the Dβ1 subunit. In the *Dβ1*-expressing neurons, this absence could simply result in loss of cholinergic signal, but there is evidence that the absence of one subunit can also alter the levels of other nAChR subunits at the level of transcription (Perry *et al.* 2021). In contrast, the R81T mutation does not result in loss of the subunit (Homem *et al.* 2020) and there is evidence that this amino acid replacement has only a subtle effect on the binding affinity of acetylcholine (Shimomura *et al.* 2006, Ihara *et al.* 2020). Thus, subsets of neurons

involved in different biological processes and behaviors may have different vulnerability to a simple reduction in neuron firing (as in *Dβ1*^{R81T}) versus complete loss of a subunit with possible nAChR compensation (as in *Dβ1Δex5*).

Using the somatic CRISPR-Cas9 system (Meltzer *et al.* 2019) and GAL4-UAS rescue system, we identified CCAP neurons as a neuronal subset where *Dβ1* expression was required for robust wing expansion. Disrupted wing expansion was observed at high frequency in our *CCAP*-GAL4 CRISPR mosaics, and this phenotype was fully rescued in *CCAP*-GAL4 and *bursicon*-GAL4 driven rescues. We also observed a mild reduction in tanning of the cuticle in *Dβ1Δex5* mutants. Furthermore, inspection of available single-cell RNA-seq datasets reveal co-expression of *Dβ1* with *CCAP, bursicon* and *partner of bursicon* in both the larval brain (Ravenscroft *et al.* 2020) and the adult ventral nerve cord (Allen *et al.* 2020) (**Figure S9***, Appendix 2*). Bursicon has long been documented as the wing expansion and cuticular tanning hormone (Fraenkel and Hsiao 1965), and the molting hormone cascade that culminates in bursicon's release from CCAP neurons is well-studied (Di Cara and King-Jones 2013). So how might Dβ1-containing nAChRs fit into this hormone cascade? The delayed release of bursicon is regulated by excitation of the CCAP neurons (Luan *et al.* 2006) and, to our knowledge, the neurotransmitter/s responsible for this excitation have not been identified. We propose the signal may be cholinergic, requiring Dβ1-containing nAChRs. However, this study did not examine the cholinergic signal and it will be important to test the electrophysiological response of CCAP neurons to acetylcholine in wildtype flies and *Dβ1* mutants to determine what current remains in the absence of Dβ1-containing nAChRs. An alternative hypothesis is that Dβ1-containing nAChRs are required in CCAP neurons during development such that loss of Dβ1 alters the connectivity and functionality of CCAP neurons. This hypothesis is also likely to explain the transcript-level loss of *CCAP*, *bursicon* and *partner of bursicon* we observed in *Dβ1Δex5*. It is also possible that altered expression of other nAChR subunits present in CCAP neurons may be contributing to the phenotypic effects of loss of Dβ1 (Perry *et al.* 2021). Based on single-cell RNA-seq data, all subunits except *Dβ3* are detected in CCAP neurons, (Allen *et al.* 2020, Ravenscroft *et al.* 2020). Ultimately, our results firmly place Dβ1-containing receptors as a key component of CCAP

neuron signaling, however investigation to further tease apart *when* and *how* Dβ1 is required will be of value.

Phenotypes that showed unsuccessful rescue (fertility) or partial rescue (longevity, climbing performance) in our CCAP rescue experiments indicate important roles for Dβ1 subunits in other neurons outside the CCAP subset. The observed reduction in *Dβ1Δex5* male courtship, and the subsequent failure to mate, could indicate a role for Dβ1-containing receptors in neurons regulating mating behaviour. Indeed, some of these neurons have already been identified as cholinergic (Acebes *et al.* 2004, Schinamen *et al.* 2014, Somers *et al.* 2017, Ishimoto and Kamikouchi 2020). Alternatively, any mating issues could be a side effect of impaired movement. Aside from poor climbing performance, we observed reduced general movement, and it is possible Dβ1-containing nAChRs are required in cholinergic muscle control (Hsu and Bhandawat 2016, Malloy *et al.* 2019). An approach similar to that used here, to specifically delete the *Dβ1* gene in neural circuits controlling male courtship, would provide insight into whether the mating issues observed are due to altered signalling in these courtship circuits, or due to a more general impact on movement.

While our experiments have yielded significant insights into roles of Dβ1, there remains considerable work to be performed on other circuits and with other nAChR subunits if we are to gain a complete picture of nAChR function in insect nervous systems. Recent developments in heterologous nAChR expression (Ihara *et al.* 2020) and single-cell sequencing (Croset *et al.* 2018, Brunet Avalos *et al*. 2019, Allen *et al*. 2020) will help accelerate this research, determining which subunits form functional subtypes, and whether those subunit combinations are natively expressed in the same neurons. Moving forward, simultaneous disruption of multiple subunits may also be required to unearth certain phenotypes. This would be useful in the identification of the nAChR α subunits co-assembling with Dβ1 to influence wing expansion. As we have seen here, this work highlights some of the reasons why nAChR-targeting insecticides became such a commercial success, yet also hints at why this insecticide class has run into issues relating to collateral damage to beneficial insect populations (Goñalons and Farina 2015, Wu-Smart and Spivak

2016, Woodcock *et al.* 2017, Crall *et al*. 2018, Sanchez-Bayo and Wyckhuys 2019, Martelli *et al.* 2020). On one hand, the severe fitness costs we have described may have safeguarded growers against widespread insecticide resistance evolving in pest species. On the other hand, our findings provide insight into how sublethal doses might be disrupting specific neuronal pathways in non-pest species. Ongoing efforts to understand native roles of insect nAChRs will be vital for refining pest control strategies and predicting the behavioral and physiological impacts on species living in insecticide-contaminated environments.

Chapter Four

Establishing a rescue system for examining the conservation of β1 subunits and resistance-conferring mutations

4.1 Introduction

In many insect species, the β1 nAChR subunit is a key target for multiple insecticides. In *Drosophila*, *Dβ1* knockout mutants show high levels of resistance to imidacloprid, nitenpyram and sulfoxaflor (Perry *et al.* 2021). In the brown planthopper, *Niliparvata lugens*, co-immunoprecipitation assays indicate Npβ1 is required for the formation of an imidacloprid binding site (Li *et al.* 2010). Similarly, electrophysiological assays indicate Amβ1 and Btβ1 are required for the formation of imidacloprid, thiacloprid and clothianidin binding sites in the bee species *Apis mellifera* and *Bombus terrestris* (Ihara *et al.* 2020).

Despite the clear importance of β1 subunits in insecticide mode of action, field-evolved resistance-conferring mutations are incredibly rare. This is almost certainly due to the detrimental fitness costs associated with loss of function, as seen in *Dβ1* knockout mutants. Flies lacking Dβ1 exhibit pleiotropic effects, including short adult lifespan, reduced locomotion, mating defects, and incomplete wing expansion (*Chapter Three*). The relatively high conservation of β1 subunits among insect species (Jones and Sattelle 2010), combined with the lack of resistant mutants in the field (with two exceptions), suggests these fitness costs are probably not restricted to *Drosophila*. Thus, any resistance-conferring mutations that reduce or abolish function of the subunit would be unlikely to thrive in field populations unless subjected to high selective pressure from insecticide exposure.

4.1.1 The R81T replacement

To date, only two species are reported to have field-evolved *β1* mutations in the field: the peach-potato aphid *Myzus persicae* (Bass *et al*. 2011) and the melon-cotton aphid *Aphis gossypii* (Koo *et al.* 2014). These sap-feeding aphids are both major agricultural pests with global distributions, and populations that have been exposed to a range of insecticides. In both species, the reported resistance to imidacloprid was conferred by a point mutation that caused an arginine to threonine replacement in the loop D region of the LBD of the β1 subunit (R81T). The same R81T replacement has since been shown to confer imidacloprid

resistance in *Drosophila* mutants (Homem *et al.* 2020), and loss of response to imidacloprid, thiacloprid and clothianidin in heterologously expressed *Drosophila* nAChRs (Ihara *et al.* 2020).

This amino acid position has long been recognised as key to the insect-specific selectivity of neonicotinoids. A threonine residue (81T) is characteristic of vertebrate subunits and causes lower imidacloprid binding affinity (Shimomura *et al.* 2006) (**Table 4.1**). Likewise, many arachnid species that are insensitive to neonicotinoids possess a glutamine residue (81Q) at the equivalent position (Dermauw *et al.* 2012, Erdmanis *et al.* 2012), although whether this difference is the primary cause of insensitivity remains to be tested.

Descriptions of the Drosophila *Dβ1*^{R81T} homozygous mutants indicate this replacement incurs fitness costs (Homem *et al.* 2020), albeit far less severe than *Dβ1* knockout mutants (*Chapter Three*). This is despite evidence that the replacement does not appear to disrupt ACh binding (Ihara *et al.* 2020). The fitness of R81T genotypes in aphid populations has not been described, however the delay with which imidacloprid resistance arose in these species (relative to other insecticides that do not target the β1 subunit) (Bass *et al.* 2011), could suggest an associated cost.

4.1.2 Using *Drosophila* to express alternative β1 subunits

While it is clear that β1 subunits play an important role in insecticide response among insect species, *in vivo* work on pest subunits is scarce because there are experimental limitations to studying a pest allele in the pest species itself. Field-evolved alleles often co-occur with metabolic resistance mutations, making it difficult to estimate the fold-resistance conferred by the target-site mutation itself. As for lab-generated alleles, despite advancements in CRISPR, it remains far more efficient to perform mutagenesis and maintain strains in the *Drosophila* model.

Table 4.1 Alignment of loop D amino acid residues from β1 (and equivalent) subunits

Species	Amino acid number of *D. melanogaster* β1 subunit										
Insects (sensitive)	77	78	79	80	**81**	82	83	84	85	86	87
D. melanogaster β1	N	V	W	L	R	L	V	W	Y	D	Y
M. persicae β1 (sensitive)	N	V	W	L	R	L	V	W	R	D	Y
A. gossypii β1 (sensitive)	N	V	W	L	R	L	V	W	R	D	Y
A. gambiae β1	N	V	W	L	R	L	V	W	S	D	Y
A. aegypti β1	N	V	W	L	R	L	V	W	S	D	Y
A. melifera β1	N	V	W	L	R	F	I	W	T	D	Y
B. mori β1	N	V	W	L	R	L	V	W	M	D	Y
L. migratoria β1	N	V	W	L	R	L	V	W	N	D	Y
N. lugens β1	N	V	W	L	R	L	V	W	N	D	Y
T. castaneum β1	N	V	W	L	R	L	V	W	N	D	Y
Insects (resistant)											
M. persicae β1 (resistant)	N	V	W	L	T	L	V	W	R	D	Y
A. gossypii β1 (resistant)	N	V	W	L	T	L	V	W	R	D	Y
Vertebrates (insensitive)											
Homo sapiens β2	N	V	W	L	T	Q	E	W	E	D	Y
Gallus gallus β2	N	V	W	L	T	Q	E	W	E	D	Y
Rattus norvegicus β2	N	V	W	L	T	Q	E	W	E	D	Y
Mus musculus β2	N	V	W	L	T	Q	E	W	E	D	Y
Arachnids (insensitive)											
H. destructor β1	N	V	W	L	Q	L	S	W	Y	D	Y
Ixodes scapularis β1	N	V	W	L	Q	L	V	W	T	D	Y
Pardosa pseudoannulata β1	N	V	W	L	Q	L	M	W	N	D	Y
Tetranychus urticae β1	N	V	W	L	E	L	R	W	N	D	Y

A *Drosophila*-based cDNA rescue system could be an efficient means to investigate the importance of any amino acid residue for both insecticide binding and native subunit function. It could be used for β1 subunits from *Drosophila* and other insect species. A similar system has proven successful in the investigation of insect α6 nAChR subunits (Perry *et al.* 2015). The *Dβ1*-TG4 driver, which lacks *Dβ1* expression and instead expresses GAL4 in *Dβ1*-expressing cells, represents an ideal rescue driver (*Chapter Three*). When used to drive wild type *Dβ1* cDNA under UAS control (UAS-*Dβ1*), this completely rescues the pleiotropic phenotypes observed in *Dβ1* null mutants. Given the relatively high amino acid conservation of insect β1 subunits, it is probable that heterospecific *β1* cDNAs could be successfully expressed in this way, and thanks to the obvious nature of *Dβ1* loss of function, visual

verification of functional rescue would require little effort. Such a system would give insight into the functional conservation of insect β1 subunits and provide a platform for investigating amino acids variants of interest in pest subunits in a controlled genetic background.

4.1.3 Chapter aims

The overall aim of this chapter is to test the *Dβ1*-TG4 rescue system with alternative *Dβ1* and *β1* cDNA alleles. Expression of Dβ1^{R81T} and Dβ1^{R81Q} subunits will provide insight into how these amino acid replacements affect native Dβ1 function and insecticide sensitivity. In the case of Dβ1^{R81T}, these results can be compared to the fitness and resistance results recently reported for *Drosophila* R81T mutants (Homem *et al.* 2020). As for Dβ1^{R81Q}, this will represent the first investigation of this amino acid replacement in a controlled genetic background. Finally, rescue will be attempted with a wild type aphid subunit, Mpβ1 (*M. persicae*). If Mpβ1 is able to functionally rescue loss of *Dβ1* and restore insecticide susceptibility, this will pave the way for future mutagenesis work on this subunit. A list of key questions is provided below.

1. Does expression of Dβ1^{R81T}, Dβ1^{R81Q,} or Mpβ1, in a *Dβ1* null background, rescue the fitness costs associated with loss of *Dβ1*?
2. Do the Dβ1^{R81T} and Dβ1^{R81Q} replacements affect imidacloprid sensitivity?
3. Does expression of Mpβ1 restore imidacloprid sensitivity to *Dβ1* null mutants?

4.2 Methods

4.2.1 Fly strains and maintenance

All fly strains used are described in **Table 4.2**. Flies were maintained on standard semolina fly media at 25°C under a 12: 12 hour light: dark cycle unless otherwise stated. Due to the low viability of *Dβ1Δex5* and *Dβ1*-TG4, any strains containing these alleles were maintained over the third chromosome TM3.GFP fluorescent balancer. For rescue crosses, virgin *Dβ1*-TG4 females were placed with *UAS; Dβ1Δex5* males in laying cages (**Figure 4.1**).

In preparation for all adult experiments, embryos were collected for 24 hours on apple juice agar plates and L1 larvae lacking a fluorescent balancer chromosome were transferred to standard semolina fly media where they were reared until adulthood. For Wiggle Index assays, L1 larvae were instead transferred to fresh apple juice agar plates supplemented with yeast paste and allowed to develop to the L2 stage.

4.2.1.1 Generating UAS-Dβ1^{R81T}

Previously, *Dβ1* cDNA had been cloned from the wild type strain *Armenia-14* into the pGEM-T Easy vector (Promega) (*Chapter Three*). Mutagenic primers (**Table 4.3**) and QuikChange II PfuUltra High Fidelity DNA Polymerase (Agilent) were then used to introduce the R81T replacement into the *Dβ1* cDNA located on this *Dβ1*-pGEM plasmid. Methylated parental DNA was digested with *Dpn*I, leaving the linear mutagenised PCR product intact. This linear product was then column-purified, circularised, sequenced (**Table 4.4**) and sub-cloned into the *Not*I site of the pUAST-attB vector (Bischof *et al.* 2007), then microinjected into attP40 (*25709 w-*) embryos. Transgenics were screened phenotypically for *w+* eye colour rescue, and molecularly using *SV40* and *25709_External_R* primers. Homozygotes were then crossed to generate the *UAS-Dβ1^{R81T}; Dβ1Δex5* strain used for rescue experiments.

Table 4.2 Fly strains used in *Chapter Four*

Name	Origin	Genotype	Reference
wAC9	Lab stock	w[1118]; +; +	Perry *et al.* 2021
25709 w-	Lab stock	y[1] M{RFP[3xP3.PB] GFP[E.3xP3]=vas-int.Dm}ZH-2A w[*]; P{y[+t7.7]=CaryP}attP40	Christesen *et al.* 2021
Dβ1Δex5	Lab stock	w[1118];+;Dβ1Δex5/TM3, P{w+mC=ActGFP}JMR2, Ser1	Perry *et al.* 2021, Christesen *et al*. 2021
Dβ1-TG4	Lab stock	w[1118];+;TI{RFP[3xP3.PB]=T-GEM}nAChRbeta1/TM3, P{w+mC=ActGFP}JMR2, Ser1	Christesen *et al.* 2021
UAS-Dβ1	Lab stock	y[1] M{RFP[3xP3.PB] GFP[E.3xP3]=vas-int.Dm}ZH-2A w[*]; P{w[+mC]=UAS-Dβ1}attP40; +	Christesen *et al.* 2021
UAS-Dβ1^{R81T}	Lab stock	y[1] M{RFP[3xP3.PB] GFP[E.3xP3]=vas-int.Dm}ZH-2A w[*]; P{w[+mC]=UAS-Dβ1.R81T}attP40; +	This study
UAS-Dβ1^{R81Q}	Lab stock	y[1] M{RFP[3xP3.PB] GFP[E.3xP3]=vas-int.Dm}ZH-2A w[*]; P{w[+mC]=UAS-Dβ1.R81Q}attP40; +	This study
UAS-Mpβ1	Lab stock	y[1] M{RFP[3xP3.PB] GFP[E.3xP3]=vas-int.Dm}ZH-2A w[*]; P{w[+mC]=UAS-Mpβ1}attP40; +	This study
UAS-Dβ1; Dβ1Δex5	Lab stock	w[*]; P{w[+mC]=UAS-Dβ1}attP40; Dβ1Δex5/TM3, P{w+mC=ActGFP}JMR2, Ser1	Christesen *et al.* 2021
UAS-Dβ1^{R81T}; Dβ1Δex5	Lab stock	w[*]; P{w[+mC]=UAS-Dβ1R81T}attP40; Dβ1Δex5/TM3, P{w+mC=ActGFP}JMR2, Ser1	This study
UAS-Dβ1^{R81Q}; Dβ1Δex5	Lab stock	w[*]; P{w[+mC]=UAS-Dβ1R81Q}attP40; Dβ1Δex5/TM3, P{w+mC=ActGFP}JMR2, Ser1	This study
UAS-Mpβ1; Dβ1Δex5	Lab stock	w[*]; P{w[+mC]=UAS-Mpβ1}attP40; Dβ1Δex5/TM3, P{w+mC=ActGFP}JMR2, Ser1	This study

Table 4.3 Primers used in *Chapter Four*

Primer name	Sequence	Description
25709_External_R1	CTTGAAGCTTTGGGCTTTTG	AttP40 insertions
SV40	CCCCCTGAACCTGAAACATA	AttP40 insertions
c46a_g47c_F	GGTAGTCGTACCAAACCAAAGTTAACCAAACGTTTGATTTCATAATTTGATTTTTCT	R81T mutagenesis
c46a_g47c_R	AGAAAAATCAAATTATGAAATCAAACGTTTGGTTAACTTTGGTTTGGTACGACTACC	R81T mutagenesis
Clone_Mpb1_F	GACCACCGTACAAGTGCCAAAG	Cloning *Mpβ1*
Clone_Mpb1_R	GATGAAAATGCTCAAGTTAGAAC	Cloning *Mpβ1*

Table 4.4 Loop D amino acid residues based on sequencing of UAS-*Dβ1* plasmids

Construct	Amino acid number of *D. melanogaster* β1 subunit										
	77	78	79	80	81	82	83	84	85	86	87
UAS-Dβ1	N	V	W	L	R	L	V	W	Y	D	Y
UAS-Dβ1^{R81T}	N	V	W	L	T	L	V	W	Y	D	Y
UAS-Dβ1^{R81Q}	N	V	W	L	Q	L	**S**	W	Y	D	Y
UAS-Mpβ1	N	V	W	L	R	L	V	W	R	D	Y
Dβ1 (reference sequence)	N	V	W	L	R	L	V	W	Y	D	Y
Mpβ1 (reference sequence)	N	V	W	L	R	L	V	W	R	D	Y

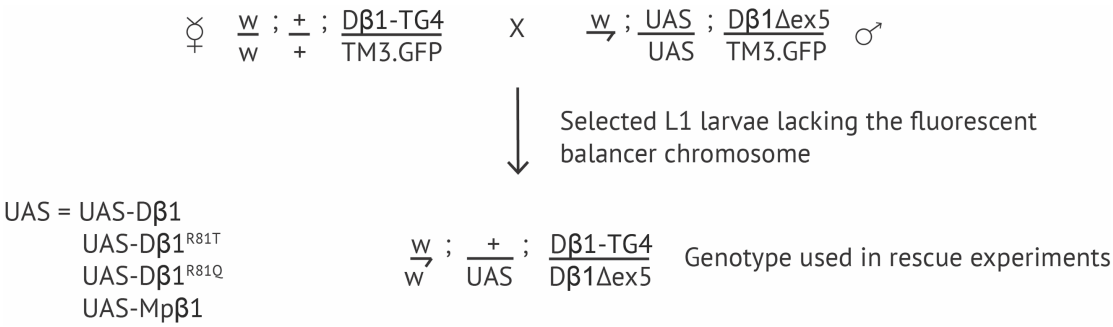


Figure 4.1 Rescue crosses

Prior to all experiments, *w; +; Dβ1-TG4* virgin females and *w; UAS; Dβ1Δex5* males were allowed to mate in laying cages. Larvae lacking the TM3.GFP balancer were then selected and reared for larval or adult experiments. For non-rescued controls, *w; +; Dβ1*-TG4 virgin females were instead mated with *w; +; Dβ1Δex5* males.

4.2.1.2 Generating Dβ1^{R81Q}

Two gBlocks (IDT) were designed; one encoding the N-terminal half of the *Dβ1* CDS and one encoding the C-terminal half of the *Dβ1* CDS (see *Appendix 3*). Both were designed with homology arms to allow Gibson Assembly into the pUAST-attB vector (Bischof *et al*. 2007). The N-terminal gBlock also included mutations resulting in a R81Q replacement and a V83S replacement (**Table 4.4**). Thus, this allele has QLS (as found in the red-legged earth mite, *Halotydeus destructor*) replacing the RLV of *D. melanogaster* (**Table 4.1**). These gBlocks were inserted into the pUAST-attB vector using the Gibson Assembly Cloning Kit (NEB), and microinjected into attP40 (*25709 w-*) embryos. Transgenics were screened phenotypically for *w+* eye colour rescue, and molecularly using *SV40* and *25709_External_R* primers. Homozygotes were then crossed to generate the *UAS-Dβ1^{R81Q}; Dβ1Δex5/TM3.GFP* strain, from which males were used in rescue crosses (**Figure 4.1**).

4.2.1.3 Generating Mpβ1

Total RNA was extracted from an urban population of *M. persicae* aphids collected in Melbourne, Australia. The *Mpβ1* open reading frame was then PCR amplified (primer sequences available in **Table 4.3**) and cloned into pGEM-T Easy (Promega). Clones were sequenced (**Table 4.4**), sub-cloned into the *Not*I site of the pUAST-attB vector (Bischof *et al*. 2007), and microinjected into attP40 (*25709 w-*) embryos. Transgenics were screened phenotypically for *w+* eye colour rescue, and molecularly using *SV40* and *25709_External_R* primers. Homozygotes were then crossed to generate the *UAS-Mpβ1; Dβ1Δex5/TM3.GFP* strain, from which males were used in rescue crosses (**Figure 4.1**).

4.2.2 Developmental mortality assays

L1 larvae were transferred from apple juice agar plates to standard semolina fly media vials, reared at 25°C for 2 weeks, then scored for stage of mortality (50 per vial, 5 independent vials, *n* = 250). Individuals that died during pupal stages P1-P11 or P12-P15 (Bainbridge and Bownes, 1981) were scored as "pupal" and "eclosing" respectively.

4.2.3 Wing morphology analysis

Adults were scored for wing morphology as previously described (*Chapter Three, Figure 3.2*) (*n* = 250). Briefly, fully expanded (FE) wings resembled wild type morphology, unexpanded (UE) wings remained tightly folded with ≤90° separating the distal and proximal portions of the wing, whilst partially expanded (PE) wings had intermediate morphologies.

4.2.4 Longevity assays

Virgin males and females were collected over 48 hours then placed on standard semolina fly media (10 males and 10 females per vial, 4 vials per genotype, *n* = 80). Vials were maintained horizontally at 25°C under a 12:12h light: dark cycle. Flies were transferred to new vials and the number of dead flies recorded every 2-3 days (or every 4-7 days late in the experiment for long-lived genotypes) until all were deceased. A Kaplan-Meier Survival Curve was constructed and significance was calculated using a Cox-Mantel test ($p < 0.05$).

4.2.5 Fertility assays

Vials used in longevity assays (*section 4.2.4*) were maintained at 25°C after removal of adult flies. Fertility was then estimated by scoring the number of viable offspring that eclose 2 weeks later. This number was divided by the number of parental females that were present in the vial (10 females per vial at the start of the experiment, 4 vials per genotype, $n = 40$) and the number of days females were present to lay eggs (2-5 days). Significance was calculated using Student's t-test ($p < 0.05$).

4.2.6 Climbing assays

Three-day-old flies were transferred without anaesthesia into clean empty vials, allowed to acclimate for 5 minutes, then tapped down 3 times on a fly pad to initiate the negative geotaxis response (Gargano *et al.* 2005) (10 males and 10 females per vial, 4 vials per genotype, $n = 80$). The vials were recorded for 10 seconds from a distance of 30cm on an iPhone 8 (Apple Inc.). QuickTime Player (Apple Inc.) was used to capture the frame occurring 6 seconds (180 frames) post-third tap down. JPEGs were then imported into Image J (Fiji, version 2.0.0, Schindelin et al. 2012) and marked with a horizontal threshold 35mm from the bottom of the vials. The number of flies above this threshold was scored manually. Significance was calculated using Tukey's test ($p < 0.05$).

4.2.7 Wiggle Index assays

A modified Wiggle Index (WI) Assay (Denecke *et al.* 2015) was used to measure larval response to the neonicotinoid imidacloprid (Pestanal®, Sigma-Aldrich). L2 larvae were transferred into a 24-well plate (25 larvae per well, 4 wells per genotype, $n = 100$) containing 200uL 5% sucrose in distilled water then recorded for 30 seconds (time = T_0) using a Panasonic 3CCD Ultra-Compact Digital Palmcorder. Immediately after recording, 50uL of insecticide solution was added to wells (or 50uL 5% sucrose for 0ppm controls), then 50uL was removed to return the well volume to 200uL. Further 30 second videos were

then taken at 15, 30, 60, 90, and 120 minutes after insecticide exposure. Raw videos were split into JPEG image sequences using the DVDVideoSoft Converter, and further processed as previously described (Denecke *et al.* 2015), generating heat maps and a numerical estimate of total motility (WI). To calculate relative movement, WI values were normalised to the WI of the respective genotype at T_0. Significance was calculated using Tukey's test ($p < 0.05$).

To measure basal larval movement, the videos for 0ppm control wells were processed as described above (25 larvae per well, 4 wells per genotype, $n = 100$). To calculate relative movement, WI values were normalised to the wAC9 mean.

4.3 Results

4.3.1 The *Dβ1^{R81T}*, *Dβ1^{R81Q}* and *Mpβ1* subunits restore native *Dβ1* function

As first shown in *Chapter Three*, the pleiotropic consequences of loss of *Dβ1* can be successfully rescued by expression of wild type *Dβ1* cDNA in *Dβ1*-expressing cells (*UAS-Dβ1* rescue). Here, we have generated cDNA constructs for the *Drosophila* alleles *Dβ1^{R81T}* and *Dβ1^{R81Q}*, and the wild type aphid subunit, *Mpβ1*, and expressed them using the same TG4 rescue system. We have seen that expression of each of these cDNA constructs is sufficient to rescue many elements of the *Dβ1* null phenotype.

For all three alleles, complete rescue was observed for developmental mortality (**Figure 4.2**), adult longevity (**Figure 4.3**), fertility (**Figure 4.4**), and wing expansion (**Figure 4.5**). Rescue of movement phenotypes was less consistent (**Figure 4.6**). *UAS-Dβ1^{R81T}* performed best in movement assays, achieving a significantly higher average larval WI value (1.9) and greater adult climbing success rate (87%) than the wild type *UAS-Dβ1* rescue (1.5, 80%). *UAS-Dβ1^{R81Q}* achieved a slightly lower average larval WI (1.4) and substantially lower climbing success rate (23%) than the *UAS-Dβ1* rescue, but both were significant compared to non-rescued *Dβ1-TG4/Dβ1Δex5* controls (1.0, 0%), indicating partial rescue of the movement phenotype. *UAS-Mpβ1* expression did not significantly increase the average larval WI (1.1), and again partially but significantly increased adult climbing success (28%) compared to non-rescued controls. Despite the incomplete rescue observed in *UAS-Dβ1^{R81Q}* and *UAS-Mpβ1* movement assays, overall these results demonstrate that *Dβ1^{R81T}*, *Dβ1^{R81Q}* and *Mpβ1* are largely able to substitute for *Dβ1* native function.

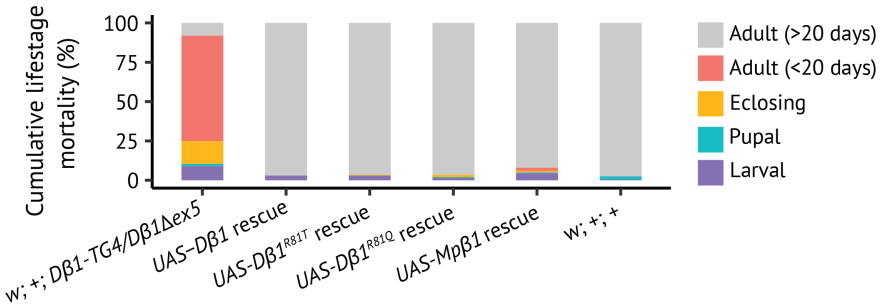


Figure 4.2 *β1* alleles rescue mortality

Percentage mortality at each lifestage (*n* = 250). Non-rescued *Dβ1-TG4/Dβ1Δex5* flies typically die during the eclosing phase or during early adulthood. This mortality was rescued by all *β1* rescue constructs tested. The genotype for all rescues is *w; UAS/+; Dβ1-TG4/Dβ1Δex5.*

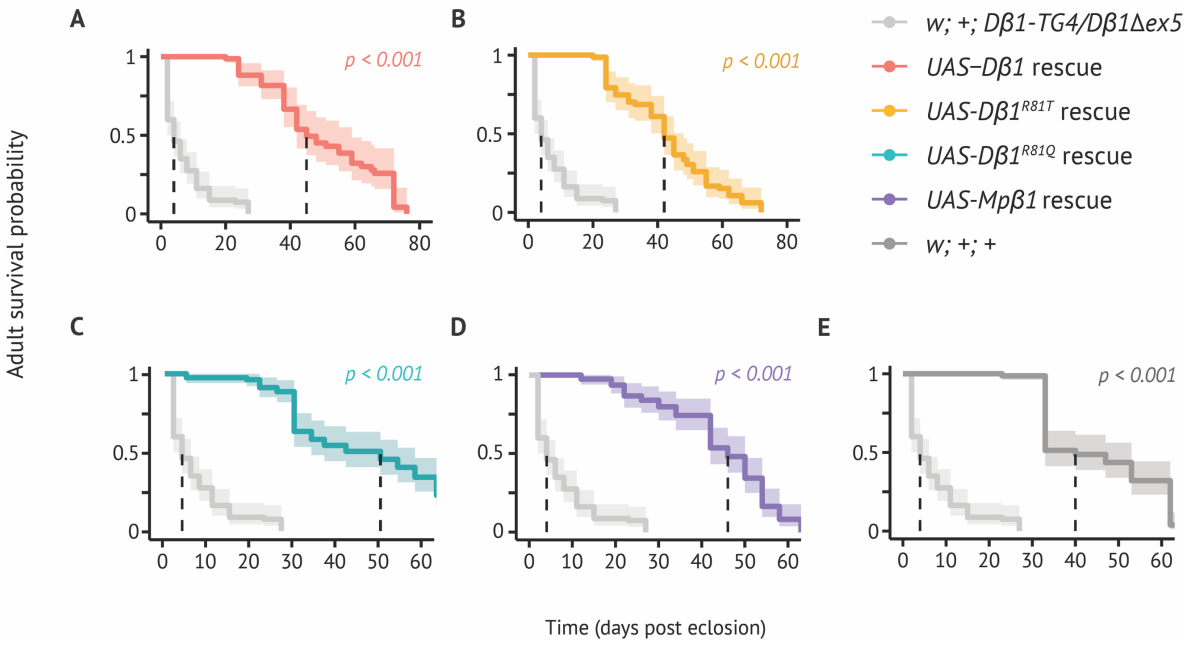


Figure 4.3 *β1* alleles rescue adult longevity

Kaplan Meier survival plots with black dashed lines marking median longevity. The 5-day median longevity of *Dβ1-TG4/Dβ1Δex5* was increased significantly in all rescue experiments. Results for *w; +; Dβ1-TG4/Dβ1Δex5* (light grey) are repeated for ease of comparison. The genotype for all rescues is *w; UAS/+; Dβ1-TG4/Dβ1Δex5.* Shading represents 95% confidence intervals (*n* = 80, Cox-Mantel test).

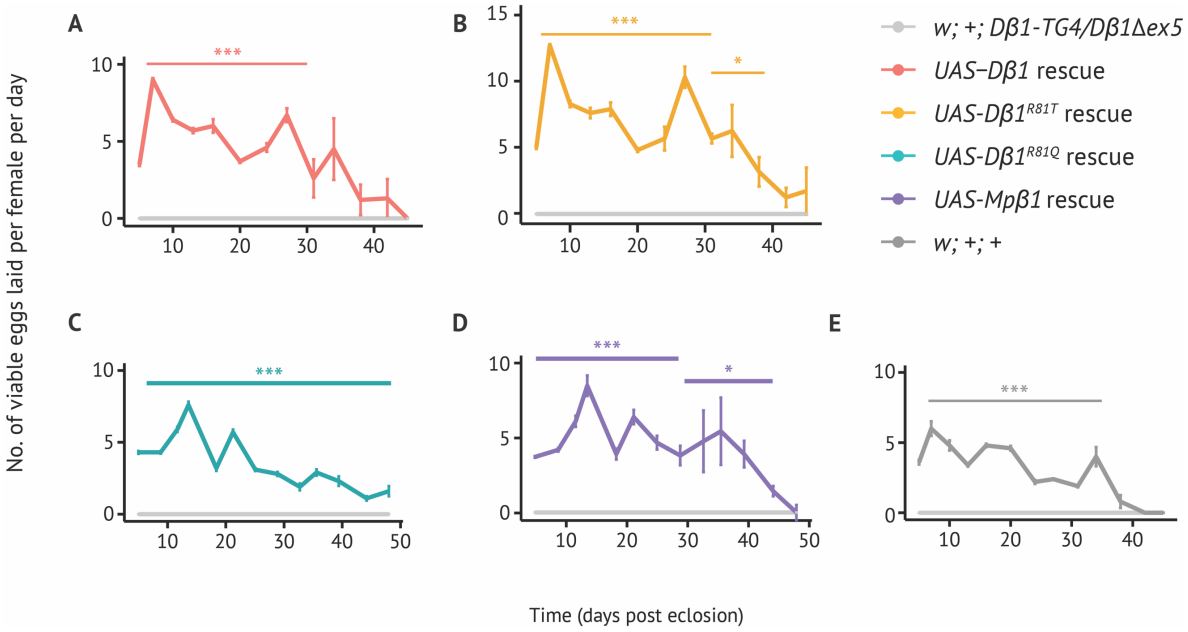


Figure 4.4 *β1* alleles rescue fertility

Number of viable eggs laid per female per day, throughout lifespan. Results for *w; +; Dβ1-TG4/Dβ1Δex5* (light grey) are repeated for ease of comparison. The genotype for all rescues is *w; UAS/+; Dβ1-TG4/Dβ1Δex5.* Error bars indicate SEM (*n* = 40, Student's t-test performed for each time point).

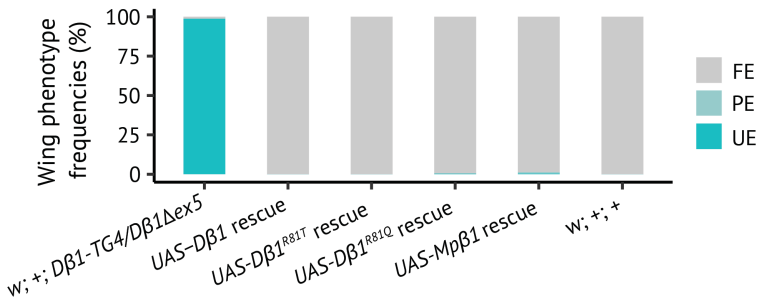


Figure 4.5 *β1* alleles rescue wing morphology

Non-rescued *Dβ1*-TG4/*Dβ1Δex5* flies exhibit unexpanded (UE) wing morphology, while those expressing a rescue construct achieved fully expanded (FE) wings (*n* = 250). Partially expanded (PE) wings were rarely observed in these genotypes. The genotype for all rescues is *w; UAS/+; Dβ1-TG4/Dβ1Δex5.*

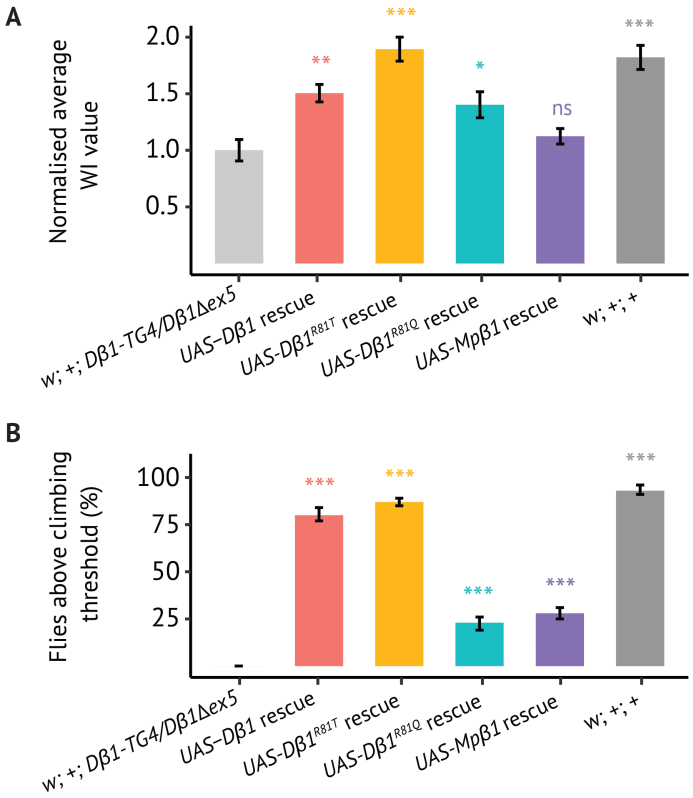


Figure 4.6 The level of rescue of larval and adult locomotor performance varies between different *β1* alleles

(**A**) Average Wiggle Index (WI) values for L2 larvae (*n* = 100). All values are normalised to the non-rescued *w; +; Dβ1-TG4/Dβ1Δex5* average WI. (**B**) Adult climbing performance (*n* = 80). For (**A**) and (**B**), the genotype for all rescues is *w; UAS/+; Dβ1-TG4/Dβ1Δex5.* All error bars indicate SEM and significance is relative to the non-rescued *w; +; Dβ1-TG4/Dβ1Δex5* (* $p < 0.05$, ** $p < 0.01$, *** $p < 0.001$, Tukey's test).

4.3.2 Responses to imidacloprid exposure

The Dβ1 subunit is required for the binding of multiple different insecticides, including the neonicotinoid imidacloprid, with removal of the subunit conferring high levels of resistance (Perry *et al*. 2021). Successful functional rescue of *Dβ1* should therefore restore sensitivity, unless there are amino acid replacements present that confer resistance themselves. A WI assay was used to quantify changes in larval movement upon exposure to 20ppm imidacloprid. Second instar larvae were filmed pre-exposure, then 15, 30, 60 and 120

minutes post-exposure, and movement was normalised to the pre-exposure baseline movement for each genotype.

Within 30 minutes of exposure to imidacloprid, a significant drop in relative movement was observed in *UAS-Dβ1* and wAC9 control larvae (both 0.2 at T_{30}) (**Figure 4.7**). This reduction in movement is typical of sensitive genotypes (Denecke *et al.* 2015). In contrast, this response was absent in resistant *Dβ1-TG4/Dβ1Δex5* larvae, with relative movement instead increasing post-exposure (2.4 at T_{120}). This was similar to the movement pattern observed in non-exposed 0ppm controls. Inspection of relative larval movement in all 0ppm controls reveals all genotypes exhibit an overall increase in movement over the course of the two-hour experiment, indicating the movement gain observed in resistant larvae was not entirely due to the presence of the insecticide (**Figure 4.7 E**).

Unexpectedly, the *UAS-Dβ1*^{R81T} response appeared similar to susceptible genotypes, with a rapid decline in relative movement post-exposure (0.4 at T_{30}). However, relative movement did remain slightly higher than *UAS-Dβ1* larvae for most of the experiment, and although this was not statistically significant, it could indicate a low level of resistance for *Dβ1*^{R81T} at this dose. In contrast, a convincing level of resistance was observed for *UAS-Dβ1*^{R81Q}, with relative movement increasing post-exposure (3.1 at T_{120}), exceeding the relative increase in movement for resistant *Dβ1-TG4/Dβ1Δex5* larvae. For *UAS-Mpβ1*, a rapid reduction in movement was observed post-exposure (0.3 at T_{30}), indicating efficient restoration of sensitivity.

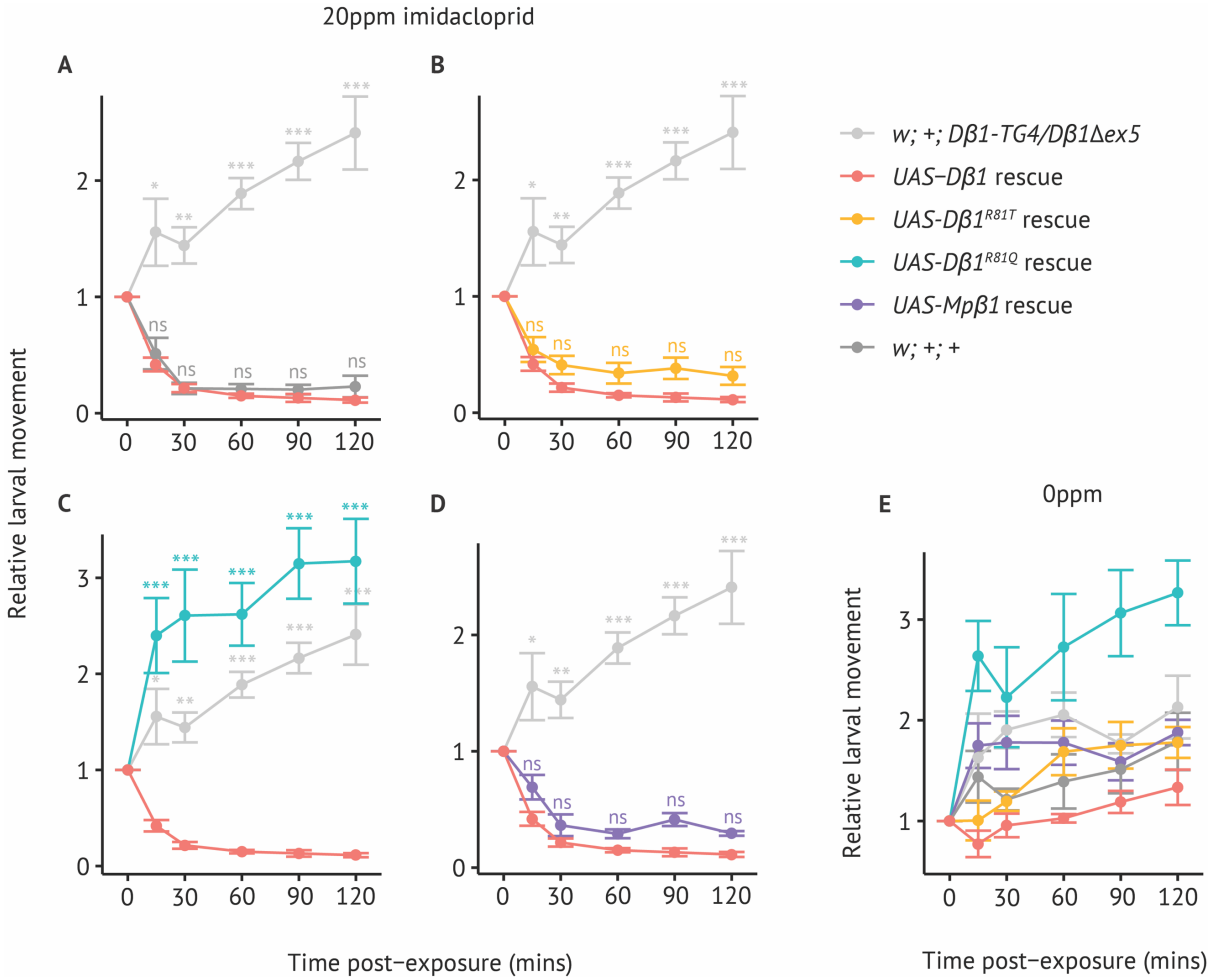


Figure 4.7 Responses of different *β1* alleles to imidacloprid exposure

(**A-D**) A WI assay was used to measure change in larval movement during a two-hour exposure to 20ppm imidacloprid (*n* = 100). Error bars indicate 95% confidence intervals and significance is relative to *UAS-Dβ1* rescue (red) (* $p < 0.05$, ** $p < 0.01$, *** $p < 0.001$, Tukey's test). Results for *UAS-Dβ1* rescue (red) and *w; +; Dβ1-TG4/Dβ1Δex5* (light grey) are repeated for ease of comparison. (**E**) 0ppm controls reveal an overall increase in larval movement after T_0 for all genotypes (*n* = 100). All WI values are normalised to the WI of the given genotype at T_0. The genotype for all rescues is *w; UAS/+; Dβ1-TG4/Dβ1Δex5.*

4.4 Discussion

The Dβ1 nAChR subunit has two opposing roles in Drosophila fitness; it plays a non-redundant role in adult viability (*Chapter Three*) and it is a key target for multiple important commercial insecticides (Perry *et al*. 2021). This duality means that *Dβ1* loss of function mutants can be highly resistant to insecticides, but are also afflicted with obvious and detrimental fitness costs. Nature's solution to this dilemma has involved field populations evolving resistance-conferring amino acid replacements in loop D of the LDB of β1 subunits (Bass *et al.* 2011, Koo *et al.* 2014), however there are difficulties associated with studying the effect of these mutations directly in pest species.

The aim of this chapter was to investigate some of these alternative *β1* alleles using the previously-tested *Drosophila* TG4 rescue system (*Chapter Three*) which allows for expression of a transgene specifically in *Dβ1*-expressing cells and in the absence of the native Dβ1 subunit. Specifically, we generated cDNA rescue constructs for two *Drosophila* alleles carrying amino acid replacements present in other species: $D\beta1^{R81T}$ (present in resistant populations of *M. persicae* and *A. gossypi* aphids) and $D\beta1^{R81Q}$ (present in naturally resistant *H. destructor* mites). To test whether this system would work with a heterospecific β1 subunit, we also generated a wild type cDNA rescue construct for the aphid *M. persicae* (*Mpβ1*). By combining the TG4 rescue system with fitness and insecticide response assays, we have been able to show how effectively these alleles can rescue native *Dβ1* function, and the extent to which they may confer resistance or restore insecticide sensitivity.

4.4.1 $D\beta1^{R81T}$

In rescue experiments using the *UAS-*$D\beta1^{R81T}$ rescue construct, this subunit was able to completely restore native *Dβ1* function, rescuing all elements of the *Dβ1* phenotype, including mortality, longevity, fertility, wing expansion, and larval and adult movement. In one respect this was unexpected, given that recent work done on genomic $D\beta1^{R81T}$ mutants indicated there were multiple fitness costs associated with this amino acid replacement in

Drosophila (Homem *et al.* 2020). These fitness costs included marked reductions in female egg laying, male longevity and adult climbing performance. On the other hand, *in vitro* electrophysiological evidence indicates that the R81T change has only a very minor impact on ACh binding for various different Dβ1-containing receptor subtypes (Ihara *et al.* 2020). On this basis, it is reasonable to suspect that the $D\beta1^{R81T}$ allele could fulfil the endogenous roles of the wild type Dβ1 subunit. A potential factor behind the inconsistent results could be the difference in the expression level of our allele and the one generated by Homem *et al.* (2020). Homem *et al.*'s $D\beta1^{R81T}$ allele was a genomic mutation, meaning its expression level was limited to the *Dβ1* native expression level, whereas our use of the GAL4-UAS system would have allowed for overexpression. If a reduction in ACh-driven signalling is the cause of any $D\beta1^{R81T}$ phenotypes, it is possible that overexpression of our construct and a subsequent increase in the number of receptors at post-synaptic membranes could have compensated for the weaker signal. Alternatively, since our rescue experiments involved crossing parental strains that each possessed wild type Dβ1, it also remains possible that maternally-inherited Dβ1 was present in our rescue animals.

Another unexpected result appeared in our insecticide response assay, with flies expressing *UAS-*$D\beta1^{R81T}$ showing a similar response to imidacloprid as wildtype. This is in contrast to Homem *et al.* (2020) who reported 32.6-fold resistance to imidacloprid in $D\beta1^{R81T}$ homozygotes. There are some factors that make it hard to directly compare these results; Homem *et al*. tested adult mortality using vials that had been coated in the insecticide, while we tested an acute change in movement in larvae bathed in insecticide solution. It is possible that Dβ1 plays a more prominent role in the response to imidacloprid in adults. This is certainly supported by the expression pattern of *Dβ1* in each life stage, with *Dβ1* expressed in a far greater proportion of neurons in the adult brain (Allen *et al.* 2020, Croset *et al.* 2018) than the larval brain (Ravenscroft *et al*. 2020) (*Appendix 2, Figure S9*). It is also possible that our *UAS-*$D\beta1^{R81T}$ larvae could have experienced better post-exposure survival than other susceptible controls, however we did not test for this. In future, it will be valuable to repeat our WI assay using a range of lower imidacloprid doses to discriminate between the sensitivity of *UAS-*$D\beta1^{R81T}$ and *UAS-Dβ1*.

Despite differences between our findings and those of Homem *et al.* (2020), it is worth noting that the level of tolerance conferred by the R81T replacement is surprisingly low in both studies. In field populations of imidacloprid-resistant R81T *M. persicae* aphids, resistant clones also overexpress the detoxification enzyme CYP6CY3 (Bass *et al*. 2011). Together, R81T and CYP6CY3 amplification confer >1000-fold imidacloprid resistance to these aphids – substantially higher than the fold-resistance observed here, and by Homem *et al.* Thus, together with Homem *et al.,* our work provides further evidence that R81T and CYP6CY3 likely act synergistically in combination but confer far less potent levels of resistance when present in isolation.

While we have addressed some reasons why our *UAS-Dβ1*^{R81T} gave similar results to the wild type *UAS-Dβ1* rescue, it is nonetheless curious when our *UAS-Dβ1*^{R81Q} allele was so convincingly unaffected by imidacloprid. Sequencing our injected *UAS-Dβ1*^{R81T} construct did reveal the correct nucleotide substitutions encoding the R81T replacement (**Table 4.4**), however it is important to question whether the *Dβ1*^{R81T} allele was the only *Dβ1* allele present in these individuals. Extraction of RNA and sequencing of the cDNA would reveal if any wild type *Dβ1* is being expressed, for example, as a result of any error during earlier crossing schemes.

4.4.2 Dβ1^{R81Q}

Many arachnid species are insensitive to neonicotinoids (Dermauw *et al.* 2012, Erdmanis *et al.* 2012), and here we provide the first experimental evidence that loop D residues may be largely responsible for this insensitivity. Our *Dβ1*^{R81Q} subunit contained two replacements, R81Q and V83S, mimicking the residues present in loop D of the insensitive mite species *H. destructor* (**Tables 4.3, 4.4**). *UAS-Dβ1*^{R81Q} rescue yielded some striking results, providing almost complete functional rescue of *Dβ1*'s endogenous roles while likely conferring a high level of imidacloprid resistance comparable to the *Dβ1* nulls. These results support the notion that the presence of the R81 residue is critical for imidacloprid binding but dispensable for ACh binding (Ihara *et al.* 2020). Testing whether the *UAS-Dβ1*^{R81Q} allele is

resistant to other neonicotinoids and other insecticide classes will be an important future experiment, as will testing of the R81Q and V83S replacements independently.

Only two elements of the *Dβ1* loss of function phenotype were not fully rescued by *UAS-Dβ1*^{R81Q} expression - larval movement and adult climbing. This suggests the *Dβ1*^{R81Q} allele is still able to fulfil normal Dβ1 signalling roles in CCAP neurons, and neurons involved in mating and longevity, but that there is still some function missing in circuits controlling movement. This could reflect the fact that movement circuits likely rely on more frequent and rapid signalling, making them more sensitive to subtle changes in ACh binding affinity than, for example, neurons like the CCAP neurons which are involved in the relatively slower process of hormone production.

4.4.3 *Mpβ1*

Mpβ1 shares only 82% identity at the amino acid level with Dβ1, yet *UAS-Mpβ1* was able to fully rescue most *Dβ1* loss of function phenotypes, including mortality, longevity, fertility, and wing expansion. This is the first report of a non-*Drosophila* β1 subunit being expressed in *Drosophila*, and reveals the high level of functional conservation between the β1 subunits in these two species. The results also indicate that Mpβ1 was able to form functional receptors with Dβ1's native binding partners despite multiple amino acid differences throughout the protein. The only fitness costs not rescued by *UAS-Mpβ1* expression were larval movement and adult climbing. As discussed for the *UAS-Dβ1*^{R81Q} rescue, this could reflect the fact that these circuits rely on more persistent firing, making them more sensitive to altered signalling. Importantly, *UAS-Mpβ1* expression was also able to fully restore the response of larvae to imidacloprid in the WI assay. Together, these results reveal that it would be possible to investigate mutated *Mpβ1* alleles, and their involvement in insecticide response, using the same TG4 system in future experiments.

4.4.4 Future directions

While we have successfully used the TG4 rescue system to express mutated Dβ1 subunits, the system's true power lies in is its ability to investigate mutated non-*Drosophila* subunits in the *Drosophila* model background. Performing site-directed mutagenesis on a cDNA plasmid *in vitro* is more convenient, and in some cases safer, than performing *in vivo* CRISPR in the species of interest. It requires minimal resources - only cDNA from the species (or alternatively, synthesised gBlocks when the insect itself is not available), and does not require maintenance of a lab population. This may reveal potential mutations that could confer resistance and allow their frequency in field populations to be monitored as part of pest management programs.

But how far, taxonomically, can we push the TG4 system for β1 subunits? We have shown that Mpβ1 is able to functionally rescue loss of Dβ1, despite only sharing 82% amino acid identity with Dβ1. We are therefore optimistic that successful rescue could be achieved using many other insect β1 subunits that share even higher identity, such as the honeybee Amβ1 (87%) and the cotton bollworm Haβ1 (91%). However, our recent preliminary work on two arachnid β1 subunits, the red-legged earth mite (Hdβ1) and two-spotted spider mite (Tuβ1) indicates evolutionary conservation may not be strong enough to rescue loss of Dβ1 using non-insect β1 subunits (unpublished).

Other nAChR subunits could also be studied using TG4 rescue. The ease of the TG4 system for generating subunit-specific drivers, combined with the availability of CRISPR knockout mutants for nine of the ten *Drosophila* subunits (Perry *et al.* 2021), means this system could theoretically be applied to study insecticide response *in vivo* for any pest subunits that are able to functionally compensate for the *Drosophila* subunit. Even for subunits that lack obvious loss of function phenotypes, restoration of sensitivity is a sufficient proxy for rescue of endogenous function (Perry *et al.* 2015), and would mean the effects of mutagenesis would be testable.

Ultimately, using the TG4 rescue system to express mutated heterospecific subunits will provide a platform for future work on resistance-conferring mutations and will reveal a great deal about the functional conservation of this evolutionarily conserved gene family. By studying pest nAChR subunits in this way, it will allow for investigation of resistance ratios associated with single amino acid changes, decoupled from the noise of metabolic resistance. It could also be used in the screening of field populations, providing insight into the best choice of insecticide to apply, and enabling identification of novel resistance-causing alleles.

Chapter Five

Discussion

Following the identification of severe phenotypes associated with the loss of function of two nAChR subunits, their endogenous roles were examined using an array of genetic tools available in *Drosophila*. The Dα5 subunit, explored in *Chapter Two*, was shown to play a role in a pathway that regulates ETH production in developing larvae. Animals lacking Dα5 were shown to phenocopy ETH mutants, and the moulting and wandering phenotypes observed were revealed to be associated with a reduction of ETH transcript. In *Chapter Three*, deletion of *Dβ1* resulted in pleiotropic consequences, including disrupted wing expansion. This wing phenotype was associated with loss of the hormone bursicon, and the bursicon-producing CCAP neurons were identified as a small subset requiring Dβ1 for normal neuronal function. Alternative alleles of *Dβ1* were also investigated in *Chapter Four*. Dβ1 subunits containing resistance-conferring amino acid replacements were able to rescue the loss of function phenotypes, indicating resistance may not always be associated with fitness costs. A non-*Drosophilid β1* allele was also able to rescue loss of Dβ1, revealing a high level of functional conservation across species and setting the stage for future work on pest subunits in the *Drosophila* model. The following sections discuss how these findings may change the way we think about insect development, nAChR dynamics and insect-insecticide interactions, as well as what future studies may build on the foundation laid here.

5.1 Neuronal control of development

Insect development, and the complex system of hormones that regulate an insect's progression through the different developmental stages, has been intensively studied over the last century (Butterworth 1980). Each of the major developmental hormones have been identified, we know how they fluctuate to drive developmental events, and we know a lot about the cells in which they are produced. However, the findings in this thesis emphasise that our knowledge of these well-studied processes is far from complete. With new technologies comes the capacity to study these processes in even greater detail at the genetic and molecular levels.

Traditionally, rising levels of one hormone are described as triggering production of the next hormone in the developmental cascade. Now, we know that loss of individual nAChR

subunits can disrupt this system, revealing that there is still considerable neuronal regulation required in addition to the endocrine regulation at major developmental transitions. That the loss of Dα5 and loss of Dβ1 each result in severe reduction of *ETH* and *CCAP* transcripts, respectively, indicates that there is a cholinergic signal required somewhere upstream of the expression of these hormone genes. For Dβ1 and CCAP there appears to be simple explanation, and cholinergic neurons that project onto the CCAP neurons have been identified using connectomic resources (Scheffer *et al.* 2020, Li *et al.* 2021). However, demonstration of the impact on the cholinergic signal itself will require further study. With respect to Dα5 and ETH, the specific cells requiring Dα5 are yet to be identified and, given the lack of innervation onto the ETH-producing Inka cells, this relationship will be more complex to resolve. Moving forward, tools that allow for silencing of specific neurons (Baines *et al.* 2001), activation of specific neurons (Klapoetke *et al.* 2014), and visualisation of active neurons (Chen *et al.* 2013) will be vital for identifying circuits involved in the neuronal control of hormone production during development.

5.2 Implications of nAChR compensation

Having examined the phenotypes associated with loss of nAChR subunits, it is important to consider what may happen at the neuronal level when a subunit is missing. The simplest possibility is that the nAChR subtype needed for cholinergic neurotransmission is lost, and any phenotypes observed are simply due to loss of a normal signal. However, it is also possible that the remaining subunits arrange to form pentameters that have subtle differences in permeability or channel activity compared to the original subtype. In this case, the presence of alternative subtypes at the membrane could alter the sensitivity of the neuron, and could ultimately contribute to the phenotype in a less predictable way.

This scenario becomes even more complex when we consider how loss of an individual subunit can influence other nAChR subunits at the transcriptional and post-translational levels. Transcriptional compensation is common among nAChR subunit deletion mutants, with RNA-seq revealing that at least one subunit (other than the deleted subunit) is significantly down-regulated or up-regulated in all existing mutants (Perry *et al.* 2021).

Compensation at the post-translational level is also a common phenomenon. This occurs when individual subunits are deleted (Champtiaux *et al*. 2002), or when insecticide-binding causes certain subunits to be degraded (Nguyen *et al.* 2021), and involves changes in trafficking or recycling to increase or decrease pentamers present at the membrane. Together, these compensation mechanisms could drastically alter normal signalling in a given neuron.

As we continue to investigate the endogenous signalling roles of nAChR subunits in specific neurons, it will be important to keep this compensation in mind and to question what deletion of an individual subunit actually entails at the neuronal level. It is clearly not a simple loss of function. Ideally, any attempts to characterise the role of a specific subunit in a neuron of interest will involve measuring the level of neuronal activity when that subunit is present or absent. This could be done using calcium reporters such as GCaMP (Chen *et al.* 2013) or electrophysiology (Murthy and Turner 2013). It would also be valuable to measure the transcript and protein levels of all other subunits, and to visualise the presence of other subunits at the membrane using a protein tagging system such as CRiMIC (Li-Kroeger *et al.* 2018). While this is a lengthy task, it would greatly improve our understanding of the dynamics of the 10 subunits and how they behave when one subunit is lost.

5.3 The trade-off between insecticide resistance and associated fitness costs

The endogenous roles of nAChRs can have a direct impact on the success of an insecticide in pest control. Traditionally, targets considered ideal for mitigating resistance are those with an associated fitness cost (Coyne 1951, Georghiou 1994). There are many cases where this approach has proven successful in delaying the appearance of resistant alleles, and the α6 and β1 subunits provide the perfect juxtaposition. Loss of the Dβ1 subunit can confer high levels of resistance to imidacloprid, and we are now aware of the fitness costs associated with this resistance. Yet there are only three reported cases of target-site imidacloprid resistance despite 30 years' intensive global use of this insecticide (Liu *et al.* 2005, Bass *et al.* 2011, Koo *et al.* 2014). In contrast, disruption of Dα6 does not have an obvious fitness cost in *Drosophila*, nor does it appear to have severe effects in other insects (Perry *et al.* 2007,

Baxter *et al.* 2010, Bao and Xu 2011, Puinean *et al.* 2013, Silva *et al.* 2016, Homem *et al.* 2020). Consequently, multiple pest species evolved resistance to the α6-targeting spinosyns within three years of the introduction of these compounds (Baxter *et al.* 2010, Bao and Xu 2011, Puinean *et al.* 2013, Silva *et al.* 2016). With this approach in mind, Dα5 may become an attractive novel target, given its essential role in larval development. Dα5's limited distribution in Dipterans would limit the range of species that could be targeted, but this would simultaneously provide the advantage of reduced collateral damage to beneficial non-Dipteran species.

Targeting subunits that have fitness costs can be effective in avoiding target-site resistance, however, this approach is not perfect. As seen for Dβ1, resistance-conferring amino acid replacements like R81T can still arise and threaten pest control efforts (Bass *et al*. 2011, Koo *et al.* 2014). While there is some evidence this replacement may be associated with some fitness costs (Homem *et al.* 2020), the findings of *Chapter Four* suggest otherwise, and the success of the *M. persicae* and *A. gossypii* aphid populations indicate fitness costs were not severe enough to mitigate resistance for these species in the field (Bass *et al.* 2011, Koo *et al.* 2014). Targeting essential subunits also fails to solve the problem of metabolic resistance, which is the most common mechanism of resistance that occurs in field populations for many classes of insecticide (Ffrench-Constant and Bass 2017, Perry *et al.* 2018).

Finally, perhaps the most important reason to challenge this fitness-cost-based approach to pest control, is the effect it may have on non-pest species. Insecticides are present at low doses throughout the environment, and it is clear that chronic exposure to these sub-lethal doses is occurring in a large number of species, including many pollinators (Gonalons and Farina 2015, Crall *et al.* 2018). This means neurons expressing the target subunits may experience chronic over-firing, and this is likely to affect the behaviours, metabolism, and developmental pathways associated with those neurons (Martelli *et al.* 2020). In the case of β1, if an insect is exposed to sub-lethal levels of imidacloprid, and some imidacloprid binds to β1-containing nAChRs on the CCAP neurons, this could disrupt the carefully-timed

production of CCAP and bursicon. Based on further findings in *Chapter Three*, chronic binding of imidacloprid elsewhere in the brain could also affect longevity, movement, and male courtship. Further studies examining how insecticide exposure may impact these key neuronal pathways could better inform the evaluation of insecticide safety, and could be taken into consideration when determining appropriate application strategies and safe residual levels in the environment.

5.4 Concluding remarks

This thesis has built on our existing knowledge of the biology of nAChRs. By examining the endogenous roles of nAChR subunits, this work has uncovered developmental and behavioural pathways that require cholinergic signalling and provided new insights into pathways that may be affected when insects evolve resistance, or are chronically exposed, to nAChR-targeting insecticides. It has also demonstrated the efficiency of many new technologies for precise genetic manipulation that we can continue to use to study the nAChR gene family.

An ultimate goal will be to define the role each subunit plays, and what subtypes exist, in each cholinergic pathway. For subunits that are functionally redundant, this may require simultaneous disruption of multiple subunits. Somatic CRISPR will continue to be an efficient tool for pinpointing neurons where expression of nAChR subunits is required for behaviour. The TG4 system will also be incredibly useful for generating subunit-specific drivers for all subunits. These TG4 drivers could be used to visualise expression patterns of individual subunits and, when converted to split-GAL4 hemi-drivers, would enable identification of co-expressed subunits. When combined with the recently-generated collection of deletion mutants (Perry *et al.* 2021), TG4 drivers could also be incorporated into rescue systems for studying resistance-conferring mutations and the functional conservation for nAChR subunits from various insect species.

Many insect neuronal pathways have been described as cholinergic, and a huge amount of research remains to enable us to partition these pathways and determine which nAChRs

subunits are required where. With the abundance of connectomic datasets emerging, knowledge of how each cholinergic neuron communicates will be essential for completely annotating the functional wiring map of the *Drosophila* brain. Continuing to explore insect neurobiology will also help manage the use of insecticides to control pests in smarter ways and in ways that prevent further devastation to the majority of insect species that are so vital to the Earth's many ecosystems.

References

Acebes A, Y Grosjean, C Everaerts, and JF Ferveur, 2004 Cholinergic control of synchronized seminal emissions in *Drosophila*. Curr. Biol. 14: 704–710.

Ali S, 2012 Nicotinic acetylcholine receptors; an examination of expression and insecticide interactions in *Drosophila melanogaster*. The University of Melbourne (PhD Thesis).

Allen AM, MC Neville, S Birtles, V Croset, CD Treiber *et al.*, 2020 A single-cell transcriptomic atlas of the adult *Drosophila* ventral nerve cord. eLife 9: e54074.

Althoff T, RE Hibbs, S Banerjee, E Gouaux, 2014 X-ray structures of GluCl in apo states reveal a gating mechanism of Cys-loop receptors. Nature 512: 333-337.

Altschul SF, W Gish, W Miller, EW Myers, DJ Lipman, 1990 Basic local alignment search tool. J. Mol. Biol. 215(3): 403-410.

Ashburner M, 1990 Puffs, genes, and hormones revisited. Cell 61: 1-3.

Bainbridge SP, and M Bownes, 1981 Staging the metamorphosis of *Drosophila melanogaster*. J. Embryol. Exp. Morphol. 66: 57–80.

Baines RA, JP Uhler, A Thompson, ST Sweeney, and M Bate, 2001 Altered electrical properties in *Drosophila* neurons developing without synaptic transmission. J. Neurosci. 21(5): 1523-1531.

Bao B and WH Xu, 2011. Identification of gene expression changes associated with the initiation of diapause in the brain of the cotton bollworm, *Helicoverpa armigera*. BMC Genom. 12, 224.

Bar-On YM, R Phillips, and R Milo, 2018 The biomass distribution on Earth. PNAS. 115(25):6506–11.

Barnstedt O, D Owald, J Felsenberg, R Brain, J-P Moszynski *et al.*, 2016 Memory-relevant mushroom body output synapses are cholinergic. Neuron 89: 1237–1247.

Bass, C., A. M. Puinean, M. Andrews, P. Cutler, M. Daniels *et al.*, 2011 Mutation of a nicotinic acetylcholine receptor β subunit is associated with resistance to neonicotinoid insecticides in the aphid *Myzus persicae*. BMC Neurosci. 12: 51.

Basset AR, C Tibbit, CP Ponting, and J-L Liu, 2013 Highly efficient targeted mutagenesis of *Drosophila* with the CRISPR/Cas9 system. Cell Rep. 4: 1-9.

Baxter, SW, M Chen, A Dawson, JZ Zhao, H Vogel *et al.,* 2010. Mis-spliced transcripts of nicotinic acetylcholine receptor *alpha6* are associated with field evolved spinosad resistance in *Plutella xylostella* (L.). PLoS Genet. 6, e1000802.

Beckmann J and Lips KS, 2013 The non-neuronal cholinergic system in health and disease. Pharmacology 92: 286–302.

Bellen HJ, MF Wangler, S Yamamoto, 2019 The fruit fly at the interface of diagnosis and pathogenic mechanisms of rare and common human diseases. Human Mol. Genetics 28: R207-R214.

Berger EM and EB Dubrovsky, 2005. Juvenile hormone molecular actions and interactions during development of *Drosophila melanogaster*. Vitam Horm 73: 175–215.

Bischof J, RK Maeda, M Hediger, F Karch, and K Basler, 2007 An optimized transgenesis system for *Drosophila* using germ-line-specific phiC31 integrases. Proc. Natl. Acad. Sci. U.S.A. 104: 3312–3317.

Bischoff N, S Wimberger, M Maresca, and C Brakebusch, 2020 Improving precise CRISPR genome editing by small molecules: is there a magic potion? Cells. 9: 1318.

Blackman RL and VF Eastop, 2000 Aphids on the world's crops: an identification and information guide.

Bossy B, M Ballivet, and P Spierer, 1988. Conservation of neural nicotinic acetylcholine receptors from *Drosophila* to vertebrate central nervous systems. EMBO Journal. 7(3): 611–618.

Boulter J, A O'Shea-Greenfield, RM Duvoisin, JG Connolly, E Wada *et al.,* 1990 Alpha-3, alpha-5, and beta-4: three members of the rat neuronal nicotinic acetylcholine receptor-related gene family form a gene cluster. J. Biol. Chem. 265: 4472–4482.

Brand AH and N Perrimon, 1993 Targeted gene expression as a means of altering cell fates and generating dominant phenotypes. Development 118: 401–415.

Brunet Avalos C, GL Maier, R Bruggmann, and SG Sprecher, 2019 Single-cell transcriptome atlas of the *Drosophila* larval brain. eLife 8: e50354.

Bustin, SA, V Benes, JA Garson, J Hellemans, J Huggett *et al.*, 2009 The MIQE guidelines: minimum information for publication of quantitative real-time PCR experiments. Clin. Chem. 55: 611–622.

Butterworth FM, 1980 Ecdysone: Introduction to the molecular mechanism of steroid action in insects.

Campos-Ortega JA and V Hartenstein, 1985 The embryonic development of *Drosophila melanogaster.*

Canver MC, DE Bauer, A Dass, YY Yien, J Chung *et al.,* 2014 Characterization of genomic deletion efficiency mediated by clustered regularly interspaced short palindromic repeats (CRISPR)/Cas9 nuclease system in mammalian cells. J. Biol. Chem. 289(31): 21312-21324.

Caussinus E, O Kanca, and M Affolter, 2012 Fluorescent fusion protein knockout mediated by anti-GFP nanobody. Nat. Struc. Mol. Biol. 19(1): 117-122.

Chamaon K, R Schulz, K Smalla, B Seidel, and E Gundelfinger, 2000 Neuronal nicotinic acetylcholine receptors of *Drosophila melanogaster*: The α-subunit Dα3 and the β-type subunit ARD co-assemble within the same receptor complex. FEBS Letters. 482(3):189–92.

Chamaon K, K Smalla, U Thomas, and E Gundelfinger, 2002 Nicotinic acetylcholine receptors of *Drosophila*: Three subunits encoded by genomically linked genes can co-assemble into the same receptor complex. J Neurochem. 80(1): 149–57.

Champtiaux N, Z-Y Han, A Bessis, FM Rossi, M Zoli, *et al.,* 2002 Distribution and pharmacology of α6-containing nicotinic acetylcholine receptors analyzed with mutant mice. J. Neurosci. 22(4): 1208–1217.

Chavez V, G Marques, J Delbecque, K Kobayashi, M Hollingsworth *et al.,* 2000 The *Drosophila disembodied* gene controls late embryonic morphogenesis and codes for a cytochrome P450 enzyme that regulates embryonic ecdysone levels. Development 127: 4115–4126.

Chen T-W, TJ Wardill, Y Sun, SR Pulver, SL Renninger *et al.,* 2013 Ultrasensitive fluorescent proteins for imaging neuronal activity. Nature. 499(7458): 295-300.

Chen W, 2021 Defining the imidacloprid target in *Drosophila melanogaster.* The University of Melbourne (PhD Thesis).

Christesen D, YT Yang, J Somers, C Robin, T Sztal *et al.,* 2017 Transcriptome analysis of *Drosophila melanogaster* third instar larval ring glands points to novel functions and uncovers a cytochrome p450 required for development. G3. 7: 467-479.

Christesen D, YT Yang, W Chen, P Batterham, T Perry, 2021 Loss of the Dβ1 nicotinic acetylcholine receptor subunit disrupts bursicon-driver wing expansion and diminishes adult viability in *Drosophila melanogaster*. Genetics (*accepted*).

Clark AC, ML del Campo, and J Ewer, 2004 Neuroendocrine control of larval ecdysis behavior in *Drosophila*: complex regulation by partially redundant neuropeptides. J. Neurosci. 24(17): 4283-4292.

Contrino S, RN Smith, D Butano, A Carr, F Hu *et al.,* 2012 modMine: flexible access to modENCODE data. Nucl. Acids Res. 40.

Corringer, PJ, N Le Novère, and JP Changeux, 2000 Nicotinic receptors at the amino acid level. Annu. Rev. Pharmacol. Toxicol. 40: 431–458.

Coyne, FP 1951 Proper use of insecticides. British Medical Journal. 2(4736): 911–912.

Crall JD, CM Switzer, RL Oppenheimer, AN Ford Versypt, B Dey *et al.*, 2018 Neonicotinoid exposure disrupts bumblebee nest behavior, social networks, and thermoregulation. Science 362: 683–686.

Croset V, CD Treiber, and S Waddell, 2018 Cellular diversity in the *Drosophila* midbrain revealed by single-cell transcriptomics. eLife 7: e34550.

Crossthwaite AJ, A Bigot, P Camblin, J Goodchild, RJ Lind *et al.*, 2017 The invertebrate pharmacology of insecticides acting at nicotinic acetylcholine receptors. J. Pestic. Sci. 42: 67–83.

Dale RP, AK Jones, C Tamborindeguy, TGE Davies, JS Amey *et al.*, 2010 Identification of ion channel genes in the *Acyrthosiphon pisum* genome. 19: 141-153.

Dani J and D Bertrand 2007. Nicotinic acetylcholine receptors and nicotinic cholinergic mechanisms of the central nervous system. Annu. Rev. Pharmacol. Toxicol. 47:699–729.

Danielsen ET, ME Moeller, N Yamanaka, Q Ou, JM Laursen *et al.,* 2016 A *Drosophila* genome-wide screen identifies regulators of steroid hormone production and developmental timing. Dev. Cell. 37: 558-570.

Denecke S, CJ Nowell, A Fournier-Level, T Perry, and P Batterham, 2015 The Wiggle Index: an open source bioassay to assess sub-lethal insecticide response in *Drosophila melanogaster*. PLoS One 10: e0145051–18.

Deng B, Q Li, X Liu, W Zhang, J Huang *et al.,* 2019 Chemoconnectomics: mapping chemical transmission in *Drosophila*. Neuron. 101: 976-893.

Dermauw W, A Ilias, M Riga, A Tsagkarakou, M Grbic *et al.,* 2012 The cys-loop ligand-gated ion channel gene family of *Tetranychus urticae*: Implications for acaricide toxicology and a novel mutation associated with abamectin resistance. Insect Biochem. Mol. Biol. 42: 455-465.

Di Cara F, and K King-Jones, 2013 How clocks and hormones act in concert to control the timing of insect development. Curr. Top. Dev. Biol. 105: 1–36.

Diao F and BH White, 2012 A novel approach for directing transgene expression in *Drosophila*: T2A-GAL4 in-frame fusion. Genetics. 190: 1139 – 1144.

Diao F, H Ironfield, H Luan, F Diao, WC Shropshire *et al.*, 2015 Plug-and-play genetic access to *Drosophila* cell types using exchangeable exon cassettes. Cell Rep. 10: 1410–1421.

Dietzl G, D Chen, F Schnorrer, K-C Su, Y Barinova *et al.,* 2007 A genome-wide transgenic RNAi library for conditional gene inactivation in *Drosophila*. Nature. 448(7150): 151-156.

Ding X, T Seebeck, Y Feng, Y Jiang, GD Davis, and F Chen, 2019 Improving CRISPR-Cas9 genome editing efficiency by fusion with chromatin-modulating peptides. The CRISPR Journal. 2(1).

Dominick OS and JW Truman, 1984 The physiology of wandering behaviour in *Manduca sexta*. I. Temporal organization and the influence of the internal and external environments. J. Exp. Biol. 110: 35-51.

Drosophila 12 Genomes Consortium, 2007 Evolution of genes and genomes on the *Drosophila* phylogeny. Nature. 450(7167): 203-218.

English BA and CK Jones, 2012 Cholinergic neurotransmission.

Erdmanis L, AO O'Reilly, MS Wiliamson, LM Field, A Turberg, and BA Wallace, 2012 Association of neonicotinoid insensitivity with a conserved residue in the loop d binding region of the tick nicotinic acetylcholine receptor. Biochem. 51(123): 4627-4629.

Fayyazuddin A, MA Zaheer, PR Hiesinger, and HJ Bellen, 2006 The nicotinic acetylcholine receptor *Dα7* is required for an escape behavior in *Drosophila*. PLoS Biol. 4: e63.

Fillippova J, A Matveeva, E Zhuravlev, and G Stepanov, 2019 Guide RNA modification as a way to improve CRISPR/Cas9-based genome-editing systems. Biochem. 167: 49-60.

Florey E, 1963 Acetylcholine in invertebrate nervous systems. Can. J. Biochem. Physiol. 41: 2619–2626.

Fraenkel G and C Hsiao, 1965 Bursicon, a hormone which mediates tanning of the cuticle in the adult fly and other insects. J. Insect Physiol. 11: 513–556.

Freeman MR, A Dobritsa, P Gaines, WA Segraves, JR Carlson, 1999 The *dare* gene: steroid hormone production, olfactory behavior, and neural degeneration in *Drosophila*. Development 126: 4591–4602.

Gargano JW, I Martin, P Bhandari, and MS Grotewiel, 2005 Rapid iterative negative geotaxis (RING): a new method for assessing age-related locomotor decline in *Drosophila*. Exp. Gerontol. 40: 386–395.

Gauthier SA and RS Hewes, 2006 Transcriptional regulation of neuropeptide and peptide hormone expression by the *Drosophila dimmed* and *cryptocephal* genes. J. Exp. Biol. 209: 1803-1815.

Geer BW, 1967 Dietary choline requirements for sperm motility and normal mating activity in *Drosophila melanogaster*. Biological Bulletin 133: 548.

Geer BW, GF Vovis, and MA Yund, 1968 Choline activity during development of *Drosophila melanogaster*. Physiological Zoology 41: 280.

Georghiou GP, 1994 Principles of insecticide resistance management. Phytoprotection, 75(4): 51.

Ghazali MFR, 2020 Profiling the molecular mechanisms underlying negative cross-resistance to insecticides using *Drosophila melanogaster*. The University of Melbourne (PhD Thesis).

Goñalons C and WM Farina, 2015 Effects of sublethal doses of imidacloprid on young adult honeybee behaviour PLoS One 10: e0140814–15.

Gratz SJ, AM Cummings, JN Nguyen, DC Hamm, LK Donohue *et al.*, 2013 Genome engineering of *Drosophila* with the CRISPR RNA-guided Cas9 nuclease. Genetics 194: 1029–1035.

Gratz SJ, FP Ukken, CD Rubinstein, G Thiede, LK Donohue *et al.*, 2014 Highly specific and efficient CRISPR/Cas9-catalyzed homology-directed repair in *Drosophila.* Genetics 196(4): 961-971.

Grauso M, RA Reenan, E Culetto, and DB Sattelle, 2002 Novel putative nicotinic acetylcholine receptor subunit genes, *Dalpha5, Dalpha6* and *Dalpha7*, in *Drosophila melanogaster* identify a new and highly conserved target of adenosine deaminase acting on RNA-mediated A-to-I pre-mRNA editing. Genetics 160: 1519–1533.

Graveley BR, AN Brooks, JW Carlson, MO Duff, JM Landolin *et al.*, 2011 The developmental transcriptome of *Drosophila melanogaster*. Nature 471: 473–479.

Greenspan RJ, 2000 Courtship in *Drosophila.* Ann. Rev. Genetics. 34: 205-232.

Grutter T and J Changeux, 2001 Nicotinic receptors in wonderland. Trends Biochem. Sci. 26(8): 459–63.

Hanaoka K and E Ohnishi, 1974 Changes in ecdysone titre during pupal-adult development in the silkworm, *Bombyx mori*. J. Insect. Physiol. 20(12): 2375-2384.

Hartenstein V, 1993 Atlas of *Drosophila* development.

Henrich V, 1995 Comparison of Ecdysteroid Production in *Drosophila* and *Manduca*: pharmacology and cross-species neural reactivity. Arch. Insect. Biochem. Physiol. 30: 239-254.

Hermans-Borgmeyer I, D Zopf, RP Ryseck, B Hovemann, H Betz, and ED Gundelfinger, 1986 Primary structure of a developmentally regulated nicotinic acetylcholine receptor protein from *Drosophila*. EMBO J. 5(7): 1503–8.

Homem RA, B Buttery, E Richardson, Y Tan, LM Field *et al.*, 2020 Evolutionary trade-offs of insecticide resistance — The fitness costs associated with target-site mutations in the nAChR of *Drosophila melanogaster*. Mol Ecol 29: 2661–2675.

Hsu CT and V Bhandawat, 2016 Organization of descending neurons in *Drosophila melanogaster*. Sci. Rep. 6:20259.

Ihara M and K Matsuda, 2018 Neonicotinoids: molecular mechanisms of action, insights into resistance and impact on pollinators. Curr. Opin. Insect. Sci. 30: 86-92.

Ihara M, S Furutani, S Shigetou, S Shimada, K Niki *et al.*, 2020 Cofactor-enabled functional expression of fruit fly, honeybee, and bumblebee nicotinic receptors reveals picomolar neonicotinoid actions. Proc. Natl. Acad. Sci. U.S.A. 117: 16283–16291.

Ishimoto H, and A Kamikouchi, 2020 A feedforward circuit regulates action selection of pre-mating courtship behavior in female *Drosophila*. Curr. Biol. 30: 396–407.e4.

Jenett A, GM Rubin, TTB Ngo, D Shepard, C Murphy *et al.* 2012 A GAL4-driver line resource for *Drosophila* neurobiology. Cell Rep. 2(4): 991-1001.

Jennings BH, 2011 *Drosophila* – a versatile model in biology and medicine. Materials Today. 14(5): 190-195.

Jonas P, A Baumann, B Merz, and ED Gundelfinger, 1990 Structure and developmental expression of the *Dα2* gene encoding a novel nicotinic acetylcholine receptor protein of *Drosophila melanogaster.* FEBS. 269(1): 264-268.

Jones AK, M Grauso, and DB Sattelle, 2005 The nicotinic acetylcholine receptor gene family of the malaria mosquito*, Anopheles gambiae*. Genomics. 85(2): 176–87.

Jones AK, V Raymond-Delpech, S Thany, M Gauthier, and DB Sattelle, 2006 The nicotinic acetylcholine receptor gene family of the honey bee, *Apis mellifera*. Genome Res. 16(11): 1422–30.

Jones AK and DB Sattelle, 2007 The cys-loop ligand-gated ion channel gene superfamily of the red flour beetle, *Tribolium castaneum*. BMC Genomics. 8:327–27.

Jones AK, and DB Sattelle, 2010 Diversity of insect nicotinic acetylcholine receptor subunits. Adv. Exp. Med. Biol. 683: 25–43.

Jones AK, AN Bera, and DB Sattelle, 2010 The cys-loop ligand-gated ion channel gene superfamily of the parasitoid wasp, *Nasonia vitripennis*. Heredity. 104: 247-259.

Kao PN, AJ Dwork, RR Kaldany, ML Silver, J Wideman *et al.*, 1984 Identification of the alpha subunit half-cystine specifically labelled by an affinity reagent for the acetylcholine receptor binding site. J. Biol. Chem. 259: 11662–11665.

Karlin A, 2002 Emerging structure of the nicotinic acetylcholine receptors. Nat. Rev. Neurosci. 3: 102–114.

Karlin A, and MH Akabas, 1995 Toward a structural basis for the function of nicotinic acetylcholine receptors and their cousins. Neuron 15: 1231–1244.

Karsai G, E Pollák, M Wacker, M Vömel, M Selcho *et al.*, 2013 Diverse in- and output polarities and high complexity of local synaptic and non-synaptic signaling within a chemically defined class of peptidergic *Drosophila* neurons. Front. Neural Circuits 7: 127.

Kearse M, R Moir, A Wilson, S Stones-Havas, M Cheung *et al.,* 2012 Geneious Basic: an integrated and extendable desktop software platform for the organization and analysis of sequence data. Bioinformatics. 28(12): 1647-1649.

Kim YJ, D Zitnan, CG Galizia, K-H Cho, and ME Adams, 2006 A command chemical triggers an innate behavior by sequential activation of multiple peptidergic ensembles. Curr. Biol. 16: 1395–1407.

Kingan TG and ME Adams, 2000 Ecdysteroids regulate secretory competence in Inka cells. J. Exp. Biol. 203: 3011-3018.

Klapoetke NC, Y Murata, SS Kim, SR Pulver, A Birdsey-Benson *et al.,* 2014 Independent optical excitation of distinct neural populations. Nat. Methods. 11(3): 338-346.

Koo HN, JJ An, SE Park, JI Kim, and GH Kim*,* 2014 Regional susceptibilities to 12 insecticides of melon and cotton aphid, *Aphis gossypii* (Hemiptera: Aphididae) and a point mutation associated with imidacloprid resistance. Crop Prot. 55: 91-97.

Lansdell SJ and NS Millar, 2000a Cloning and heterologous expression of Dα4, a Drosophila neuronal nicotinic acetylcholine receptor subunit: Identification of an alternative exon influencing the efficiency of subunit assembly. Neuropharmacology. 39(13): 2604-2614.

Lansdell SJ and NS Millar, 2000b The influence of nicotinic receptor subunit composition upon agonist, alpha-bungarotoxin and insecticide (imidacloprid) binding affinity. Neuropharmacology 39: 671–679.

Lansdell S and N Millar, 2002 Dβ3, an atypical nicotinic acetylcholine receptor subunit from *Drosophila*: Molecular cloning, heterologous expression and coassembly. J Neurochem. 80(6): 1009–18.

Lansdell, SJ, T Collins, J Goodchild, and NS Millar, 2012 The *Drosophila* nicotinic acetylcholine receptor subunits *Dα5* and *Dα7* form functional homomeric and heteromeric ion channels. BMC Neurosci 13: 73.

Lendvai B and ES Vizi, 2008 Nonsynaptic chemical transmission through nicotinic acetylcholine receptors. Physiol. Rev. 88(2): 333-349.

Li T-R and M Bender, 2000 A conditional rescue system reveals essential functions for the ecdysone receptor (EcR) gene during molting and metamorphosis in *Drosophila.* Development. 127: 2897-2905.

Li J, Y Shao, Z Ding, H Bao, Z Liu *et al.*, 2010 Native subunit composition of two insect nicotinic receptor subtypes with differing affinities for the insecticide imidacloprid. Insect Biochem. Mol. Biol. 40: 17–22.

Li F, JW Lindsay, EC Marin, N Otto, M Dreher *et al.*, 2020 The connectome of the adult *Drosophila* mushroom body provides insights into function. eLife 9: e62576.

Li-Kroeger D, O Kanca, PT Lee, S Cowan, MT Lee *et al.*, 2018 An expanded toolkit for gene tagging based on MiMIC and scarless CRISPR tagging in *Drosophila.* eLife 7: 38709.

Liu Z, MS Williamson, SJ Lansdell, I Denholm, Z Han, and NS Millar, 2005 A nicotinic acetylcholine receptor mutation conferring target-site resistance to imidacloprid in *Nilaparvata lugens* (brown planthopper). PNAS 102(24): 8420-8425.

Losey JE and M Vaughan, 2006 The economic value of ecological services provided by insects. BioScience. 56(4): 311-323.

Luan HJ, WC Lemon, NC Peabody, JB Pohl, PK Zelensky *et al.*, 2006 Functional dissection of a neuronal network required for cuticle tanning and wing expansion in *Drosophila*. J. Neurosci. 26: 573–584.

Luong HNB, 2018 *In vivo* functional characterization of nicotinic acetylcholine receptors in *Drosophila melanogaster*. The University of Melbourne (PhD Thesis).

Malina A, CJF Cameron, F Robert, M Blanchette, J Dostie, and J Pelletier, 2015 PAM multiplicity marks genomic target sites as inhibitory to CRISPR-Cas9 editing. Nat. Comm. 6: 10124.

Malloy CA, E Somasundaram, A Omar, U Bhutto, M Medley *et al.*, 2019 Pharmacological identification of cholinergic receptor subtypes: modulation of locomotion and neural circuit excitability in *Drosophila* larvae. Neuroscience 411: 47–64.

Marchal E, H Vandersmissen, L Badisco, S Van de Velde, H Verlinden, *et al.,* 2010 Control of ecdysteroidogenesis in prothoracic glands of insects: A review. Peptides 31: 506– 519.

Martelli F, 2020 Systemic impacts of low dose insecticide exposures in *Drosophila*: a mechanism centred on oxidative stress. The University of Melbourne (PhD Thesis).

Martelli, F., Z. Zhongyuan, J. Wang, C-O. Wong, N. E. Karagas *et al.*, 2020 Low doses of the neonicotinoid insecticide imidacloprid induce ROS triggering neurological and metabolic impairments in *Drosophila*. Proc. Natl. Acad. Sci. U.S.A. *In press.*

Matsuda K, M Shimomura, M Ihara, M Akamatsu, and DB Sattelle, 2005 Neonicotinoids show selective and diverse actions on their nicotinic receptor targets: electrophysiology, molecular biology, and receptor modeling studies. Biosci. Biotechnol. Biochem. 69: 1442–1452.

McBrayer Z, H Ono, M Shimell, J-P Parvy, RB Beckstead *et al.*, 2007 Prothoracicotropic hormone regulates developmental timing and body size in *Drosophila*. Developmental Cell 13: 857–871.

McKay BE, AN Placzek, and JA Dani, 2007 Regulation of synaptic transmission and plasticity by neuronal nicotinic acetylcholine receptors. Biochem. Pharmacol. 74(8): 1120-1133.

Melcher C and MJ Pankratz, 2005 Candidate gustatory interneurons modulating feeding behavior in the *Drosophila* brain. PloS Biol. 3(9): e305.

Meltzer H, E Marom, I Alyagor, O Mayseless, V Berkun *et al.*, 2019 Tissue-specific (ts)CRISPR as an efficient strategy for *in vivo* screening in *Drosophila.* Nat. Commun. 10: 2113.

Meng X, G Wahlstrom, T Immonen, M Kolmer, M Tirronen *et al.,* 2002 The *Drosophila hugin* gene codes for myostimulatory and ecdysis-modifying neuropeptides. Mech. Dev. 117: 5-13.

Mesce KA and SE Fahrbach, 2002 Integration of endocrine signals that regulate insect ecdysis. Front. Neuroendocrinol. 23: 179-199.

Millar NS, 2003 Assembly and subunit diversity of nicotinic acetylcholine receptors. Biochem. Soc. Trans. 31: 869–874.

Millar NS and I Denholm, 2007 Nicotinic acetylcholine receptors: targets for commercially important insecticides. Invert. Neurosci. 7: 53–66.

Millar NS and PC Harkness, 2008 Assembly and trafficking of nicotinic acetylcholine receptors (Review). Mol. Membrane. Biol. 25(4): 279-292.

Mirth C, JW Truman, and LM Riddiford, 2005 The role of the prothoracic gland in determining critical weight for metamorphosis in *Drosophila melanogaster*. Curr. Biol. 15: 1796–1807.

Mitchell J, 2012. Nitenpyram resistance in *Drosophila melanogaster*. The University of Melbourne (PhD Thesis).

Moris-Sanz, M, A Estacio-Gómez, E Sánchez-Herrero, and FJ Díaz-Benjumea, 2015 The study of the Bithorax-complex genes in patterning CCAP neurons reveals a temporal control of neuronal differentiation by Abd-B. Biol. Open 4: 1132–1142.

Murthy M and G Turner, 2013 Whole-cell *in vivo* patch-clamp recordings in the *Drosophila* brain. *Drosophila Neurobiol.*

Nagarkar-Jaiswal S, PT Lee, ME Campbell, K Chen, S Anguiano-Zarate *et al.,* 2015 A library of MiMICs allows tagging of genes and reversible, spatial and temporal knockdown of proteins in *Drosophila*. eLife 4: e05338.

Nemecz A, MS Prevost, A Menny, and P-J Corringer, 2016 Emerging molecular mechanisms of signal transduction in pentameric ligand-gated ion channels. Neuron. 90.

Nguyen J, R Ghazali, P Batterham, and T Perry, 2021 Inhibiting the proteasome reduces molecular and biological impacts of the natural product insecticide, spinosad. Pest. Man. Sci.

Nijhout HF, 1975 A threshold size for metamorphosis in the tobacco hornworm *Manduca sexta* (L.). Biol. Bull. 149: 214-225.

O'Brien MA and PH Taghert, 1998 A peritracheal neuropeptide system in insects: release of myomodulin-like peptides at ecdysis. J Exp Biol 201: 193-209.

Ou Q, A Magico, and K King-Jones, 2011 Nuclear receptor DHR4 controls the timing of steroid hormone pulses during *Drosophila* development. PLoS Biol. 9(9): e1001160.

Park Y, V Fillippov, SS Gill, and ME Adams, 2002 Deletion of the ecdysis-triggering hormone gene leads to lethal ecdysis deficiency. Development. 129: 493-503.

Park JH, AJ Schroeder, C Helfrich-Forster, FR Jackson, and J Ewer, 2003 Targeted ablation of CCAP neuropeptide-containing neurons of *Drosophila* causes specific defects in execution and circadian timing of ecdysis behavior. Development 130: 2645–2656.

Pearce SL, DF Clarke, PD East, S Elfekih, KHJ Gordon *et al.*, 2017 Genomic innovations, transcriptional plasticity and gene loss underlying the evolution and divergence of two highly polyphagous and invasive *Helicoverpa* pest species. BMC Biol. 15: 63.

Perry T, J McKenzie, and P Batterham, 2007 A Dα6 knockout strain of *Drosophila* melanogaster confers a high level of resistance to spinosad. Insect Biochem. Mol. Biol. 37(2): 184–88.

Perry T, DG Heckel, JA McKenzie, and P Batterham, 2008 Mutations in *Dα1* or *Dβ2* nicotinic acetylcholine receptor subunits can confer resistance to neonicotinoids in *Drosophila melanogaster*. Insect Biochem. Mol. Biol. 38: 520–528.

Perry T, JQ Chan, P Batterham, GB Watson, C Geng *et al.*, 2012 Effects of mutations in *Drosophila* nicotinic acetylcholine receptor subunits on sensitivity to insecticides targeting nicotinic acetylcholine receptors. Pestic. Biochem. and Phys. 102: 56–60.

Perry T, J Somers, YT Yang, and P Batterham, 2015 Expression of insect α6-like nicotinic acetylcholine receptors in *Drosophila melanogaster* highlights a high level of conservation of the receptor: spinosyn interaction. Insect Biochem. Mol. Biol.

Perry T and P Batterham, 2018 Harnessing model organisms to study insecticide resistance. Curr. Opin. Insect. Sci. 27: 61-67.

Perry T, W Chen, R Ghazali, YT Yang, D Christesen *et al.,* 2021 Role of nicotinic acetylcholine receptor subunits in the mode of action of neonicotinoid, sulfoximine and spinosyn insecticides in *Drosophila melanogaster*. Insect. Biochem. Mol. Biol. 131: 103547.

Petersen TN, S Brunak, G von Heijne, and H Nielsen, 2011 SignalP 4.0: discriminating signal peptides from transmembrane regions. Nat Methods 8: 785–786.

Petryk A, J Warren, G Marques, M Jarcho, Gilbert L *et al.,* 2003. Shade is the *Drosophila* P450 enzyme that mediates the hydroxylation of ecdysone to the steroid insect molting hormone 20- hydroxyecdysone. PNAS. 100: 13773–13778.

Port F, HM Chen, T Lee, and SL Bullock, 2014 Optimized CRISPR/Cas tools for efficient germline and somatic genome engineering in *Drosophila*. Proc. Natl. Acad. Sci. U. S. A. 111: E2967–E2976.

Port F and SL Bullock, 2016 Augmenting CRISPR applications in *Drosophila* with tRNA-flanked sgRNAs. Nat. Methods. 13(10): 852-856.

Puinean AM, SJ Lansdell, T Collins, P Bielza, and NS Millar, 2013 A nicotinic acetylcholine receptor transmembrane point mutation (G275E) associated with resistance to spinosad in *Frankliniella occidentalis*. J Neurochem. 124(5): 590–601.

Quik M, D Zhang, M McGregor, and T Bordia, 2015 Alpha7 nicotinic receptors as therapeutic targets for Parkinson's disease. Biochem. Pharmacol. 97(4): 399-407.

Ravenscroft TA, J Janssens, P-T Lee, B Tepe, PC Marcogliese *et al.,* 2020 *Drosophila* voltages-gated sodium channels are only expressed in active neurons and are localized to distal axonal initial segment-like domains. J. Neurosci. 40(42): 7999 – 8024.

Ren XQ, SB Cheng, MW Treuil, J Mukherjee, J Rao, *et al.*, 2005 Structural determinants of α4β2 nicotinic acetylcholine receptor trafficking. J. Neurosci. 25: 6676–6686.

Rewitz K, R Rybczynski, J Warren, L Gilbert, 2006 The Halloween genes code for cytochrome P450 enzymes mediating synthesis of the insect moulting hormone. Biochemical Society Transactions 34: 1256–1260.

Rewitz KF, N Yamanaka, LI Gilbert, MB O'Connor, 2009 The insect neuropeptide PTTH activates receptor tyrosine kinase torso to initiate metamorphosis. Science 326: 1403–1405.

Riddiford LM, 1993 Hormones and *Drosophila* development. Cold Spring Harbor Laboratory Press, Cold Spring Harbor, NY, pp. 899-940.

Robinson SW, P Herzyk, JAT Dow, DP Leader, 2013. FlyAtlas: database of gene expression in the tissues of *Drosophila melanogaster*. Nucleic Acids Res 41: 744– 750.

Saldago VL and TC Sparks, 2005 The Spinosyns: chemistry, biochemistry, mode of action, and resistance. Agrochemical Discovery.

Sánchez-Bayo F and KAG Wyckhuys, 2019 Worldwide decline of the entomofauna: a review of its drivers. Biol. Conserv. 232: 8–27.

Sattelle DB, AK Jones, BM Sattelle, K Matsuda, R Reenan *et al.*, 2005 Edit, cut and paste in the nicotinic acetylcholine receptor gene family of *Drosophila melanogaster*. Bioessays 27: 366–376.

Sawruk E, P Schloss, H Betz, and B Schmitt, 1990a Heterogeneity of *Drosophila* nicotinic acetylcholine receptors: SAD, a novel developmentally regulated a-subunit. EMBO Journal. 9(9): 2671-2677.

Sawruk E, C Udri, H Betz, and B Schmitt, 1990b SBD, a novel structural subunit of the Drosophila nicotinic acetylcholine receptor, shares its genomic localization with two α-subunits. FEBS Letters. 273(1-2): 177–81.

Scheffer LK, CS Xu, M Januszewski, Z Lu, S Takemura *et al.,* 2020 A connectome and analysis of the adult *Drosophila* central brain. eLife. 9: 57443.

Schinaman JM, RL Giesey, CM Mizutani, T Lukacsovich, and R Sousa-Neves, 2014 The KRÜPPEL-like transcription factor DATILÓGRAFO is required in specific cholinergic neurons for sexual receptivity in *Drosophila* females. PLoS Biology 12: e1001964.

Schindelin J, I Arganda-Carreras, E Frise, V Kaynig, M Longair *et al.*, 2012 Fiji: an open-source platform for biological-image analysis. Nat. Methods. 9(7): 676-682.

Schloss P, H Betz, C Schroder, and ED Gundelfinger, 1991 neuronal nicotinic acetylcholine receptors in *Drosophila*: antibodies against an α-like and a non-α-subunit recognize the same high-affinity α-bungarotoxin binding complex. J. Neurochem.

Schoofs A, S Huckesfeld, P Schlegel, A Miroschnikow, M Peters *et al.,* 2014 Selection of motor programs for suppressing food intake and inducing locomotion in the *Drosophila* brain. PLoS Biol. 12(6): e1001893.

Schulz R, E Sawruk, C Mülhardt, S Bertrand, A Baumann, *et al.,* 1998 Dα3, a new functional alpha subunit of nicotinic acetylcholine receptors from *Drosophila*. J Neurochem. 71(2): 853–862.

Schulz R, S Bertrand, K Chamaon, K Smalla, E Gundelfinger, and D Bertrand, 2000 Neuronal nicotinic acetylcholine receptors from *Drosophila*: Two different types of α subunits coassemble within the same receptor complex. J Neurochem. 74(6): 2537–2546.

Segraves WA and DS Hogness, 1990 The E75 ecdysone-inducible gene responsible for the 75B early puff in *Drosophila* encodes two new members of the steroid receptor superfamily. Genes. Dev. 4: 204-219.

Seguela P, J Wadiche, K Dineley-Miller, JA Dani, and JW Patrick, 1993 Molecular cloning, functional properties, and distribution of rat brain alpha7: a nicotinic cation channel highly permeable to calcium. J. Neurosci. 13(2): 596-604.

Setiawan L, X Pan, AL Woods, MB O'Connor, and IK Hariharan, 2018 The BMP2/4 ortholog Dpp can function as an inter-organ signal that regulates developmental timing. Life. Sci. Alliance. 1(6): e201800216.

Shao Y-M, K Dong, C-X Zhang, 2007 The nicotinic acetylcholine receptor gene family of the silkworm, *Bombyx mori*. BMC Genomics. 8:324.

Shapiro H, 1932 The rate of oviposition in the fruit fly, *Drosophila*. Biol. Bull. 63(3): 456-471.

Sharma S, R Kooner, and R Arora, 2017 Insect pests and crop losses.

Shi M, Z Yue, A Kuryatov, JM Lindstrom, and A Sehgal, 2014 Identification of Redeye, a new sleep-regulating protein whose expression is modulated by sleep amount. eLife 3: e01473.

Shi X, Y-K Zhu, X-M Xia, K Qiao, H-Y Wang, and K-Y Wang, 2012 The mutation in nicotinic acetylcholine receptor *β1* subunit may confer resistance to imidacloprid in *Aphis gossypii*. J. Food Agric. Environ. 10: 1227–1230.

Shimada-Niwa Y and R Niwa, 2014 Serotonergic neurons respond to nutrients and regulate the timing of steroid hormone biosynthesis in *Drosophila.* Nat. Comm. 5: 5778.

Shimomura M, H Okuda, K Matsuda, K Komai, M Akamatsu, and DB Sattelle, 2002 Effects of mutations of a glutamine residue in loop D of the a7 nicotinic acetylcholine receptor on agonist profiles for neonicotinoid insecticides and related ligands. British. J. Pharmacol. 137: 162-169.

Shimomura M, M Yokota, M Ihara, M Akamatsu, DB Sattelle, *et al.,* 2006 Role in the selectivity of neonicotinoids of insect-specific basic residues in loop D of the nicotinic acetylcholine receptor agonist binding site. Mol. Pharmacol. 70: 1255–1263.

Siegmund T, and G Korge, 2001 Innervation of the ring gland of *Drosophila melanogaster*. J. Comp. Neurol. 431: 481–491.

Silva WM, M Berger, C Bass, M Williamson, DM Moura *et al.,* 2016. Mutation (G275E) of the nicotinic acetylcholine receptor alpha6 subunit is associated with high levels of resistance to spinosyns in *Tuta absoluta* (Meyrick) (Lepidoptera: gelechiidae). Pestic. Biochem. Physiol. 131: 1–8.

Snapp E, 2005 Design and use of fluorescent fusion proteins in cell biology. Curr. Protoc. Cell. Biol.

Somers J, J Nguyen, C Lumb, P Batterham, and T Perry, 2015 *In vivo* functional analysis of the *Drosophila melanogaster* nicotinic acetylcholine receptor Dalpha6 using the insecticide spinosad. Insect Biochem. Mol. Biol. 64, 116–127.

Somers J, HNB Luong, J Mitchell, P Batterham, and T Perry, 2017 Pleiotropic effects of loss of the *Dα1* Subunit in *Drosophila melanogaster*: implications for insecticide resistance. Genetics 205: 263–271.

Sparks TC, AJ Crossthwaite, R Nauen, S Banba, D Cordova *et al.,* 2020 Insecticides, biologics and nematicides: Updates to IRAC's mode of action classification - a tool for resistance management. Pesticide. Biochem. Physiol. 167: 104587.

Sparks TC, FJ Wessels, BA Lorsbach, BM Nugent, GB Watson, 2019. The new age of insecticide discovery-the crop protection industry and the impact of natural products. Pestic. Biochem. Physiol. 161, 12–22.

Sparks TC, GD Thompson, HA Kirst, MB Hertlein, LL Larson *et al.*, 1998 Biological activity of the spinosyns, new fermentation derived insect control agents, on Tobacco Budworm (Lepidoptera: Noctuidae) larvae. J. Econom. Entomo. 91(6): 1277-1283.

St. John PA, 2009 Cellular trafficking of nicotinic acetylcholine receptors. Acta. Pharmaco. Sin. 30(6): 656-662.

Stokes C, M Treinin, and RL Papke, 2015 Looking below the surface of nicotinic acetylcholine receptors. Trends. Pharmacol. Sci. 36(8): 514-523.

Thany SH, G Lenaers, V Raymond-Delpech, DB Sattelle, and B Lapied, 2007 Exploring the pharmacological properties of insect nicotinic acetylcholine receptors. Trends Pharmacol. Sci. 28: 14–22.

Tierney ML, N Unwin, 2000 Electron microscopic evidence for the assembly of soluble pentameric extracellular domains of the nicotinic acetylcholine receptor. J. Mol. Biol. 303: 185–196.

Tomizawa, M, and JE Casida, 2005 Neonicotinoid insecticide toxicology: mechanisms of selective action. Annu. Rev. Pharmacol. Toxicol. 45: 247-268.

Van Hiel, MB, P Van Wielendaele, L Temmerman, S Van Soest, K Vuerinckx et al., 2009 Identification and validation of housekeeping genes in brains of the desert locust *Schistocerca gregaria* under different developmental conditions. BMC Mol. Biol. 10: 56.

Venken KJT, JW Carlson, KL Schultze, H Pan, Y He *et al.*, 2009 Versatile P[acman] BAC libraries for transgenesis studies in *Drosophila melanogaster.* Nat. Methods. 6(6): 431-446.

Venken KJT, KL Schulze, NA Haelterman, H Pan, Y He *et al.,* 2011 MiMIC: a highly versatile transposon insertion resource for engineering *Drosophila melanogaster* genes. Nat. Methods 8: 737–U80.

Verkuiji SA and MG Rots, 2019 The influence of eukaryotic chromatin state on CRISPR-Cas9 editing efficiencies. Curr. Opin. Biotechnol. 55: 68-73.

Veverytsa L, and DW Allan, 2012 Temporally tuned neuronal differentiation supports the functional remodeling of a neuronal network in *Drosophila*. Proc. Natl. Acad. Sci. U.S.A. 109: e748–e756.

Von Heijne, 1990 The signal peptide. J. Membrane. Biol. 115: 195-201.

Wang X, X Meng, C Liu, H Gao, Y Zhang, and Z Liu, 2015 Cys-loop ligand-gated ion channel gene discovery in the *Locusta migratoria manilensis* through the neuron transcriptome. Gene. 561(2): 276-282.

Wang J, H Ma, Y Zuo, Y Yang, and Y Wu, 2020 CRISPR-mediated gene knockout reveals nicotinic acetylcholine receptor (nAChR) subunit α6 as a target of spinosyns in *Helicoverpa armigera*. 76(9): 2925-2931.

Watson GB, SW Chouinard, KR Cook, C Geng, JM Gifford *et al.,* 2010 A spinosyn-sensitive *Drosophila melanogaster* nicotinic acetylcholine receptor identified through chemically induced target site resistance, resistance gene identification, and heterologous expression. Insect Biochem. Mol. Biol. 40: 376–384.

Watson GB, MR Loso, JM Babcock, JM Hasler, TJ Letherer *et al.,* 2011 Novel nicotinic action of the sulfoximine insecticide sulfoxaflor. Insect. Biochem. Mol. Biol.

Wilson AL, O Courtenay, LA Kelly-Hope, TW Scott, W Takken *et al.,* 2020 The importance of vector control for the control and elimination of vector-borne diseases. PLoS Neg. Trop. Diseases.

Wonnacott S, 1997 Presynaptic nicotinic ACh receptors. Trends. Neurosci. 20: 92-98.

Woodcock BA, JM Bullock, R. Shore, MS Heard, MG Pereira *et al.*, 2017 Country-specific effects of neonicotinoid pesticides on honey bees and wild bees. Science 356: 1393–1395.

Wu M, JE Robinson, and WJ Joiner, 2014 SLEEPLESS is a bifunctional regulator of excitability and cholinergic synaptic transmission. Curr. Biol. 24: 621–629.

Wu-Smart J, and M Spivak, 2016 Sub-lethal effects of dietary neonicotinoid insecticide exposure on honey bee queen fecundity and colony development. Sci. Rep. 6: 32108.

Yamanaka N, G Marques, and MB O'Connor, 2015 Vesicle-mediated steroid hormone secretion in *Drosophila melanogaster*. Cell. 163(4): 907-919.

Yao X, F Song, F Chen, Y Zhang, J Gu *et al.,* 2008 Amino acids within loops D, E and F of insect nicotinic acetylcholine receptor β subunits influence neonicotinoid selectivity. Insect Biochem. Mol. Biol. 38(9): 834-840.

Zheng Z, JS Lauritzen, E Perlman, CG Robinson, M Nichols *et al.*, 2018 A complete electron microscopy volume of the brain of adult *Drosophila melanogaster*. Cell 174: 730–743.

Zinke I, C Kirchner, LC Chao, MT Tetzlaff, and MJ Pankratz*,* 1999 Suppression of food intake and growth by amino acids in *Drosophila*: the role of *pumpless*, a fat body expressed gene with homology to vertebrate glycine cleavage system. Development. 126: 5275-5284.

Appendices

Appendix 1

CRISPR methods used in attempts to generate a *Dα5* genomic deletion

Different CRISPR strategies became available over the course of the project. These strategies are each described in detail in their own section. All fly strains used in CRISPR experiments are listed in **Table A1** and all sgRNA sequences are listed in **Table A2**. Primer sequences are provided within each section.

A1.1 *In vitro* transcribed sgRNAs

Target sites in the 5'UTR (sgRNA_5'UTR) and exon 2 (sgRNA_exon2) were chosen using the *CRISPR Optimal Target Finder* (Gratz *et al.* 2014). Full length sgRNAs were then generated using the recommended protocol with minor modifications (Bassett *et al.* 2013). Briefly, specific sgRNA primers (**Table A3**) and the *core_sgRNA_R* primer were amplified using *Q5 High-Fidelity DNA polymerase* (NEB) and the PCR products were purified. *In vitro* transcription was then performed using the T7 *mMessage mMACHINE Kit* (Life Technologies). sgRNAs were purified by phenol chloroform extraction and isopropanol precipitation then co-microinjected into *actin-Cas9* embryos. Surviving injectees and F_1 offspring were crossed to *Dbal* flies and molecularly tested for the presence of a deletion using *Dα5_5'UTR_HMA_F/Dα5_exon2__HMA_R* primers.

Table A1 Fly strains used for CRISPR

Name	Origin	Genotype	Stock #	Reference
actin-Cas9	BDSC	*y[1] M{w[+mC]=Act5C-Cas9.P}ZH-2A w[*]; +; +*	54590	
nanos-Cas9	BDSC	*y[1] M{w[+mC]=nos-Cas9.P}ZH-2A w[*]; +; +*	54591	
25709 w-	Lab stock	*y[1] M{RFP[3xP3.PB] GFP[E.3xP3]=vas-int.Dm}ZH-2A w[*]; P{y[+t7.7]=CaryP}attP40; +*	24749 (X), 25709 (II,III)	Christesen *et al.* 2021
25709 v-	BDSC	*y[1] v[1] P{y[+t7.7]=nos-phiC31\int.NLS}X; P{y[+t7.7]=CaryP}attP40; +*	25709	Bischof *et al*. 2007
pCFD4-5'UTR-exon2	Lab stock	*y[1] M{RFP[3xP3.PB] GFP[E.3xP3]=vas-int.Dm}ZH-2A w[*]; P{pCFD4-5'UTR-exon2}attP40; +*		This study
pCFD4-5'UTR-exon12	Lab stock	*y[1] v[1] P{y[+t7.7]=nos-phiC31\int.NLS}X; P{pCDF4-5'UTR-exon12}attP40; +*		This study
pCFD5-exon2,3,4,6	Lab stock	*y[1] v[1] P{y[+t7.7]=nos-phiC31\int.NLS}X; P{pCDF5-exon2,3,4,6}attP40; +*		This study
Dbal	Lab stock	*w[*]; If[*]/CyO; Sb/TM6b, Tb[1]*		Perry *et al.* 2021

Abbreviations: BDSC (Bloomington *Drosophila* Stock Center)

Table A2 sgRNA sequences

Name	Targeted region	Sequence
sgRNA_5'UTR	5'UTR	GGAAATAGATTCCAACCACT
sgRNA_exon2	exon 2	ACTCTATCATGTCTCGATAT
sgRNA_5'UTR^{v2}	5'UTR	GTTGGTATTAAGGGCAGCCC
sgRNA_exon2^{v2}	exon 2	GGCTCGACATTGCATGTAGG
sgRNA_exon12	exon 12	TAACCACCTCGCCCATATGG
sgRNA_exon3	exon 3	GGACGTTCTAGTGTATTATA
sgRNA_exon4	exon 4	TCGTGTCTATACGTTCCGCC
sgRNA_exon6	exon 6	ATTGCCTCCATGGCCTTGCT

Table A3 CRISPR primers (*in vitro* transcribed sgRNAs)

Name	Sequence	Description
Dα5_sgRNA_5'UTR_F	GAAATTAATACGACTCACTATAGGAAATAGATTCCAACCACTGTTTTAGAGCTAGAAATAGC	Generating sgRNAs
Dα5_sgRNA_exon2_F	GAAATTAATACGACTCACTATAACTCTATCATGTCTCGATATGTTTTAGAGCTAGAAATAGC	Generating sgRNAs
core_sgRNA_R	AAAAGCACCGACTCGGTGCCACTTTTTCAAGTTGATAACGGACTAGCCTTATTTTAACTTGCTATTTCTAGCTCTAAAAC	Generating sgRNAs
Dα5_5'UTR_HMA_F	TTCAGACTGTTGGGGGAAGT	Detecting deletion
Dα5_exon2_HMA_R	CACGTGAAGTTGCCACTGTT	Detecting deletion

Highlighting: *Dα5*-specific 20bp regions of homology. Correspond to the sgRNA sequences in Table A2.

A1.2 pU6-5'UTR and pU6-exon2

Two new sgRNAs targeting the 5'UTR (sgRNA_5'UTR^{v2}) and exon 2 (sgRNA_exon2^{v2}) were designed using the *CRISPR Optimal Target Finder* (Gratz *et al.* 2014) and integrated individually into pU6 plasmids (Addgene: 45946) using the recommended protocol (Gratz *et al.* 2013) (**Table A4**). Both plasmids were sequenced and then co-microinjected into *actin-Cas9* and *nanos-Cas9* embryos. Surviving injectees and F_1 offspring were crossed to *Dbal* flies and molecularly tested for the presence of a deletion using *Dα5_5'UTR_FA/Dα5_exon2_RA* primers.

Table A4 CRISPR primers (pU6-5'UTR and pU6-exon2)

Name	Sequence	Description
Dα5_pU6_sgRNA_5'UTR_F	GTTGGTATTAAGGGCAGCCCGTTTTAGAGCTAGAAATAGCAAG	Generating sgRNAs
Dα5_pU6_sgRNA_exon2_F	GGCTCGACATTGCATGTAGGGTTTTAGAGCTAGAAATAGCAAG	Generating sgRNAs
Dα5_5'UTR_FA	GCATGAAGCAAGCCCAGAAA	Detecting deletion
Dα5_exon2_RA	GGCAACACAACGACAACTCC	Detecting deletion

Highlighting: *Dα5*-specific 20bp regions of homology. Correspond to the sgRNA sequences in Table A2.

A1.3 pCFD4-5'UTR-exon2

sgRNA_5'UTR^{v2} and sgRNA_exon2^{v2} were integrated into a modified pCFD4 plasmid (Addgene: 49411). This plasmid, which allows for tandem expression of two sgRNAs, had been previously modified to include the *white*$^{+}$ marker instead of the original *vermillion*$^{+}$ marker (pCFD4*w*$^{+}$). Both sgRNAs were integrated into pCFD4*w*$^{+}$ using the protocol published by Port *et al.* (2014). Briefly, sgRNA primers (**Table A5**) and *Q5 High-Fidelity DNA polymerase* (NEB) were used to run a PCR with pCFD4*w*$^{+}$ as the template. This PCR product, and the pCFD4w+ backbone, were then digested with *Bbs*I, gel purified, assembled by *Gibson Assembly* (NEB) and sequenced.

pCFD4-5'UTR-exon2 was then microinjected into two different fly strains. For G_0 CRISPR editing, it was microinjected into *actin-Cas9* embryos. Surviving injectees and F_1 offspring were crossed to *Dbal* flies and molecularly tested for the presence of a deletion using *Dα5_5'UTR_FC/Dα5_exon2_RD* primers.

Table A5 CRISPR primers (pCFD4-5'UTR-exon2)

Name	Sequence	Description
Dα5_pCFD4_5'UTR_F	TATATAGGAAAGATATCCGGGTGAA CTTCGTTGGTATTAAGGGCAGCCCGT TTTAGAGCTAGAAATAGCAAG	Generating sgRNA plasmid
Dα5_pCFD4_exon2_R	ATTTTAACTTGCTATTTCTAGCTCTAA AACCCTACATGCAATGTCGAGCCGA CGTTAAATTGAAAATAGGTC	Generating sgRNA plasmid
vermillion_F	ATCACTTGAGGTGAAAGTGC	Detecting transgenic insertion
25709_R	CTTGAAGCTTTGGGCTTTTG	Detecting transgenic insertion
Dα5_5'UTR_FC	ATACAAAATCGGAGACCACG	Detecting deletion
Dα5_exon2_RD	AAATACTCGCATCCCACTCG	Detecting deletion

Highlighting: *Dα5*-specific 20bp regions of homology. Correspond to the sgRNA sequences in Table A2

For generation of a transgenic sgRNA fly strain, pCFD4-5'UTR-exon2 was microinjected into attP40 (*25709 w*$^{-}$) embryos. Transgenics were identified phenotypically by *w*$^{+}$ eye colour rescue, and molecularly using *vermillion_F/25709_R* primers. Flies homozygous for the pCFD4-5'UTR-exon2 insertion were generated by self-crossing. Homozygous

males were then crossed to *actin-Cas9* or *nanos-Cas9* virgin females, producing F_1 offspring with all components required for CRISPR editing. F_1 offspring were crossed to *DbaI* flies and molecularly tested for the presence of a deletion using *Dα5_5'UTR_FC/Dα5_exon2_RD* primers.

A1.4 pCFD4-5'UTR-exon12

An sgRNA targeting exon 12 was designed using *crisprflydesign.org* and, with sgRNA_5'UTR^{v2}, integrated into the original pCFD4 plasmid (Addgene: 49411) using the published protocol described above (Port *et al.* 2014) (**Table A6**). pCFD4-5'UTR-exon12 was then microinjected into attp40 (*25709 v-*) embryos. Transgenics were identified phenotypically by v^+ eye colour rescue, and molecularly using *vermillion_F/25709_R* primers. Flies homozygous for the pCFD4-5'UTR-exon12 insertion were generated by self-crossing. Homozygous males were then crossed to *actin-Cas9 or nanos-Cas9* virgin females, and F_1 offspring were crossed to *DbaI* flies. Individuals were molecularly tested for the presence of a deletion using *Dα5_5'UTR_FC/Dα5_exon12_R* primers.

Table A6 CRISPR primers (pCFD4-5'UTR-exon12)

Name	Sequence	Description
Dα5_pCFD4_5'UTR_F	TATATAGGAAAGATATCCGGGTGAA CTTCGTTGGTATTAAGGGCAGCCCGT TTTAGAGCTAGAAATAGCAAG	Generating sgRNA plasmid
Dα5_pCFD4_exon12_R	ATTTAACTTGCTATTTCTAGCTCTAAA ACATCATTGGCAATGTCATTGCGACG TTAAATTGAAAATAGGTC	Generating sgRNA plasmid
vermillion_F	ATCACTTGAGGTGAAAGTGC	Detecting transgenic insertion
25709_R	CTTGAAGCTTTGGGCTTTTG	Detecting transgenic insertion
Dα5_5'UTR_FC	ATACAAAATCGGAGACCACG	Detecting deletion
Dα5_exon12_R	TAACCACCTCGCCCATATGG	Detecting deletion

Highlighting: *Dα5*-specific 20bp regions of homology. Correspond to the sgRNA sequences in Table A2.

.

A1.5 pCFD5-exon2,3,4,6

sgRNAs targeting exons 2,3,4 and 6 were designed using *crisprflydesign.org* and integrated into the multiplex sgRNA plasmid pCFD5 (Addgene: 73914) using the recommended protocol (Port and Bullock 2016). Briefly, sgRNA primers (**Table A7**) and *Q5 High-Fidelity DNA polymerase* (NEB) were used to run three individual PCR reactions with pCFD5 as the template. These PCR products, plus *BbsI*-digested pCFD5 backbone, were then gel purified and assembled by Gibson Assembly (NEB). The resulting plasmid, pCFD5-exon2,3,4,6, was sequenced and microinjected into attP40 (*25709 v*-) embryos. Transgenics were screened phenotypically for v^+ eye colour rescue, and molecularly using *vermillion_F/25709_R* primers. Flies homozygous for the pCFD5-exon2,3,4,6 insertion were generated by self-crossing. Homozygous males were then crossed to *actin-Cas9* virgin females, producing F_1 offspring with all components required for CRISPR editing. Individuals were molecularly tested for the presence of a deletion using *Dα5_5'UTR_FC/Dα5_intron6_R*, *Dα5_exon2_FC/Dα5_intron6_R* or *Da5_exon4_F/Da5_intron6_R* primers.

Table A7 CRISPR primers (pCFD5-exon2,3,4,6)

Name	Sequence	Description
Dα5_pCFD5_PCR1_F	GCGGCCCGGGTTCGATTCCCGGCCGATG CAGGCTCGACATTGCATGTAGGGTTTTA GAGCTAGAAATAGCAAG	Generating sgRNA plasmid
Dα5_pCFD5_PCR1_R	TATAATACACTAGAACGTCCTGCACCAGC CGGGAATCGAACCC	Generating sgRNA plasmid
Dα5_pCFD5_PCR2_F	GGACGTTCTAGTGTATTATAGTTTTAGAG CTAGAAATAGCAAG	Generating sgRNA plasmid
Dα5_pCFD5_PCR2_R	GGCGGAACGTATAGACACGATGCACCAG CCGGGAATCGAACCC	Generating sgRNA plasmid
Dα5_pCFD5_PCR3_F	TCGTGTCTATACGTTCCGCCGTTTTAGAG CTAGAAATAGCAAG	Generating sgRNA plasmid
Dα5_pCFD5_PCR3_R	ATTTTAACTTGCTATTTCTAGCTCTAAAAC AGCAAGGCCATGGAGGCAATTGCACCAG CCGGGAATCGAACCC	Generating sgRNA plasmid
vermillion_F	ATCACTTGAGGTGAAAGTGC	Detecting transgenic insertion
25709_R	CTTGAAGCTTTGGGCTTTTG	Detecting transgenic insertion
Dα5_5'UTR_FC	ATACAAAATCGGAGACCACG	Detecting deletion
Dα5_exon2_FC	ACATAAGACTGTGTGCACGC	Detecting deletion
Dα5_exon4_F	AAAACGGCCAGTGCGAATTC	Detecting deletion
Dα5_intron6_R	CAGTTTGGTGTGCCTCTGGA	Detecting deletion

Highlighting: *Dα5*-specific 20bp regions of homology. Correspond to the sgRNA sequences in Table A2.

Appendix 2

Supplementary material for Christesen *et al.* 2021 (*Chapter Three*)

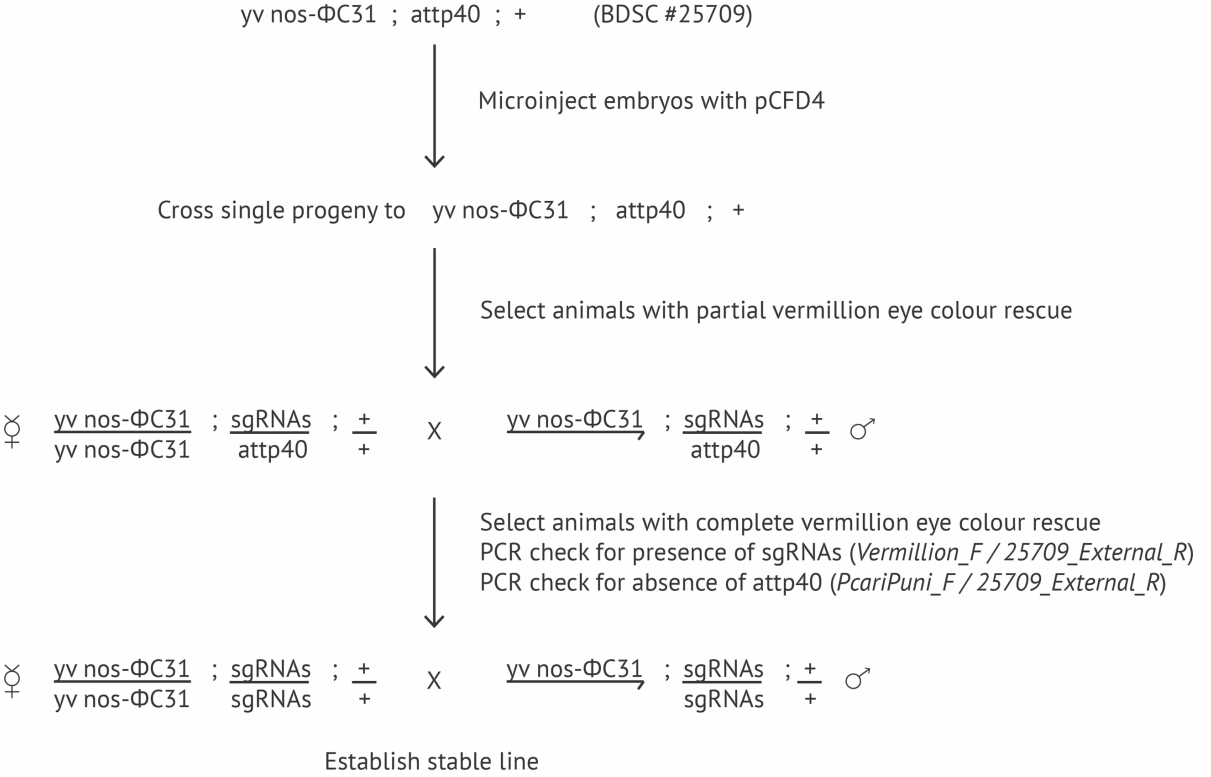


Figure S1 Crossing scheme used to generate transgenic sgRNA strains

This crossing scheme was repeated for two different pCFD4 plasmids. In pCFD4-*Dβ1*, "sgRNAs" refers to *5'UTR_sgRNA* and *sgRNA2*, while in pCFD4-*Dβ1-ex3,* "sgRNAs" refers to 5'*UTR_sgRNA* and *sgRNA1*. sgRNA positions are shown in Figure 1. All fly strains are described in Tables S1 and S2. Primer sequences are available in Table S3.

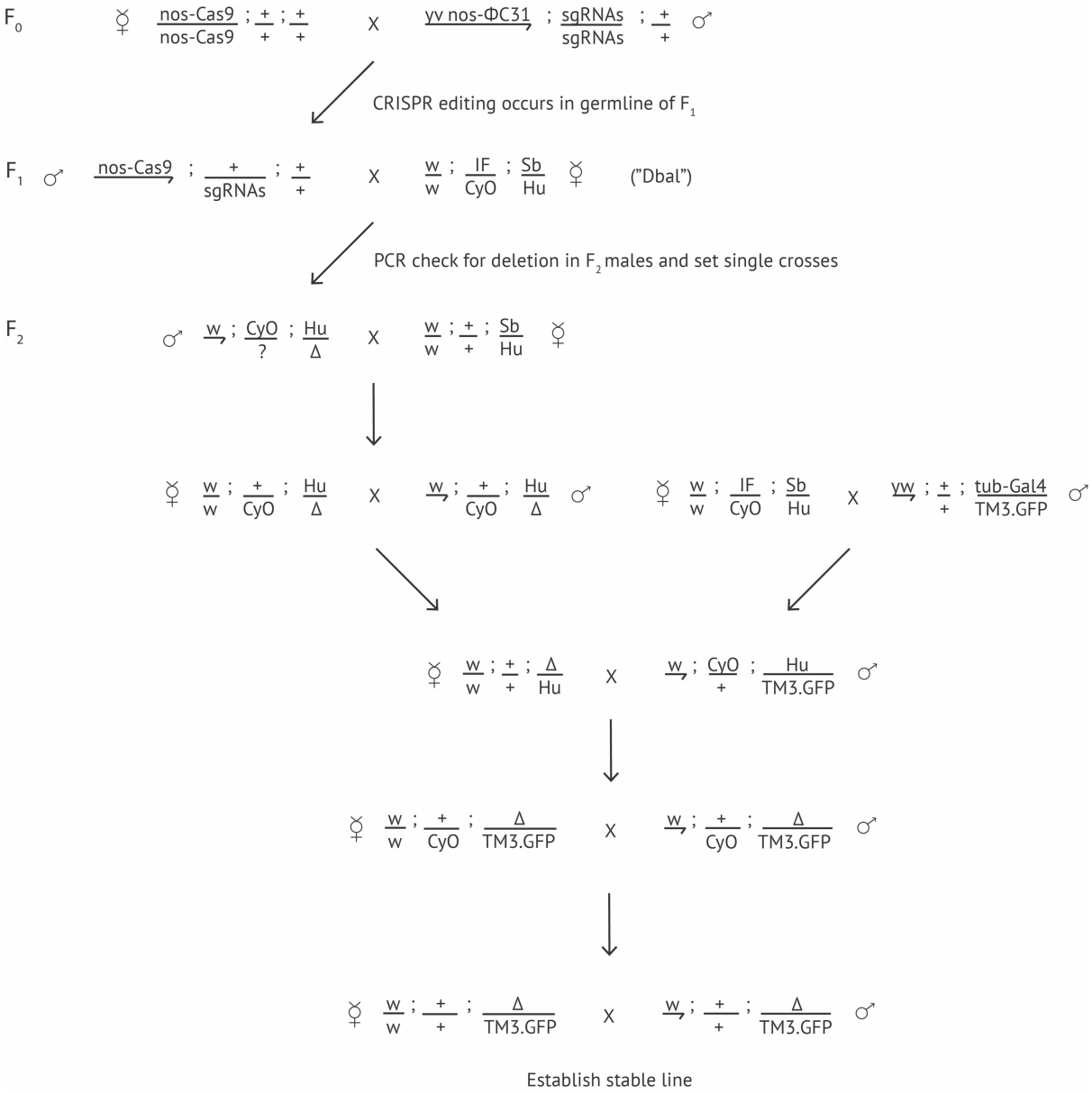


Figure S2 Crossing scheme used to generate genomic deletion strains

This crossing scheme was used to generate the *Dβ1Δe5* and *Dβ1Δex3* strains. For *Dβ1Δe5,* the F_0 sgRNA males were *pCFD4-Dβ1*. For *Dβ1Δe3,* the F_0 sgRNA males were *pCFD4-Dβ1-ex3*. All fly strains are described in Tables S1 and S2. Primer sequences are available in Table S3.

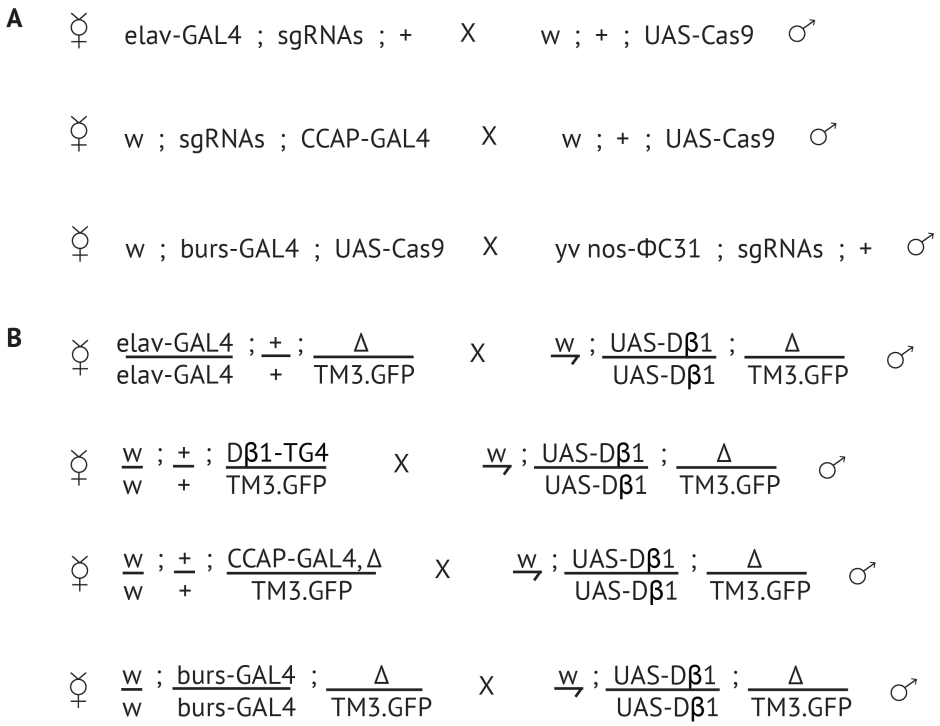


Figure S3 Crosses performed in tissue-specific somatic CRISPR and tissue-specific rescue experiments

A list of the crosses performed for (**A**) tissue-specific somatic CRISPR experiments, and (**B**) tissue-specific rescue experiments. "sgRNAs" always refers to the pair of sgRNAs present in *pCFD4-Dβ1* (*5'UTR_sgRNA/sgRNA2*). The deletion (Δ) used in all rescue crosses is *Dβ1Δex5*. All fly strains are described in Tables S1 and S2.

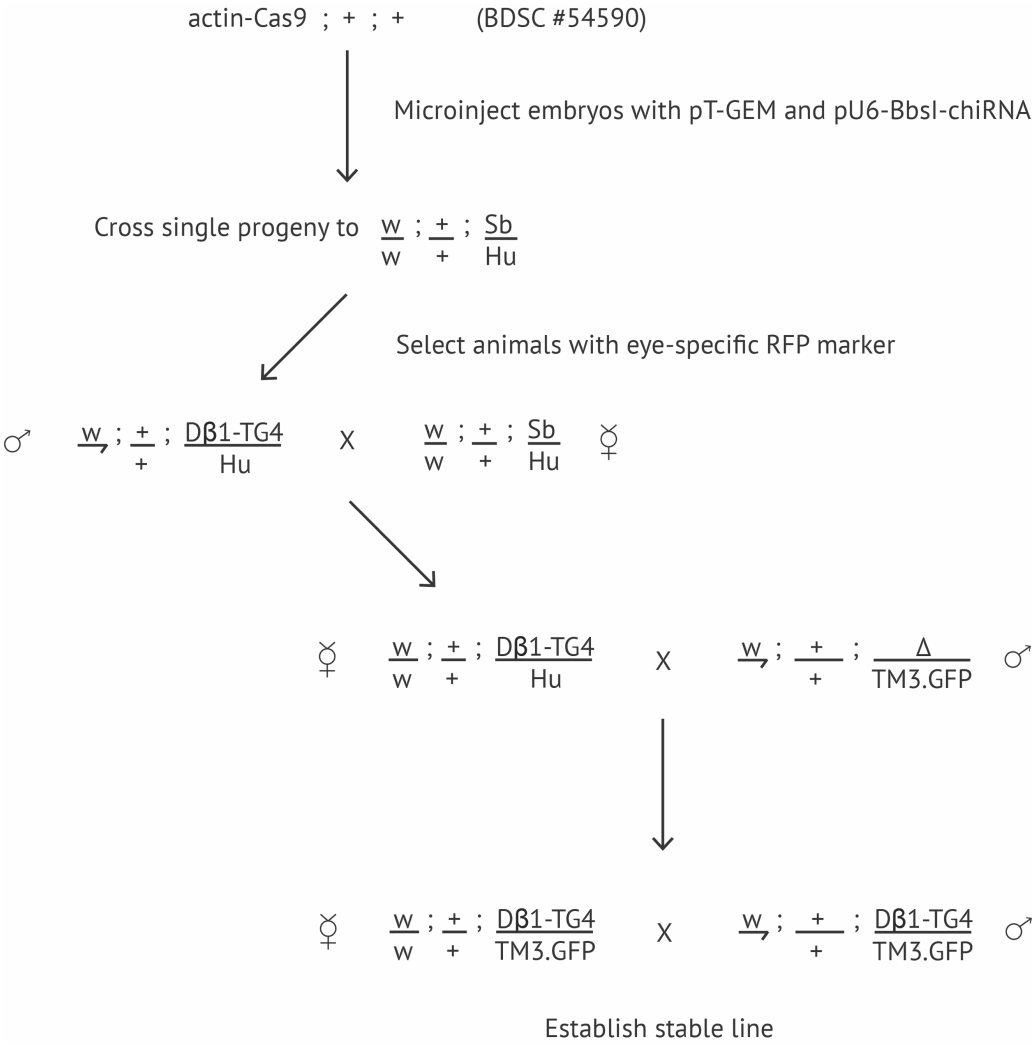


Figure S4 Crossing scheme used to generate the *Dβ1*-TG4 strain

All fly strains are described in Tables S1 and S2.

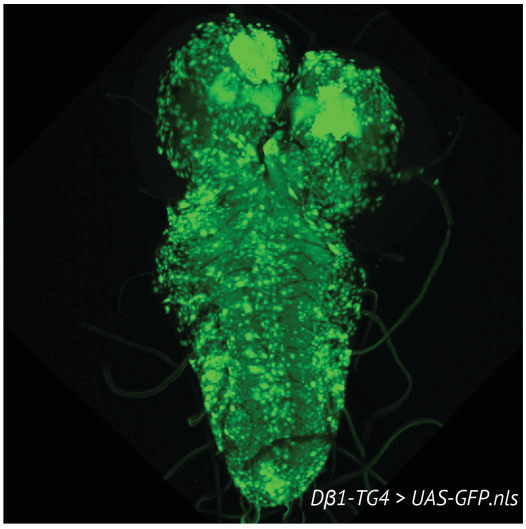


Figure S5 Expression pattern of *Dβ1*-TG4 in larval brain

Virgin *Dβ1*-TG4 females were crossed to UAS-GFP.nls reporter males and brains dissected from offspring in the wandering third instar larval stage. Widespread expression was detected in the brain lobes and ventral nerve cord.

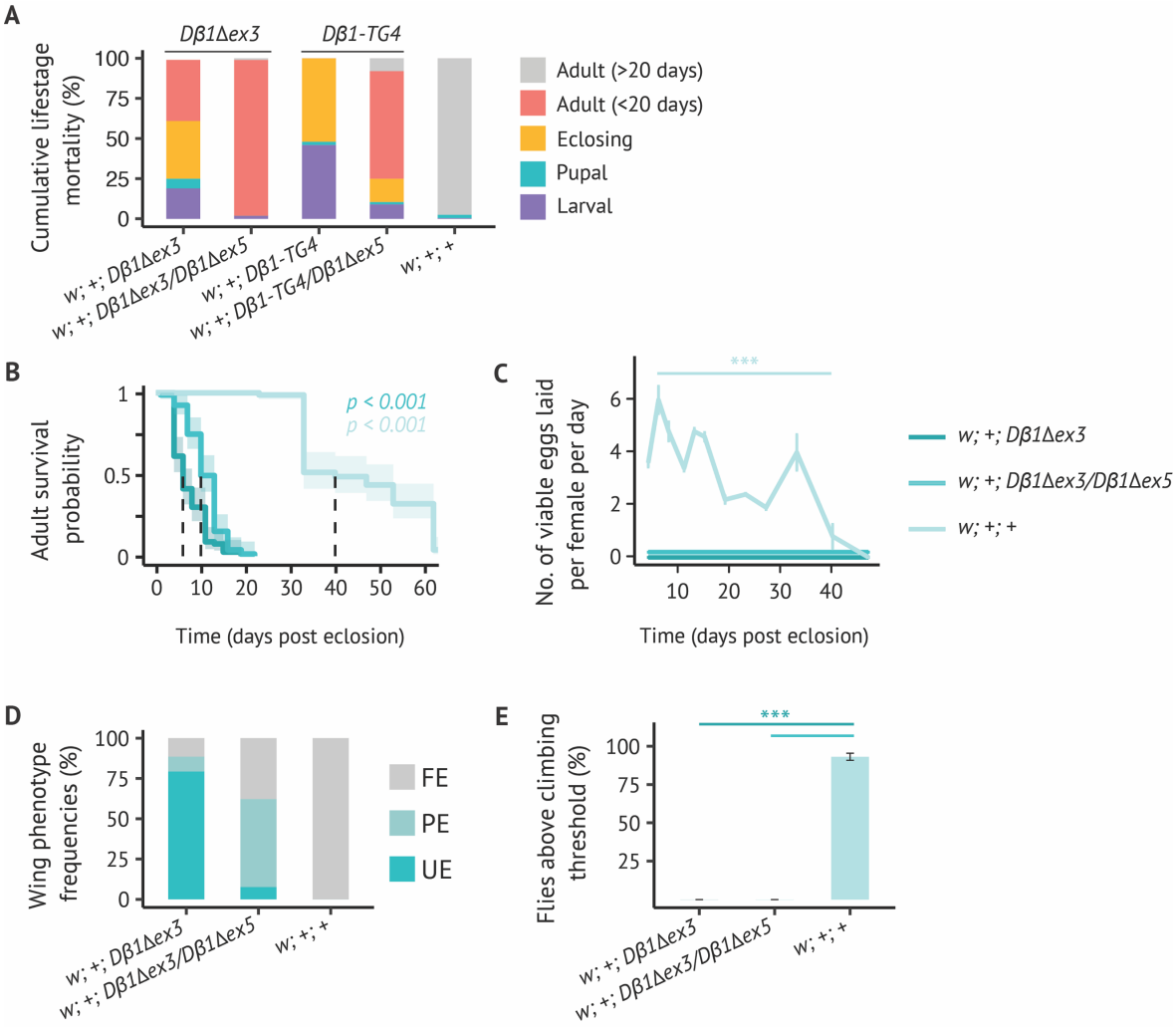


Figure S6 Fitness effects for the smaller deletion, *Dβ1Δex3*, and *Dβ1*-TG4

Dβ1Δex3 (a deletion) and *Dβ1*-TG4 (a T2A-GAL4 insertion) were examined in homozygosis and in transheterozygosis with *Dβ1Δex5*. The background control strain is wAC9 (*w; +; +*). (**A**) Developmental mortality was common in homozygotes, most notably for *Dβ1*-TG4 where 0% survived to adulthood (*n* = 250). Since homozygous *Dβ1*-TG4 adults could not be collected, and transheterozygous *Dβ1*-TG4 adults are already presented in Figures 2 and 3, these genotypes are absent from (**B-E**). (**B**) Kaplan-Meier survival plots with black dashed lines marking median longevity. Longevity was significantly low in homozygotes and transheterozygotes relative to the wAC9 control. Shading represents 95% confidence intervals (*n* = 80, Cox-Mantel test). (**C**) Number of viable eggs laid per female per day, throughout lifespan. No egg laying was observed for homozygotes or transheterozygotes. Error bars indicate SEM (*n* = 40, *** $p < 0.001$, Student's t-test performed for each time point). (**D**) Wing expansion was disrupted in most homozygotes and transheterozygotes (*n* = 250). UE, unexpanded; PE, partially expanded; FE, fully expanded. (**E**) Homozygotes and transheterozygotes failed all climbing assays. Error bars indicate SEM (*n* = 80, *p* *** < 0.001, Tukey's HSD pair-wise test).

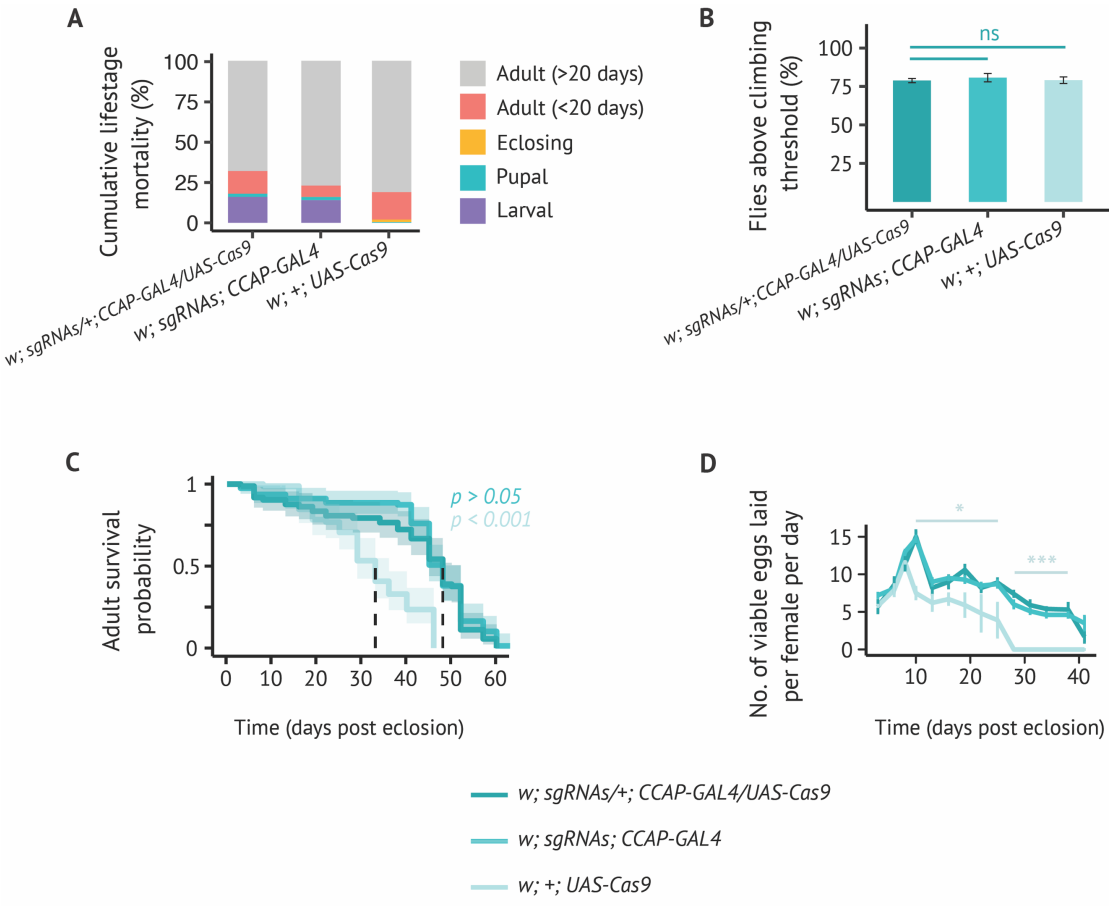


Figure S7 *CCAP*-GAL4 CRISPR has no additional fitness effects

Deletion of *Dβ1* specifically in CCAP neurons (*CCAP*-GAL4 CRISPR) has no detrimental effect relative to the parental controls in multiple fitness assays (except for wing expansion, Figure 5). (**A**) Proportion of deaths occurring at each developmental lifestage through to early and late adulthood (n = 250). (**B**) Percentage of individuals that successfully passed a 45mm threshold in climbing assays. Error bars indicate SEM (n = 80, $p > 0.05$, Tukey's test). (**C**) Kaplan-Meier survival plot with black dashed lines marking median longevity. Longevity was significantly shorter in the UAS-Cas9 parental control, but no difference was observed between the other genotypes. Shading represents 95% confidence intervals (n = 80, Cox-Mantel test). (**D**) Number of viable eggs laid per female per day, throughout lifespan. Fertility was significantly lower for the UAS-Cas9 parental control, but no difference was observed between the other genotypes. Error bars indicate SEM (n = 40, * $p < 0.05$, *** $p < 0.001$, Student's t-test performed for each time point).

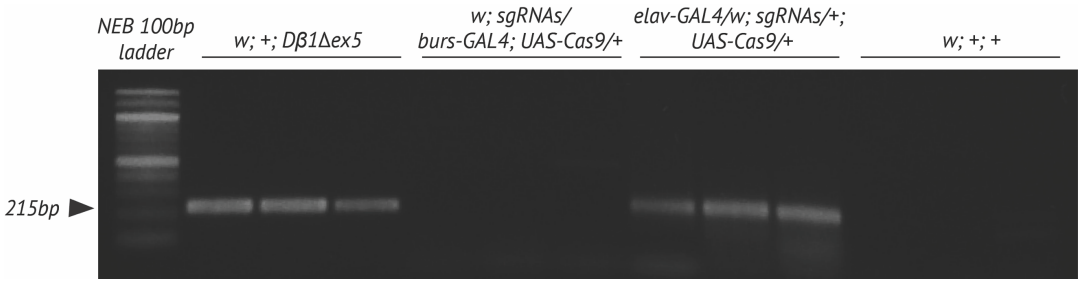


Figure S8 CRISPR editing is not detected in *burs*-GAL4 CRISPR flies

DNA was extracted from pooled samples of 10 adult flies, and deletions in *Dβ1* detected using *Dβ1_5'UTR_sgRNA_HMA_F/Dβ1_sgRNA2_HMA_R* primers. Deletions were detected in all *Dβ1Δex5* and *elav*-GAL4 CRISPR samples, but not in *burs*-GAL4 CRISPR samples or wAC9 controls. Primer sequences are available in Table S3.

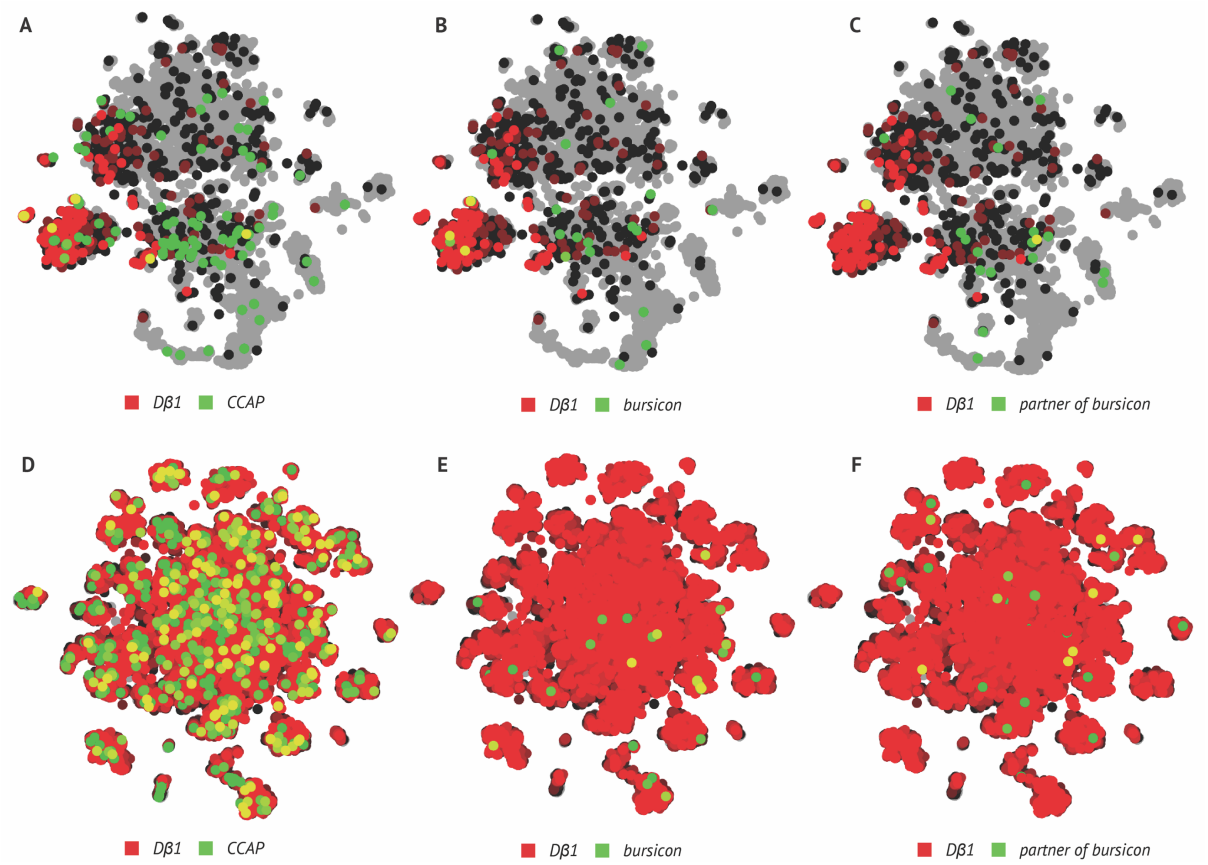


Figure S9 Available single-cell RNA-seq data reveal coexpression of *Dβ1*, *CCAP, bursicon* and *partner of bursicon*

Two-dimensional representation of cells in the larval brain (**A-C**) and the cells in the adult ventral nerve cord (**D-F**). Cells expressing *Dβ1* are red, cells expressing either *CCAP, bursicon* or *partner of bursicon* are green, and cells that express both genes have a blended colour (if expression is equal, cells appear yellow). Datasets for the larval brain (Ravenscroft *et al.* 2020) and the adult ventral nerve cord (Allen *et al.* 2020) were accessed via Scope (https://scope.aertslab.org/).

Table S1 Fly strains used

Name	Origin	Description	Genotype	Stock #	Reference
wAC9	Lab stock	Autosomes from BDSC #54590 and X chromosome from VDRC #60000. This is the background strain for a collection of nAChR CRISPR mutants.	w[1118]; +; +		Perry *et al.* 2021
25709 v-	BDSC	2nd chromosome attP landing site.	y[1] v[1] P{y[+t7.7]=nos-phiC31\int.NLS}X; P{y[+t7.7]=CaryP}attP40	25709	Bischof *et al*. 2007
pCFD4-Dβ1	Lab stock	Transgenic sgRNA stock. sgRNAs targeting Dβ1 5'UTR and Dβ1 exon 5 are ubiquitously expressed (5'UTR_sgRNA and sgRNA2).	y[1] v[1] P{y[+t7.7]=nos-phiC31\int.NLS}X; P{pCFD4-Dβ1}attP40		Perry *et al.* 2021
nanos-Cas9	BDSC	Cas9 driven during oogenesis by *nanos* regulatory sequences.	y[1] M{w[+mC]=nos-Cas9.P}ZH-2A w[*]	54591	
actin-Cas9	BDSC	Cas9 driven by Actin5c promotor.	y[1] M{w[+mC]=Act5C-Cas9.P}ZH-2A w[*]	54590	
UAS-Cas9	BDSC	3rd chromosome Cas9 under control of the UAS promotor.	w[1118]; P{y[+t7.7] w[+mC]=UAS-Cas9.C}attP2	54595	
Dbal	Lab stock	2nd and 3rd chromosomes have balancers and marker chromosomes.	w[*]; If[*]/CyO; Sb/TM6b, Tb[1]		Perry *et al.* 2021
elav Dbal	Lab stock	2nd and 3rd chromosomes have balancers and marker chromosomes. elav-GAL4 X chromsome is from BDSC #458.	P{w[+mW.hs]=GawB}elav[C155]; If[*]/CyO; Sb/TM6b, Tb[1]		
w;+; Sb/Hu	Lab stock	3rd chromosome has balancer and marker chromosome	w[*]; +; Sb/TM6b, Tb[1]		
tub-GAL4/ TM3.GFP	Lab stock	A fluorescent third chromosome balancer. All other chromosomes from BDSC #5138.	y[1] w[*]; +; P{w[+mC]=tubP-GAL4}LL7/TM3, P{w+mC=ActGFP}JMR2, Ser1		
Dβ1Δex5	Lab stock	Contains a deletion in the Dβ1 gene from the 5'UTR to exon 5. Maintained over fluorescent third chromosome balancer.	w[1118];+;Dβ1Δex5/TM3, P{w+mC=ActGFP}JMR2, Ser1		Perry *et al.* 2021
elav-GAL4	BDSC	Pan-neuronal GAL4 expression.	P{w[+mW.hs]=GawB}elav[C155]	458	
CCAP-GAL4	BDSC	GAL4 expression in the CCAP-neurons.	y[1] w[*]; Bl[1]/CyO, y[+]; P{w[+mC]=CCAP-GAL4.P}9	25686	
burs-GAL4	BDSC	GAL4 expression in the bursicon-positive CCAP-neurons.	w[*]; P{w[+mC]=Burs-GAL4.P}P12	40972	
Armenia-14	Lab stock	Wild type strain.	.+;+;+		Perry *et al*. 2008
UAS-GFP.nls	BDSC	Reporter strain. Nuclear-localised GFP under control of the UAS promotor.	w[1118]; P{w[+mC]=UAS-GFP.nls}14	4775	

Table S2 Fly strains generated

Name	Description	Genotype
25709 w-	Autosomes from BDSC #25709 (2nd chromosome attP landing site) and X chromosome from BDSC #24749 (w).	y[1] M{RFP[3xP3.PB] GFP[E.3xP3]=vas-int.Dm}ZH-2A w[*]; P{y[+t7.7]=CaryP}attP40
pCFD4-Dβ1-ex3	Transgenic sgRNA stock. sgRNAs targeting Dβ1 5'UTR and Dβ1 exon 3 are ubiquitously expressed (5'UTR_sgRNA and sgRNA1).	y[1] v[1] P{y[+t7.7]=nos-phiC31\int.NLS}X; P{pCFD4-Dβ1-ex3}attP40
Dβ1Δex3	Contains a deletion in the Dβ1 gene from the 5'UTR to exon 3. Maintained over fluorescent third chromosome balancer.	w[1118];+;Dβ1Δex3/TM3, P{w+mC=ActGFP}JMR2, Ser1
Dβ1-TG4	Contains a T2A-GAL4 cassette in the first coding intron of the Dβ1 gene. Maintained over fluorescent third chromosome balancer.	w[1118];+;TI{RFP[3xP3.PB]=T-GEM}nAChRbeta1/TM3, P{w+mC=ActGFP}JMR2, Ser1
elav-GAL4; Dβ1sgRNAs	Pan-neuronal GAL4 expression. Ubiquitous expression of sgRNAs targetting Dβ1 5'UTR and Dβ1 exon 5 (5'UTR_sgRNA and sgRNA2).	P{w[+mW.hs]=GawB}elav[C155]; P{pCFD4-Dβ1}attP40; +
Dβ1sgRNAs; CCAP-GAL4	GAL4 expression in the CCAP-neurons. Ubiquitous expression of sgRNAs targetting Dβ1 5'UTR and Dβ1 exon 5 (5'UTR_sgRNA and sgRNA2).	w[*]; P{pCFD4-Dβ1}attP40; P{w[+mC]=CCAP-GAL4.P}9
burs-GAL4; UAS-Cas9	GAL4 expression in the bursicon-positive CCAP-neurons. Cas9 under control of the UAS promotor.	w[*]; P{w[+mC]=Burs-GAL4.P}P12; P{y[+t7.7] w[+mC]=UAS-Cas9.C}attP2
UAS-Dβ1	Dβ1 cDNA under control of the UAS promotor.	y[1] M{RFP[3xP3.PB] GFP[E.3xP3]=vas-int.Dm}ZH-2A w[*]; P{w[+mC]=UAS-Dβ1}attP40; +
UAS-Dβ1; Dβ1Δex5	Dβ1 cDNA under control of the UAS promotor. Dβ1Δex5 deletion maintained over fluorescent third chromosome balancer.	w[*]; P{w[+mC]=UAS-Dβ1}attP40; Dβ1Δex5/TM3, P{w+mC=ActGFP}JMR2, Ser1
elav-GAL4; Dβ1Δex5	Pan-neuronal GAL4 expression. Dβ1Δex5 deletion maintained over fluorescent third chromosome balancer.	P{w[+mW.hs]=GawB}elav[C155]; +; Dβ1Δex5/TM3, P{w+mC=ActGFP}JMR2, Ser1
CCAP-GAL4, Dβ1Δex5	GAL4 expression in the CCAP-neurons. The third chromosome CCAP-GAL4 driver has been recombined with the Dβ1Δex5 deletion. Maintained over fluorescent third chromosome balancer.	w[*];+;Dβ1Δex5, P{w[+mC]=CCAP-GAL4.P}9/TM3, P{w+mC=ActGFP}JMR2, Ser1
burs-GAL4; Dβ1Δex5	GAL4 expression in the bursicon-positive CCAP-neurons. Dβ1Δex5 deletion maintained over fluorescent third chromosome balancer.	w[*]; P{w[+mC]=Burs-GAL4.P}P12; Dβ1Δex5/TM3, P{w+mC=ActGFP}JMR2, Ser1

Table S3 Primers used

Primer name	Sequence	Experiment
Dβ1_sgRNA_5'UTR	TATATAGGAAAGATATCCGGGTGAACTTCGAAAGCTCT CTCATTTCTAAAGGGTTTTAGAGCTAGAAATAGCAAG	CRISPR
Dβ1_sgRNA_1	ATTTTAACTTGCTATTTCTAGCTCTAAAACTAGTCGGCCT CATCCCACTGCGACGTTAAATTGAAAATAGGTC	CRISPR
Dβ1_sgRNA_2	ATTTTAACTTGCTATTTCTAGCTCTAAAACTCCTATTCAT GAAGCGCCCTCGACGTTAAATTGAAAATAGGTC	CRISPR
Dβ1_sgRNA_5'UTR_HMA_F	ACAGCTGATAGGGCCAACTG	CRISPR
Dβ1_sgRNA1_HMA_R	GTCCGGCTTCCAAACCTT	CRISPR
Dβ1_sgRNA2_HMA_R	CTGATATGCTTGGGCAGCTC	CRISPR
Vermillion_F	ATCACTTGAGGTGAAAGTGC	CRISPR
25709_External_R1	CTTGAAGCTTTGGGCTTTTG	CRISPR, AttP40 insertions
SV40	CCCCCTGAACCTGAAACATA	AttP40 insertions
PcaryPuni_F	GTTTAGAGCAGCCGAAT	AttP40 insertions
Dβ1_clone_F	CATGTCCCTGGAGTAAGTG	Cloning Dβ1
Dβ1_clone_R	CTGCTCCAAGTCCTCACTC	Cloning Dβ1
Dβ1_RT_F	GAGTTCATTGCCGAGCACTT	qRT-PCR
Dβ1_RT_R	AAATCTCGATGATGCGATCC	qRT-PCR
CCAP_RT_F	TACAATGGAAGTACGAGAAGC	qRT-PCR
CCAP_RT_R	GCGTTTGAATAGCGAGAAT	qRT-PCR
bursiconA_RT_F (bursicon)	CTTGGCGACGATTGTCAGGT	qRT-PCR
bursiconA_RT_R (bursicon)	GGGACAGAATAGCGAGACGG	qRT-PCR
bursiconB_RT_F (partner of bursicon)	GGCACTGGCGACGAGAACTG	qRT-PCR
bursiconB_RT_R (partner of bursicon)	GGCAGCAGTAGCACTCTTTCAG	qRT-PCR
Rp32_ RT_F	CCAGTCGGATCGATATGCTAA	qRT-PCR
Rp32_RT_R	GTTCGATCCGTAACCGATGT	qRT-PCR
CG13220_RT_F	TGGGCAGTGCCTTCTACATTT	qRT-PCR
CG13220_RT_R	CGTACGCACCTCGCTTGTT	qRT-PCR

Table S4 MIQE

Sample	Details	Checklist
Source	If cancer, was biopsy screened for adjacent normal tissue?	*Drosophila melanogaster* whole 1-day old virgin adults
Method of preservation	Liquid N2/RNAlater/formalin	Liquid N2
Storage time (if appropriate)	If using samples >6 months old	<1 month old
Handling	Fresh/frozen/formalin	Frozen
Extraction method	Trizol/columns	TRIsure (Bioline)
RNA: DNA-free	Intron-spanning primers/no RT control	Intron-spanning primers, DNaseI, PCR check
Concentration	Nanodrop/ribogreen/microfluidics	Fluorometric quantitation (Qubit)
RNA: integrity	Microfluidics/3':5' assay	Agarose gel
Inhibition-free	Method of testing	Dilution curve, PCR efficiency <100%
Assay optimisation/validation		
Amplicon details	Exon location, amplicon size	Dβ1: 196bp CCAP: 101bp burs: 210bp pburs: 196bp RpL32: 121bp CG13220: 121bp
Primer sequence	Even if previously published	See **Table S3**
In silico	BLAST/Primer-BLAST/m-fold	Primer-BLAST, electrophoresis, melt curve
empirical	Primer concentration/annealing temperature	
Priming conditions	Oligo-dT/random/combination/target-specific	oligo-dT
PCR efficiency	Dilution curve	Dβ1: 106.3% CCAP: 109.2% burs: 92.4% pburs: 82.9% RpL32: 85.4% CG13220: 90.6%
Linear dynamic range	Spanning unknown targets	5-fold serial dilution
Limits of detection	LOD detection/accurate quantification	Dβ1: 25.19 CCAP: 31.21 burs: 30.54 pburs: 28.19 RpL32: 23.32 CG13220: 29.45
RT/PCR		
Protocols	Detailed description, concentrations, volumes	12.5uL total reaction. 5uL SYBR green Master Mix, 0.25uL F, 0.25uL R, 4.5uL H20 and 2.5uL Template. Initial denaturation: 95deg 5min Denaturation: 95deg 10sec Annealing: 60deg 30sec (x40 cycles)
Reagents	Supplier, lot number	QuantiFast SYBR green PCR kit, Qiagen
Duplicate RT	DCq	Triplicate
NTC	Cq & melt curves	CT value & melt curve not detected
NAC	DCq beginning:end of qPCR	N/A
Positive control	Inter-run calibrators	Inter-run calibrator
Data analysis		
Specialist software	e.g. QBAsePlus	N/A
Statistical justification	e.g. biological replicates	3 biological replicates for each genotype
Transparent, validated normalisation	e.g. GeNorm summary	Target and housekeeper validated at the same life stage

Table S5 Statistical significance for fertility data
Corresponds to data presented in Figure 2D. p values calculated using Student's t-test.

Experimental genotype	Control genotype	Time (days post eclosion)	p value	Annotation
w: +; Dβ1Δex5	w; +; +	4	0.000	***
		6	0.000	***
		8	0.000	***
		11	0.000	***
		13	0.000	***
		15	0.000	***
		19	0.000	***
		23	0.000	***
		27	0.000	***
		33	0.001	**
		40	0.113	ns
		47	1.000	ns
elav-GAL4/w; sgRNAs/+; UAS-Cas9/+	elav-GAL4; sgRNAs; +	3	0.002	**
		5	0.032	*
		10	0.000	***
		13	0.003	**
		16	0.027	*
		19	0.033	*
		23	0.050	*
		29	0.012	*
		33	0.011	*
		36	0.122	ns
		39	0.189	ns
elav-GAL4/w; sgRNAs/+; UAS-Cas9/+	w; +; UAS-Cas9	3	0.001	**
		5	0.000	***
		10	0.002	**
		13	0.025	*
		16	0.042	*
		19	0.107	ns
		23	0.972	ns
		29	0.142	ns
		33	1.000	ns
		36	1.000	ns
		39	1.000	ns
elav-GAL4/w; UAS-Dβ1/+; Dβ1Δex5	elav-GAL4; +; Dβ1Δex5	3	0.000	***
		5	0.000	***
		8	0.000	***
		11	0.000	***
		14	0.000	***
		17	0.000	***
		20	0.053	ns
		23	0.260	ns
		26	1.000	ns
		29	1.000	ns
		33	1.000	ns
		36	1.000	ns
		40	1.000	ns
elav-GAL4/w; UAS-Dβ1/+; Dβ1Δex5	w; UAS-Dβ1; Dβ1Δex5	3	0.000	***
		5	0.000	***
		8	0.000	***
		11	0.000	***
		14	0.000	***
		17	0.000	***
		20	0.053	ns
		23	0.260	ns
		26	1.000	ns
		29	1.000	ns
		33	1.000	ns
		36	1.000	ns
		40	1.000	ns

w; UAS-Dβ1/+; Dβ1-TG4/Dβ1Δex5	w; +; Dβ1-TG4/Dβ1Δex5	5	0.000	***
		7	0.000	***
		10	0.000	***
		13	0.000	***
		16	0.000	***
		20	0.000	***
		24	0.000	***
		27	0.000	***
		31	0.083	ns
		34	0.067	ns
		38	0.280	ns
		42	0.356	ns
		45	1.000	ns

Appendix 3

gBlocks used to generate *Dβ1*^{R81Q} cDNA

Db1QLS_Nterm_gBlock:

GAATACAAGAAGAGAACTCTGAATAGGGAATTGGGAATTCGTTAACAGATCTGCGGCCGCGGGAATTCGATTCAT
GGAGTCTTCCTGCAAATCCTGGCTGTTGTGCAGCATCCTGGTGCTTGTGGCCTTTTCGTTGGTCAGTGCATCCGAAG
ATGAAGAGCGCTTGGTGCGTGACCTCTTTCGAGGCTACAATAAACTCATACGACCCGTACAGAATATGACACAAAA
AGTTGGAGTAAGATTTGGTTTGGCGTTCGTACAGCTAATCAATGTCAATGAGAAAAATCAAGTTATGAAATCAAAC
GTTTGGTTACAGTTGTCCTGGTACGACTACCAGCTGCAGTGGGATGAGGCCGACTACGGCGGCATCGGGGTGTTGC
GTCTGCCCCCCGACAAGGTTTGGAAGCCGGACATTGTGCTCTTCAATAATGCCGATGGCAACTACGAGGTGCGCTA
CAAGTCCAACGTGCTGATTTATCCCACGGGAGAGGTCCTGTGGGTTCCTCCGGCCATTTACCAGAGCTCCTGCACCA
TCGATGTGACCTACTTCCCCTTCGATCAGCAGACCTGTATCATGAAGTTCGGATCGTGGACCTTCAATGGAGATCAG
GTCTCATTGGCGCTCTATAATAATAAGAACTTTGTGGATCTGTCGGATTACTGGAAGTCCGGCACCTGGGACATTAT
AGAGGTGCCCGCCTATCTGAACGTTTACGAGGGCGATAGCAACCACCCCACGGAGACTGACATCACATTCTACATC
ATCATCCGGCGAAAGACTCTCTTCTACACTGTGAATTTAATTCTGCCC

Db1_Cterm_gBlock:

CGGCGAAAGACTCTCTTCTACACTGTGAATTTAATTCTGCCCACGGTGCTGATTTCCTTCCTCTGCGTCTTGGTATTTT
ACCTGCCAGCCGAGGCCGGCGAAAAGGTTACGCTCGGAATTAGCATTTTGCTGTCACTGGTTGTGTTCCTGTTGCTG
GTGTCGAAGATTCTGCCACCAACGTCGCTGGTGCTGCCACTGATCGCCAAATATTTGCTGTTCACCTTCATCATGAAC
ACGGTTTCCATCCTGGTGACCGTGATCATCATCAACTGGAACTTCCGGGGGCCGCGCACCCACCGCATGCCCATGTA
CATCCGCTCCATCTTCCTGCACTACCTGCCCGCCTTCCTATTCATGAAGCGCCCTCGGAAGACCCGCCTGCGCTGGAT
GATGGAGATGCCCGGAATGAGCATGCCCGCCCATCCTCATCCCTCCTACGGCTCGCCAGCGGAGCTGCCCAAGCAT
ATCAGCGCCATCGGCGGCAAGCAATCCAAGATGGAGGTCATGGAGTTGTCCGACCTGCATCACCCCAACTGCAAGA
TCAACCGCAAGGTCAACAGTGGTGGGGAACTTGGCCTGGGTGACGGTTGTCGCCGGGAGAGCGAGTCCTCCGATT
CCATCCTGCTCTCTCCGGAGGCCAGCAAGGCCACCGAGGCGGTGGAGTTCATTGCCGAGCACTTGCGGAACGAGG
ATCTGTACATTCAGACCCGCGAAGATTGGAAGTACGTGGCCATGGTGATCGATCGCTTGCAACTATACATCTTCTTC
ATTGTGACCACGGCCGGAACGGTGGGCATTCTGATGGATGCTCCGCATATTTTCGAGTACGTTGATCAGGATCGCA
TCATCGAGATTTACAGGGGAAAGTAAGCGAGTGAGGACTTGGAGCAGGCCGCGGCTCGAGGGTACCTCTAGAGG
ATCTTTGTGAAGGAACCTTACTTCT